Universiteit
Leiden
The Netherlands

Nucleosome stacking in chromatin fibers probed with single-molecule force- and torque-spectroscopy

Kaczmarczyk, A.

Citation

Kaczmarczyk, A. (2019, June 19). *Nucleosome stacking in chromatin fibers probed with single-molecule force- and torque-spectroscopy*. *Casimir PhD Series*. Retrieved from https://hdl.handle.net/1887/74050

Version:	Not Applicable (or Unknown)
License:	Leiden University Non-exclusive license
Downloaded from:	https://hdl.handle.net/1887/74050

Note: To cite this publication please use the final published version (if applicable).

Cover Page

Universiteit Leiden

The handle http://hdl.handle.net/1887/74050 holds various files of this Leiden University dissertation.

Author: Kaczmarczyk, A.
Title: Nucleosome stacking in chromatin fibers probed with single-molecule force- and torque-spectroscopy
Issue Date: 2019-06-19

Nucleosome stacking in chromatin fibers probed with single-molecule force- and torque-spectroscopy

Nucleosome stacking in chromatin fibers probed with single-molecule force- and torque-spectroscopy

PROEFSCHRIFT

ter verkrijging van
de graad van Doctor aan de Universiteit Leiden,
op gezag van Rector Magnificus prof. mr. C.J.J.M. Stolker,
volgens besluit van het College voor Promoties
te verdedigen op woensdag 19 juni 2019
klokke 11:15 uur

door

Artur Kaczmarczyk

geboren te Ruda Śląska, Polen
in 1988

Promotores:	Prof. dr. ir. S. J. T. van Noort Prof. dr. N. H. Dekker (Delft University of Technology)
Promotiecommissie:	Prof. dr. J. Lipfert (Ludwig-Maximilian-University, Munich, Germany) Dr. F. Mattiroli (Hubrecht Institute, Utrecht) Prof. dr. E. R. Eliel Prof. dr. H. Schiessel Prof. dr. T. Schmidt

©2019 Artur Kaczmarczyk. All rights reserved.

Cover: Little silhouettes pulling and twisting chromatin inside a cellular matrix.
(image of silhouettes adapted from: Sergey Nivens/Shutterstock.com)

Casimir PhD Series, Delft-Leiden, 2019-22
ISBN 978-90-8593-398-4
An electronic version of this thesis can be found at
https://openaccess.leidenuniv.nl

This work was supported by the Netherlands Organisation for Scientific Research (NWO/OCW), as part of the Frontiers of Nanoscience program, and by the NWO-VICI Research Program Project 680-47-616.

To my parents

"The true delight is in the finding out rather than in the knowing."
Isaac Asimov

Contents

1 Introduction **1**
- 1.1 From DNA through nucleosomes to chromatin . . . 2
- 1.2 Regulation of the structure of chromatin fibers . . . 5
- 1.3 Single-molecule magnetic tweezers for studying the dynamics of chromatin . . 7
- 1.4 Mechanical properties of a stretched and supercoiled DNA . . . 10
- 1.5 Statistical mechanics . . . 12
- 1.6 Outline of this thesis . . . 13

2 Methods for probing chromatin structure with magnetic tweezers **21**
- 2.1 Introduction . . . 22
- 2.2 List of materials . . . 24
- 2.3 DNA cloning . . . 27
- 2.4 DNA digestion and labelling . . . 27
- 2.5 Chromatin reconstitution . . . 28
- 2.6 Electrophoretic band shift assay . . . 29
- 2.7 Assembly of the flow cell chamber . . . 30
- 2.8 Flow cell functionalization . . . 33
- 2.9 Dynamic force spectroscopy on chromatin fibers . . . 35
- 2.10 Data analysis . . . 39
- 2.11 Additional notes . . . 44

3 Single-molecule force spectroscopy on histone H4 tail-cross-linked chromatin reveals fiber folding **53**
- 3.1 Introduction . . . 54
- 3.2 Results . . . 56
  - 3.2.1 Chromatin with short NRL folds into a stiffer structure than chromatin with long NRL . . . 56
  - 3.2.2 The H4 tail mediates the nucleosome-nucleosome interactions in folded chromatin fibers . . . 58
  - 3.2.3 H4-V21C/H2A-E64C mutations affect chromatin stacking . . . 60
- 3.3 Discussion and conclusions . . . 63
- 3.4 Materials and methods . . . 67
  - 3.4.1 Chromatin reconstitution and cross-linking . . . 67
  - 3.4.2 Sample preparation . . . 67
  - 3.4.3 Magnetic tweezers . . . 68
  - 3.4.4 Data analysis . . . 68
- 3.5 Supplementary Figures . . . 69

4 Chromatin fibers stabilize nucleosomes under torsional stress 77
4.1 Introduction . . . 78
4.2 Results . . . 81
4.2.1 Chromatin fibers fold into left-handed superhelices that absorb positive twist . . . 81
4.2.2 Nucleosome unstacking is influenced by torque . . . 84
4.2.3 Positive twist can stabilize and destabilize chromatin fibers . . . 86
4.2.4 The torsional modulus of chromatin fibers can be determined experimentally and computationally . . . 90
4.2.5 The response of chromatin fibers to torsion does not vary with NRL . . . 92
4.3 Discussion and conclusions . . . 94
4.4 Materials and methods . . . 99
4.4.1 DNA constructs and chromatin assembly . . . 99
4.4.2 Flow cell preparation . . . 99
4.4.3 Magnetic tweezers . . . 100
4.4.4 Magnetic torque tweezers . . . 100
4.5 Supplementary Information . . . 101
4.5.1 Model of elastic response of DNA to torsion . . . 101
4.5.2 Model of elastic response of chromatin to torsion . . . 103
4.5.3 Distribution of the linking number between the chromatin fiber and DNA handles . . . 104
4.5.4 Computational determination of twist-induced chromatin unstacking . . . 105
4.6 Supplementary Figures . . . 107

5 Linker histone H1 stabilizes nucleosome stacking in chromatin fibers 127
5.1 Introduction . . . 128
5.2 Results . . . 130
5.2.1 Chromatin higher-order structure is stabilized by the linker histone . . . 130
5.2.2 Chromatin unstacking enhances H1 dissociation . . . 133
5.2.3 Quantification of discrete unstacking steps reveals asymmetric unwrapping of chromatosomes . . . 135
5.3 Discussion and conclusions . . . 138
5.4 Materials and methods . . . 141
5.4.1 DNA and chromatin preparation . . . 141
5.4.2 Chromatin with linker histone . . . 142
5.4.3 Flow cells . . . 142
5.4.4 Magnetic tweezers . . . 143
5.5 Supplementary Information . . . 143
5.5.1 Non-equilibrium statistical mechanics model . . . 143
5.5.2 Quantification of discrete unfolding steps . . . 147
5.6 Supplementary Figures . . . 151

6 Summary 161

Samenvatting 165

Publications 169

Curriculum Vitae 171

Chapter 1

Introduction

The genetic information stored in eukaryotic cells is encoded in billions of DNA base pairs. Cells can accommodate such an immensely long genetic code by organizing it into a hierarchical DNA-protein complex called chromatin. To understand this phenomenon, the structure of chromatin has been studied extensively over the last decades. In particular, major progress has been made in resolving the structure of its fundamental component called the nucleosome, and in visualizing the most condensed states such as mitotic chromosomes. However, knowing these structural details is not sufficient to determine how chromatin sustains a tight packing in a tiny cell and simultaneously grants access to genes. Unravelling the mechanism of chromatin (un)folding is therefore essential to comprehend the process of gene expression. It appears that the coordination of key cellular processes involving DNA must be accompanied with dynamic changes in the chromatin structure. Thanks to the continuous development of single-molecule techniques, it is now possible to explore the dynamics of chromatin condensation with high spatial and temporal resolution. The folding of chromatin will be the subject of this thesis.

The focus of this dissertation is the response of well-defined chromatin fibers to mechanical stress induced by force and torque. The presented work consists of an experimental approach involving the application of novel magnetic tweezers, and makes use of theoretical modelling based on statistical mechanics. The obtained results enable us to quantify the mechanical properties of individual chromatin fibers. Importantly, these features cannot be measured by traditional methods that report only on time- and/or ensemble-averaged properties of a larger sample. Using single-molecule methods, new insights that are relevant in the context of gene regulation can be inferred and employed further in epigenetic studies.

The first chapter of the thesis introduces the concepts and theoretical background. Initially, the main structural features of DNA, nucleosomes, and chromatin fibers are described. Then, the principle of magnetic tweezers is presented, and this is followed by the introduction of the statistical mechanics employed in modelling. Finally, a brief overview of the contents of the following chapters is provided.

1.1 From DNA through nucleosomes to chromatin

Genomes of eukaryotic organisms are stored in a cell nucleus in the form of DNA. The DNA consists of two complementary, long chains of polynucleotides that wind around each other and form a double helix. Each nucleotide is composed of a deoxyribose (a carbohydrate), a phosphate group and one of four available nitrogen bases (adenine, thymine, cytosine or guanine). The sequence of the base pairs in the polynucleotide strand defines the unique genetic code that is translated into functional proteins that build the cells [1].

In order to ensure that genes are passed on to the next generation, the eukaryotic DNA is stored and protected in a designated compartment of a cell called

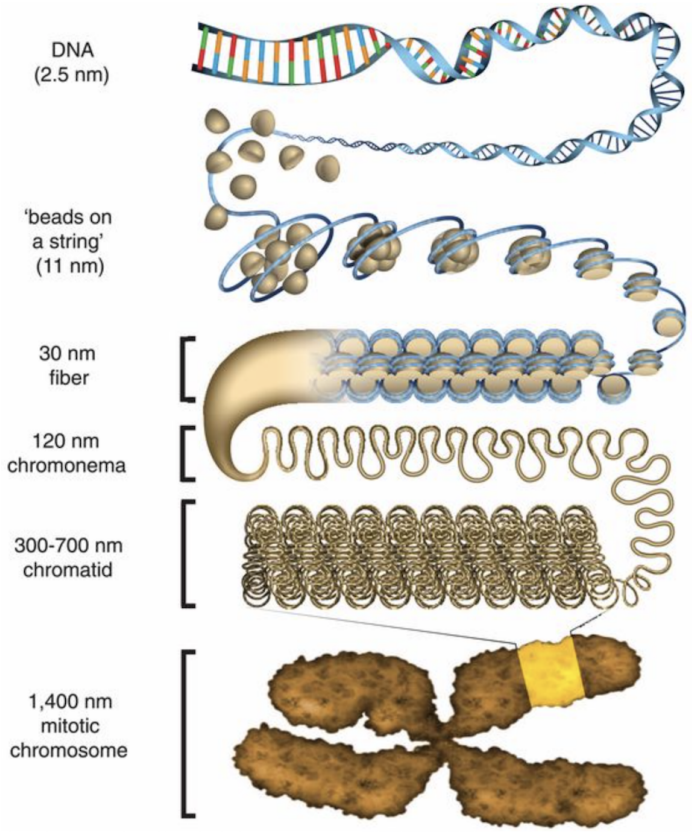

Figure 1.1
Hierarchical model of chromatin folding. Schematic representation of DNA compaction into chromatin. The DNA (top) is wrapped around histone octamers and the resulting "beads-on-a-string" structure folds into a higher-order chromatin structure called "the 30 nm fiber". Further condensation leads to thicker fibers named as chromonema and chromatid. The most compacted state of chromatin is the mitotic chromosome (bottom) that has a diameter of 1.4 μm. This graphical image is adapted from *Science, 2017 Jul 28; 357(6349).*

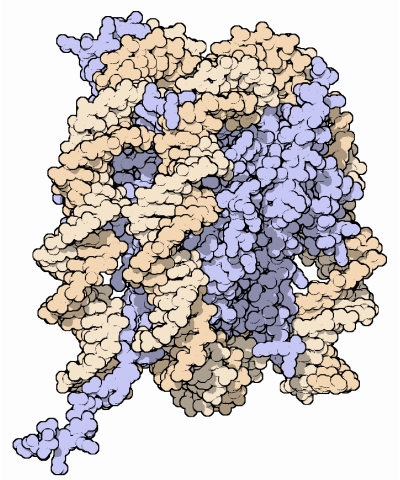

Figure 1.2
Crystal structure of the nucleosome. 147 base pairs of DNA form a double helix, depicted in orange, and wrap around the histone proteins that constitute the histone octamer (blue). This graphical image is adapted from: PDB, https://cdn.rcsb.org/pdb101/motm/images/1aoi.gif.

the nucleus. At the same time, the DNA must remain accessible to facilitate the transcription of genes into mRNA and to control all metabolic processes. Maintaining the balance between the packing and the accessibility becomes highly challenging, especially in eukaryotic organisms that feature a complex and diverse metabolism. This large complexity correlates with the size of the genome that is present in every cell. For example, the DNA of every human cell is composed of 3 billion base pairs, which would measure more than 1 meter in a stretched configuration [2]. It has been suggested that such a long strand would still fit by itself inside a micrometer-size nucleus, given that the thickness of the DNA is only 2 nm [3]. However, the consequence of random packing of the DNA would be disastrous for cells. The probability of finding a specific DNA sequence in a disorganized spool of billions of base pairs would be low enough to affect the vitality of any living system. In multicellular organisms, only specific fragments of their genome are expressed in different cell types at a given time, and therefore more sophisticated mechanisms of DNA organization have evolved. The efficient compaction of eukaryotic genomes is accomplished by folding of DNA into nucleosomes and further condensation of nucleosomal arrays into chromatin that has many levels of compaction (Fig. 1.1). In this thesis, the dynamics of nucleosomal arrays folded into compact chromatin fibers is studied by single-molecule force- and torque-spectroscopy.

Chromatin is a complex of DNA and histone proteins that interact with each other in a well-defined manner. The basic repetitive unit of chromatin,

called the nucleosome, is a structure formed by 147 base pairs of DNA wrapped 1.65 times around a histone octamer (Fig. 1.2) [4]. There are four types of histones that constitute an octamer, and each of the histones is present in two copies. Histones H3 and H4 form the tetrasome $(H3-H4)_2$, which complexes with two H2A-H2B dimers. An optional fifth histone, called the linker histone (H1 or H5), can bind to nucleosomes and form a structure named the chromatosome [5]. In Chapters 3 and 4 of this thesis, nucleosomal arrays without linker histone are investigated and in Chapter 5, chromatin with the linker histone is studied.

The structure of the nucleosome has been resolved by X-ray crystallography to 2.8 Å resolution [6]. It has been shown that nucleosomal components vary - specifically the DNA sequence wrapped around the histone core, as well as some chemical groups that modify the canonical histone proteins. The physical properties of nucleosomes are also affected by the ionic strength of the solution in which they are present [7]. As a result, nucleosomes are highly dynamic structures and can undergo spontaneous unwrapping or sliding along the DNA. These transient states can be stabilized by chromatin remodellers or modifications in the structure of DNA (*e.g* methylation of DNA bases) and histones (*e.g* methylation, acetylation, ubiquitinylation of the flexible histone tails) [8–10]. Multiple studies have shown that these dynamic changes in nucleosome composition are crucial for granting access to the genetic information [11–13]. It remains less understood, however, what the mechanism of accessing the DNA is, given the crowded environment of a cell nucleus that contains a multitude of nucleosomes that may interact with each other into more condensed fibers.

In vivo, nucleosomes are connected by short fragments of the linker DNA (20 - 80 bp), and the resulting "beads-on-a-string" are thought to form heterogeneous, liquid-like chromatin composed of "clutches" of nucleosomes [14]. However, structural studies of oligonucleosomes *in vitro* have indicated that they form secondary (higher-order) structures upon nucleosome stacking [15]. The most common model, known as the "30 nm fiber", implies that neighboring nucleosomes are constrained at the exterior of the fiber, while the linker DNA resides at its center [16]. The exact configuration of stacked nucleosomes and the topology of the linker DNA has remained a topic of debate, mainly due to the heterogeneous and dynamic nature of chromatin and the lack of techniques that can directly resolve the structure of such fibers.

The overall structure of chromatin may be driven by the interactions between the nucleosomes [17]. In this dissertation, this issue is specifically addressed by employing the conditions that facilitate the internucleosomal contacts. Additionally, the specific Widom-601 DNA sequence was used in order to control the positioning of the reconstituted nucleosomes on the DNA template [18, 19]. By these means, well-defined chromatin fibers were formed, and their stability and dynamics could be studied using magnetic tweezers.

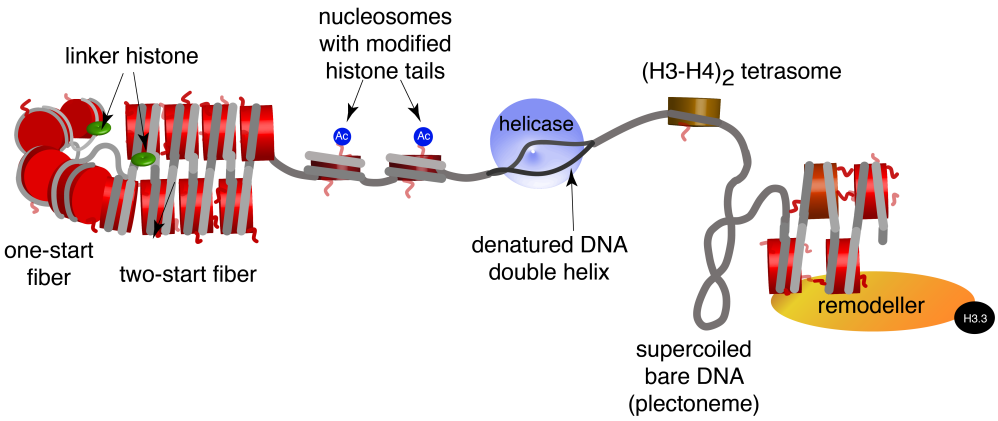

Figure 1.3
Multiple factors regulate the level of DNA compaction. Schematic drawing, showing the complexity of chromatin compaction that may exist *in vivo*. The DNA double helix (grey) is wrapped around globular histone octamers with protruding flexible tails (red) and form nucleosomes. Linker histones (green) can bind to some of the nucleosomes and form chromatosomes. The neighboring nucleosomes and chromatosomes can interact with each other and constrain the linker DNA between them either in bent (in a one-start fiber) or straight configuration (in a two-start fiber). Modifications of histones, such as *e.g* acetylation of the histone tail (dark blue points), or the activity of remodellers (orange), regulate the level of chromatin compaction. Some molecular motors such as *e.g.* helicase (blue) or polymerase bind to chromatin, predominantly to the fragments of accessible bare DNA. While executing their functions, the proteins generate torsional stress that results in the formation of supercoils (plectonemes and/or denatured DNA helix) which can further affect the structure of chromatin.

1.2 Regulation of the structure of chromatin fibers

In the earliest reports describing the higher-order organization of chromatin, arrays of nucleosomes were shown to form a supercoiled fiber, described as a solenoidal filament [29]. An alternative configuration to this, the zig-zag (two-start) geometry, was suggested when the high-resolution crystal structure of short fibers was presented [15]. In this model, the linker DNA wraps back and forth between the two stacks of nucleosomes. Many subsequent studies pointed to the two-start folding of nucleosome arrays, especially those with nucleosomes separated by short linker DNA [30, 31]. However, Robinson *et al.* probed the compaction of nucleosome arrays with longer linker DNA (30 - 70 bp), and found that the measured dimensions of the fibers were incompatible with the two-start model. Thus, the relative abundance of different variations of the higher-order structures remains still a matter of debate.

The extensive research on chromatin has provided detailed descriptions of factors that contribute to changes in chromatin compaction (see Table 1.1).

factor	role in the chromatin folding
Nucleosome Repeat Length (NRL)	Nucleosome Repeat Length (NRL) is a parameter that defines the number of base pairs wrapped around a histone octamer (147 bp) and the length of the DNA connecting consecutive nucleosomes (linker DNA). Linker DNA lengths varying between 20 - 90 bp were found *in vivo*, depending on the underlying DNA sequence, cell type, and other factors. From the mechanistic point of view, the shorter the DNA linkers, the more constrained the internucleosomal flexibility. This implies that arrays with larger spacing between nucleosomes permit for different geometries of the linker DNA (including its bending). Moreover, due to the helical twist of the DNA (36° per 1 base pair), the length of linkers defines the rotational orientation of adjacent nucleosomes [20]. Thus, NRLs with 10 base pairs increments are frequently employed in *in vitro* studies to retain the same rotational setting of nucleosomes in chromatin arrays. In this thesis, NRLs of 167 and 197 bp were used to probe the geometry of chromatin fibers and the topology of the linker DNA in those (see Chapter 2,3,4,5).
linker histone (H1, H5)	Linker histones are additional histone proteins that bind to the nucleosomal dyad and seal the nucleosome, preventing the unwrapping of the DNA [21]. Linker histones are abundant in chromatin with larger NRLs and their suggested function is to enhance chromatin condensation [22] (see Chapter 5).
histone tails interaction	Histone tails are flexible chains of positively charged N-terminal domain of the core histones or C-terminal domain of the histone H2A. As they protrude from the nucleosome, they interact with globular domains of neighboring nucleosomes or recruit other proteins involved in the regulation of chromatin structure (*e.g* chromatin remodellers) [23]. Histone tails feature a range of post-translational modifications (acetylation, phosphorylation, methylation) [8]. A key role is played by the tail of histone H4 and its interaction with the acidic patch of histone H2A that mediate the stacking of nucleosomes into a "30 nm fiber" (see Chapter 3).
histone variants	A number of histone variants has been reported to affect the stability of nucleosomes, *e.g* H2A.X, H2A.Z, macro-H2A, H3.3, CENP-A [24]. These histone variants mostly lack certain docking domains recognized in canonical histones by enzymatic remodellers [25].
non-histone proteins	Other non-histone proteins that organize chromatin such as HP1 or HMG have been identified. HP1 interacts with histones H3 and H4 and is thought to act similarly to linker histones [26]. HMG proteins bind to nucleosomes, outcompeting the interaction with linker histones, and by this means they destabilize chromatin [5]. A group of "polycomb complexes" targets the modified histones, such as methylated histone H3 [27].
torsional stress	Supercoiling of the DNA is generated by polymerases during DNA replication and transcription and can regulate the stability of nucleosomes [28] (see Chapter 4).

Table 1.1
Selected factors that influence the stability of nucleosomes and the higher-order structure of chromatin.

For example, the location and spacing between nucleosomes were shown to be correlated with the rate of DNA transcription. Torsional stress generated by the molecular motors (*e.g.* polymerases, helicases) was suggested to be one of the main regulators of genome architecture [32]. The stability of nucleosomes can also be modulated by the presence of linker histones, chromatin remodellers, and histone modifications [5, 24]. However, mechanistic explanations of this regulation, especially in the context of chromatin fibers are largely missing. The first single-molecule experiments that resolved dynamic changes in chromatin focused on individual nucleosomes and sparsely decorated nucleosomal arrays [33–36]. In this thesis, it is shown that stacking of nucleosomes into a fiber changes its mechanical properties and hence may affect the response of chromatin to these factors.

1.3 Single-molecule magnetic tweezers for studying the dynamics of chromatin

Single-molecule force spectroscopy techniques such as optical tweezers (OT), magnetic tweezers (MT) or atomic force microscopy (AFM) can directly monitor the folding and unfolding of individual biomolecules [37, 38]. In these methods, the molecule of interest is attached to an object (*e.g* 1 μm bead, functionalized glass or a cantilever) and is subsequently stretched by external forces. In OT (Fig. 1.4A), a high-intensity laser with a high numerical aperture lens generates a force that traps a bead in the focus of the beam [39]. In AFM (Fig. 1.4B), the position of a cantilever with a tethered molecule is changed and by this means the force is exerted. In MT (Fig. 1.4C), forces are exerted by a magnetic field that acts on a paramagnetic bead tethered to a biomolecule [40].

The force in all these single-molecule force spectroscopy techniques can be generally described by Hooke's law:

$$F = k \cdot x \tag{1.1}$$

where F is the force, x is the displacement of the molecule from the equilibrium (in the elastic limit), and k is the stiffness of the system (reflected in the fluctuations of the tether). One can either change the displacement and measure the force in a position clamp or *vice versa* - exert the force of a known value and measure the displacement (extension) of the molecule in a force clamp. Both approaches result in force-distance curves that provide information about the mechanical properties of the tethered molecule, such as its persistence length or a contour length.

In this study, magnetic tweezers were used to probe the dynamics of DNA and chromatin tethers. One of the major advantages of MT over OT and AFM is the possibility of multiplexing [41]. This means that within a single measurement, dozens of individual molecules can be tracked in real-time. This

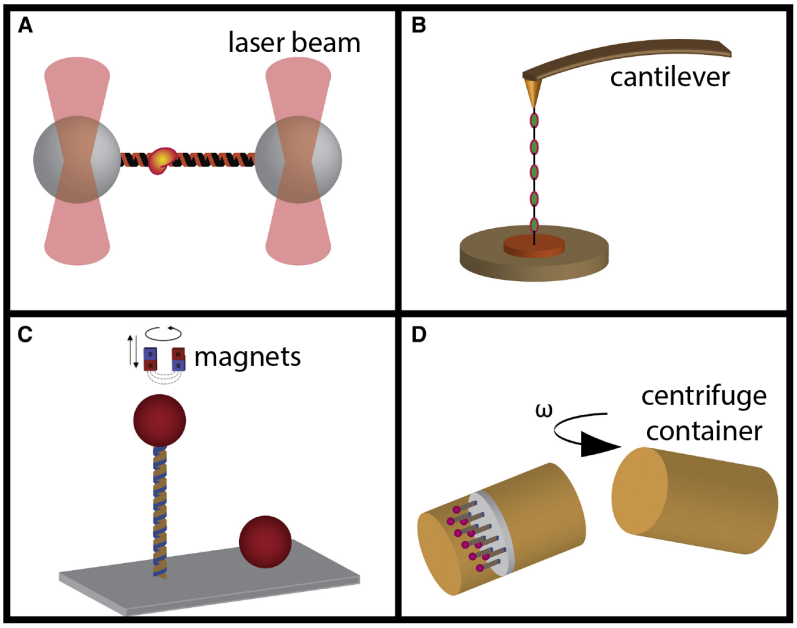

Figure 1.4
Schematics of single-molecule force spectroscopy techniques. A) In optical tweezers, focused laser beams are used to trap dielectric particles. **B)** In atomic force microscopy, flexible cantilevers apply direct forces to the molecule of interest. **C)** In magnetic tweezers, forces are applied by a magnetic field. **D)** In the centrifuge force microscope, centrifugal forces are exerted to a tethered sample. This graphical image is adapted from *Biophysical Journal 115, 2279 - 2285, December 18, 2018.*

is particularly relevant for complex biological molecules composed of many subunits, such as chromatin fibers. Moreover, magnetic tweezers allow to precisely control not only forces but also the twist or the torque by the rotation of the magnet [42]. Such feature makes MT a suitable tool to investigate the effect of torsion on the wrapping of DNA into nucleosomes. Applying twist to reconstituted chromatin fibers can therefore mimic the effect of torsional stress that is generated *in vivo*.

In magnetic tweezers, wide-field transmission microscopy, using LED illumination, is employed to record the images of the beads, and real-time image processing is used to resolve their 3D position over time [42, 43]. When the beads are a few μm out of focus, they generate strong diffraction patterns in the focal plane. The exact profile of those patterns is correlated with the distance of the bead from this focal plane along the optical axis (z-direction). By comparison of the image with a reference pattern, it is possible to measure the position of the bead with respect to the focus with nanometer accuracy.

Displacement of the beads (and hence the tethered molecules) is induced by changing the magnetic field gradient exerted by stationary magnets or

electromagnets. The magnetic field gradient is influenced by the orientation of the two magnets and the gap size between those, whereas the magnitude of the magnetic field $\vec{B}$ is determined by the type of magnets and the material and diameter of the paramagnetic beads used in the experiment. The force $\vec{F}$ exerted on a paramagnetic bead is given by:

$$\vec{F} = \frac{1}{2}\vec{\bigtriangledown}(\vec{m} \cdot \vec{B}) \tag{1.2}$$

where $\vec{m}$ is the induced magnetic moment of the bead in the external magnetic field $\vec{B}$. The distance between the bead and the magnets (in the order of few millimeters) is much larger than the typical displacement of the tethered bead (less than 1 μm), and therefore the force is constant at specific magnet position, irrespective of tether motion. By moving the magnets towards (or from) the flow cell, the gradient of the magnetic field is increased (or decreased), increasing (or reducing) the applied force [44].

The magnetic field gradient and the induced magnetic moment can be modelled for a specific magnet geometry and magnetic beads, which allows to quantify the exerted forces [45]. However, a more accurate approach of force calibration involves the measurement of the average displacement of the tethered bead due to its Brownian motion:

$$F = \frac{k_{\mathrm{B}} T L}{< \delta\ x^2 >} \tag{1.3}$$

where k_{B} is the Boltzmann constant, T is the temperature, L the measured length of the tether, and $< \delta x^2 >$ is the variance of the bead displacement in the image plane. Using this relation, the force can be quantified empirically for a known magnet and bead configuration. Due to the limited acquisition frequency of the camera, certain corrections must be performed to account for image blurring and aliasing [46].

Besides force, torque can also be applied using the magnets [47, 48]. The magnetic field $\vec{B}$ will cause the magnetic moment of the bead to align with the field, but due to a slight anisotropy in the magnetization of the bead, a small component of the magnetic moment, $\vec{m_0}$ does not align. This causes a torque on the bead given by: $\Gamma\ = (\vec{m_0} \times \vec{B})$.

By employing a magnet configuration that decreases the horizontal component of the magnetic field (for example cylindrical magnets with a small side magnet attached to it, as shown in Chapter 4), it is possible to directly measure the restoring torque of the over- or under-wound tethered molecule [49, 50].

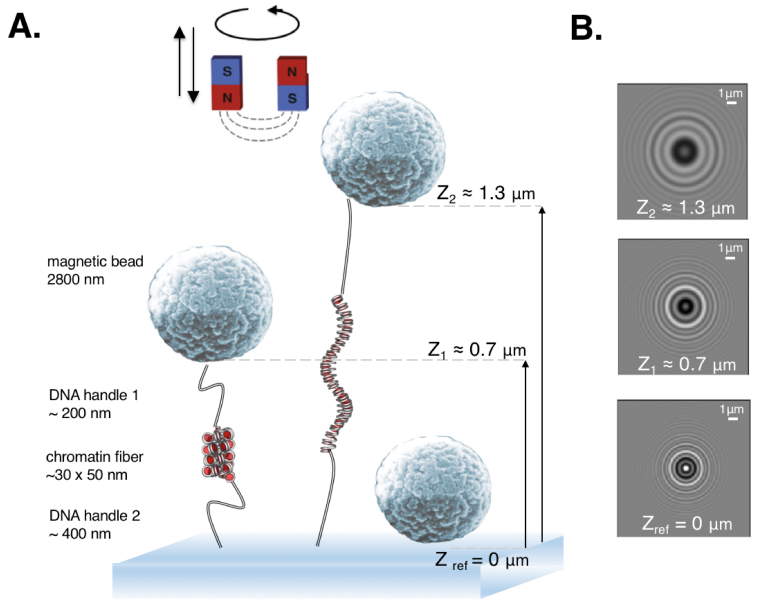

Figure 1.5
Schematic representation of a magnetic tweezers experiment. A) A chromatin fiber (red) flanked by DNA handles on both sides (grey lines) is tethered between a glass slide (blue) and a magnetic bead (grey textured). The magnetic field, introduced by a pair of cubic magnets (red and blue), induces a force on the bead which results in unfolding of the chromatin fiber. The height of the magnetic bead reflects the extension of the tether. **B)** The exact profile of the diffraction pattern recorded by the camera reflects the distance between the bead and the focal plane.

1.4 Mechanical properties of a stretched and supercoiled DNA

In order to understand the mechanical properties of chromatin, it is essential to recapitulate the features of DNA that have been well established by single-molecule force- and torque-spectroscopy.

To a good approximation, a DNA molecule behaves like an elastic isotropic rod that in solution bends locally as a result of thermal fluctuations [51]. This causes the end-to-end distance of the polymer to be shorter than its contour length (the length of the polymer in the fully stretched configuration). Small forces can stretch such entropically coiled DNA without changing the intrinsic structure of the DNA.

A model called the inextensible worm-like-chain (WLC) can be employed to describe this extension of the DNA in terms of its end-to-end distance as a function of force [52]. In this dissertation, the extensible WLC model is used, which includes both the aforementioned entropic stretching and the elastic

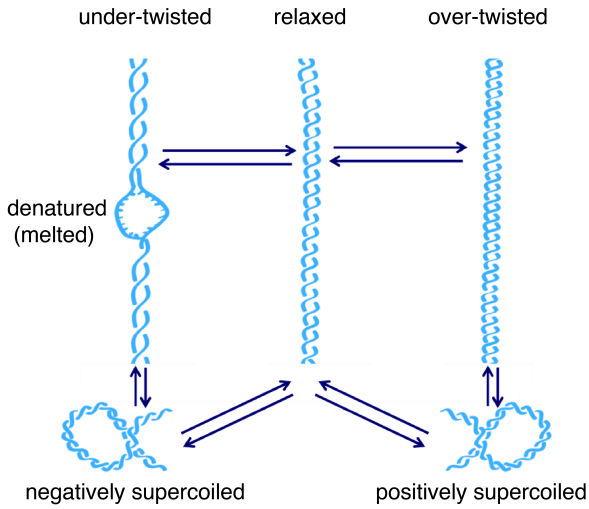

Figure 1.6
Topological properties of supercoiled DNA. In the absence of turns, DNA can exist as a relaxed molecule (center) with a right-handed chirality. Over-winding (right) DNA increases the twist density or form a positively supercoiled structure (plectoneme). Under-winding DNA (left) decreases the twist density and may induce DNA denaturation (melting bubble) or form a negatively supercoiled structure (plectoneme). This graphical image is adapted from *Biophysical Journal, 2014; 106(1174-1181).*

elongation (referring to the increasing distance between DNA base pairs):

$$z_{\mathrm{DNA}}(f, L) = L\left[1 - \frac{1}{2}\sqrt{\frac{k_{\mathrm{B}}T}{fA}} + \frac{f}{S}\right]. \tag{1.4}$$

where f is the force, L the contour length of the DNA, A the stretching persistence length that defines its flexibility ($\sim$ 50 nm), k_{B} the Boltzmann constant, T the temperature and S the DNA stretching modulus (that equals $\sim$ 1100 pN, and reflects the force at which the elastically elongated DNA would measure twice its contour length).

In vivo, DNA exists mainly as a double-stranded helix with a right-handed chirality (B-DNA) [1]. The topology of DNA can be characterized by its linking number that describes how many times the two DNA strands are interwound [53]. The linking number (Lk_0) of a relaxed B-DNA molecule with N base pairs equals:

$$Lk_0 = \frac{N}{Tw_0} \tag{1.5}$$

where Tw_0, corresponding to the number of base pairs that make 1 full helical turn, equals 10.5. The linking number of DNA is a sum of its twist (Tw) and

writhe (Wr). Twist refers to the density of the helical winding and indicates the total number of turns in the double-stranded DNA helix. Writhe is a measure of the looping of DNA and it quantifies the number of times that the double helix crosses itself (Fig. 1.6). For a relaxed, linear DNA molecule, $Wr = 0$ and $Lk_0 = Tw$.

The linking number changes when turns are applied to the DNA helix tethered, for example, in the magnetic tweezers set-up. Provided that both DNA strands are anchored at their ends (referred later on in Chapter 4 as "rotationally constrained"), turns of the magnets can change the twist (Tw) and/or writhe (Wr) of the DNA molecule. Over-twisting (positive twist) occurs when anti-clockwise turns are applied (Tw increases). Under-twisting (negative twist) is induced upon the application of clockwise rotation (Tw decreases). Excessive negative twist initially results in torque build-up, but it is limited by the subsequent denaturation (or melting) of the DNA ($Tw = 0$). Excessive positive twist also results in the build-up of torque, followed by the change in writhe. The latter results from the formation of plectonemic supercoils (that occur also at negative twist when forces are sufficiently low).

The overall change in the linking number is then governed by the sum of the changes in twist and writhe:

$$\Delta\ Lk = \Delta\ Tw + Wr \tag{1.6}$$

1.5 Statistical mechanics

Statistical mechanics is employed in this thesis as a tool to quantitatively interpret the experimental results. This branch of statistical physics is very effective in describing stochastic behaviour of a system that consists of a large number of components, based on the distribution of energy among them. Here, statistical mechanics is used to infer the properties of a DNA-chromatin tether that is in thermodynamic equilibrium. At different levels of force and torque, both DNA and chromatin fibers can be in different states. For DNA, previously introduced twisted, plectonemic and melted states can be separately identified. For chromatin, states such as stacked nucleosomes, partially unwrapped nucleosomes, and fully unwrapped nucleosomes are distinguished. In general, each state i has its characteristic free energy G_i. The probability P_i that the system occupies given state i within an overall distribution of states is:

$$P_i = \frac{\exp(-\frac{G_i}{k_\mathrm{B}T})}{\sum_i \exp(-\frac{G_i}{k_\mathrm{B}T})} \tag{1.7}$$

where $k_\mathrm{B}T$ is the Boltzmann constant at room temperature (4.1 pN $\cdot$ nm).

In this thesis, such formalism is applied to the extension of chromatin fibers. The probability of a given state (characterized by its extension z_i) is calculated

at room temperature and is force-dependent:

$$P_i(F) = \frac{\exp(-\frac{\Delta\ G_i(z_i) - f z_i}{k_B T})}{\sum_i \exp(-\frac{\Delta\ G_i(z_i) - f z_i}{k_B T})} \tag{1.8}$$

where $\Delta\ G_i(z_i)$ is the free energy of a given state.

Knowing the probability of each state (Eq. 1.8), the average extension of the entire tether can be calculated as:

$$< z(F) >= \sum_i z_i P_i \tag{1.9}$$

1.6 Outline of this thesis

In this thesis, the mechanical properties of individual chromatin fibers are studied. Specifically, the phenomenon of nucleosome stacking in such fibers is investigated in great detail with multiplexed magnetic tweezers. By combining single-molecule force spectroscopy with a nucleosome cross-linking assay, our structural model describing the compliance of chromatin fibers [54] is reinforced. Moreover, the first direct measurements of torque in compact chromatin fibers are introduced, and finally, the role of the linker histone H1 in chromatin folding is studied. All reported observations contribute to a better understanding of the function of chromatin higher-order structures in genome organization and processing.

A detailed description of the methodology that is used in all parts of this work is presented in Chapter 2. It is followed by three chapters (Chapter 3, 4, and 5) that address the role of nucleosome-nucleosome interactions in chromatin folding. By stabilizing the higher-order structure of chromatin using chemical cross-linking (Chapter 3), by measuring or constraining torque (Chapter 4), and by the addition of protein linker histones (Chapter 5), new structural features of chromatin fibers were inferred and interesting changes of such structures were characterized.

In **Chapter 2**, the process of the chromatin assembly, data acquisition, and analysis routines are described in a protocol-like fashion. Initially, sample preparation methods, such as DNA cloning and chromatin reconstitution, are introduced which are followed by technical specifications of the instruments employed in the experiments. Next, the statistical mechanics model, established in Ref. [54], is recapitulated and the method of fitting the experimental data with this model is described in a step-by-step manner.

In **Chapter 3**, the force-spectroscopy experiments on chromatin fibers with mutated histones are presented. Using these genetically modified histones (H4-V21C, H2A-E64C) in the chromatin assembly process allowed to induce covalent bonds between adjacent nucleosomes via histone tails in a controlled manner.

Such site-specific cross-linking stabilized the secondary structure of chromatin fibers against stretching and provided direct evidence of nucleosome stacking in folded chromatin fibers. Importantly, this phenomenon occurs in chromatin fibers with the Nucleosome Repeat Length of both 167 and 197. This supports the hypothesis of two different higher-order structures of chromatin fibers.

The experiments presented in **Chapter 4** were performed on rotationally constrained chromatin fibers. This allowed to study the structural changes of chromatin induced by the application of twist. In addition to regular magnetic tweezers, magnetic torque tweezers were also used to probe the torque build-up in twisted chromatin tethers. A torsional spring model was developed to quantify the torsional flexibility of chromatin fibers and to infer the topology of compact chromatin fibers. Remarkably, a new phenomenon of twist-induced nucleosome restacking was found which indicates that torsional stress might stabilize nucleosome stacking.

In **Chapter 5**, the role of the linker histone H1 in chromatin folding is investigated. Linker histones are supplementary histone proteins that have been suggested to induce additional condensation of chromatin fibers. Here, the mechanisms of folding and unfolding were compared between fibers with and without linker histone H1. However, rather than higher compaction, which was not observed, increased stability of nucleosome stacking was found in H1(+) chromatin fibers. A novel non-equilibrium model and a new step-finding algorithm were introduced to quantify the discrete unstacking events induced by stretching chromatin fibers with the linker histone.

In the **Chapter 6**, the main conclusions are summarized and an outlook on the future work, that may shed more light on the structure and dynamics of chromatin fibers, is presented.

Bibliography I

[1] Bruce Alberts et al. *Molecular Biology of the Cell, 5th Edition*. 2008. ISBN: 978-0-8153-4105-5.

[2] Philip Nelson. *Biological Physics: Energy , Information , Life*. 2002. ISBN: 0-7167-4372-8.

[3] Helmut Schiessel. *Biophysics for Beginners: A Journey through the Cell Nucleus*. Taylor Francis Group, LLC, 2013. ISBN: 978-981-4241-65-6.

[4] Roger D. Kornberg. "Structure of chromatin". In: *Annu Rev Biochem.* 46 (1977), pp. 931–54.

[5] Nicole Happel and Detlef Doenecke. "Histone H1 and its isoforms: Contribution to chromatin structure and function". In: *Gene* 431 (2009), pp. 1–12. ISSN: 03781119. DOI: 10.1016/j.gene.2008.11.003.

[6] Karolin Luger et al. "Crystal structure of the nucleosome core particle at 2.8Å resolution". In: *Nature* 389 (1997), pp. 251–260. ISSN: 0028-0836. DOI: 10.1038/38444.

[7] Abdollah Allahverdi et al. "Chromatin compaction under mixed salt conditions: Opposite effects of sodium and potassium ions on nucleosome array folding". In: *Scientific Reports* 5 (2015), p. 8512. ISSN: 20452322. DOI: 10.1038/srep08512.

[8] Gregory D. Bowman and Michael G. Poirier. "Post-translational modifications of histones that influence nucleosome dynamics". In: *Chemical Reviews* 115 (2015), pp. 2274–2295. ISSN: 15206890. DOI: 10.1021/cr500350x.

[9] Karolin Luger and Timothy J. Richmond. "The histone tails of the nucleosome". In: *Current Opinion in Genetics and Development* 8.2 (1998), pp. 140–146. ISSN: 0959437X. DOI: 10.1016/S0959-437X(98)80134-2.

[10] J. Widom. "Role of DNA sequence in nucleosome stability and dynamics". In: *Quarterly Reviews of Biophysics* 34 (2001), pp. 269–324. ISSN: 0033-5835. DOI: doi:10.1017/S0033583501003699.

[11] J. L. Workman and R. E. Kingston. "Alteration of nucleosome structure as a mechanism of transcriptional regulation". In: *Annu. Rev. Biochem* 67 (1998), pp. 545–79. DOI: 10.1146/annurev.biochem.67.1.545.

[12] Brent Brower-Toland et al. "Specific contributions of histone tails and their acetylation to the mechanical stability of nucleosomes". In: *Journal of Molecular Biology* 346.1 (2005), pp. 135–146. ISSN: 00222836. DOI: 10.1016/j.jmb.2004.11.056.

[13] Keda Zhou, Guillaume Gaullier, and Karolin Luger. "Nucleosome structure and dynamics are coming of age". In: *Nature Structural & Molecular Biology* 26 (2019), pp. 3–13. ISSN: 1545-9993. DOI: 10.1038/s41594-018-0166-x.

[14] Maria Aurelia Ricci et al. "Chromatin fibers are formed by heterogeneous groups of nucleosomes in vivo". In: *Cell* 160.6 (2015), pp. 1145–1158. ISSN: 10974172. DOI: 10.1016/j.cell.2015.01.054.

[15] Thomas Schalch et al. "X-ray structure of a tetranucleosome and its implications for the chromatin fibre". In: *Nature* 436.7047 (2005), pp. 138–141. ISSN: 00280836. DOI: 10.1038/nature03686.

[16] Philip J. J. Robinson et al. "EM measurements define the dimensions of the '30-nm' chromatin fiber: evidence for a compact, interdigitated structure." In: *Proceedings of the National Academy of Sciences of the United States of America* 103.17 (2006), pp. 6506–11. ISSN: 0027-8424. DOI: 10.1073/pnas.0601212103.

[17] Nikolay Korolev, Alexander P. Lyubartsev, and Lars Nordenskiöld. "A systematic analysis of nucleosome core particle and nucleosome-nucleosome stacking structure". In: *Scientific Reports* 8.1 (2018), p. 1543. ISSN: 2045-2322. DOI: 10.1038/s41598-018-19875-0.

[18] P. T. Lowary and J. Widom. "New DNA sequence rules for high affinity binding to histone octamer and sequence-directed nucleosome positioning". In: *Journal of Molecular Biology* 276.1 (1998), pp. 19–42. ISSN: 00222836. DOI: 10.1006/jmbi.1997.1494.

[19] Andrew Flaus and Tom Owen-Hughes. "Mechanisms for nucleosome mobilization". In: *Biopolymers* 68.4 (2003), pp. 563–578. ISSN: 00063525. DOI: 10.1002/bip.10323.

[20] Sergei A. Grigoryev. "Nucleosome spacing and chromatin higher-order folding". In: *Nucleus (United States)* 3.6 (2012), pp. 493–9. ISSN: 19491034. DOI: 10.4161/nucl.22168.

[21] Robert T. Simpson. "Structure of the chromatosome, a chromatin particle containing 160 base pairs of DNA and all the histones". In: *Biochemistry* 17.25 (1978), pp. 5524–5531. ISSN: 0006-2960. DOI: 10.1021/bi00618a030.

[22] Philip J. J. Robinson and Daniela Rhodes. "Structure of the '30 nm' chromatin fibre: A key role for the linker histone". In: *Current Opinion in Structural Biology* 16.3 (2006), pp. 336–343. ISSN: 0959440X. DOI: 10.1016/j.sbi.2006.05.007.

[23] Marta Garcia-Ramirez, Feng Dong, and Juan Ausio. "Role of the histone 'tails' in the folding of oligonucleosomes depleted of histone H1". In: *Journal of Biological Chemistry* 267.27 (1992), pp. 19587–19595. ISSN: 00219258.

[24] Karolin Luger, Mekonnen L. Dechassa, and David J. Tremethick. "New insights into nucleosome and chromatin structure: An ordered state or a disordered affair?" In: *Nature Reviews Molecular Cell Biology* 13.7 (2012), pp. 436–447. ISSN: 14710072. DOI: 10.1038/nrm3382.

[25] Andrew J. Bannister and Tony Kouzarides. "Regulation of chromatin by histone modifications." In: *Cell research* 21.3 (2011), pp. 381–95. ISSN: 1748-7838. DOI: 10.1038/cr.2011.22.

[26] Joel C. Eissenberg and Sarah C.R. Elgin. "The HP1 protein family: Getting a grip on chromatin". In: *Current Opinion in Genetics and Development* 10.2 (2000), pp. 204–210. ISSN: 0959437X. DOI: 10.1016/S0959-437X(00)00058-7.

[27] Guohong Li and Danny Reinberg. "Chromatin higher-order structures and gene regulation". In: *Current Opinion in Genetics and Development* 21.2 (2011), pp. 175–186. ISSN: 0959437X. DOI: 10.1016/j.gde.2011.01.022.

[28] Nick Gilbert and Bernard Ramsahoye. "The relationship between chromatin structure and transcriptional activity in mammalian genomes". In: *Briefings in Functional Genomics and Proteomics* 4.2 (2005), pp. 129–142. ISSN: 14739550. DOI: 10.1093/bfgp/4.2.129.

[29] J. T. Finch and A. Klug. "Solenoidal model for superstructure in chromatin." In: *Proceedings of the National Academy of Sciences* 73.6 (1976), pp. 1897–1901. ISSN: 0027-8424. DOI: 10.1073/pnas.73.6.1897.

[30] Benedetta Dorigo et al. "Nucleosome arrays reveal the two-start organization of the chromatin fiber". In: *Science* 306.5701 (Nov. 2004), pp. 1571–1573. ISSN: 00368075. DOI: 10.1126/science.1103124.

[31] Feng Song et al. "Cryo-EM study of the chromatin fiber reveals a double helix twisted by tetranucleosomal units". In: *Science* 344.6182 (2014), pp. 376–380. ISSN: 10959203. DOI: 10.1126/science.1251413.

[32] Christophe Lavelle. "DNA torsional stress propagates through chromatin fiber and participates in transcriptional regulation". In: *Nature Structural and Molecular Biology* 15.2 (2008), pp. 123–125. ISSN: 15459993. DOI: 10.1038/nsmb0208-123.

[33] Shirley Mihardja et al. "Effect of force on mononucleosomal dynamics". In: *Proceedings of the National Academy of Sciences* 103.43 (2006), pp. 15871–15876. ISSN: 0027-8424. DOI: 10.1073/pnas.0607526103.

[34] Maxim Y. Sheinin et al. "Torque modulates nucleosome stability and facilitates H2A/H2B dimer loss". In: *Nature Communications* 4 (2013), p. 2579. ISSN: 20411723. DOI: 10.1038/ncomms3579.

[35] Aurélien Bancaud et al. "Structural plasticity of single chromatin fibers revealed by torsional manipulation". In: *Nature Structural and Molecular Biology* 13.5 (2006), pp. 444–450. ISSN: 15459993. DOI: 10.1038/nsmb1087.

[36] Brent D. Brower-Toland et al. "Mechanical disruption of individual nucleosomes reveals a reversible multistage release of DNA". In: *Proceedings of the National Academy of Sciences* 99.4 (2002), pp. 1960–1965. ISSN: 0027-8424. DOI: 10.1073/pnas.022638399.

[37] Orkide Ordu, Alexandra Lusser, and Nynke H. Dekker. "Recent insights from in vitro single-molecule studies into nucleosome structure and dynamics". In: *Biophysical Reviews* 8.S1 (2016), pp. 33–49. ISSN: 18672469. DOI: 10.1007/s12551-016-0212-z.

[38] Helen Miller et al. "Single-molecule techniques in biophysics: A review of the progress in methods and applications". In: *Reports on Progress in Physics* 81.2 (2018). ISSN: 00344885. DOI: 10.1088/1361-6633/aa8a02.

[39] Joost van Mameren, Gijs J.L. Wuite, and Iddo Heller. "Introduction to optical tweezers: Background, system designs, and commercial solutions". In: *Methods in Molecular Biology*. Vol. 1665. 2018, pp. 3–23. ISBN: 9781617792816. DOI: 10.1007/978-1-4939-7271-5_1.

[40] Franz J. Giessibl. "Advances in atomic force microscopy". In: *Reviews of Modern Physics* 75.3 (2003), pp. 949–983. ISSN: 00346861. DOI: 10.1103/RevModPhys.75.949.

[41] Noah Ribeck and Omar A. Saleh. "Multiplexed single-molecule measurements with magnetic tweezers". In: *Review of Scientific Instruments* 79.9 (2008), p. 094301. ISSN: 00346748. DOI: 10.1063/1.2981687.

[42] I. D. Vilfan et al. *Magnetic Tweezers for Single-Molecule Experiments*. Ed. by Peter Hinterdorfer and Antoine Oijen. New York, NY: Springer US, 2009, pp. 371–395. ISBN: 978-0-387-76497-9. DOI: 10.1007/978-0-387-76497-9_13. arXiv: 9809069v1 [gr-qc].

[43] Marteen Kruithof et al. "Subpiconewton dynamic force spectroscopy using magnetic tweezers." In: *Biophysical journal* 94.6 (2008), pp. 2343–2348. ISSN: 00063495. DOI: 10.1529/biophysj.107.121673.

[44] Charlie Gosse and Vincent Croquette. "Magnetic tweezers: Micromanipulation and force measurement at the molecular level". In: *Biophysical Journal* 82.6 (2002), pp. 3314–3329. ISSN: 00063495. DOI: 10.1016/S0006-3495(02)75672-5.

[45] Jan Lipfert, Xiaomin Hao, and Nynke H Dekker. "Quantitative modeling and optimization of magnetic tweezers." In: *Biophysical journal* 96.12 (2009), pp. 5040–9. ISSN: 1542-0086. DOI: 10.1016/j.bpj.2009.03.055.

[46] Zhongbo Yu et al. "A force calibration standard for magnetic tweezers". In: *Review of Scientific Instruments* 85.12 (2014), p. 123114. ISSN: 10897623. DOI: 10.1063/1.4904148.

[47] T. R. Strick et al. "The Elasticity of a Single Supercoiled DNA Molecule". In: *Science* 271.5257 (1996), pp. 1835–1837. ISSN: 0036-8075. DOI: 10.1126/science.271.5257.1835.

[48] Maarten M. van Oene et al. "Biological Magnetometry: Torque on Superparamagnetic Beads in Magnetic Fields". In: *Physical Review Letters* 114.21 (2015), p. 218301. ISSN: 0031-9007. DOI: 10.1103/PhysRevLett.114.218301.

[49] Jan Lipfert et al. "Magnetic torque tweezers: Measuring torsional stiffness in DNA and RecA-DNA filaments". In: *Nature Methods* 7.12 (2010), pp. 977–980. ISSN: 15487091. DOI: 10.1038/nmeth.1520.

[50] Amit Sharma and Alfonso Mondragón. "DNA topoisomerases". In: *Current Opinion in Structural Biology*. Methods in Molecular Biology 5.1 (1995). Ed. by Duncan J. Clarke, pp. 39–47. ISSN: 0959440X. DOI: 10.1016/0959-440X(95)80007-N.

[51] Claude Bouchiat et al. "Estimating the persistence length of a worm-like chain molecule from force-extension measurements". In: *Biophysical Journal* 76.1 (1999), pp. 409–413. ISSN: 00063495. DOI: 10.1016/S0006-3495(99)77207-3.

[52] J. F. Marko. "Stretching must twist DNA". In: *Europhysics Letters* 38.3 (1997), pp. 183–188. ISSN: 02955075. DOI: 10.1209/epl/i1997-00223-5.

[53] He Meng et al. "Coexistence of Twisted, Plectonemic, and Melted DNA in Small Topological Domains". In: *Biophysical Journal* 106.5 (2014), pp. 1174–1181. ISSN: 00063495. DOI: 10.1016/j.bpj.2014.01.017.

[54] He Meng, Kurt Andresen, and John van Noort. "Quantitative analysis of single-molecule force spectroscopy on folded chromatin fibers". In: *Nucleic Acids Research* 43.7 (2015), pp. 3578–3590. ISSN: 13624962. DOI: 10.1093/nar/gkv215.

Chapter 2

Methods for probing chromatin structure with magnetic tweezers

Magnetic tweezers form a unique tool to study the topology and mechanical properties of chromatin fibers. Chromatin is a complex of DNA and proteins that folds the DNA in such a way that meter-long stretches of DNA fit into the micron-sized cell nucleus. Moreover, it regulates accessibility of the genome to the cellular replication, transcription, and repair machinery. However, the structure and mechanisms that govern chromatin folding remain poorly understood, despite recent spectacular improvements in high-resolution imaging techniques. Single-molecule force spectroscopy techniques can directly measure both the extension of individual chromatin fragments with nanometer accuracy and the forces involved in the (un)folding of single chromatin fibers. Here, we report detailed methods that allow one to successfully prepare *in vitro* reconstituted chromatin fibers for use in magnetic tweezers-based force spectroscopy. The higher-order structure of different chromatin fibers can be inferred from fitting a statistical mechanics model to the force-extension data. These methods for quantifying chromatin folding can be extended to study many other processes involving chromatin, such as the epigenetic regulation of transcription.

This chapter is based on: Kaczmarczyk A., Brouwer T.B., Pham C., Dekker N.H, van Noort S.J.T : "Probing chromatin structure with magnetic tweezers", in: Nanoscale Imaging - Methods and Protocols, Springer, 1814:297-323 (2018).

2.1 Introduction

Chromatin is a DNA-protein complex that organizes and compacts DNA in the nucleus of eukaryotic cells. The basic unit of a chromatin is a nucleosome, which consists of 147 base pairs of DNA turning 1.65 times around a histone protein octamer. The histone octamer is composed of a $(H3\text{-}H4)_2$ histone tetramer and two H2A-H2B histone dimers [1, 2]. Nucleosomes interact with each other via histone tails and form higher-order chromatin structures [3–5].

Eukaryotic DNA is subject to many processes such as replication and transcription. To regulate these processes, the structure and composition of chromatin fibers must be very dynamic [6]. Previous studies have shown how the nucleosome positioning, post-translational histone modifications, and chromatin remodelers can alter the stability of nucleosomes and may modulate the structure of chromatin [7–10]. Using X-ray crystallography [11], electron microscopy [12–15], or atomic force microscopy [16], researchers have established detailed structures of the nucleosome and small arrays of nucleosomes. However, as the structure of chromatin fibers becomes more complex and disordered as their size increases, these techniques have their limits in contributing to an examination of higher-order chromatin structure. Moreover, they do not typically address the dynamical rearrangements of chromatin fibers that are essential for the genomic transactions occurring in eukaryotic nucleus. In contrast, single-molecule force spectroscopy techniques are capable of tracking and manipulating the extension of chromatin fibers in real-time and under physiological conditions, providing unique means to study their structure, assembly, and disassembly.

Magnetic tweezers represent an especially powerful tool for the study of chromatin folding, as they permit the straightforward application of both tension and torsion [17, 18] as well as multiplexing [19, 20]. Precise control of the force combined with nanometer accuracy measurements of the extension of individual fibers will help to elucidate the molecular mechanisms that control chromatin condensation and the regulation of processes involving chromatin. In our assay, chromatin fibers are tethered between a glass slide and a paramagnetic bead. As the distance between a pair of magnets and the beads reduces, the beads experience an increasing force, which is directly applied to the tethered fibers.

In this methods chapter, we describe how a DNA substrate containing an array of nucleosome positioning sequences is prepared (Section 2.3) and functionalized for magnetic tweezers experiments (Section 2.4). This involves labelling of one end of the DNA with digoxigenin and the other end with biotin. Subsequently, the DNA substrate is loaded with histone proteins resulting in well-defined reconstituted chromatin fibers (Section 2.5). Though protein chaperones (*i.e.* NAP-1) can load histones on DNA into arrays of nucleosomes [21], we employ salt-dialysis reconstitution in which positively charged histones assemble onto the negatively charged DNA as the salt concentration is slowly decreased [22]. To ensure a well-defined composition and spacing of

the nucleosomes in the chromatin fiber, we use a DNA template with tandem repeats of Widom-601 positioning sequences [23]. The quality of chromatin assembly is assessed using agarose gel electrophoresis (Section 2.6) which shows different mobility of incomplete and overcomplete chromatin fibers compared to stoichiometric assemblies of chromatin fibers.

We use a homebuilt magnetic tweezers microscope and custom flow cells to immobilize and manipulate individual chromatin fibers. The flow cell design constitutes an aluminum holder that fixes two cover slides and PDMS (polydimethylsiloxane) layer that seals the channel between the two slides. The holder has two channels for a buffer exchange and a large aperture for illumination of the sample (Section 2.7). After functionalizing the chamber (Section 2.8), chromatin fibers are injected into a flow cell and tethered between a glass slide and a magnetic bead. The chromatin fiber is manipulated by changing the force on the beads by moving the magnets (Section 2.9). The resulting changes in tether end-to-end distance are measured by a bead-tracking algorithm and are subsequently analyzed with a statistical mechanics model (Section 2.10). Following these procedures yields a detailed characterization of the mechanical properties of single-folded chromatin fibers.

2.2 List of materials

1. **DNA cloning**
- Ampicillin-resistant pUC18 plasmid with tandem repeats of the Widom-601 sequence (see Note 1)
- XL1-blue E. coli competent cells stored at -80 °C (see Note 2)
- ThermoMixer C Eppendorf12 ^{TM} 5424R Microcentrifuge (Eppendorf)
- Shaker KS 130 (IKA KS)
- Luria-Bertani (LB) medium and LB agar plate
- NucleoBond Xtra Midi kit (Macherey-Nagel)

2. **DNA digestion and labeling**
- Restriction enzymes: Bse*YI*, Bsa*I* (New England Biolabs)
- NEBuffer 3.1 (with bovine serum albumin) - 10× concentrated (New England Biolabs)
- Promega Wizard SV Gel and PCR cleanup kit (Promega)
- BioDrop μLITE spectrophotometer (Isogen Life Science)
- 1× Tris/Borate/EDTA buffer (TBE)
- dNTPs (100 mM) (Roche)
- GeneRuler DNA Ladder Mix (Thermo Fisher Scientific)
- Klenow Fragment (2 U/μL), LC (Thermo Fisher Scientific)
- Reaction buffer for Klenow Fragment (10×) (Thermo Fisher Scientific)
- Digoxigenin-11-dUTP (1 mM) (Roche)
- Biotin-16-dUTP (1 mM) (Roche)
- UV transilluminator ChemiDoc XRS+ (Bio-Rad)

3. **Chromatin reconstitution**
- Slide-A-Lyzer mini dialysis tubes, 10000 MWCO (Thermo Scientific)
- Low-binding pipette tips (VWR)
- Magnetic stirrer with a heat plate (VWR)
- Glass beaker (1 L)
- Econo gradient pump (Bio-Rad)
- Histone Octamer, Recombinant Human (stored at -20 °C) (EpiCypher)
- 1.5 L of miliQ H_2O (4 °C)
- 50× Tris/EDTA (TE), pH 7.5
- 5 M NaCl
- high salt buffer (80 mL of 5 M NaCl +4 mL of 50× Tris/ EDTA (TE) + miliQ H_2O up to 200 mL)
- Low salt buffer (980 mL of miliQ HO + 20 mL of 50× Tris/ EDTA (TE))

4. **Electrophoretic band shift assay**
- Agarose Standard (Roth)
- PowerPac Basic Power Supply (Bio-Rad)

- KuroGEL Midi 13 Electrophoresis Horizontal (VWR)
- GeneRuler DNA Ladder Mix (Thermo Fisher Scientific)
- 5× Tris/boric acid (TB
- Loading buffer (20% glycerol, 20 mM Tris, 1 mM EDTA, bromophenol blue)
- Ethidium bromide (10000×) (Thermo Fisher Scientific)

5. **Assembly of the flow cell chamber**

- Aluminum flow cell frame, custom-built (Fig. 2.1)
- Perspex mold, custom-built (Fig. 2.1)
- Cover slip 24 × 40 mm, # 1.5 thickness (Menzel Gläser)
- Cover slip 24 × 60 mm, # 1.5 thickness (Menzel Gläser)
- Sylgard 184 silicone elastomer kit PDMS (Sylgard)
- FEP tubing (1/1600 OD × 0.02000 ID) (Upchurch Scientific)
- Electrical wire (∼ 0.0200 OD) (Nexans)
- Embossing tape (Dymo)
- N2 Spray Gun Assembly (NCI)
- Vacuum controller CVC 3000 and Diaphragm pump MZ 2 NT (Vacuubrand)
- M4 screws
- Ultrasonic cleaning bath USC-TH (VWR)
- Microscope slide (75 × 26 × 1 mm) (Menzel Gläser)
- Glass beakers (100 mL + 250 mL)
- Cover slip holder (custom-made)
- 2-Propanol

6. **Flow cell functionalization**

- Dynabeads M-270 Streptavidin or MyOne Streptavidin (Invitrogen)
- Microscope slide (75 × 26 × 1 mm)
- Pentyl acetate, puriss. p.a., ≥ 98.5 % (GC) (Sigma-Aldrich)
- 1% nitrocellulose in pentyl acetate (Ladd Research Industries)
- Anti-digoxigenin - from sheep (Sigma-Aldrich)
- Bovine serum albumin (BSA) heat shock fraction, pH 7, ≥ 98% (Sigma-Aldrich)
- Dynal Invitrogen Bead Separations (Invitrogen)
- Tween-20 (Sigma-Aldrich)
- Sodium azide (NaN_3) (Merck)
- 1 M HEPES, pH 7.5
- 2 M KCl
- 20 mM $MgCl_2$
- 1× Tris/EDTA (TE)
- Plastipak 1 mL syringe (BD)
- Sterican 18G single-use needle (B. Braun)
- Tygon tubing (0.8 mm ID/0.8 mm wall)

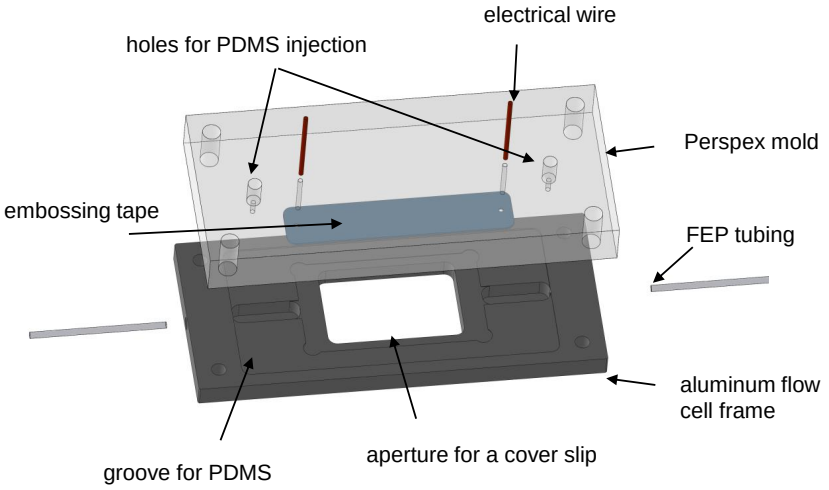

Figure 2.1
Components of the flow cell chamber. A custom-built Perspex mold is mounted onto a custom-built aluminum flow cell frame that holds a 24 × 40 mm cover slip. Subsequently, PDMS is injected into the chamber between the mold and the groove of the metal frame.

7. **Hardware**

- 25 Mpix Condor camera (CMOS Vision GmbH)
- Frame grabber Camera Link PCIe-1433 (National Instruments)
- NIKON CFI Plan Fluor objective (NA = 1.3, 40×, oil, Nikon Corporation)
- Infinity-corrected tube lens ITL200 (Thorlabs)
- 100 μW, 20 mA LED collimator emitting at 645 nm (IMM Photonics GmbH)
- Computer T7610 (Dell) with a 10 core Intel Xeon 2.8 GHz processor (Intel) and 32 GB DDR3 memory
- Multi-axis piezo scanner P-517.3CL (Physik Instrumente GmbH Co.)
- 5 mm cube magnets N50 (Supermagnete, Webcraft GmbH)
- Two-phase hollow shaft stepper motor (Casun)
- M-126.2S1 Translation Stage for a magnet (Two Physik)
- M-126.2S1 Translation Stage for objective (Two Physik)
- Syringe pump (Prosense B. V.)

2.3 DNA cloning

1. **Cell transformation with pUC18 plasmid**. Thaw about 100 μL of XL1-blue competent cells on ice and add $\sim$ 1 μL of a plasmid. Mix gently and incubate on ice for at least 30 min. Induce a 42 °C heat shock of about 90 - 120 s with the ThermoMixer. Place the sample back on ice for 1 min and add 900 μL of LB medium. Shake gently (240 rpm) and incubate for 30 - 60 min at 37 °C. Centrifuge the sample for 1 min at 14000 rpm (18500 $\times$ G), remove the supernatant, and then resuspend the sample in 100 μL LB medium. Spread the sample on an LB agar plate with ampicillin, and incubate upside-down at 37 °C overnight.

2. **Cell culture**. Select a single colony and inoculate in 500 mL flask with 250 mL LB medium with ampicillin. Incubate overnight at 37 °C while shaking (320 rpm). Next day, centrifuge the culture (14000 rpm [18500 $\times$ G] at 4 °C for 10 min). Discard the supernatant and keep the cell pellet.

3. **Plasmid DNA isolation**. Isolate and purify the plasmid DNA using NucleoBond Xtra Midi kit using the manufacturer's protocol.

2.4 DNA digestion and labelling

1. **Plasmid digestion with Bsa*I* and Bse*YI***. Linearize the plasmid DNA with two restriction enzymes in a buffer that contains maximally 50 ng/μL of the substrate in 1$\times$ NEBuffer 3.1 (see Note 3). Digest overnight at 37 °C. Subsequently, inactivate the enzyme by incubating the reaction at 80 °C for 20 min. Purify the digested DNA with the PromegaWizard SV Gel and PCR cleanup kit (see Note 4).

2. **DNA labelling with biotin tag**. Mix the purified DNA, the Klenow fragment (5 units per 100 μL of a reaction volume), and a regular, non-tagged dNTP complementary to the first nucleotide at one side of the digested DNA, here CTP (see Note 5 and Fig. 2.2B), together with biotin-16-dUTP (final concentration of dNTPs is 20 μM). Incubate for 2 h at 37 °C. Purify the DNA with the Promega Wizard SV Gel and PCR cleanup kit.

3. **DNA labelling with digoxigenin tag**. Mix the biotinylated DNA; the Klenow fragment (5 units per 100 μL of a reaction volume); a regular, non-tagged dNTP complementary to the first single nucleotide at the other side of the digested DNA (Fig. 2.2C); and digoxigenin-11-dUTP (final concentration of dNTPs is 20 μM). Incubate 2 h at 37 °C. Purify the DNA with the Promega Wizard SV Gel and PCR cleanup kit.

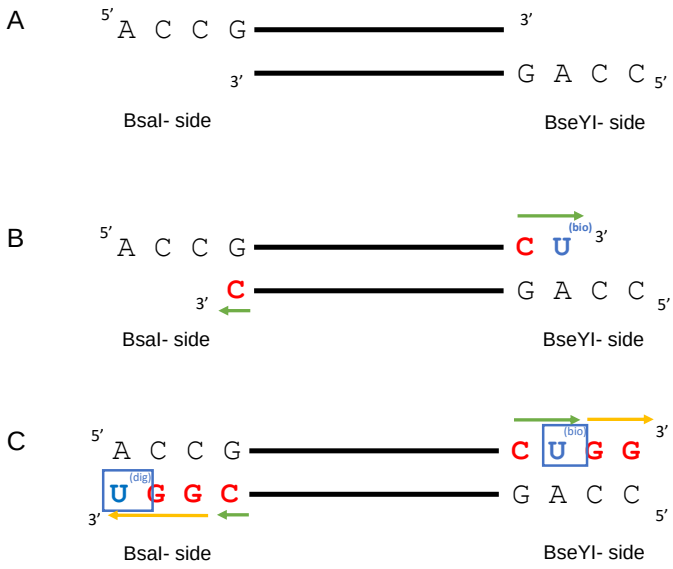

Figure 2.2
Labelling of the DNA with a single biotin and digoxigenin tag. A) The pUC18 plasmid digested with Bsa*I* and Bse*YI* has single-stranded overhangs at both sides. **B)** A Klenow reaction with biotin-dUTP and free nucleotides other than dGTP (here dCTP) results in incorporation of a biotin only at the Bse*YI* side. **C)** Subsequently, the DNA is purified and a second Klenow reaction with dGTP and digoxigenin-dUTP results in binding of a digoxigenin at the Bsa*I* side.

2.5 Chromatin reconstitution

The DNA is mixed with histone octamers in a high salt buffer [24]. Subsequently, the salt concentration is slowly reduced by dialysis to first assemble $(H3\text{-}H4)_2$ tetrasomes on the 601-DNA. At low salt concentration, histone dimers H2A-H2B bind to the tetrasomes, and full nucleosomes are formed. The nucleosome reconstitution depends critically on the histone:DNA ratio. Excess histones yield additional tetrasomes and nucleosomes on the DNA handles, and excess DNA yields undersaturated fibers. Therefore, each reconstitution is done in a titration series.

1. **Preparation of histone:DNA titrations**. Prepare at least five batches with increasing histone:DNA ratios. Each batch contains at least 500 ng of DNA in a total volume of 50 μL. The minimal DNA concentration (m/v) is then 10 ng/μL, and the minimal molar concentration of the 601 DNA (excluding the DNA handles) is 0.1 μM. Center the titrations at 1:1 molar ratio between 601 segments and histone octamer (Table 2.1). See Note 6 for an explanation of the calculation method.

component	I	II	III	IV	V	VI
180 ng/μL 601-DNA (μL)	7	7	7	7	7	7
200 ng/μL histone octamer (μL)	2	3	4	5	6	7
330 ng/μL competitor DNA (μL)	1	1	1	1	1	1
final DNA conc μL	0.179	0.179	0.179	0.179	0.179	0.179
final octamer conc μL	0.074	0.111	0.148	0.185	0.222	0.259
high salt buffer μL	40	39	38	37	36	35
total volume μL	50	50	50	50	50	50
octamer:DNA ratio	0.4	0.6	0.8	1.0	1.2	1.4

Table 2.1
The composition of individual titrations used for chromatin reconstitution. Samples with increasing octamer : DNA ratio are prepared to account for lower reproducibility while pipetting small volumes.

2. **Salt gradient dialysis**. Cool down all the buffers before starting the assembly (see Note 7). Insert a magnet rod into a beaker that contains 200 mL of high salt buffer. Put the dialysis tubes on a floater, and incubate for 15 min in this buffer to allow the membranes to soak. Transfer 50 μL of histone:DNA mixtures into the dialysis tubes using the low-binding pipette tips (see Note 8). Rinse the Econo gradient pump with miliQ H_2O and subsequently with the low salt buffer. Connect the pump as in Fig. 2.3. Set the flow rate at 0.9 mL/min to ensure a gradual decrease of the salt concentration in the dialysis tubes. Switch on the magnet plate to properly mix the incoming low salt buffer with the high salt buffer (see Note 9).

3. **Collecting the reconstituted samples**. After approximately 18 h, 900 mL of the buffer is pumped to the waste bottle. Transfer the content of the dialysis tubes into separate low-binding tubes. Store the chromatin samples at 4 °C for maximally 5 weeks. Rinse the tubing of the pump with miliQ H_2O.

2.6 Electrophoretic band shift assay

Quality assessment using agarose gel electrophoresis helps to select chromatin fibers with the optimal histone:DNA ratio prior to a single-molecule experiment. Due to their size and charge, reconstituted chromatin fibers migrate slower through a gel than a bare DNA template (Fig. 2.4).

1. **Gel preparation**. Dissolve 0.7 g of agarose gel in 100 mL of 0.2× TB buffer by heating the solution in a microwave (700 W, 1 min). Pour the melted agarose solution in a large gel tray. Place a 20 μL well comb in the gel. Let the agarose solidify for $\sim$ 45 min.

2. **Sample loading**. Put the gel together with its tray into an electrophoresis chamber. Fill it with the 0.2× TB buffer. Gently remove the comb. Load 3 μL

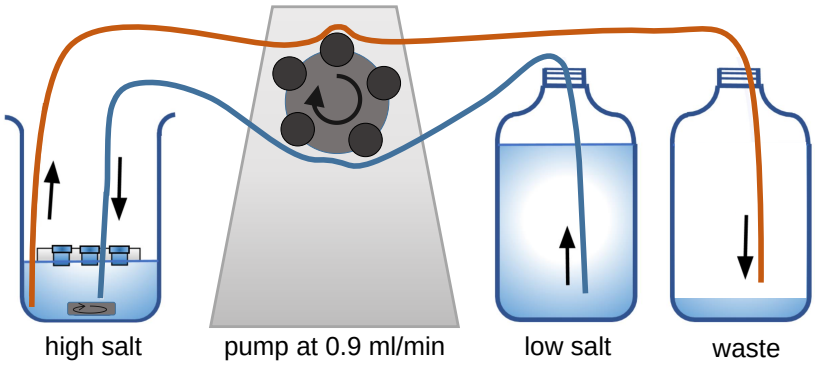

Figure 2.3
Schematic representation of the dialysis system controlled by a peristaltic pump. Samples are dialyzed against a high salt buffer. Subsequently, a low salt buffer is pumped into the beaker with dialyzed samples, while an equal volume is flown out into a waste bottle to ensure a constant volume and a gradual decrease of salt concentration in the dialysis tubes.

of GeneRuler DNA Ladder into the first and the last well. Pipette the DNA-only substrate ($\sim$ 200 ng) mixed with a 10 $\times$ loading dye (final concentration 1 $\times$) into the second well. Load 10 μL of reconstituted chromatin samples mixed with the 10$\times$ loading dye (final concentration 1$\times$) to subsequent wells.

3. **Running the electrophoresis**. Put the lid on the electrophoresis chamber, and connect to the power source. Run at 100 V for 2.5 h to ensure a good separation of bands.

4. **Staining with EtBr**. Remove the tray with the gel and place it carefully in a container with 1000 mL of 1$\times$ EtBr. Incubate while shaking for 30 min.

5. **Destaining**. Move the gel on its tray to a container with a distilled water and incubate for 15 min.

6. **Gel imaging**. Visualize the bands on the ChemiDoc UV. Select the optimal histone:DNA titration for single-molecule experiments. Choose the titration ratio with a smaller shift than the bare DNA that does not exhibit any excessive assembly on a competitor DNA (lane 5 in Fig. 2.4, see Note 10).

2.7 Assembly of the flow cell chamber

A properly assembled flow cell chamber can be reused for numerous experiments when it is handled gently and is not contaminated during an assembly. Only the top 24 $\times$ 60 mm cover slip, with a functionalized surface, needs to be

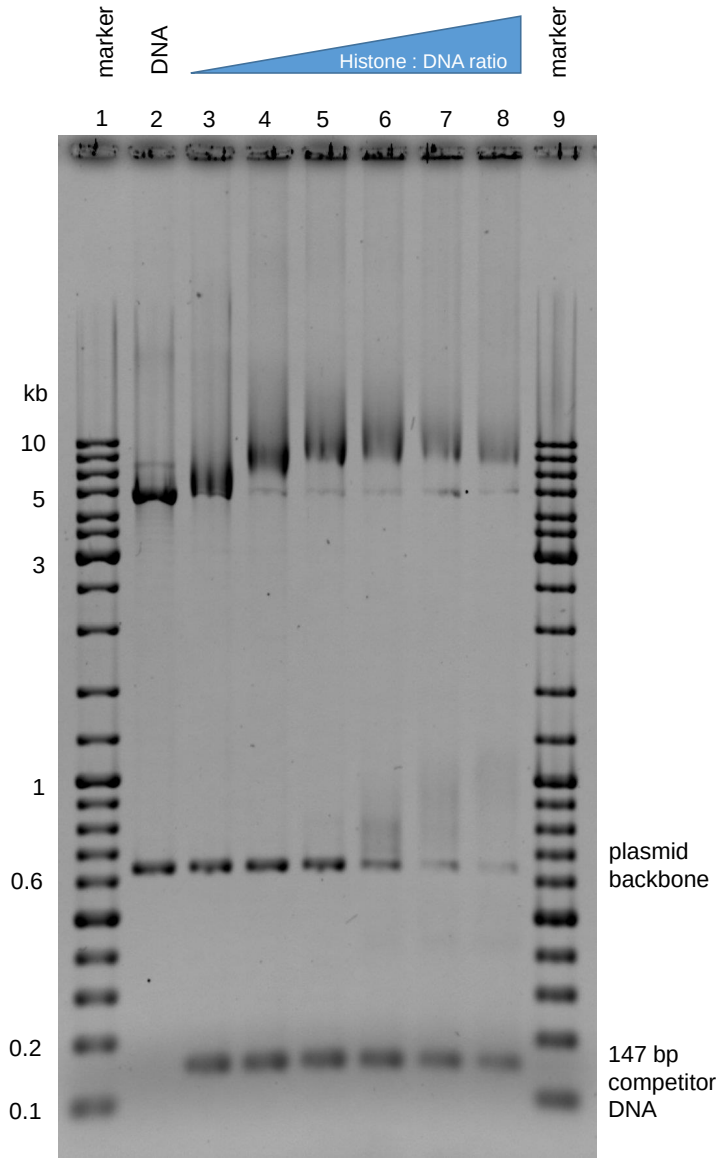

Figure 2.4
Electrophoretic mobility shift assay of reconstituted chromatin fibers. With the increasing histone concentration, chromatin fibers migrate slower through the agarose gel. The consecutive bands on the gel (lanes 3 - 8) are gradually shifted with respect to the bare DNA band (lane 2). The plateau in the band shift reflects a full saturation of chromatin fibers and indicates that excessive histones start to assemble on the non-601 DNA, resulting in additional band shift of the plasmid backbone and the competitor DNA (lanes 6 - 8). The sample in lane 5 exhibits a full saturation of the 601 arrays and no excessive assembly on the competitor DNA; therefore it was chosen for single-molecule experiments.

replaced.

1. **Cleaning**. Remove the top glass slide from the flow cell and any leftovers of PDMS from the Perspex molds and the aluminum holders. Wash thoroughly with miliQ H_2O and 2-propanol. Make sure that no PDMS remains inside the inlets of the molds and the holders. Dry under N_2 gas stream (Fig. 2.5A).

2. **PDMS preparation**. Mix PDMS (polydimethylsiloxane) base and curing agent in a 10:1 ratio (viscous and nonviscous component, respectively) (Fig. 2.5B). Prepare at least 2 - 3 mL per flow cell. Mix vigorously with a pipette tip for 2 min (see Note 11). Put under a vacuum chamber for 2 h in order to degas the viscous polymer.

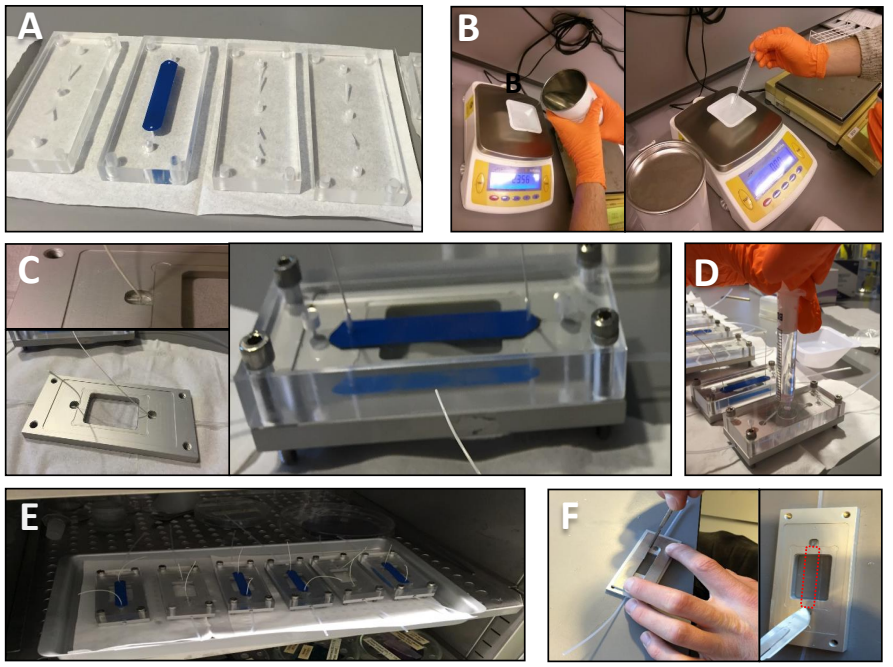

Figure 2.5
Assembly of flow cell chambers. A) Perspex molds are cleaned and dried. **B)** The PDMS base and the curing agent are weighted, mixed, and degassed. **C)** During the degassing process, aluminum flow cell holders, cover glasses, wiring, and Perspex molds are mounted. **D)** The PDMS solution is injected into chambers. **E)** Flow cells are cured at 65 ^{o}C. **F)** Perspex molds are removed and a channel is cut out from a flat, cured PDMS layer (red dotted line) indicates the part of PDMS that was cut out.

3. **Assembling a flow cell chamber**. Insert a stiff electric wire into two 10-cm-long pieces of FEP tubing. Insert the tubes into a metal frame such that the electric wire protrudes out of the inner outlet of the holder, near the central aperture of the flow cell. Do the same on the other side of the flow cell (Fig. 2.5C,

left). Put a clean glass cover slip (24 × 40 mm) onto the aperture. Mount the Perspex mold tightly onto the flow cell with M4 screws (Fig. 2.5C, right). Make sure that the electric wires protrude through the holes in the top of this mold and that the cover slip remains in its place. The end of the FEP tubing must remain inside the outlet near the aperture of the aluminum holder.

4. **Casting PDMS**. Gently inject the degassed PDMS with a syringe into the assembled flow chambers through one of the holes on top of the Perspex molds. Push the syringe slowly until the whole chamber is filled with the PDMS and the excess of polymer starts to leak out of the second hole in the mold (Fig. 2.5D). Prevent incorporating air bubbles into the chamber. Cure the assembly in an oven at 65 °C for at least 2 h to initiate the polymerization of PDMS (Fig. 2.5E).

5. **Cutting the channel in a cured PDMS**. Loosen the screws and gently remove the electric wires and the Perspex mold such that the FEP tubing and the cured PDMS remain intact. The large groove of the aluminum holder should be filled with a transparent, smooth, and solid layer of PDMS that covers its whole surface and, as a result, immobilizes the 24 × 40 mm cover slip firmly on the aluminum holder. Carefully cut a rectangular channel in the PDMS layer above the cover slip (Fig. 2.5F) (see Note 12). The channel connects the two holes in the PDMS that are left after removing the electric wire from the FEP tubes.

2.8 Flow cell functionalization

A cover slip (24 × 60 mm) coated with anti-digoxigenin is put on top of the cured PDMS layer, closing the cut out channel. Buffer can be flushed in and out through the FEP tubes that connect the two sides of the flow channel. After an experiment, the cover slip can be replaced, and the flow cell may be reused for another experiment.

A. Cover slip functionalization

1. **Cleaning**. Put several 24 × 60 mm cover slips in a holder, and sonicate in 2-propanol for 15 min in an ultrasonic cleaner. Dry the cover slips under N_2 gas stream.

2. **Coating with nitrocellulose**. Clean a 100 mL beaker and a 1 mm microscopy slide with 2-propanol. Cover the bottom of the beaker with 5 mL of a 0.1 % nitrocellulose in pentyl acetate. Put the slide vertically into the beaker, immersing its bottom edge. Gently bring a 24 × 60 mm cover slip into the liquid, parallel to the microscopy slide, and make use of capillary forces to fill the gap in between the two glasses with nitrocellulose solution. Remove the cover slip

after 30 s and dry the glasses under a stream of N_2. Store the slides in a closed container with the coated side up.

B. Flow cell assembly prior to an experiment

1. **Cleaning**. When recycling a used flow cell, remove and discard the 24 × 60 mm cover slip with a scalpel. Clean the PDMS surface, the bottom 24 × 40 mm cover slip, and the FEP tubing with miliQ H_2O and subsequently with 2-propanol.

2. **Sealing the flow cell**. Put a new functionalized 24 × 60 mm cover slip in the middle of the PDMS layer, covering the channel, with the nitrocellulose-coated side facing inward. Gently press the glass to seal the flow cell channel. Connect one side of the FEP tubing to a 1 mL syringe. Insert the tubing on the opposite side of the flow cell into an Eppendorf tube containing 1 mL of miliQ H_2O, and suck the liquid into the flow cell. Prevent any air to get inside the flow channel.

3. **Incubation of anti-digoxigenin**. Insert 300 μL of 10 ng/μL anti-digoxigenin (dissolved in miliQ H_2O) into a flow cell the same way as in the previous step. Incubate for 2 h at 4 °C.

4. **Passivation of the glass slide surface**. Mix 1 mL of 4 % BSA (dissolved in miliQ H_2O) with 50 μL of 2 % Tween-20. Rinse the flow cell with the solution as previously. Seal the inlet and outlet tubes and incubate overnight at 4 °C. At this stage, the flow cell can be stored for maximally 1 week.

C. Tethering chromatin fibers

1. **Preparation of the measurement buffer**. Use a 10 × concentrated solution of the stock buffer (Table 2.2), and prepare 10 mL of the measurement buffer (Table 2.3).

2. **Washing the flow cell**. Flush out the passivation buffer with 1 mL of the measurement buffer.

component		final concentration
KCl	37.28 g	1 M
NaN_3	3.25 g	100 mM
Tween-20	5 mL	1%
1 M HEPES pH 7.5	50 mL	100 mM
mili Q H_2O	fill up to 500 mL	-

Table 2.2
The composition of the 10× measurement buffer.

component		final concentration
10 × measurement buffer	1 mL	100 mM KCl, 10 mM NaN_3 10 mM HEPES pH 7.5 0.1% Tween-20
20 mM $MgCl_2$	1 mL	2 mM
4 % BSA	0.5 mL	0.2 %
mili Q H_2O	7.5 mL	-

Table 2.3
The composition of the measurement buffer.

3. **Introducing DNA/chromatin**. Dilute 1 μL of reconstituted chromatin fibers ($\sim$ 20 ng/μL) in 500 μL of the measurement buffer. Gently flush in the chromatin into the flow cell with a 1 mL syringe. Incubate for 10 min at room temperature.

4. **Washing the magnetic beads**. Add 20 μL of magnetic beads from the stock to 20 μL of 1× TE in a low-retention Eppendorf tube, and mix by filling and releasing the pipette a couple of times. Pull down the beads from the solution using a magnet stand. Discard the supernatant. Resuspend the beads in 20 μL of 1× TE. Repeat the washing step three times.

5. **Attaching beads**. Dilute 1 μL of washed M270 or 0.5 μL of MyOne beads in 500 μL of the measurement buffer. Gently flush the beads into the flow cell with a syringe. Incubate for 10 min at room temperature.

2.9 Dynamic force spectroscopy on chromatin fibers

1. **Magnetic tweezer initialization**. Start up the magnetic tweezers microscope, including motor controllers, CMOS camera, and LED (Fig. 2.6). Move the magnet to its highest position relative to the objective.

2. **Mounting the functionalized flow cell on the microscope stage**. Put the flow cell on the stage such that the topside of the 24 × 60 mm cover slip is in focus (add immersion oil if an oil objective is used). Tighten the flow cell with screws. Connect one of the tubes to the pump and the other to a reservoir containing the measurement buffer. Rinse the flow chamber with the measurement buffer to remove loose beads. Use a minimal flow rate ($<$ 0.1 mL/min) to prevent sample degradation by excessive drag forces.

3. **Adjusting the objective position**. Lower the objective until the beads appear out of focus and multiple diffraction rings are visible.

4. **Finding a field of view with tethered beads**. Move the microscope table manually to a region of the flow cell where multiple beads are distributed throughout the field of view (Fig. 2.7). Select regions of interest (ROIs) around

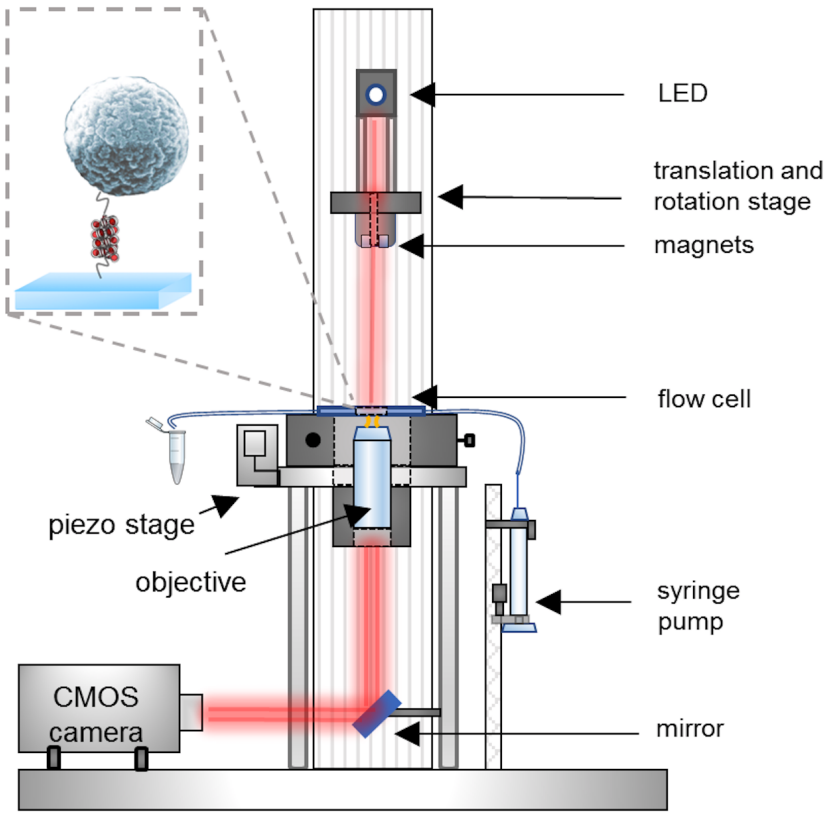

Figure 2.6
Schematic representation of the magnetic tweezers setup (a front view with the cross section of the microscope stage). The sample is illuminated by a collimated LED light beam that is guided through the objective and reflected by the mirror toward the CMOS camera. Forces and torques are generated by two cubic magnets mounted on a translation and rotation stage. A piezo stage allows controlling the focus of the microscope. A syringe pump is used to exchange buffers in the flow cell during an experiment. Inset: a chromatin fiber flanked by short DNA handles, tethered in a flow cell between a cover slip and a magnetic bead (not to scale).

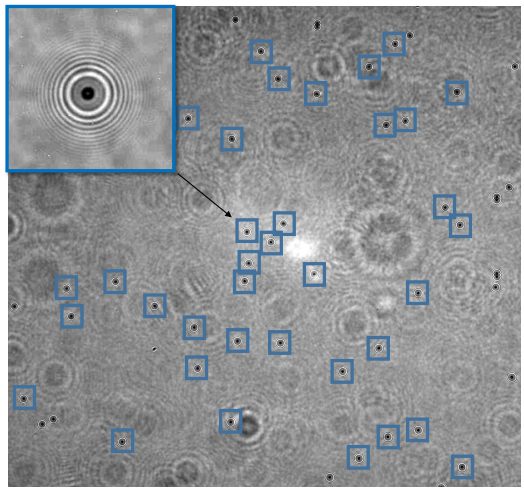

Figure 2.7
Selection of beads before tracking. Distribution of tethered magnetic beads on the imaged region of a flow cell. Small regions of interest (ROIs) were selected to track the diffraction rings of individual magnetic beads. Inset: a zoom of one of the selected ROIs.

the beads manually or using an automatic bead finder algorithm (Fig. 2.7, inset). Set a size of the ROIs such that multiple diffraction rings are included, depending on the bead size, objective magnification, and pixel size of the camera.

5. **Tracking calibration**. Using the piezo stage, move the sample through the focus, and record the diffraction ring pattern of a bead. Subsequent image analysis relates the objective position to the changes of the diffraction profile. Correct for the difference in refraction index between the aqueous flow channel and the immersion medium of the objective. For oil objectives, this is a factor 0.88 (see Note 13).

6. **Force calibration**. Calibrate the force as a function of the magnet height by measuring the lateral thermal fluctuations of a bead and the tether height at several magnet positions. Using equipartition theorem, the force can be calculated as the product of the bead height, Boltzmann constant, and absolute temperature divided by the variance of the lateral position [25, 26] (see Note 14).

7. **Setting the magnet trajectory to define a force ramp**. Define a trajectory of the magnet from a position where the force is close to 0 pN to a force up to $\sim$ 7 pN during the first measurement. Prevent sample degradation due to excessive exposure to force. To maintain fiber integrity, minimize the duration of the high-force part in the force trajectory, so the fibers can refold

to its initial state before histones dissociate (see Note 15). We use a magnet velocity of $\sim$ 0.5 mm/s in both directions. Fig. 2.8A shows the extension of a chromatin fiber tethered with a MyOne bead upon stretching twice with low forces.

8. **Rotation experiment for checking for individually tethered DNA molecules.** Subsequently, set the magnet position to a force of approximately 0.5 pN, and define a new trajectory that controls the magnet rotation. Turn the magnet at least 15 times in both directions. Because the tether is rarely attached to the very bottom of the bead, each bead trajectory should describe a circle in the X, Y plane, even when the DNA is not rotationally constrained (Fig. 2.8B). However, when more than one tether is attached to the same bead, the trajectory will deviate from a circle (Fig. 2.8C).

9. **Selection of good tethers**. Discard beads that exhibit too large extensions, indicating incompletely reconstituted chromatin fibers or bare DNA. Also discard too short tethers and beads that have irregular X, Y fluctuations caused by nonspecific sticking of the bead or the chromatin to the surface. The extension of the tether should be close to the contour length of the DNA substrate minus the length of the 601 array.

10. **Probing chromatin folding**. Fiber folding is reversible up to forces of $\sim$ 7 pN. Multiple force trajectories can be applied to the same tethers.

11. **Complete chromatin unfolding**. Perform a high-force stretching experiment to induce the complete unpeeling of histone octamers/tetramers from the DNA template. This is informative as the unwrapping of the final

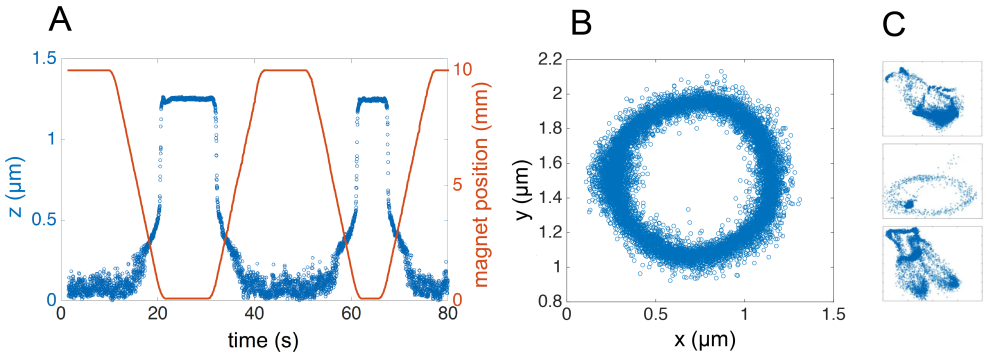

Figure 2.8
Quality assessment of a selected tether. A) Force-induced unfolding and refolding of a chromatin fiber tethered with a MyOne bead. Multiple stretching and refolding cycles with low forces ($<$ 10 pN) are not destructive to the sample. **B)** A bead follows a circle in the X, Y plane upon magnet rotation unless more than one chromatin fiber is attached to a single bead. Note that the thicker spot on the left side of the circle results from an extended period before and after rotation of the magnets. **C)** Anomalous XY tracks upon rotation of the magnets that indicate multiple tethers on a bead.

wrap of DNA from the histone core results in distinctive 25 nm steps that are indicative for each nucleosome or tetrasome. Define a magnet trajectory to apply a force ramp from 0 to 50 - 60 pN (see Note 16) to observe these discrete steps in extension. The number of steps should correlate with the number of the 601 sequence repeats on the DNA template. Analyze the results (Section 2.10).

12. **Select another field of view**. Move to another field of view in the same flow cell. Make sure that the displacement is large enough to ensure that the beads in the new field of view have not been exposed to high forces during the previous experiment. Displacements should typically be larger than the magnet size, *i.e.*, more than 5 mm.

2.10 Data analysis

The force-extension graphs are characterized by transitions from a folded fiber through an array of partially unwrapped nucleosomes to fully unwrapped nucleosomes (Fig. 2.9A). We fit the force-extension curves with a statistical mechanics model developed by Meng *et al.* [27] (Fig. 2.9B). The model quantifies all conformational changes of DNA and chromatin fibers upon stretching. By fitting the data to the model, we obtain parameters like fiber's stiffness, unfolding energy, number of nucleosomes, and number of tetrasomes (Table 2.4). The model contains a large number of parameters that capture the complexity of the fiber. It includes a degeneracy factor that is not easily implemented in analytical *formulae*, but is straightforward to implement numerically. We typically observe discrete variations of fiber compositions, indicating one or more missing or additional nucleosomes, despite best efforts to reconstitute the fibers. Moreover, the high-force transitions are not in equilibrium, whereas the model is only valid for equilibrium transitions. For these reasons, one cannot simply fit the curves using a standard Levenberg-Marquardt algorithm. Instead, model parameters are fit sequentially, using only the parameters which are relevant in a limited force regime. Subsequent fits on the same fiber in different force regimes use the thus obtained parameters as fixed constants.

1. **Correction for drift**. A difference in the extension between the beginning and the end of the time trace (Fig. 2.10A) may result from mechanical drift of the microscope (see Note 17). We use a linear drift term to enforce maximal overlap and a horizontal trend in the extension versus time plot.

2. **Determining the offset**. Determine the offset in the z-direction by fitting an extensible WLC with fixed contour length, persistence length, and stretch modulus (Table 2.4) to the most extended part of the curve, *i.e.*, at forces above 30 pN (Fig. 2.10B).

3. **Fitting the number of nucleosomes**. Start with the number of nucleosomes equal to the number of tandem repeats of the Widom-601 sequence on the DNA used for chromatin assembly. Adjust or fit the number of nucle-

A

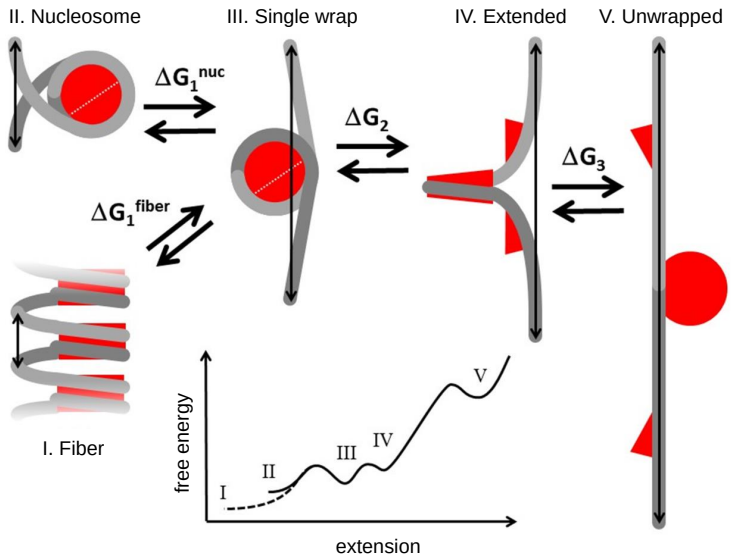

B

	extension	energy
DNA	$z_{DNA}(f,L) = L\left[1 - \frac{1}{2}\sqrt{\frac{k_BT}{fA}} + \frac{f}{S}\right]$	$G_{DNA}(f,L) = -L\left[f - \sqrt{\frac{fk_BT}{A}} + \frac{f^2}{2S}\right] + fz_{DNA}$
fiber	$z_{fiber}(f) = \frac{f}{k} + z_0$	$G_{fiber}(f) = \frac{f^2}{2k}$
total	$z_{tot}(f) = \sum_i n_i z_i(f) + z_{DNA}(f)$	$G_{tot}(f) = \sum_i n_i G_i(f) + G_{DNA}(f)$

degeneracy	$D(\text{state}) = \prod_{i<j} \binom{n_i + n_j}{n_i}$

mean equilibrium extension	$\langle z_{tot}(f) \rangle = \frac{\sum_{states} z_{tot}(f) D(state) e^{-(G_{tot} - F z_{tot})/k_BT}}{\sum_{states} D(state) e^{-(G_{tot} - F z_{tot})/k_BT}}$

Figure 2.9
Quantification of force-induced structural transitions in chromatin fibers using a statistical mechanics model (Fig. adapted from Meng et al. [27]). A) Fiber stretching proceeds through four stages of nucleosome unfolding. **B)** Analytical formulas that describe the extension of each nucleosome state as a function of force. A persistence length (nm), f force (pN), k_B Boltzmann constant, G free energy (k_BT), k stiffness (pN/nm), z tether extension (nm), L contour length (nm), S DNA stretching modulus (pN), T temperature (K), D degeneracy factor, n_i number of nucleosomes in a particular state i.

parameter	
DNA persistence length	50 nm
DNA stretch modulus	1100 pN
Number of nucleosomes (N)	15 or 30
Nucleosome Repeat Length (NRL)	167 or 197 bp
Contour length	2030 + N · NRL (bp)
Folded length of a single nucleosome	1.5 nm
Unwrapped base pairs of the 1st (outer) nucleosomal turn	56 bp
Unwrapped length in the intermediate transition	5 nm

Table 2.4
Fixed parameters of the statistical mechanics model used in data analysis.

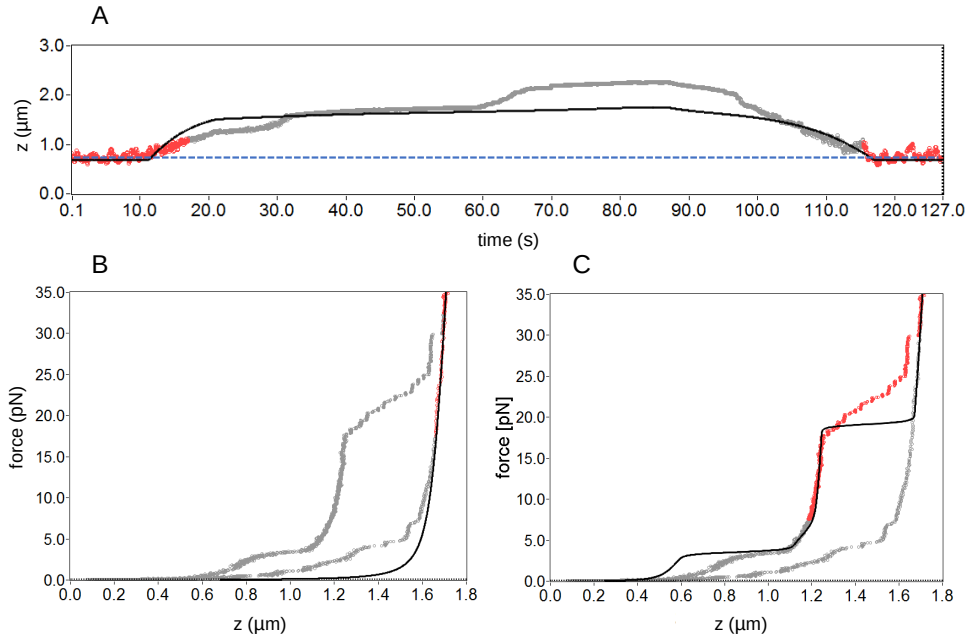

Figure 2.10
Initial procedures of the data analysis. A) Quantifying the mechanical drift. Data points from the beginning and the end of the time trace (red) are recorded at the same magnet position and should align with an arbitrary straight, horizontal line. The difference in height of selected regions before and after the alignment is divided by the duration of the measurement to estimate the linear drift factor (nm/s). **B)** Finding the z-offset. Data points with the highest z-coordinate (red) are aligned with the fitted WLC model with a persistence length of 50 nm and a given contour length (Table 2.4). **C)** Quantifying the number of nucleosomes. The staircase-like curve is selected (red), and the distance between the first and the last step is measured. The obtained extension is divided by 25 nm to estimate the number of nucleosomes and tetrasomes assembled on the tether.

osomes to obtain the best fit in the range between 8 and 15 pN (Fig. 2.10C) (see Note 18). When fitting, the number of nucleosomes should approximate an integer number.

4. **Fitting the unfolding steps**. Check that the number of steps in the force range between 8 and 40 pN agrees with the number of nucleosomes. A Student's t-test is used to compare the 3 - 6 neighboring data points to identify discrete steps (Fig. 2.10A). The step size corresponds with the difference between the extension of the last partially wrapped nucleosome and the fully unwrapped nucleosome conformation, *i.e.*, states IV and V in Fig. 2.9A (see Note 19).

5. **Fitting the low-force regime**. Fit the part of the trace between 0.5 and 8 pN to obtain the fiber stiffness, unstacking free energy and the free energy of the intermediate transition (k_BT) (Fig. 2.10B). The plateau width at 3 - 5 pN depends on the number of nucleosomes that stack and form a folded fiber. We observed that the plateau width is not always consistent with the number of nucleosomes as determined from the high-force region, described in the previous step [27]. In all experiments, the plateau size indicated that the number of stacked nucleosomes is less or equal to the number of high-force unwrapping events. The difference is attributed to tetrasomes that feature the same unwrapping steps at high force but lack the ability to fold into more condensed structures [5]. The number of tetrasomes is also fitted from the low-force region.

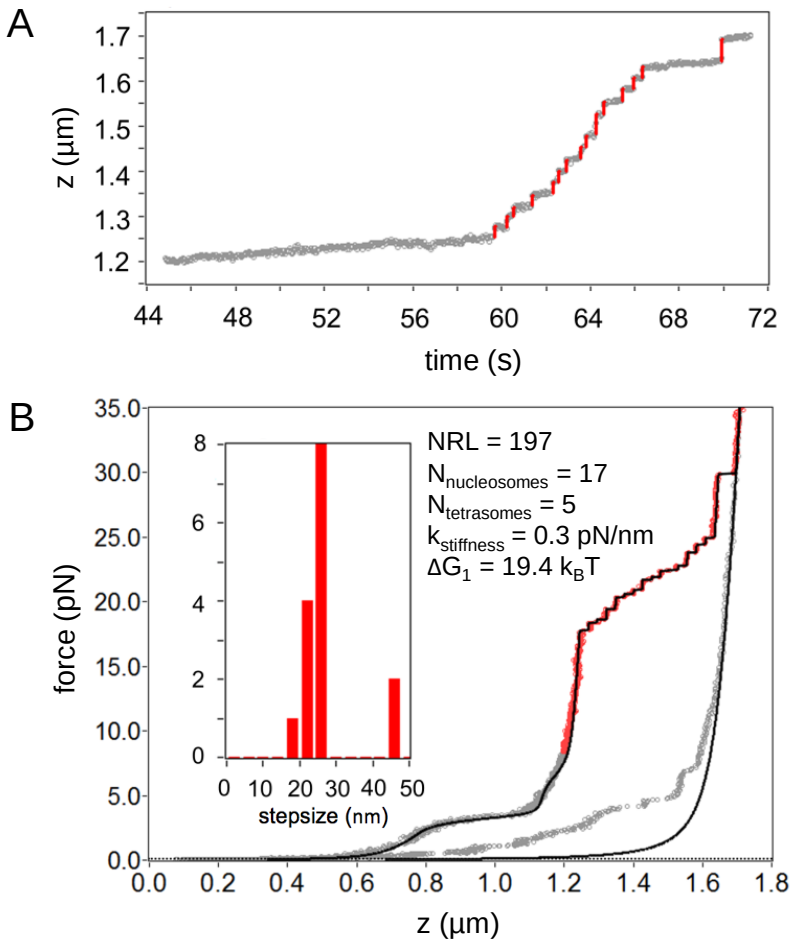

Figure 2.11
Fitting the data to the statistical mechanics model. A) Step size analysis. The same part of the trace remains selected as in Fig. 2.10C. A Student's t-test is performed to quantify the sizes of steps that occur in the 10 - 40 pN force regime. **B)** Fitting the plateau of the force-extension curve at the low-force regime to characterize the chromatin fiber folding. *Inset*: histogram of the measured step sizes and fitted parameters - NRL nucleosome repeat length, $N_{nucleosomes}$ fitted number of assembled nucleosomes and tetrasomes, $N_{tetrasomes}$ fitted number of tetrasomes, $k_{stiffness}$ stiffness of a folded fiber (pN/nm), ΔG_1 free energy of the first transition (k_BT.)

2.11 Additional notes

Note 1. We use plasmid constructs with multiple repeats of the Widom- 601 sequence (*tggagaatcccggtgccgaggccgctcaattggtcgtagacagc tctagcaccgcttaaacgcacg-tacgcgctgtcccccgcgttttaaccgccaaggggat tactccctagtctccaggcacgtgtcagatatatacatcctgt*) that are spaced with 20 bp or 50 bp of non-601 linker DNA (Nucleosome Repeat Length = 167 bp or 197 bp, respectively). In addition to the 601-repeats, we keep about 1 kbp of flanking DNA on both sides, yielding the following DNA substrates:
15 × 601 (167) - 5185 bp
15 × 601 (197) - 5635 bp
30 × 601 (167) - 7690 bp
25 × 601 (197) - 7605 bp

The flanking DNA helps to keep the chromatin fiber away from the surface of the flow chamber or the bead and facilitate selecting tethers that are not stuck to one of the surfaces. On the downside, additional nucleosomes can form on this DNA, putting high demands on the reconstitution stoichiometry.

Note 2. When handling frozen competent cells, it is important to keep them cold. Frozen cells are very sensitive to temperature fluctuations, and therefore plasmid transformation may not work if the cells are not incubated on ice.

Note 3. The reaction volume for digestion of 1 μg of isolated plasmid DNA is 20 - 50 μL. A minimum of 5 - 10 units of each enzyme is required for complete digestion of 1 μg of DNA in 1 h. For an overnight incubation, the amount of enzyme can be therefore lower. Enzyme should not exceed 10% of the total reaction volume.

Note 4. The maximum binding capacity is approximately 40 μg per column. Multiple elutions from the spin columns and longer incubation time are recommended to improve the yield of DNA purification.

Note 5. Selection of nucleotides is based on the sequences of the "sticky end" resulting from an enzymatic digestion. A regular, non-tagged nucleotide other than UTP should be complementary to the first nucleotide at one side of the digested DNA substrate. Absence of this nucleotide in the first Klenow reaction prevents incorporation of tagged UTP on the other side of the DNA substrate. The presence of other nucleotides could result in labelling the DNA with the same tag on both sides. This would not allow for DNA tethering in a flow cell as the bead and the surface have orthogonal binding proteins.

Note 6. Typically, we use a 4535 bp DNA construct containing about 2200 bp of 601 sequence repeats. The rest is a random sequence of the plasmid backbone. A typical DNA concentration after labelling is $\sim$ 250 ng/μL. Since the nucleosome contains roughly equal weights of protein and DNA, one can easily set up a good titration scheme:

(a) Use 4 μL of DNA per dialysis tube (in total 1000 ng of DNA).

(b) DNA handles are 50 % of the total DNA; therefore in total there is

500 ng of 601 DNA that should fold into nucleosomes. This amount divided by the molar mass of a single 601 repeat (10^5 g/M) and then by the total volume (5×10^{-6} l) results in ~ 0.1 μM molar concentration of the DNA substrate that is supposed to form nucleosomes.

(c) We use 200 ng/μL aliquots of histone octamer, so 2.5 μL of this aliquot needs to be added to end up with a solution with 500 ng of protein.

(d) Add high salt buffer for samples to obtain a final volume of 50 μL.

(e) Prepare tubes with the same amount of DNA, and vary the volume of histones (1.5, 2, 2.5, 3, 3.5 μL) to accommodate a loss of histones by sticking to tubes and pipette tips and uncertainties in histone and DNA concentrations.

Note 7. Keep all the buffers at 4 °C and perform the dialysis in a cold room.

Note 8. Low-binding (siliconized) pipette tips and tubing prevent sticking of histone octamers and reconstituted chromatin fibers. This is especially important when small volumes are used.

Note 9. To enforce that the volume in the beaker with dialysis tubes remains constant, make sure that the same amount of the low salt buffer is pumped into the beaker as the high salt buffer is pumped out. This can conveniently be achieved using a peristaltic pump with a double head.

Note 10. Competitor DNA starts to reconstitute into nucleosomes when all 601 sequences are occupied with histones. A band shift of the competitor DNA therefore indicates saturation of the chromatin fibers. Fibers with a minimal oversaturation, *i.e.*, having a small excess of histones assembled on the flanking DNA around 601 repeats, are preferred for magnetic tweezers experiments over subsaturated, incompletely folded fibers.

Note 11. Mix the viscous and nonviscous components of PDMS intensively for at least 2 min. Incomplete mixing will impede homogenous polymerization.

Note 12. Make sure that the FEP tubing does not get loose while removing the Perspex molds and the electrical wires. After its removal, the flow cell should contain two fixed pieces of the FEP tubing and a flat PDMS surface that completely covers and immobilizes the 24 $\times$ 40 mm cover slip in the central aperture of the holder. The cured PDMS is a flat, transparent layer that fills the cavity between the aluminum holder and the Perspex mold. Some Perspex molds have a blue embossing tape stripe attached to its bottom side. The void that is left by the embossing tape after curing the PDMS and the removal of the Perspex mold forms the actual flow channel. This channel can be increased in height by cutting out the remaining layer of cured PDMS that was left underneath the embossing tape, with a scalpel. When no embossing tape is used, the entire channel can be cut out at the location where the embossing tape would be. The channel dimension should be smaller than the dimensions of the cover slip in order to keep the glass in its place. The aluminum holder remains an intrinsic part of the flow cell for convenient mounting on the microscope and connections with tubing.

Note 13. Various methods have been published to quantify changes in the diffraction pattern of the bead [28–30]. We use the 3D FFT algorithm to correlate the measured ROIs with a computer-generated model image (Brouwer *et al.*, *in prep.*). The empirical relation between the objective position and the diffraction pattern is interpolated for tracking the bead in the z-direction.

Note 14. For a particular magnetic tweezer setup and magnets, the force calibration only needs to be performed once. As chromatin features large changes in extension as a function of force, which impedes thermal fluctuations, the calibration is done with a bare DNA molecule, prior to chromatin experiments. Typically, a double exponential decay of the force with magnet height is obtained, which is characteristic for a given batch of beads and a particular pair of magnets with a fixed configuration. In force spectroscopy experiments on chromatin, the force-magnet position relation for the appropriate bead size is used to convert magnet position to force. The *Invitrogen* beads feature a rather constant magnetic content. The variation is sufficiently small to use the same force calibration for all beads from the same batch. Other beads may have larger variations in magnetic strength. Our flow cells have a reproducible height. The offset of the magnet position can be obtained from measuring the height at which the magnets touch the top of the flow channel. This is easily recognized as beads will abruptly move out of focus.

Note 15. A first experiment involves checking the quality of tethers. Some beads are directly stuck to the surface. Others feature multiple tethers or nonspecific interactions between the chromatin and surface. An initial force ramp is used to select tethers that feature force-extension relation that is indicative of a proper chromatin fiber. In the buffer conditions used in our method and at the pulling rate lower than 0.2 pN/s, the structural transitions in the fiber remain in equilibrium. Unstacking of the nucleosomes in the chromatin fiber can be reversed upon releasing the force. This may not be the case when a chromatin fiber is not properly folded (a hysteresis is observed between a pulling and a release curve) or in other experimental conditions. Importantly, extended exposure to forces above 3 pN should be avoided, as histone H2A/H2B dimers tend to dissociate above this threshold.

Note 16. The pulling rate is higher in the high-force regime (above 10 pN) compared to the low-force regime. Depending on the pulling rate, unwrapping steps occur at different forces.

Note 17. Mechanical drift can be measured more precisely by tracking the z-extension of a bead stuck to the flow cell surface. When the z-position of such a stuck bead does not remain constant, its position can be subtracted from other extension traces to correct for drift.

Note 18. Individual chromatin fibers may have more or less nucleosomes than the number of 601 repeats on the DNA template. The measured change in extension between the first unwrapping step and the last unwrapping step, divided by 25 nm, should correspond with the fitted number of nucleosomes.

A force plateau at 3 - 5 pN that is smaller than expected indicates the presence of tetrasomes, next to nucleosomes.

Note 19. The average step size should be close to 25 nm. Occasionally, two unwrapping events can occur simultaneously, resulting in a double-sized step. When the number of nucleosomes obtained in the previous step does not match the number of steps observed in this force region, the amount of wrapped DNA and/or the extension of the extended conformations can be adjusted. Typically, step sizes and extensions are within 0.5 nm of the average values obtained from multiple experiments. In this force regime, the non-equilibrium steps in the force-extension curves and all points in between are assigned to discrete levels. Each level corresponds to a WLC with a contour length that is reduced by an integer number times the amount of DNA that is wrapped in a single-wrapped nucleosome or tetrasome.

Acknowledgements

We are grateful to Nicolaas Hermans, He Meng, Kurt Andresen, Orkide Ordu, and Ineke de Boer for the help in establishing these methods. This work was supported by the Netherlands Organisation for Scientific Research (NWO/OCW), as part of the Frontiers of Nanoscience program, by the NWO-VICI research program, project 680-47-616.

Bibliography II

[1] Roger D. Kornberg. "Structure of chromatin". In: *Annu Rev Biochem.* 46 (1977), pp. 931–54.

[2] Karolin Luger et al. "Crystal structure of the nucleosome core particle at 2.8Å resolution". In: *Nature* 389 (1997), pp. 251–260. ISSN: 0028-0836. DOI: 10.1038/38444.

[3] Benedetta Dorigo et al. "Nucleosome arrays reveal the two-start organization of the chromatin fiber". In: *Science* 306.5701 (Nov. 2004), pp. 1571–1573. ISSN: 00368075. DOI: 10.1126/science.1103124.

[4] Yujie Chen et al. "Asymmetric unwrapping of nucleosomal DNA propagates asymmetric opening and dissociation of the histone core". In: *Proceedings of the National Academy of Sciences* 114.2 (2017), pp. 334–339. ISSN: 0027-8424. DOI: 10.1073/pnas.1611118114.

[5] Artur Kaczmarczyk et al. "Single-molecule force spectroscopy on histone H4 tail-cross-linked chromatin reveals fiber folding". In: *Journal of Biological Chemistry* 292.42 (2017), pp. 17506–17513. ISSN: 1083351X. DOI: 10.1074/jbc.M117.791830.

[6] Nick Gilbert and Bernard Ramsahoye. "The relationship between chromatin structure and transcriptional activity in mammalian genomes". In: *Briefings in Functional Genomics and Proteomics* 4.2 (2005), pp. 129–142. ISSN: 14739550. DOI: 10.1093/bfgp/4.2.129.

[7] Karolin Luger and Timothy J. Richmond. "The histone tails of the nucleosome". In: *Current Opinion in Genetics and Development* 8.2 (1998), pp. 140–146. ISSN: 0959437X. DOI: 10.1016/S0959-437X(98)80134-2.

[8] J. Widom. "Role of DNA sequence in nucleosome stability and dynamics". In: *Quarterly Reviews of Biophysics* 34 (2001), pp. 269–324. ISSN: 0033-5835. DOI: doi:10.1017/S0033583501003699.

[9] J. L. Workman and R. E. Kingston. "Alteration of nucleosome structure as a mechanism of transcriptional regulation". In: *Annu. Rev. Biochem* 67 (1998), pp. 545–79. DOI: 10.1146/annurev.biochem.67.1.545.

[10] Gregory D. Bowman and Michael G. Poirier. "Post-translational modifications of histones that influence nucleosome dynamics". In: *Chemical Reviews* 115 (2015), pp. 2274–2295. ISSN: 15206890. DOI: 10.1021/cr500350x.

[11] Thomas Schalch et al. "X-ray structure of a tetranucleosome and its implications for the chromatin fibre". In: *Nature* 436.7047 (2005), pp. 138–141. ISSN: 00280836. DOI: 10.1038/nature03686.

[12] Sergei A. Grigoryev. "Nucleosome spacing and chromatin higher-order folding". In: *Nucleus (United States)* 3.6 (2012), pp. 493–9. ISSN: 19491034. DOI: 10.4161/nucl.22168.

[13] Philip J. J. Robinson et al. "EM measurements define the dimensions of the '30-nm' chromatin fiber: evidence for a compact, interdigitated structure." In: *Proceedings of the National Academy of Sciences of the United States of America* 103.17 (2006), pp. 6506–11. ISSN: 0027-8424. DOI: 10.1073/pnas.0601212103.

[14] Feng Song et al. "Cryo-EM study of the chromatin fiber reveals a double helix twisted by tetranucleosomal units". In: *Science* 344.6182 (2014), pp. 376–380. ISSN: 10959203. DOI: 10.1126/science.1251413.

[15] Andrew Routh, Sara Sandin, and Daniela Rhodes. "Nucleosome repeat length and linker histone stoichiometry determine chromatin fiber structure." In: *Proceedings of the National Academy of Sciences of the United States of America* 105.26 (2008), pp. 8872–8877.

[16] Katarzyna M. Krzemien et al. "Atomic force microscopy of chromatin arrays reveal non-monotonic salt dependence of array compaction in solution". In: *PLoS ONE* 12.3 (2017). Ed. by Yamini Dalal, e0173459. ISSN: 19326203. DOI: 10.1371/journal.pone.0173459.

[17] Marteen Kruithof et al. "Subpiconewton dynamic force spectroscopy using magnetic tweezers." In: *Biophysical journal* 94.6 (2008), pp. 2343–2348. ISSN: 00063495. DOI: 10.1529/biophysj.107.121673.

[18] Orkide Ordu, Alexandra Lusser, and Nynke H. Dekker. "Recent insights from in vitro single-molecule studies into nucleosome structure and dynamics". In: *Biophysical Reviews* 8.S1 (2016), pp. 33–49. ISSN: 18672469. DOI: 10.1007/s12551-016-0212-z.

[19] Noah Ribeck and Omar A. Saleh. "Multiplexed single-molecule measurements with magnetic tweezers". In: *Review of Scientific Instruments* 79.9 (2008), p. 094301. ISSN: 00346748. DOI: 10.1063/1.2981687.

[20] Iwijn De Vlaminck et al. "Highly parallel magnetic tweezers by targeted DNA tethering". In: *Nano Letters* 11.12 (2011), pp. 5489–5493. ISSN: 15306984. DOI: 10.1021/nl203299e.

[21] Alexandra Lusser and James T. Kadonaga. "Strategies for the reconstitution of chromatin." In: *Nature Methods* 1.1 (2004), pp. 19–26. DOI: 10.1038/nmeth709.

[22] Van A. T. Huynh, Philip J. J. Robinson, and Daniela Rhodes. "A method for the in vitro reconstitution of a defined '30 nm' chromatin fibre containing stoichiometric amounts of the linker histone". In: *Journal of Molecular Biology* 345.5 (2005), pp. 957–968. ISSN: 00222836. DOI: 10.1016/j.jmb.2004.10.075.

[23] P. T. Lowary and J. Widom. "New DNA sequence rules for high affinity binding to histone octamer and sequence-directed nucleosome positioning". In: *Journal of Molecular Biology* 276.1 (1998), pp. 19–42. ISSN: 00222836. DOI: 10.1006/jmbi.1997.1494.

[24] Andrew Flaus. "Principles and practice of nucleosome positioning in vitro". In: *Frontiers in Life Science* 5.1-2 (2011), pp. 5–27. ISSN: 21553769. DOI: 10.1080/21553769.2012.702667.

[25] T. R. Strick et al. "The Elasticity of a Single Supercoiled DNA Molecule". In: *Science* 271.5257 (1996), pp. 1835–1837. ISSN: 0036-8075. DOI: 10.1126/science.271.5257.1835.

[26] Zhongbo Yu et al. "A force calibration standard for magnetic tweezers". In: *Review of Scientific Instruments* 85.12 (2014), p. 123114. ISSN: 10897623. DOI: 10.1063/1.4904148.

[27] He Meng, Kurt Andresen, and John van Noort. "Quantitative analysis of single-molecule force spectroscopy on folded chromatin fibers". In: *Nucleic Acids Research* 43.7 (2015), pp. 3578–3590. ISSN: 13624962. DOI: 10.1093/nar/gkv215.

[28] Yoshie Harada et al. "Direct observation of DNA rotation during transcription by escherichia coli RNA polymerase". In: *Nature* 409.6816 (2001), pp. 113–115. ISSN: 00280836. DOI: 10.1038/35051126.

[29] Bob M. Lansdorp et al. "A high-speed magnetic tweezer beyond 10,000 frames per second". In: *Review of Scientific Instruments* 84.4 (2013), p. 044301. ISSN: 00346748. DOI: 10.1063/1.4802678.

[30] J. P. Cnossen, D. Dulin, and N. H. Dekker. "An optimized software framework for real-time, high-throughput tracking of spherical beads". In: *Review of Scientific Instruments* 85.10 (2014). ISSN: 10897623. DOI: 10.1063/1.4898178.

Chapter 3

Single-molecule force spectroscopy on histone H4 tail-cross-linked chromatin reveals fiber folding

The eukaryotic genome is highly compacted into a protein-DNA complex called chromatin. The cell controls access of transcriptional regulators to chromosomal DNA via several mechanisms that act on chromatin-associated proteins and provide a rich spectrum of epigenetic regulation. Elucidating the mechanisms that fold chromatin fibers into higher-order structures is therefore key to understanding the epigenetic regulation of DNA accessibility. Here, using histone H4-V21C and histone H2A-E64C mutations, we employed single-molecule force spectroscopy to measure the unfolding of individual chromatin fibers that are reversibly cross-linked through the histone H4 tail. Fibers with covalently linked nucleosomes featured the same folding characteristics as fibers containing wild-type histones but exhibited increased stability against stretching forces. By stabilizing the secondary structure of chromatin, we confirmed a nucleosome repeat length (NRL)-dependent folding. Consistent with previous crystallographic and cryo-EM studies, the obtained force-extension curves on arrays with 167 bp NRLs best supported an underlying structure consisting of zig-zag, two-start fibers. For arrays with 197 bp NRLs, we previously inferred solenoidal folding, which was further corroborated by force-extension curves of the cross-linked fibers. The different unfolding pathways exhibited by these two types of arrays and reported here extend our understanding of chromatin structure and its potential roles in gene regulation. Importantly, these findings imply that chromatin compaction by nucleosome stacking protects nucleosomal DNA from external forces up to 4 piconewtons.

This chapter is based on: Kaczmarczyk A., Allahverdi A., Brouwer T.B., Nordenskiöld L., Dekker N.H., and van Noort S.J.T., "Single-molecule force spectroscopy on histone H4 tail cross-linked chromatin reveals fiber folding" Journal of Biological Chemistry, 292 (42), 17506-17513 (2017).

3.1 Introduction

The eukaryotic genome is highly compacted into the protein-DNA complex called chromatin. The basic unit of chromatin organization comprises 147 base pairs of DNA wrapped in 1.7 turns around an octamer of proteins, consisting of the core histones H2A, H2B, H3 and H4 [1]. This Nucleosome Core Particle (NCP) has been shown to form a barrier [2] as well as a binding site [3] for proteins involved in DNA metabolism, such as those responsible for replication, transcription and DNA repair. The cell modulates access to chromosomal DNA by remodeling it [4] *via* active nucleosome translocation [5], post-translational modifications of histones [6], and/or the binding of other proteins like the linker histone or HP1 [7, 8], providing a rich spectrum of regulation.

The accessibility of chromosomal DNA can further be modulated by folding strings of nucleosomes into higher order chromatin structures, driven by nucleosome-nucleosome interactions. This secondary structure remains controversial [9] despite extensive efforts in exploring it using Electron Microscopy (EM) [10, 11], crystallography [12], Analytical Ultra Centrifugation (AUC) [13, 14] and structural modelling [15–17]. These studies generally support a preferential stacking of nucleosomes in a face-to-face fashion, mediated by the H4 tail [12, 18]. However, the geometrical constraints of short linker DNA between the consecutive nucleosomes may inhibit such interactions and therefore variations in the DNA linker length may influence the resulting higher order folding [19]. This is especially relevant in the context of epigenetics since the expression of particular genes can be correlated with the occupancy and spacing of nucleosomes on the DNA [20, 21]. For example, the expulsion of nucleosomes in the promotor regions facilitates the accessibility of the underlying DNA sequence to polymerases [22]. However, a fundamental understanding of the mechanisms involved in this epigenetic regulation requires a significant advance in our knowledge of chromatin folding.

Although nucleosomal arrays readily fold into 30 nm fibers *in vitro*, their existence *in vivo* has been questioned [23]. Nevertheless, it seems likely that interactions between nucleosomes will occur in a crowded eukaryotic nucleus [24], and given the heterogeneity in nucleosome spacing [25], it is relevant to uncover how the length of the linker DNA affects nucleosome-nucleosome contacts and the chromatin structure that is induced by those interactions. Tandem arrays of the Widom-601 sequence, which force the nucleosomes into well-defined positions, have been instrumental in structural studies of chromatin [26–28]. The most detailed structures show chromatin fibers that form two stacks of nucleosomes connected by straight linker DNA, as shown in the crystal structure of a tetra-nucleosome [12]. The same tetra-nucleosomal geometry was recently visualized by cryo-EM [10], implying that a two-start configuration is the predominant structure of chromatin fibers.

Other studies, however, indicate that arrays of nucleosomes may form

alternative structures [29]. In particular, the one-start or solenoid structure has been proposed early on [30]. Robinson *et al.* demonstrated that the diameter of folded chromatin fibers, as measured with EM, is independent of the DNA linker length [11], which is difficult to reconcile with a two-start helix with straight linker DNA. The relatively irregular folding of these fibers impeded averaging of structures, leaving the linker DNA unresolved.

Probing the mechanical response of chromatin to tension constrains some of the proposed models of the underlying structure. In single-molecule force spectroscopy, the extension of individual chromatin fibers is measured as a function of the applied force [31, 32]. Previously, we introduced a detailed interpretation of the force-extension relation with a statistical mechanics model that quantifies extensions and transitions between all chromatin conformations upon stretching [33]. From our analysis, we inferred a two-start folding of 167-NRL fibers and a one-start folding of 197-NRL. The two-start organization was recently confirmed using single-molecule force spectroscopy on 177- and 187-NRL fibers [34]. The interpretation that 197-NRL fibers fold as a one-start solenoid, which was also inferred from EM studies [11], has been challenged [17, 35], arguing that the obtained linear extension of the chromatin fibers can be achieved by gradual unwrapping of DNA from the nucleosome cores. To clarify this issue, it is important to resolve at what force and extension the nucleosome-nucleosome contacts are broken.

Both of the suggested folding geometries imply stacking of nucleosomes, which has been proposed to be mediated by electrostatic interactions between the H4 tail and the acidic patch on the H2A-H2B dimer [36]. An elegant way to study such tail-mediated nucleosome interactions was developed by Dorigo *et al.*, who cross-linked neighboring nucleosomes by introduction of two cysteines, one in the acidic patch and one at the end of the H4-tail [18]. The reversible cross-linking process is controlled by the redox potential of the measurement buffer. Under oxidizing conditions, a covalent disulfide bond between two cysteines in adjacent nucleosomes mimics the suggested native structure of the H4 tails in stacked nucleosomes. Both gel electrophoresis and EM imaging confirmed the two-start folding of cross-linked fibers by showing that odd and even nucleosomes form two separate stacks [18].

Here, we combine cysteine-mediated nucleosome cross-linking with single-molecule dynamic force spectroscopy. This approach brings the advantage of being able to distinguish the signatures of rupturing nucleosome-nucleosome contacts from those of gradually unwrapping nucleosomal DNA. As long as the nucleosome-nucleosome stacking is not disrupted, *i.e.* H4-mediated interactions between nucleosomes are not broken, the introduction of disulfide links between nucleosomes should not change the force-extension relation. The obtained force-extension curves of cross-linked nucleosomes should in this case overlap with those of either arrays containing wild-type (WT) nucleosomes or reduced Cys-mutant (MT) nucleosomes. Both the stretching stiffness and

the extension at the rupture force would be unaffected by the disulfide bonds. Alternatively, if the linear stretching of folded chromatin fibers mainly involves DNA unwrapping, cross-linking the nucleosomes with the H4 tails should inhibit large extension of the fiber. Thus, single-molecule force spectroscopy of cross-linked chromatin fibers should be able to discriminate different unfolding pathways of a chromatin fiber. The results presented in this work clearly reveal H4 tail-mediated nucleosome stacking and one- and two-start structures for 167- and 197-NRLs, respectively.

3.2 Results

3.2.1 Chromatin with short NRL folds into a stiffer structure than chromatin with long NRL

We first briefly recapitulate our previous force spectroscopy results on chromatin fibers and how the force-extension data can be interpreted. We employ a statistical physics model that quantifies the changes in extension of each intermediate nucleosome conformation upon stretching the fiber and explicitly takes variations in the fiber composition into account. The force-dependent extension of the tether is obtained by the sum of the extensions of each nucleosome and the extension of the bare DNA handles at the flanks of the chromatin fiber, which are modelled by a Worm-Like-Chain. The features of individual chromatin fibers are captured by fitting this model to the experimental force-extension curves (Fig. 3.1A).

A characteristic feature of the force-extension curves of folded chromatin fibers is the force plateau at 3 - 4 pN. We will refer to this region as the unstacking transition of the chromatin fiber. At forces below this transition, the fiber is folded into a condensed structure that is stabilized by nucleosome-nucleosome interactions. In this regime, the fiber extension increases linearly with applied force, like a Hookean spring. When the force exceeds the rupture force, the extension of the total fiber rapidly increases to about 1 μm (Fig. 3.1A and B). This extension corresponds to about 30 nm per nucleosome and is consistent with a single wrap of DNA remaining around each histone core. The unstacking transition is modeled with a force-dependent equilibrium in which the stacking energy is balanced with the work done by the bead. For a more detailed description, we refer to Ref. [33].

Only at forces exceeding 7 pN does the second wrap of DNA start to be released. As opposed to the low force ruptures, this second transition is not in equilibrium, resulting in clear, well-defined steps of 25 nm for each unfolding event (Fig. 3.1C). We note that the release of DNA from singly wrapped octameric nucleosomes, as present after the unstacking transition, cannot be distinguished from the unfolding of tetrasomes, which consist of two copies of the histones H3 and H4 wrapped by a single turn of DNA; both would result

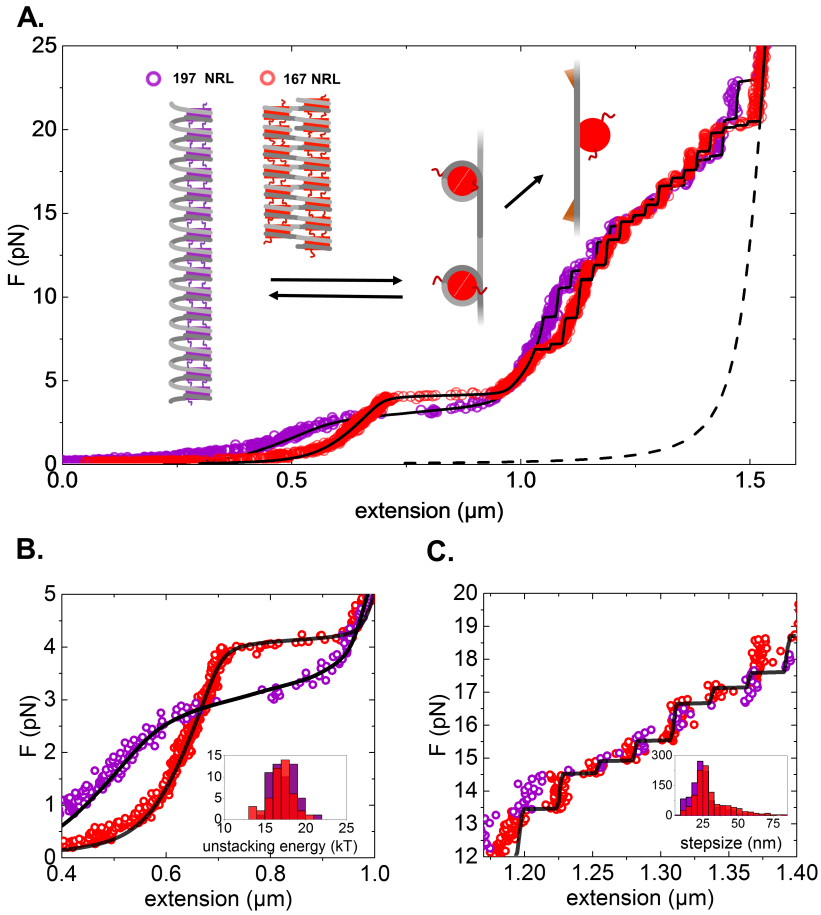

Figure 3.1
Wild-type histone chromatin fibers with 167 and 197 bp NRLs respond differently to applied force. A) Force-extension curve of a chromatin fiber reconstituted on 15 × 167 bp DNA (20 bp linker DNA; red) and 15 × 197 bp DNA (50 bp linker DNA; violet). As a reference, the WLC extension of a 4.4 kbp DNA is plotted (black dotted line). Fitted black curves correspond to the statistical mechanics model for chromatin unfolding described in Meng *et al.* [33]. The graphs represent conformational changes upon stretching. A folded fiber initially stretches linearly until nucleosome-nucleosome interactions rupture and simultaneous release of 56 bp of nucleosomal DNA. The remaining nucleosomal DNA releases in two steps, a small 5 nm step around 6 pN and ∼ 25 nm step at higher forces. Note that tetrasomes only feature the last step. **B)** Zoom of the low-force part of the force-extension curve, representing the stretching of the folded fiber. Compared with 197 bp NRL fibers, 167 bp NRL fibers are more condensed (although extra tetrasomes or hexasomes in this fiber shift the curve to higher condensation), are stiffer, have a higher rupture force, and rupture cooperatively. The unstacking transition is in equilibrium, and the fiber refolds as the force is released (data not shown). *Inset*: histogram of the fitted unstacking energy per nucleosome for both types of fibers. **C)** Zoom of the high-force regime of the force-extension diagram. The remaining wrapped DNA unfolds in a non-equilibrium fashion, resulting in a staircase-like extension curve. *Inset*: histogram of the step sizes.

in the appearance of 25 nm steps. The force-dependent extension of the entire fiber is defined by sum of the force-dependent extensions of each nucleosome, tetrasome, hexasomes and the flanking DNA. The number of nucleosomes and tetrasomes are fitted to the force-extension curve of each individual fiber, yielding the black lines in Fig. 3.1. All force-extension curves feature a similar unfolding pathway, though the detailed composition and interaction parameters may differ between individual fibers.

Several features of the force-extension curves depend on the Nucleosome Repeat Length (NRL). Compared to 197-NRL fibers, 167-NRL fibers exhibit an increased rupture force of 3.5 pN and 4 pN respectively and an almost 4 times larger slope in the low force regime that precedes unstacking transition (Fig. 3.1B). For the 167-NRL fiber, the latter feature results in a maximal extension of the fiber before the unstacking transition of about 5 nm per nucleosome, compared to roughly 10 nm per nucleosome for 197-NRL fibers. Furthermore, 167-NRL fibers feature a sharp force plateau, implicating cooperative unfolding, whereas the more gradual unstacking of 197-NRL fibers indicates independent ruptures of stacked nucleosomes. Interestingly, the stacking energy, which can be approximated by the product of the rupture force and the length of the force plateau divided by the number of stacked nucleosomes, is the same for both fibers (Fig. 3.1B, inset). This suggests that similar nucleosome-nucleosome interactions govern the folding of the two types of nucleosomal arrays into higher order structures.

These results and those of our previous studies imply a two-start zig-zag structure for the 167-NRL fibers and a one-start solenoidal folding for the 197-NRL fibers. However, this interpretation has been questioned [9], arguing that the excessive bending of the linker DNA does not allow for stacking of neighboring nucleosomes. Moreover, it was suggested that stacking of nucleosomes involves more than just histone tail-mediated interactions and would require a close-packed stack of nucleosomes, which is inconsistent with an extension of up to 10 nm per nucleosome. Clearly, identifying the exact structural nature of the unstacking transition will help to address these issues.

3.2.2 The H4 tail mediates the nucleosome-nucleosome interactions in folded chromatin fibers

In the absence of DNA, H4-V21C and H2A-E64C mutant histones readily dimerize under oxidizing conditions, while remaining largely separate in the presence of a reducing agent such as DTT (Fig. 3.2A). When these histones are folded into a chromatin fiber, H2A-H4 cross-linking stabilizes the mutant (MT) fiber against a stretching force (Fig. 3.2B). Indeed, cross-linked chromatin fibers remain condensed up to much larger forces than fibers in reduced conditions, which exhibit an unstacking plateau similar to WT-fibers. The difference in extension is more than 500 nm at 5 pN for a fiber containing 15 nucleosomes, or

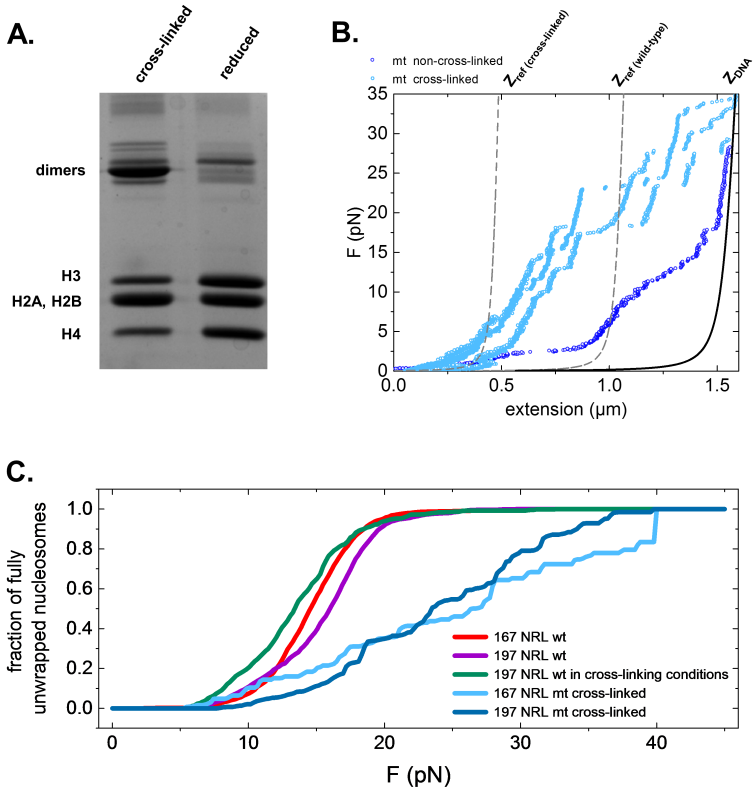

Figure 3.2

Cross-linking mutant histones introduces covalent bonds between nucleosomes in folded chromatin fibers. A) 18% SDS-PAGE of H4-V21C/H2A-E64C double mutant *X. laevis* histone octamers in reducing and oxidizing conditions. Apart from the three bands corresponding to H4, H2A-H2B, and H3 histones, additional bands are visible due to the formation of histone dimers through the disulfide bridge. Multiple dimers can be formed because of endogenous cysteines in H3 and newly introduced cysteines in both H4 and H2A. **B)** Force-extension curves of cross-linked 197 bp NRL fibers (light blue) and a WT-197 bp NRL fiber (dark blue). Dashed lines represent WLC curves of DNA with the same extension as chromatin fibers at 7 pN. These curves were used to calculate the fraction of fully unwrapped nucleosomes. **C)** Fraction of unfolded nucleosomes as a function of force for the wild-type and cross-linked fibers. Wild-type and non-cross-linked fibers of both NRLs feature full unwrapping of nucleosomes in a force range between 6 and 22 pN. In cross-linked fibers, only 30% of the nucleosomes are fully unwrapped at 22 pN. Full unwrapping is only achieved at 40 pN.

about 30 nm per nucleosome. Moreover, at forces above 10 pN, we observe large, discrete, and irregular rupture events on cross-linked MT-fibers (Fig. 3.2B), as opposed to clear 25 nm steps (Fig. 3.1B) for WT-fibers. Similar to WT-fibers, this transition is irreversible and the refolding curve does not overlap with a stretching curve (Fig. S2). Not all histones dissociate from the DNA though, as the refolding curve significantly deviates from that of bare DNA, as described by a WLC, at forces below 25 pN. Compared to WT-fibers, this deviation appears to be slightly bigger for the cross-linked fibers, but large variations were observed.

To quantify the unfolding more precisely, we computed the fraction of fully unwrapped nucleosomes as a function of force (Fig. 3.2C) for all types of fibers. Whereas forces of 20 pN are sufficient to unwrap more than 90 % of the nucleosomal DNA in WT-fibers and MT-fibers under reduced conditions, only about a third of the nucleosomal DNA is released in cross-linked MT-fibers (Fig. 3.2C, 167 and 197-NRL in light and dark blue curves, respectively). To unwrap more than 90 % of the nucleosomal DNA in cross-linked MT-fibers, forces in the range of 35 - 40 pN are required. Thus, efficient cross-linking of Cys-residues is achieved in folded fibers when the redox potential is sufficiently low.

In contrast to the observed differences in the high force regime, inspection of the low force regime reveals that here the mechanical properties of the cross-linked MT-fibers are very similar to those of folded WT-fibers. For 167-NRL fibers (Fig. 3.3A), close overlap is observed for the force-extension curves below the 4 pN unstacking plateau. Both fibers yield the same stiffness ($p = 4 \times 10^{-12}$). At 4.5 pN the WT-fiber undergoes the unstacking transition, whereas the cross-linked MT-fiber continues to stretch in almost linear fashion. The force-extension curves of the 197-NRL fibers also feature substantial overlap up to the unstacking plateau (Fig. 3.2), whereupon the curves start to deviate. Again both fibers yield the same stiffness ($p = 2 \times 10^{-12}$). As in the case of the WT-fibers, the cross-linked 197-NRL MT-fiber exhibits reduced stiffness relative to the cross-linked 167-NRL MT-fiber. We therefore conclude that the mechanical properties of the folded fibers at forces below the unstacking transition are unaffected by cross-linking. This is noteworthy as it implies that contacts between the H4 tail and the H2A acidic patch remain intact throughout the linear stretching regime.

3.2.3 H4-V21C/H2A-E64C mutations affect chromatin stacking

One would expect that MT-fibers under reducing conditions and WT-fibers exhibit similar force-extension behavior, but instead we found that MT-fibers are generally more extended at low force (Fig. 3.4A and B). This difference can be understood by explicitly accounting for the numbers of nucleosomes, hexasomes

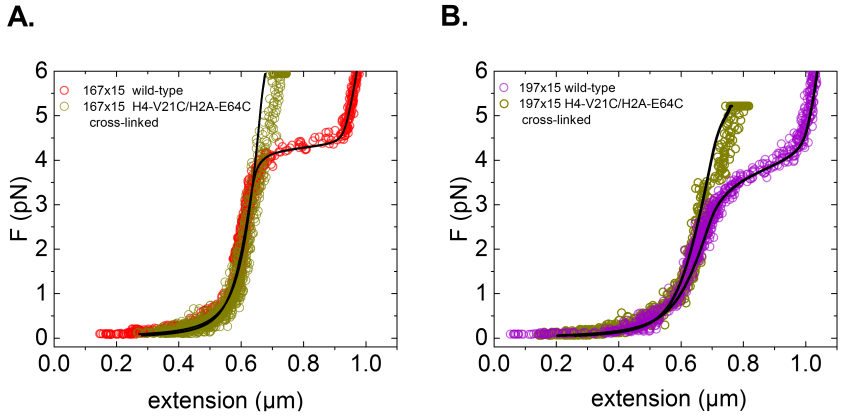

Figure 3.3
Cross-linked fibers do not feature the characteristic chromatin - unstacking transition at 4 pN. A) The typical force plateau of 167-bp NRL fibers at 4.5 pN is not observed in cross-linked fibers. Until unstacking, the force-extension curves overlap. **B)** Comparison between a cross-linked MT-fiber and a WT 197 bp NRL fiber shows a similar stabilization of the fiber. Note that these fibers have a different number of tetrasomes and hexasomes, resulting in a small offset between the curves. The small transition at 3.5 pN in the cross-linked 197 bp NRL MT-fiber may indicate that one of the nucleosome pairs is not properly cross-linked. Fitting the curves yields the same values for the fiber stiffness of cross-linked and non-cross-linked fibers.

and tetrasomes present in the fibers. Fitting the data to our physical model of chromatin stretching shows that MT-fibers generally contain fewer nucleosomes, yet more tetrasomes, than their WT equivalents. Consider, for example, the 167-NRL WT-fiber and the corresponding MT-fiber shown in Fig. 3.4A. The WT-fiber is found to contain 14 nucleosomes and 5 tetrasomes, whereas the MT-fiber contains 9 nucleosomes and 10 tetrasomes (fit results with residuals are listed in Fig. S3 and S4). As both fibers contain 19 nucleosomal particles in total, their extensions at forces exceeding 5 pN are very similar. In a similar fashion, we fitted 15 nucleosomes and 8 tetrasomes for the 197-NRL WT-fiber shown in Fig. 3.4, whereas the 197-NRL MT-fiber contained 9 nucleosomes and 15 tetrasomes. These fit results are typical for our reconstitutions and may reflect an inherently lower stability of nucleosomes in MT-fibers. If so, H2A-H2B dimers may more easily dissociate. H2A-H2B dissociation will result in less nucleosome-wrapped DNA (as tetrasomes only wrap a single turn of DNA) and less nucleosomes that stack on each other (for which the acidic patch on H2A-H2B is required). Both effects will increase the extension of the fiber at forces below the unstacking transition. These differences in fiber composition, however, do not impact the stiffness of WT- and cross-linked MT-fibers, which

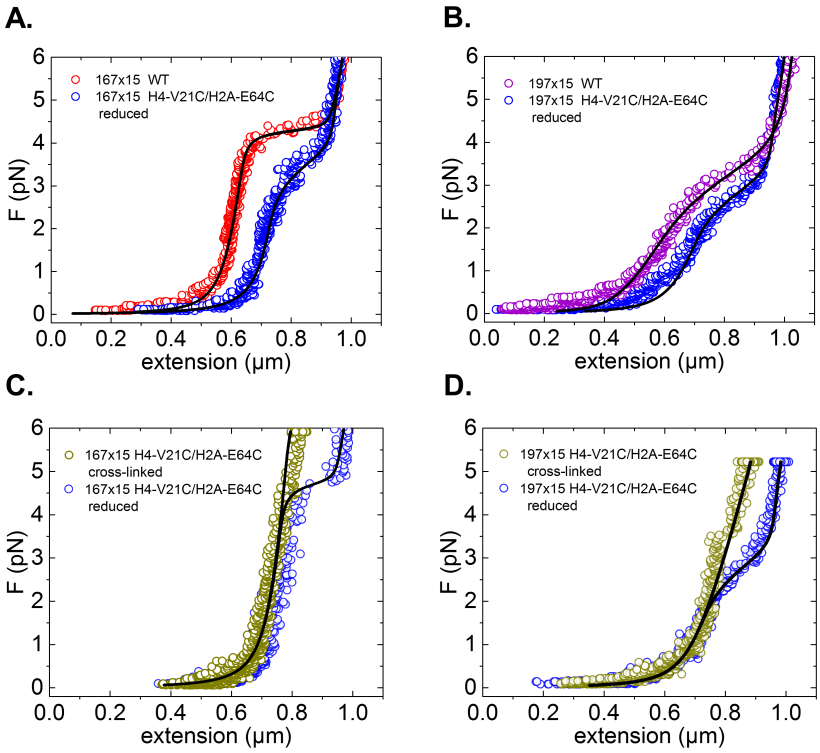

Figure 3.4
Cross-linking of individual fibers does not affect their mechanical properties. **A)** Low-force regime of the force-extension curve of a chromatin fiber assembled on 15 × 167 bp DNA with WT-octamers (red curve) and H4-V21C/H2A-E64C octamers (dark blue) under reducing conditions. **B)** Low force regime of the force-extension curve of a chromatin fiber assembled on 15 × 197 bp DNA with WT-octamers (purple curve) and H4-V21C/H2A-E64C octamers (dark blue) under reducing conditions. The difference in the plateau height between WT- and MT-fibers in both graphs indicates a reduced interaction strength. The smaller width of force plateaus of the MT-fibers should be attributed to a smaller number of H2A-H2B dimers than in the WT-fibers. **C and D)** Low-force regime of the force-extension curves of the same MT-chromatin fibers as shown in A and B under reduced (blue) and oxidized conditions (green). The tether was first pulled when cross-linked in oxidizing buffer and then in reducing buffer (light blue). Removal of cross-links recovers the force plateau. Importantly, before fiber rupture, the force-extension behaviors of the MT-fibers overlap with the curves obtained when cross-linked.

continue to reflect the stiffness characteristic for their NRL (Fig. S3 and S4).

We can further exclude the effects of differences in the composition of individual fibers by exposing individual fibers sequentially to cross-linking and reducing conditions. We first applied forces up to 6 pN on MT-fibers under cross-linking conditions (Fig. 3.4C and D, green curves). Next, we flushed in DTT to disrupt cross-linking and repeated the pulling experiment (Fig. 3.4C and D, blue curves). As before, the force-extension curves of cross-linked and reduced MT-fibers largely overlap at forces below the unstacking transition, with the differences in stiffness between 167 and 197-NRL fibers being independent of the presence of cross-linking. Because cross-linking of H4-V21C to H2A-E64C does not affect the mechanical properties of the folded fiber, but does inhibit the unstacking transition (Fig. 3.3), we can unequivocally attribute this unstacking transition in both 167-NRL and 197-NRL fibers to the rupture of H4 tail-mediated nucleosome stacking, rather than the gradual unwrapping of the nucleosomal DNA.

3.3 Discussion and conclusions

The folding of chromatin fibers is a highly-debated topic that has been addressed mainly by studying regularly spaced 601-arrays reconstituted in vitro. In order to elucidate how the Nucleosome Repeat Length influences the secondary structure and dynamics of chromatin, we performed a single-molecule force spectroscopy study on 167- and 197-NRL nucleosomal arrays reconstituted with wild-type histone octamers and compared their response to that of fibers composed of double mutant (H4-V21C, H2A-E64C) histone octamers. Using these two point mutations, we could attribute the nature of nucleosome stacking in folded chromatin fibers to these specific residues. Importantly, up to the unstacking transition, we observed the same mechanical properties in cross-linked and WT-fibers, which underscores the role of the H4 tail in nucleosome-nucleosome interactions that drive higher order folding.

Successful cross-linking in the flow-cell was confirmed by the increased rupture forces of the individual fibers (Fig. 3.4), and could be reversed by flushing a reducing agent into the buffer. We speculate that the large changes in extension at forces exceeding 10 pN (Fig. 3.2B) represent the disassembly of clusters of covalently linked nucleosomes from the DNA.

All force-extension curves showed a linear extension of the folded fibers in the low force regime. The overlap between WT-fibers and MT-fibers below 3 pN (Fig. 3.3) implies that cross-linked MT-fibers share the same structure as equivalent fibers assembled with WT-histone octamers. We can therefore pin-point the predominant stacking interaction to the two mutated residues, though additional interactions between other tails and neighboring nucleosomes cannot be excluded. Linking the nucleosomes by the disordered, flexible tails

explains the very low stiffness of the fibers and the linear large extension that we report here and in previous work.

Our MT-nucleosomes still carried the native H3-C110 residue, which could form di-sulfide bonds with the cysteines in H4-V21C and H2A-E64C. We cannot exclude the formation of such cross-links in our chromatin fibers. However, the H3-C110 residues are deeper buried in the nucleosome structure and therefore less accessible. In the low force range we observed the same mechanical properties for the fibers under oxidizing and reducing conditions, suggesting that only the anticipated H4-V21C - H2A-E64C disulfide bonds are formed, mimicking native H4 tail - H2A acidic patch interactions.

The cross-linking approach has a significant advantage in the single-molecule force spectroscopy assay. Covalently fixing the state of the fiber in absence of force allowed us to decouple the mechanical properties of 197-NRL fibers from spontaneous fiber unfolding. The results obtained with the WT-fibers show that the maximum extension of the folded 197-NRL fiber is $\sim$ 10 nm per nucleosome. Considering a height of a nucleosome of approximately 6 nm, a gap of $\sim$ 4 nm remains between two stacked nucleosomes in the stretched fiber. The H4 tails have just enough length to span this gap. The cross-linked MT-fibers can be stretched several nm per nucleosome more, prior to the occurrence of rupture transitions at $\sim$ 8 pN. This additional length may result from elastic deformation of the nucleosome, and it cannot be excluded that part of the H4 tail is pulled out of the nucleosome core at such high forces. The observed extension shows, however, that nucleosome-nucleosome stacking does not require close packing of the stacked nucleosomes.

We detected a higher abundance of tetrasomes in MT-fibers, which could result from weaker stacking interactions between nucleosomes. We observed that the unstacking plateau occurs at lower forces, 3.5 pN *vs.* 4 pN for 167-NRL and 2.5 pN *vs.* 3 pN for 197-NRL for non-cross-linked MT-fibers. Replacing the glutamic acid residue in H2A by a polar cysteine reduces the charge of the acidic patch and may consequently decrease electrostatic nucleosome-nucleosome interactions and therefore the stability of nucleosome stacking. The small extension of the 197-NRL fiber at 3.5 pN (Fig. 3.3B) may represent the unstacking of a few non-cross-linked nucleosomes, indicating that cross-linking may not have been achieved fully in these fibers. Interestingly, the rupture force for single nucleosomes (which cannot stack and can only unwrap) is 2.5 pN [33]. Thus, unwrapping of nucleosomal DNA in the absence of stacking could account for the appearance of the unstacking transition at 2.5 pN; consistent with this interpretation, we observe a more gradual unstacking transition for 167 MT-fibers under reducing conditions (Figure 3.4A). Likewise, sedimentation velocity analysis of 167- and 177 MT-fibers under reducing conditions indicated a reduced degree of condensation for MT-fibers relative to WT-fibers [18]. As a secondary effect, destabilization of the nucleosome-nucleosome interactions may enhance H2A-H2B dimer dissociation, leading to fibers with

a larger tetrasome/nucleosome ratio. This may be particularly relevant for the single-molecule force spectroscopy assay presented here, in which the fibers are highly diluted [37].

We can exclude, however, that the increased number of tetrasomes in MT-fibers inhibited H2A-H4 mediated nucleosome stacking, in the case that all nucleosomes would be interspersed by tetrasomes. The same fibers under cross-linking conditions continue to stretch linearly beyond 3.5 pN (Fig. 3.4C and D), demonstrating the establishment of covalent H2A-H4 cross-linking. Thus, both comparisons between ensembles of WT- and cross-linked MT-fibers, and between individual cross-linked and reduced MT-fibers, indicate that the unstacking plateau should be attributed to the unstacking of nucleosomes rather than to the unwrapping of nucleosomal DNA.

The most detailed structural studies on folded chromatin fibers used short NRLs [10, 12] and clearly resolved a two-start helix. Our experiments on WT-chromatin arrays with short NRL (167) showed that these fibers fold into rather stiff tethers that unstack cooperatively, in line with such a two-start helix. Longer repeat lengths, however, are more common in higher eukaryotes, which makes it highly relevant to resolve their topology. Robinson *et al.* reported that the dimensions of folded fibers with larger NRLs are incompatible with two-start folding [11]. Compared to 167-NRL, 197-NRL fibers appear less stiff and rupture at smaller forces. The distribution of the unstacking energy in 197-NRL fibers is slightly broader than that of 167-NRL fibers (3.1B, inset), which may indicate more heterogeneity. Consequently, thermal fluctuations will induce larger variations in extension and enhanced spontaneous unstacking of nucleosomes in the folded fibers. Such a more disordered and dynamic structure of chromatin fibers with long NRL renders studying their organization using structural techniques more challenging.

It is relevant to point out that our measurements were performed at physiological salt concentrations (*i.e.* 100 mM NaCl, see Methods). The recent results obtained with force spectroscopy and cryo-EM on 167- and 177-NRL fibers by Li *et al.* [34] were acquired at much lower salt concentrations (10 mM HEPES, pH 8.0, 0.1 mM EDTA, and optionally 1.5 mM $MgCl_2$), which could strengthen interactions between histones and DNA, driving the fibers in more compacted, closely-packed structures. Whereas Li *et al.* report step-like transitions for unstacking, a sign of non-equilibrium transitions, our force-extension curves on WT-fibers feature a gradual unstacking plateau that can be reversibly refolded. Such behavior indicates more frequent nucleosome unstacking and restacking events, which may be relevant *in vivo*, where nucleosomal DNA seems readily accessible.

The current results place strong constraints on structural models of 30 nm fibers. Such models should be compatible, upon the application of force, with an extension of up to 10 nm per nucleosome while maintaining the base of the H4 tail (residue H4 Asn24) and the acidic patch (residue H2A Glu64) in

the adjoining nucleosome within ~ 3.5 nm (the maximal extension of the H4 tail [16]). For 197-NRL fibers, this spatial constraint excludes any higher order nucleosome-nucleosome stacking other than a one-start model. For shorter fibers such as the 167-NRL, the constraint, set experimentally by the maximal extension per nucleosome, is partially relieved as these fibers are found to have a smaller maximal extension before rupture; in accordance with all other experimental evidence, this points to a two-start structure. The 10 nm linear extension per nucleosome for 197-NRL fibers clearly points to a one-start helix, as such extension in two-start models would require distances between stacked nucleosomes that exceed the length of the H4 tail.

An alternative interpretation of the extension of the fiber before the unstacking transition would be the gradual unwrapping of nucleosomal DNA [9]. Such a model would be incompatible with our data, as DNA unwrapping increases the distance between the nucleosomes to lengths that cannot be bridged by the H4 tail. The covalent bond that we introduced by cross-linking furthermore prohibits any conformational changes that require changes of interacting nucleosomes upon stretching, by unstacking and restacking with other nucleosomes. We therefore conclude that stacking between neighboring nucleosomes in a one-start helix is the most likely structure for the 197-NRL fibers studied here.

Additional measurements can be envisioned that further test the folding pathway reported here. Clipping of the histone tails, acetylation of H4K16 and the depletion of Mg^{2+} should all affect fiber folding by reducing the histone tail-mediated stacking interaction between the nucleosomes. We did observe a lower interaction energy for these cases (data not shown) but, like for the MT-fibers under reducing conditions, we predominantly observed accompanying degradation of fiber composition, leading to fibers containing mostly tetrasomes. We speculate that the lack of higher order structure makes the fiber more fragile when exposed to the drag forces that are unavoidable when flushing the flow cell. Therefore, it appears that nucleosome stacking and nucleosome stability in fibers may be correlated in our experimental setup. The current approach of strengthening nucleosome stacking, rather than weakening, allows for better control of the fiber's composition.

Though our work focuses on the physical properties of regular arrays of nucleosomes *in vitro*, the linker length dependence of nucleosome stacking may have important consequences for chromatin structure *in vivo*. It is conceivable that the variable linker length that has been reported for native chromatin can result in irregular chromatin structures, which would match recent reports on the absence of higher order structure [38] or the observation of pebbles of locally condensed structures [24]. Alternating stacking between neighbors, next-neighbors or more distant nucleosomes, could locally modulate the accessibility of the chromatin and hence play an important role in epigenetic regulation.

For linker lengths of 20 and 50 bp, we established that nucleosome stacking

protects nucleosomal DNA from external forces up to about 4 pN. This may be the most important ramification of the current work. Despite extensive extension of the chromatin fibers, nucleosome stacking remains intact in this force regime, which will reduce accessibility of the DNA and will therefore affect the activity of all nuclear processes that require access to DNA.

3.4 Materials and methods

3.4.1 Chromatin reconstitution and cross-linking

A plasmid-based on pUC18 (Novagen) containing 15 tandem repeats of the Widom-601 sequence spaced by either 20 bp or 50 bp of a linker DNA (NRL = 167 and 197, respectively) was digested with Bsa*I* and Bse*YI*, yielding linear fragments of 4535 bp for 167- and 4985 bp for 197-NRL substrates. A Klenow reaction was used to fill in the single-stranded ends with dUTP-digoxigenin (at Bsa*I* site) or dUTP-biotin (at the Bse*YI* site). Wild-type and H4-V21C/H2A-E64C double mutant *Xenopus laevis* histone octamers were purified and reconstituted as described in [33]. Prior to reconstitution, MT-histone octamers were diluted in high salt buffer (2 M NaCl, 1× TE, pH 7.5) containing 100 mM DTT to reduce the cysteine residues as in Ref. [18]. For both WT- and MT-histone octamers, reconstitution was performed using salt-gradient dialysis under reducing conditions (20 mM beta-mercaptoethanol). Optimal reconstitution was selected from a titration of histone/DNA ratios evaluated by agarose gel electrophoresis (Fig. S1). To induce the disulfide bridging between neighboring nucleosomes arrays reconstituted with H4-V21C/H2A-E64C, a second dialysis was performed with buffer without any oxidizing agents, but supplemented with 2 mM $MgCl_2$.

3.4.2 Sample preparation

A clean coverslip was coated with 0.1 % nitrocellulose (Ladd Research) in amylacetate solution and then mounted onto a poly-di-methysiloxane (PDMS, Dow Corning) flow cell containing a 10 × 40 × 0.4 mm^3 flow channel. The flow cell was incubated with 3 μg/ml anti-digoxigenin (Roche) for 2 h and then passivated with 4 % bovine serum albumin (w/v) and 0.1 % Tween-20 overnight. 20 ng/ml of reconstituted fibers in the measurement buffer (MB: 100 mM NaCl, 2 mM $MgCl_2$, 10 mM HEPES pH 7.6, 10 mM NaN_3, 0.2 % BSA, 0.1 % Tween-20) were flushed into the flow cell and incubated in a room temperature for 10 min, followed by flushing in 1 μm or 2.8 μm diameter streptavidin-coated superparamagnetic beads (MyOne/M270 respectively, Invitrogen) diluted in MB. Untethered beads were flushed out with MB buffer 10 min later.

3.4.3 Magnetic tweezers

We employed home-built multiplexed magnetic tweezers (Brouwer *et al., in preparation*). The extensions of the molecules were measured in real time at a frame rate of 30 Hz with a CMOS camera (CMOS Vision Condor). We applied a continuously increasing force by moving the magnet towards the flow cell at a constant velocity. Force ramps typically lasted 30 s. Subsequently, we reversed the magnet trajectory to decrease the force. We used a double exponential function that was calibrated prior to the experiment to calculate the exerted force [32]. The resulting force-extension plots were aligned at high force with a worm-like-chain with a contour length equal to that of the DNA employed in reconstitution (Fig. 3.1A).

3.4.4 Data analysis

We used LabVIEW software to analyze the obtained time traces of tether extension as a function of magnet position. The resulting force-extension curves were fitted to a statistical mechanics-based model described previously [33].

The cumulative distribution of rupture forces was calculated using:

$$_{\text{unwrapped}}(F) = \frac{z_{\text{measured}}(F) - z_{\text{ref}}(F)}{z_{\text{DNA}}(F) - z_{\text{ref}}(F)} \tag{3.1}$$

where $z_{\text{measured}}(F)$ is the extension of the tether at force F, $z_{\text{DNA}}(F)$ is the contour length of the DNA fully unwrapped from all nucleosomes and $z_{\text{ref}}(F)$ is the extension of the tether above a force threshold of 7 pN. $P_{\text{unwrapped}}(F)$ is set to 0 for negative values, which would correspond to more than one turn of wrapped DNA per nucleosome. The cumulative distribution is normalized using the total number of nucleosomal steps that were found in multiple pulling curves.

To determine the significance of the overlap between two force-extension curves we performed a Student t-test:

$$t = \frac{|k_{\text{wt}} - k_{\text{mt}}|}{\sqrt{SE_{\text{wt}}^2 - SE_{\text{mt}}^2}} \tag{3.2}$$

where k_{wt}, k_{mt} are the fitted slopes of the force-extension curves below between 0.5 and 3 pN for WR and MT fibers, SE_{wt}, SE_{mt} is the standard error of the fit. The two-tailed p-value was calculated for N degrees of freedom, equal to the number of data points minus the number of variables in the fit.

Acknowledgements

We are grateful to Nikolay Korolev, Nicolaas Hermans, Orkide Ordu, and Josko de Boer for valuable discussions and comments and Chi Pham and Ineke de Boer for DNA preparation.

3.5 Supplementary Figures

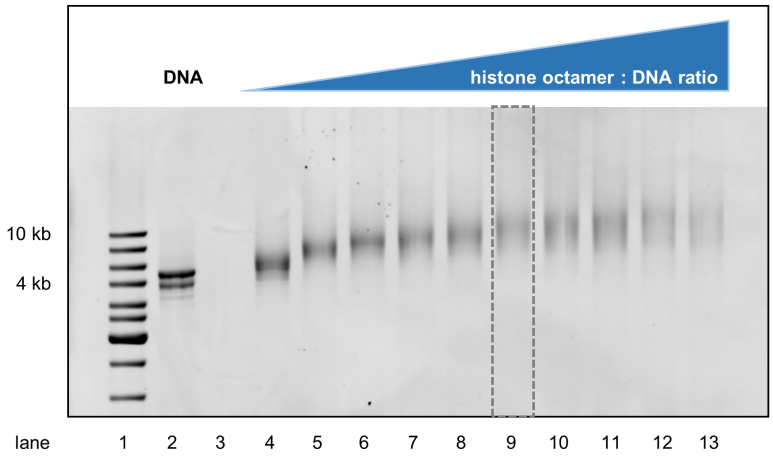

Figure S1
Band shift assay. 0.7 % agarose gel run in 0.2× TB depicts the assembly of DNA with histone octamers into a nucleosomal array. The best stoichiometry of protein versus DNA was determined experimentally by titration of the octamer:DNA ratio. With the increasing histone concentration, the chromatin fiber becomes more saturated and migrates slower through the agarose gel. Band-shift reaches a plateau at the saturation level, after which nucleosomes reconstitute on the DNA handles. For our experiments, we used the reconstitutions corresponding to lane 9.

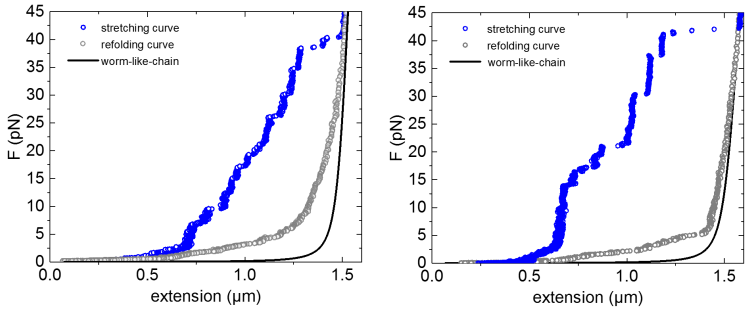

Figure S2
Force-extension curves of cross-linked chromatin fibers with depicted hysteresis between a stretching curve (blue) and a refolding curve (grey). Hysteresis is only observed at forces higher than 10 pN.

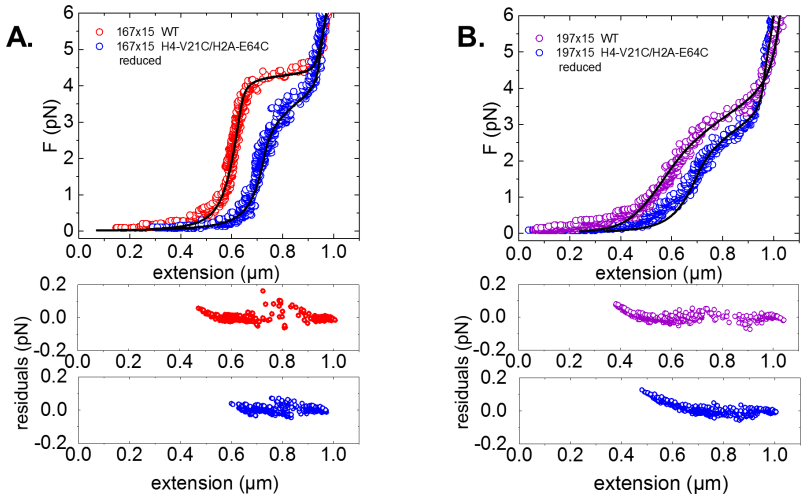

	WT	Cys
k [pN/nm]	1.1	1.1
dG [k_BT]	19.3	16.1
N ($N_{tetrasomes}$)	19 (5)	19/10

	WT	Cys
k [pN/nm]	0.19	0.24
dG [k_BT]	16.5	16.5
N ($N_{tetrasomes}$)	23 (8)	24 (15)

Figure S3

Overview of the force-extension curves presented in Fig. 4. A, B along with the residuals of the fit by the statistical mechanics model (above 0.5 pN) and fitted parameters [33].

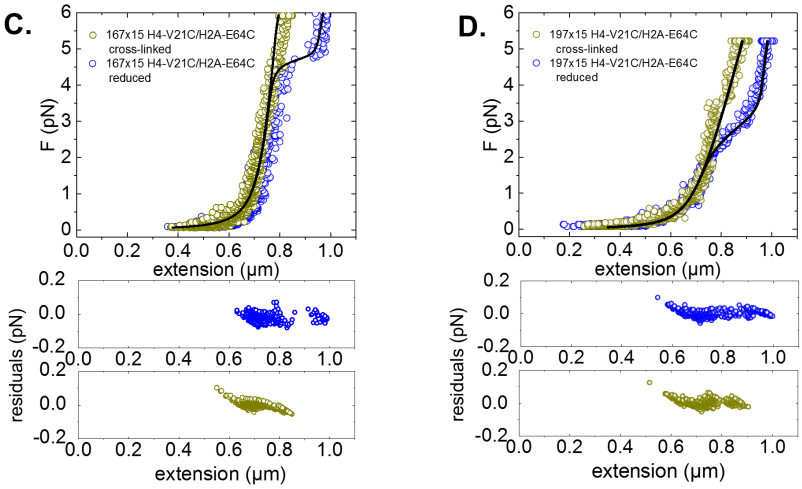

	Cys_DTT	Cys
k [pN/nm]	1.1	1.1
dG [k_BT]	21.4	-
N ($N_{tetrasomes}$)	19(10)	

	Cys_DTT	Cys
k [pN/nm]	0.24	0.24
dG [k_BT]	16.5	-
N ($N_{tetrasomes}$)	24(15)	

Figure S4

Overview of the force-extension curves presented in Fig. 4. C, D along with the residuals of the fit by the statistical mechanics model (above 0.5 pN) and fitted parameters [33].

Bibliography III

[1] Karolin Luger et al. "Crystal structure of the nucleosome core particle at 2.8Å resolution". In: *Nature* 389 (1997), pp. 251–260. ISSN: 0028-0836. DOI: 10.1038/38444.

[2] Jan Bednar et al. "The nature of the nucleosomal barrier to transcription: Direct observation of paused intermediates by electron cryomicroscopy". In: *Molecular Cell* 4.3 (1999), pp. 377–386. ISSN: 10972765. DOI: 10.1016/S1097-2765(00)80339-1.

[3] Young Jun Park and Karolin Luger. "Histone chaperones in nucleosome eviction and histone exchange". In: *Current Opinion in Structural Biology* 18.3 (2008), pp. 282–289. ISSN: 0959440X. DOI: 10.1016/j.sbi.2008.04.003.

[4] Yahli Lorch, Barbara Maier-Davis, and Roger D. Kornberg. "Mechanism of chromatin remodeling". In: *Proceedings of the National Academy of Sciences* 107.8 (2010), pp. 3458–3462. ISSN: 0027-8424. DOI: 10.1073/pnas.1000398107.

[5] Jerry L. Workman. "Nucleosome displacement in transcription". In: *Genes and Development* 20.15 (2006), pp. 2009–2017. ISSN: 08909369. DOI: 10.1101/gad.1435706.

[6] Michael Shogren-Knaak et al. "Histone H4-K16 acetylation controls chromatin structure and protein interactions." In: *Science* 311.5762 (2006), pp. 844–847. ISSN: 1095-9203. DOI: 10.1126/science.1124000.

[7] Andrew Routh, Sara Sandin, and Daniela Rhodes. "Nucleosome repeat length and linker histone stoichiometry determine chromatin fiber structure." In: *Proceedings of the National Academy of Sciences of the United States of America* 105.26 (2008), pp. 8872–8877.

[8] Joel C. Eissenberg and Sarah C.R. Elgin. "The HP1 protein family: Getting a grip on chromatin". In: *Current Opinion in Genetics and Development* 10.2 (2000), pp. 204–210. ISSN: 0959437X. DOI: 10.1016/S0959-437X(00)00058-7.

[9] Jean Marc Victor et al. "Pulling chromatin apart: Unstacking or Unwrapping?" In: *BMC Biophysics* 5 (2012), p. 21. ISSN: 2046-1682. DOI: 10.1186/2046-1682-5-21.

[10] Feng Song et al. "Cryo-EM study of the chromatin fiber reveals a double helix twisted by tetranucleosomal units". In: *Science* 344.6182 (2014), pp. 376–380. ISSN: 10959203. DOI: 10.1126/science.1251413.

[11] Philip J. J. Robinson et al. "EM measurements define the dimensions of the '30-nm' chromatin fiber: evidence for a compact, interdigitated structure." In: *Proceedings of the National Academy of Sciences of the United States of America* 103.17 (2006), pp. 6506–11. ISSN: 0027-8424. DOI: 10.1073/pnas.0601212103.

[12] Thomas Schalch et al. "X-ray structure of a tetranucleosome and its implications for the chromatin fibre". In: *Nature* 436.7047 (2005), pp. 138–141. ISSN: 00280836. DOI: 10.1038/nature03686.

[13] Abdollah Allahverdi et al. "Chromatin compaction under mixed salt conditions: Opposite effects of sodium and potassium ions on nucleosome array folding". In: *Scientific Reports* 5 (2015), p. 8512. ISSN: 20452322. DOI: 10.1038/srep08512.

[14] Sarah J. Correll, Michaela H. Schubert, and Sergei A. Grigoryev. "Short nucleosome repeats impose rotational modulations on chromatin fibre folding". In: *EMBO Journal* 31.10 (2012), pp. 2416–2426. ISSN: 02614189. DOI: 10.1038/emboj.2012.80.

[15] J. Langowski and H. Schiessel. "Chromatin simulations". In: *Computational studies of RNA and DNA* (2006), pp. 605–634. DOI: 10.1007/978-1-4020-4851-3_24.

[16] Davood Norouzi et al. "Topological diversity of chromatin fibers: Interplay between nucleosome repeat length, DNA linking number and the level of transcription". In: *AIMS Biophysics* 2.4 (2015), pp. 613–629. ISSN: 2377-9098. DOI: 10.3934/biophy.2015.4.613.

[17] Tatiana Nikitina et al. "DNA topology in chromatin is defined by nucleosome spacing". In: *Science Advances* 3.10 (2017). ISSN: 23752548. DOI: 10.1126/sciadv.1700957.

[18] Benedetta Dorigo et al. "Nucleosome arrays reveal the two-start organization of the chromatin fiber". In: *Science* 306.5701 (Nov. 2004), pp. 1571–1573. ISSN: 00368075. DOI: 10.1126/science.1103124.

[19] Sergei A. Grigoryev. "Nucleosome spacing and chromatin higher-order folding". In: *Nucleus (United States)* 3.6 (2012), pp. 493–9. ISSN: 19491034. DOI: 10.4161/nucl.22168.

[20] Cizhong Jiang and B. Franklin Pugh. "Nucleosome positioning and gene regulation: Advances through genomics". In: *Nature Reviews Genetics* 10.3 (Mar. 2009), pp. 161–172. ISSN: 14710056. DOI: 10.1038/nrg2522.

[21] Nick Gilbert and Bernard Ramsahoye. "The relationship between chromatin structure and transcriptional activity in mammalian genomes". In: *Briefings in Functional Genomics and Proteomics* 4.2 (2005), pp. 129–142. ISSN: 14739550. DOI: 10.1093/bfgp/4.2.129.

[22] Marco Tompitak, Cedric Vaillant, and Helmut Schiessel. "Genomes of Multicellular Organisms Have Evolved to Attract Nucleosomes to Promoter Regions". In: *Biophysical Journal* 112.3 (2017), pp. 505–511. ISSN: 00063495. DOI: 10.1016/j.bpj.2016.12.041.

[23] Kazuhiro Maeshima, Saera Hihara, and Mikhail Eltsov. "Chromatin structure: Does the 30-nm fibre exist in vivo?" In: *Current Opinion in Cell Biology* 22.3 (2010), pp. 291–297. ISSN: 09550674. DOI: 10.1016/j.ceb.2010.03.001.

[24] Maria Aurelia Ricci et al. "Chromatin fibers are formed by heterogeneous groups of nucleosomes in vivo". In: *Cell* 160.6 (2015), pp. 1145–1158. ISSN: 10974172. DOI: 10.1016/j.cell.2015.01.054.

[25] David J. Clark. "Nucleosome positioning, nucleosome spacing and the nucleosome code". In: *Journal of Biomolecular Structure and Dynamics* 27.6 (2010), pp. 781–793. ISSN: 15380254. DOI: 10.1080/073911010010524945.

[26] P. T. Lowary and J. Widom. "New DNA sequence rules for high affinity binding to histone octamer and sequence-directed nucleosome positioning". In: *Journal of Molecular Biology* 276.1 (1998), pp. 19–42. ISSN: 00222836. DOI: 10.1006/jmbi.1997.1494.

[27] J. Widom. "Role of DNA sequence in nucleosome stability and dynamics". In: *Quarterly Reviews of Biophysics* 34 (2001), pp. 269–324. ISSN: 0033-5835. DOI: doi:10.1017/S0033583501003699.

[28] Andrew Flaus. "Principles and practice of nucleosome positioning in vitro". In: *Frontiers in Life Science* 5.1-2 (2011), pp. 5–27. ISSN: 21553769. DOI: 10.1080/21553769.2012.702667.

[29] Elena F. Koslover et al. "Local geometry and elasticity in compact chromatin structure". In: *Biophysical Journal* 99.12 (2010), pp. 3941–3950. ISSN: 15420086. DOI: 10.1016/j.bpj.2010.10.024.

[30] J. T. Finch and A. Klug. "Solenoidal model for superstructure in chromatin." In: *Proceedings of the National Academy of Sciences* 73.6 (1976), pp. 1897–1901. ISSN: 0027-8424. DOI: 10.1073/pnas.73.6.1897.

[31] Fan-Tso Chien and John van Noort. "10 Years of Tension on Chromatin: Results From Single Molecule Force Spectroscopy." In: *Current Pharmaceutical Biotechnology* 10.5 (2009), pp. 474–485. DOI: 10.2174/138920109788922128.

[32] Marteen Kruithof et al. "Subpiconewton dynamic force spectroscopy using magnetic tweezers." In: *Biophysical journal* 94.6 (2008), pp. 2343–2348. ISSN: 00063495. DOI: 10.1529/biophysj.107.121673.

[33] He Meng, Kurt Andresen, and John van Noort. "Quantitative analysis of single-molecule force spectroscopy on folded chromatin fibers". In: *Nucleic Acids Research* 43.7 (2015), pp. 3578–3590. ISSN: 13624962. DOI: 10.1093/nar/gkv215.

[34] Wei Li et al. "FACT Remodels the Tetranucleosomal Unit of Chromatin Fibers for Gene Transcription". In: *Molecular Cell* 64.1 (2016), pp. 120–133. ISSN: 10974164. DOI: 10.1016/j.molcel.2016.08.024.

[35] Tamar Schlick, Jeff Hayes, and Sergei Grigoryev. "Toward convergence of experimental studies and theoretical modeling of the chromatin fiber". In: *Journal of Biological Chemistry* 287.8 (2012), pp. 5183–5191. ISSN: 00219258. DOI: 10.1074/jbc.R111.305763.

[36] Yujie Chen et al. "Asymmetric unwrapping of nucleosomal DNA propagates asymmetric opening and dissociation of the histone core". In: *Proceedings of the National Academy of Sciences* 114.2 (2017), pp. 334–339. ISSN: 0027-8424. DOI: 10.1073/pnas.1611118114.

[37] Cyril Claudet et al. "Histone octamer instability under single molecule experiment conditions". In: *Journal of Biological Chemistry* 280.20 (2005), pp. 19958–19965. ISSN: 00219258. DOI: 10.1074/jbc.M500121200.

[38] Kazuhiro Maeshima et al. "Liquid-like behavior of chromatin". In: *Current Opinion in Genetics and Development* 37 (2016), pp. 36–45. ISSN: 18790380. DOI: 10.1016/j.gde.2015.11.006.

Chapter 4

Chromatin fibers stabilize nucleosomes under torsional stress

Torsional stress generated during DNA replication and transcription has been suggested to facilitate nucleosome unwrapping and thereby the progression of polymerases. However, the propagation of twist in condensed chromatin remains yet unresolved. Here, we have measured how force and torque impact chromatin fibers with a Nucleosome Repeat Length (NRL) of 167 and 197. We found that both types of fibers fold into a left-handed superhelix that can be stabilized by positive torsion. We observed that the structural changes induced by twist were reversible, indicating that chromatin has a large degree of elasticity. Our direct measurements of torque additionally confirmed the hypothesis of chromatin fibers as a twist buffer. Using a statistical mechanics-based torsional spring model, we extracted values of the chromatin twist modulus and the linking number per stacked nucleosome that were in good agreement with values measured experimentally. Overall, our findings indicate that the supercoiling generated by DNA processing enzymes can be largely accommodated by the higher-order structure of chromatin.

This chapter is based on: Kaczmarczyk A., Meng H, Ordu O., van Noort S.J.T., Dekker N.H.: "Chromatin fibers stabilize nucleosomes under torsional stress", *submitted*.

4.1 Introduction

In eukaryotic cells, the accessibility of DNA is regulated at the level of chromatin. The fundamental repetitive unit of chromatin is the nucleosome, which consists of 147 base pairs of DNA wrapped around a wedge-shaped histone octamer composed of an $(H3\text{-}H4)_2$ tetramer and two H2A-H2B dimers [1, 2]. Normally, nucleosomes constitute a barrier for polymerases and other enzymes involved in DNA transactions [3]. However, they are also dynamic structures that can be influenced by *e.g* thermal fluctuations [4, 5], DNA supercoiling [6], post-translational histone modifications [7], activity of chromatin remodellers [8–10] or the presence of linker histones [11, 12]. These mechanisms provide the means to modulate nucleosome stability, and hence influence the structure of chromatin.

In the genome, nucleosomes are spaced by so-called linker DNA of 20 - 90 bps [13, 14], but they can nonetheless interact with each other *via* histone tails to form higher-order chromatin structures *e.g.* fibers. The topology of such chromatin fibers *in vivo* has remained a matter of debate, in part due to the heterogeneity of chromatin and its dynamic nature [15, 16]. While many detailed models have emerged from structural studies of nucleosomal arrays *in vitro* and *in silico* [17–20], how the stability of nucleosomes and the accessibility of the DNA can be modulated in compact chromatin remains unclear. Possibly, such stacking of nucleosomes into chromatin fibers imposes an additional barrier for molecular motors that act on DNA, and as such contributes to gene regulation.

A primary regulator of gene expression is supercoiling - the over- or under-twisting of the right-handed DNA double helix (with 10.4 base pairs per 1 helical turn [21]) that results from bending or unwinding of DNA during replication or transcription. During the latter process, RNA polymerase (RNAp) generates large torsional stresses at rates up to seven DNA supercoils per second [22]. More specifically, as described by the "twin supercoiled domain" model, RNAp overwinds DNA ahead of the transcription fork and underwinds DNA behind it [22, 23]. It has been suggested that the positive torsion ahead of a eukaryotic RNAp could destabilize nucleosomes [24], whilst the negative torsion in its wake could facilitate their reassembly (Fig. 4.1A). Such phenomenon was corroborated *in vivo* by Teves and Henikoff, who employed MNase digestion assay to resolve twist-induced changes in nucleosome occupancy [25]. A genome-wide study of the supercoiling density within large topological domains also showed that overwound and underwound regions differed in the degree of chromatin compaction [26]: actively transcribed, gene-rich *loci* were found to be under-wound and less compacted relative to transcriptionally silent regions of densely packed chromatin. This complex interplay between transcription, supercoiling, and chromatin compaction has only been investigated at the mechanistic level in the context of single nucleosomes [27]. Thus, it remains unknown how torsional stress affects the compact chromatin fibers formed by multiple interacting

nucleosomes.

To understand the propagation of twist in chromatin, it is crucial to resolve the topology of DNA in a folded chromatin fiber. The nucleosomal DNA winds around a histone octamer 1.65 times in a left-handed manner [2] and has a slightly lower helical twist density than bare DNA. As a result, the linking number (corresponding to the sum of twist and writhe of DNA) of a single nucleosome equals −1 [28]. However, it does not follow that the topological properties of chromatin fibers can simply be inferred from the number of nucleosomes they contain, because the linker DNA that connects nucleosomes forms additional loops due to nucleosome stacking. This process is mediated by nucleosome-nucleosome interactions between the H4-tail and the acidic patch of the H2A histone, and was shown to be energetically favorable *in vitro* [29, 30]. Such stacking of nucleosomes is expected to maintain a level of chromatin folding in the crowded environment of cell nucleus despite variation in lengths of the linker DNA [14]. While some *in vivo* studies suggest an unstructured organization of nucleosomes in a cell nucleus [31–34], more recent *in vivo* work by Risca *et al.* revealed contacts between alternating nucleosomes, as measured by nucleosome mapping with a resolution of 50 - 500 bp [35]. Using cryo-EM, Cai *et al.* resolved the structures of HeLa nucleosomes *in situ* and, based on the linker DNA density, proposed that nucleosomes were likely to interact with each other [36]. Thus, an understanding of the impact of twist generated on chromatin fibers by DNA processing enzymes should take into account nucleosome-nucleosome stacking.

In vitro single-molecule force spectroscopy techniques have provided a detailed view of the dynamics of condensed chromatin fibers and their unfolding. For example, experiments on native chromatin extracted from cells and stretched by optical or magnetic tweezers quantified the piconewton (pN) forces that maintain its higher-order structure [37, 38]. In our earlier work, we showed that reconstituted nucleosomal arrays form compact fibers in physiological buffer conditions, even without the presence of the linker histone H1 [39]. We also studied the compliance of fibers assembled with different Nucleosome Repeat Lengths (NRL) and inferred that chromatin arrays with short linker DNA of 20 bp (NRL = 167 bp) fold into two-start fibers, whereas those with longer linker DNA of 50 bp (NRL = 197 bp) fold into one-start, solenoidal fibers. This was consistent with a distinct folding for 197-NRL [40] fibers relative to 167-NRL fibers [17] measured via EM and X-ray crystallography, respectively. Irrespective of the linker DNA length, in our force spectroscopy assay fibers underwent a reversible unstacking transition at 3 - 5 pN, a force higher than the 2.5 pN rupture force required to partially unwrap a single nucleosome [41]. The impact of nucleosome-nucleosome interactions was further highlighted in experiments where neighboring nucleosomes were cross-linked between the H4-tails and the acidic patch of histone H2A, resulting in an increase in the rupture force without affecting the compliance of the fiber [42]. These experiments, all performed on rotationally unconstrained molecules, collectively indicate that

nucleosome-nucleosome interactions form the driving force behind chromatin condensation into a "30 nm fiber" and contribute to their resilience under mechanical stress.

Single-molecule experiments focusing on the role of torsion have examined individual tetrasomes, nucleosomes or sparsely decorated chromatin fibers. For example, Vlijm *et al.* demonstrated spontaneous flipping of $(H3\text{-}H4)_2$ tetrasomes between left- and right-handed wrapped states of the DNA, suggesting that this could contribute to the torsional plasticity of chromatin [43]. Similar transient states were not detected in nucleosomes, yet isolated nucleosomes could absorb some of the imposed twist by adapting their conformation and thereby reduce the build-up of torque. Earlier, Sheinin *et al.* [44] investigated the force-induced unfolding of single nucleosomes from a rotationally constrained DNA template. Here, the application of force to pre-twisted nucleosomes primarily facilitated the eviction of H2A-H2B dimers and had only a moderate effect on the $(H3\text{-}H4)_2$ tetrasome unwrapping relative to rotationally relaxed samples. The response to twist of sparsely decorated nucleosomal arrays under torsional constraint was investigated by Bancaud *et al.* [45, 46], who reported a large degree of torsional plasticity of chromatin and attributed this to a chiral transition of nucleosomes from a left-handed into a right-handed wrapped state. However, as the use of a low salt buffer in these experiments prevented the folding of nucleosomal arrays into compact fibers, neither the stacking between nucleosomes nor DNA unwrapping from nucleosomes could be probed. Under conditions that more closely resemble the *in vivo* context (*i.e.* 100 mM KCl and 2 mM $MgCl_2$), nucleosomes are known to stack into a condensed fiber [47], and the torsional response is therefore expected to differ.

Here, we report a comprehensive study of reconstituted chromatin fibers in physiological salt concentrations under force and torque. We found that chromatin fibers responded anisotropically to torsion and, importantly, maintained their compacted higher-order structure. Only when the tension exceeded 3 pN did positive torque facilitate the unstacking of the fiber. Interestingly, however, further positive supercoiling restored the higher-order structure. We quantified the torsional elasticity of compact chromatin fibers by analyzing the rotation-extension curves using a torsional spring model that captures this twist-induced unfolding and refolding of chromatin. The obtained low torsional stiffness of chromatin was supported by direct torque measurements using magnetic torque tweezers. Based on this quantitative analysis, we established structural parameters of folded chromatin fibers, such as the topology of the linker DNA and the chirality of the fiber. As similar phenomena were detected in chromatin fibers with NRL = 167 bp and NRL = 197 bp, this indicated that both two-start and one-start chromatin fibers form left-handed superhelices that can absorb excessive positive twist. This elastic response allows chromatin to function as a twist reservoir that can accommodate positive supercoiling. Our findings provide new insights into the mechanism of supercoiling and the stability of

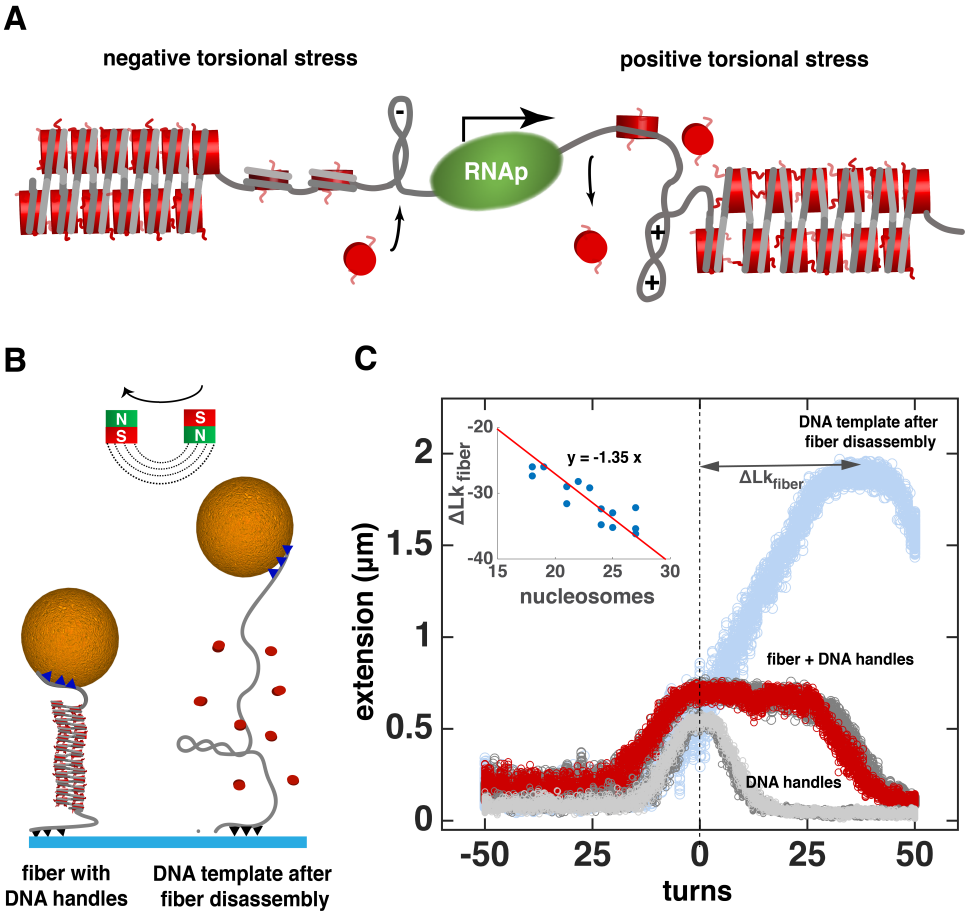

Figure 4.1
The application of turns to reconstituted chromatin fibers allows to mimic the effect of torsional stress *in vivo*. See the detailed figure caption on the next page.

chromatin during torque-inducing processes such as transcription.

4.2 Results

4.2.1 Chromatin fibers fold into left-handed superhelices that absorb positive twist

We studied torsional properties of chromatin fibers reconstituted on tandem repeats of 601-DNA sequences (30·167 bp and 25·197 bp) flanked by 2 kbps nucleosome-free DNA handles (jointly referred to below as the 'chromatin tether'). The samples were tethered at either end by multiple bonds to a magnetic bead or to the surface of a flow cell, respectively, to constrain their overall linking

Figure 4.1
Applying turns to reconstituted chromatin fibers mimics the effect of torsional stress *in vivo*. **A)** Schematic summarizing the current understanding of the response of chromatin to transcription-generated torsional stress. Progressing RNA polymerase (RNAp) generates positive DNA supercoils, ahead of the transcription bubble, that destabilize nucleosomes (red). Negative supercoils that form behind RNAp facilitate nucleosome assembly. In this study, we explore how the folding of nucleosomal arrays into chromatin affects the propagation of the torsional stress. **B)** Schematic of single-molecule magnetic tweezers used to apply tension and torsion to reconstituted chromatin. Fibers containing ∼30 regularly spaced nucleosomes (red) are flanked by (∼ 2 kb) DNA handles (grey) to allow for tethering between a paramagnetic bead (gold) and the glass slide of a flow chamber. The DNA handles include multiple biotin or digoxigenin anchors (triangles), respectively, to constrain the linking number of the tether. A pair of cubic magnets (red and green squares) is used to exert a constant stretching force on the paramagnetic bead, and hence on the tether. To apply rotations to the tethers, the magnets are rotated in either a positive (counter-clockwise) or negative (clockwise) direction. Throughout, the lengths of the tethers are monitored by tracking the positions of the paramagnetic beads in 3D in real-time. Disassembly of chromatin fibers was achieved by either exerting forces $>$ 15 pN or adding heparin to the buffer. **C)** Rotation-extension curves of DNA and chromatin under a force of 0.5 pN. At this force, the rotation curve of bare DNA handles (grey) is symmetric with respect to zero turns. The rotation curve of a chromatin fiber (red) is asymmetric with respect to zero turns and exhibits a broad apex at positive turns. At approximately +25 turns, the tether buckles (*i.e.* starts to shorten in extension) due to the formation of positive plectonemic supercoils in the DNA handles. Note that the initial dataset obtained by rotating from negative to positive turns fully overlaps with the subsequent dataset obtained by rotating in the reverse direction (dark grey). Upon the addition of heparin to the same tether, the rotation-extension curve (blue) exhibits a maximal extension that exceeds that of the folded fiber by a factor of three. Furthermore, the apex of the curve is shifted by +34 turns, from which we deduce the negative linking number of the folded chromatin fiber (main text). *Inset*: the linking number of a chromatin fiber, quantified by the shift between rotation-extension curves of chromatin fibers versus bare DNA, is proportional to the number of assembled nucleosomes. The red line is a linear fit to the data with a slope of -1.35 ± 0.02 turn per nucleosome (n = 14). Underlying rotation-extension curves are shown in Supplementary Fig. S1.

number (Fig. 4.1B). All experiments were performed in a buffer (Methods) that induces stacking of nucleosomes into compact fibers [42].

We first performed a series of experiments in which we measured the extension of the 167-Nucleosome Repeat Length (NRL) chromatin tethers at a constant tension of 0.5 pN while applying a sequence of 50 positive turns, 100 negative turns and 50 positive turns (thereby returning to the starting point). In the absence of applied turns (designated as zero turns in all plots), the tether was assumed to be in a fully torsionally relaxed state. The resulting rotation-extension diagram of the chromatin tether (Fig. 4.1, red) showed an asymmetric response of chromatin to applied positive and negative twist. In particular, the extension exhibited a broad plateau that persisted for more than 25 positive turns. This differs substantially from the response of a bare DNA molecule of comparable length to applied turns (Fig. 4.1, grey). Beyond 25 turns, applying more positive turns to the chromatin tether induced a linear

shortening (or buckling), as is also observed for bare DNA once the accumulation of positive twist has led to the build-up of a critical torque [48]. The delay in buckling of the chromatin tether relative to bare DNA at the same force implies that the chromatin fiber was able to absorb some positive twist, reducing the build-up of torque and thereby delaying the formation of plectonemic supercoils (or plectonemes) in the DNA handles. In contrast, when negative turns were applied, the buckling occurred after applying the same number of negative turns as in bare DNA (-5 turns). This shows that negative twist could not be absorbed by the chromatin fibers and instead propagated to the DNA handles, resulting in buckling once a critical torque had built up [48, 49]. Importantly, all rotation-extension curves were fully reversible (red and dark grey curves in Fig. 4.1C), as opposed to the magnetic tweezers experiments on sparsely decorated nucleosomal arrays [46]. This indicates that the structural changes occurred in thermodynamic equilibrium and that histone disassembly can be excluded at the applied forces and induced torques studied here. Jointly, the extensive plateau and lack of hysteresis in the rotation - extension curve indicate that chromatin fibers can accommodate substantial torsional stress while maintaining nucleosome-nucleosome stacking.

We subsequently quantified the amount of twist stored in a relaxed folded chromatin fiber. To do so, the sample described above was exposed *in situ* to heparin. This polyanion outcompeted the electrostatic DNA-histone interactions, resulting in the disassembly of nucleosomes [50]. Dissociation of a single histone octamer from rotationally constrained DNA increases the contour length by > 50 nm [43], while the linking number of the tether remains fixed [45]. Following the heparin treatment, the maximal extension of the nucleosome-free DNA was indeed $\sim$3 times larger than that of the folded fiber (Fig. 4.1C, blue), indicative of nucleosome disassembly. The most extended state, corresponding to rotationally relaxed DNA, was observed at $+34$ turns. Under the assumption that the chromatin fiber contains 25 nucleosomes (see Materials and Methods), this allows us to estimate the linking number of a fiber per nucleosome Lk_{fiber}. In this particular chromatin tether, this parameter equals $\frac{-34}{25} = -1.4$. A more precise quantification can be obtained by determining the number of nucleosomes (and tetrasomes) for each individual fiber using fits to their respective force-extension curves [39]. A plot of Lk_{fiber} as a function of the number of assembled nucleosomes for 14 different tethered 167-NRL chromatin fibers is shown in Fig. 4.1C (inset), wherein we included a correction of $\Delta Lk = -0.4$ per tetrasome present [43]. The slope of a linear fit to this data yielded a more accurate measure of the Lk_{fiber} of -1.35 ± 0.02. This is a larger negative number, by -0.35, than the linking number of a single isolated nucleosome [28]. We attribute the more negative linking number per nucleosome to the higher-order structure of the chromatin fiber, in which segments of linker DNA are constrained in such a way as to impart negative chirality to the fibers. In summary, chromatin fibers with 167-NRL thus fold into a left-handed superhelix that does not overwind

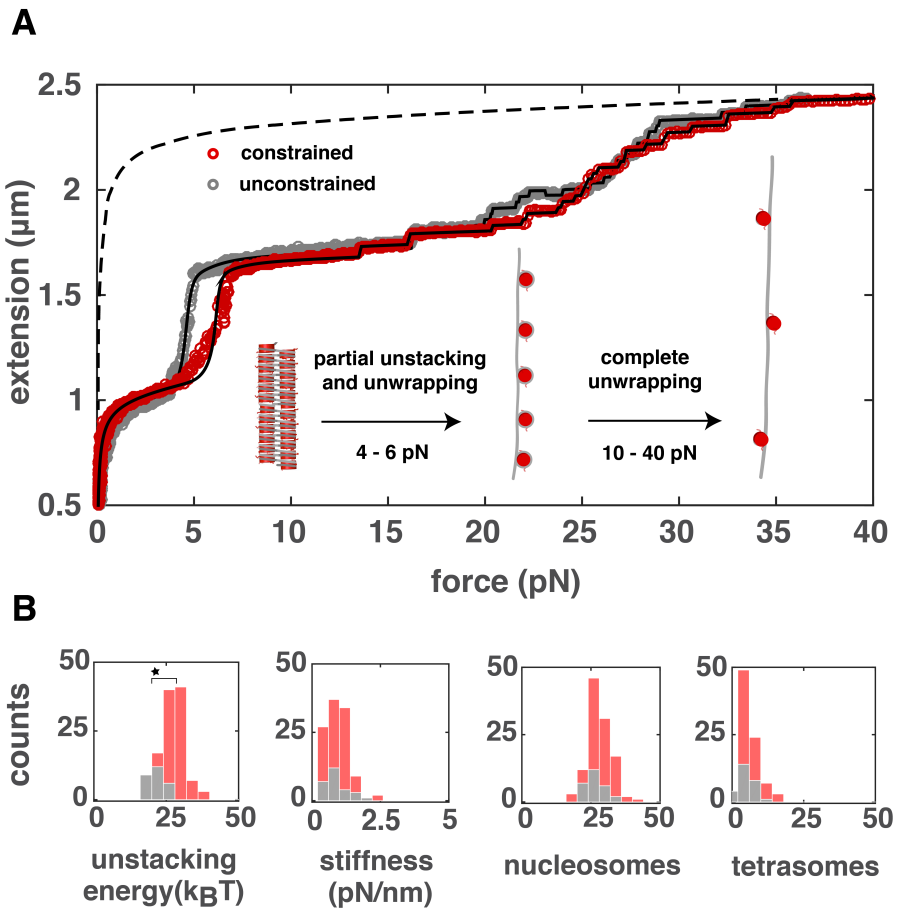

Figure 4.2
The stacking of nucleosomes is stabilized by the presence of rotational constraint.
See the detailed figure caption on the next page.

upon the application of negative turns. Nevertheless, they can be underwound by the application of positive turns until the accumulated torque in the chromatin tether exceeds the DNA buckling torque and plectonemes form in the DNA handles.

4.2.2 Nucleosome unstacking is influenced by torque

The higher-order structure of chromatin fibers is maintained by the stacking interactions between nucleosomes [30, 42]. We compared the forces necessary to rupture these interactions and unwrap DNA from the nucleosomes in rotationally unconstrained chromatin tethers *versus* rotationally constrained ones. The force-induced conformational changes in chromatin fibers with 167-NRL are shown in

Figure 4.2
The stacking of nucleosomes is stabilized by the presence of rotational constraint. **A)** Force-extension (F-E) curves of 167-NRL chromatin fibers assembled on a rotationally constrained (red) or unconstrained (grey) 601-DNA template. Both curves were fit to the statistical mechanics model (black lines) derived in Ref. [39] and briefly summarized in Chapter 2. From these fits, the number of nucleosomes $N_{\text{nucleosomes}}$ and tetrasomes $N_{\text{tetrasomes}}$ in the fibers were determined. These equaled 25 and 1, respectively in both tethers. The F-E response for 7.0 kb DNA according to the WLC model is co-plotted (dashed line). Below 1 pN, the response of the tethers to force reflects the entropic elasticity of the DNA handles that flank the folded chromatin fiber. Subsequently, in a linear regime between 1-4 pN, the stretching elasticity of the fiber dominates the F-E curve. Beyond 4 pN, in the rotationally unconstrained tether, the unstacking transition is observed, which results in a gain in extension of nearly 0.5 μm due to the release of linker DNA between nucleosomes and ∼56 bp of unwrapped DNA per nucleosome. In the rotationally constrained tether, the unstacking transition occurs at a higher force of 6.5 pN. Further increases in force result in a gradual increase in extension (∼ 10 bp per nucleosome) [39] and from ∼ 10 pN onwards, in a step-wise unwrapping of the remaining 80 bp of DNA from each octamer (or tetramer). Beyond 35 pN, the extension of the tether equals that of bare DNA, indicating complete unwrapping of DNA from the nucleosomes. The inset depicts the conformational changes of DNA and chromatin induced by the increasing force. **B)** Distributions of parameters that result from quantitative analysis of rotationally constrained (n = 112, red) and unconstrained (n = 21, grey) 167-NRL fibers with the statistical mechanics model [39]. The fibers contain on average 27 ± 3 and 27 ± 4 assembled core particles (either nucleosomes or tetrasomes), respectively. The deduced stretching stiffnesses of 1.0 ± 0.5 (for rotationally constrained fibers) and 0.9 ± 0.4 pN/nm (for rotationally unconstrained fibers) are similar to those obtained in our previous work [39, 42]. The mean unstacking energy of 27 ± 4 $k_{\text{B}}T$ in rotationally constrained fibers is significantly larger (p-value = 0.05) than in unconstrained fibers (21 ± 2 $k_{\text{B}}T$).

Fig. 4.2A. The unfolding profiles below 4 pN are identical both in rotationally unconstrained (grey) and constrained molecules (red), indicating that the fiber compliances remain the same. The profiles diverge, however, in the range of 4 - 6 pN. Here, the abrupt increase in extension (by nearly 0.5 μm) is associated with the unstacking transition, which comprises unstacking of nucleosomes, release of linker DNA and unwrapping of 56 bp of DNA per nucleosome [39]. Notably, a higher force (by nearly 2 pN) was required to rupture nucleosome-nucleosome interactions in the rotationally constrained tether relative to the unconstrained one. At higher forces between 13 - 35 pN, the remaining wrapped DNA was released in discrete steps in a manner that was independent of rotational constraint.

Fitting the force-extension curves of rotationally constrained and unconstrained 167-NRL fibers to a previously developed statistical mechanics model [39] yielded the number of nucleosomes in each chromatin fiber (on average 25), as well as a number of physical parameters that characterize the individual fiber. For example, for rotationally constrained tethers, we obtained an unstacking free energy of 27 ± 4 $k_{\text{B}}T$ (n = 112), compared to 21 ± 2 $k_{\text{B}}T$ for unconstrained tethers (n = 21) (Fig. 4.2B). In the low force regime, the stretching stiffness of the chromatin fibers equaled 1 ± 0.5 pN/nm (mean ± SD) in the presence

of rotational constraint, and 0.9 ± 0.4 pN/nm without. In this regime, the extension of 167-NRL fibers is unaffected by the presence of rotational constraint. For 197-NRL fibers, we report similar findings compared to 167-NRL fibers. For example, attaining the unstacking transition required a higher force by nearly 2 pN relative to rotationally unconstrained fibers (Fig. S2A). The stretching stiffness (0.2 ± 0.1 pN/nm), previously measured on rotationally unconstrained fibers to be smaller than that of 167-NRL fibers due to the different geometry of their higher order structure [39, 42], is found to be independent of torsional constraint (Fig. S2B).

Overall, the primary consequence of torsional constraint in the context of stretching was the higher force necessary to induce chromatin fiber unstacking. This can be understood by considering that the rupture of internucleosomal contacts in a rotationally constrained folded chromatin fiber must be accompanied by a large decrease in its writhe. At fixed linking number, this must be compensated by increased twist in the DNA handles. It thus appears that the high energy cost of over-twisting DNA will delay the onset of the unstacking transition but does not alter the unwrapping of the last turn of DNA from nucleosomes once it does occur.

4.2.3 Positive twist can stabilize and destabilize chromatin fibers

We have further characterized the response of chromatin fibers to torsion by twisting fibers at three different forces. Prior to twisting, we performed a stretching experiment, as described above, to assess the fiber composition. For example, by fitting the force-extension curve of the 167-NRL fiber in Fig. 4.3A, we inferred that it contained 30 (± 2) nucleosomes and remained fully folded at forces below 4 pN. The application of turns at the lowest force of 0.5 pN (Fig. 4.3B, orange) resulted in the asymmetric rotation-extension curve comparable to the one presented in Fig. 4.1C (red). The same phenomenon was observed when positive turns were applied at 2 pN (Fig. 4.3B, dark red). Also here, the extension remained constant up to 25 positive turns, suggesting that the induced twist was absorbed by the chromatin fiber. Only when a larger number of turns was applied, *i.e.* $\Delta Lk > 25$, did the tether extension shortened, suggestive of the formation of DNA plectonemes in the DNA handles. The application of negative turns at a force of 2 pN did not affect the tether extension. Assuming that the chromatin fiber also does not accommodate negative twist at this force, this would be consistent with the well-established torque-induced melting (or denaturation) of the DNA helix in the flanking handles [48].

To obtain more insight into the origin of the torsional plasticity of chromatin fibers, we performed direct torque measurements (plotted *versus* the number of applied turns) on the chromatin tether at the same force of 2 pN (Fig. 4.3D). For comparison, the anticipated build-up of torque in a bare DNA tether is shown

as a dotted line (separately measured data presented in Fig. S6C). In short, for bare DNA the application of either positive or negative turns resulted in the build-up of twist in the molecule and a concomitant increase in torque. At negative turns, once the torque equaled the denaturation torque, it saturated and remained constant. At positive turns, once the torque equaled the (force-dependent) critical torque for buckling, it also saturated. For the chromatin tether, we observed that at positive turns the build-up of torque proceeded more slowly compared to bare DNA. Even after the application of 30 turns, the chromatin tether had accumulated less than 10 pN·nm of torque, whereas at the same force, the application of only 7 turns to bare DNA would yield a torque of 17 pN·nm. Frequently, the build-up of torque in the chromatin tether was preceded by a near-zero torque plateau (that could last up to $\sim$ 20 positive turns). In contrast, the build-up of torque at negative turns closely followed that of the torque curve for bare DNA. This indicates, as did the rotation-extension experiments at the same force, that the application of negative turns to chromatin tethers translates into the build-up of torque in the DNA handles.

When we continued to probe the response of chromatin fibers to the rotation, but now under an applied force of 5 pN, different signatures were observed (Fig. 4.3B, light red). Upon applying positive turns, the tether extension was found to increase, until at 18 turns a maximal length was reached. This length corresponded to that of a fully unstacked fiber (compare maximal lengths in Fig. 4.3A, B). Subsequently, further application of turns resulted in shortening of the tether. This we attribute to the restacking of nucleosomes into a folded fiber. Thus, the unstacking transition of chromatin is facilitated by the application of positive turns, but excessive positive turns restabilize nucleosome stacking and the reassembly of chromatin higher-order structure.

The folding of the chromatin fiber at excessive twist was confirmed in a separate experiment in which the fiber was pre-twisted in the positive direction prior to a pulling and release cycle (Fig. S3A). Under these conditions, the unstacking transition occurred at lower force at $\Delta Lk = +10$ than at $\Delta Lk = 0$ (consistent with a reduction in the nucleosome unstacking force), whereas at $\Delta Lk = +20$ turns the unstacking force increased again (consistent with a re-introduction of nucleosome stacking). In contrast, the unstacking force was not affected by the application of negative turns (Fig. S3B). These two experiments, performed either at constant force or at constant twist, reveal an interesting property of chromatin fibers: initially, the application of positive twist decreases the extent to which fibers are folded, but the application of a larger number of positive turns, *i.e* >1 turn per nucleosome, refolds the fiber into a condensed state with newly stacked nucleosomes.

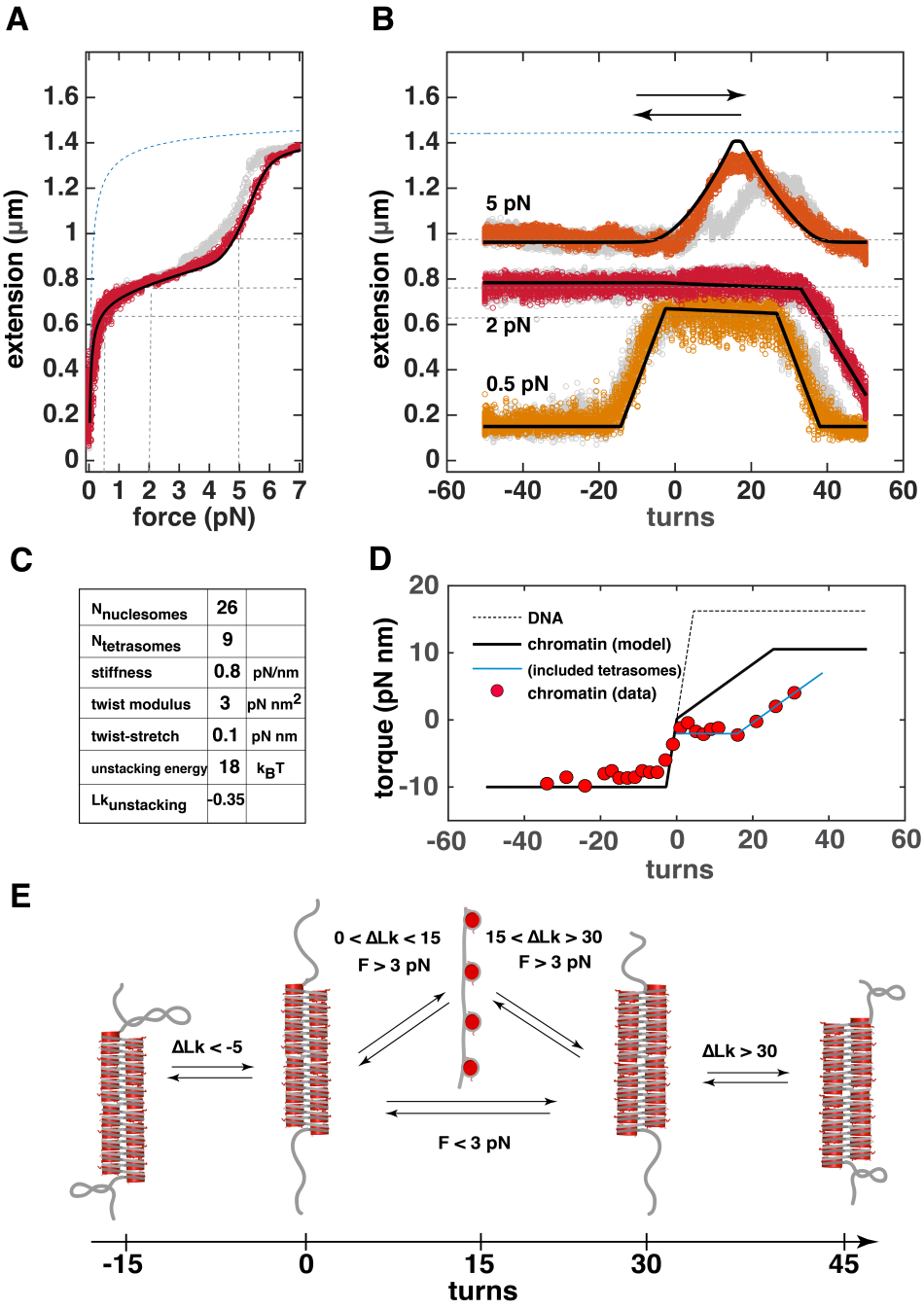

Figure 4.3
167-NRL fibers fold into a left-handed two-start helix that refolds upon the application of excess positive turns. See the figure caption on the next page.

Figure 4.3
167-NRL fibers fold into a left-handed two-start helix that refolds upon the application of excess positive turns. A) Force-extension curve of a rotationally constrained 30·167 chromatin fiber. The initially compacted fiber is stretched under force (red) and observed to unstack at 5.5 pN. When the force is subsequently decreased, the fiber is observed to refold to its initial configuration (grey). The solid black line reflects the best fit to the statistical mechanics model with $N_{\text{nucleosomes}} = 26, N_{\text{tetrasomes}} = 9$, unstacking energy $\Delta G_1 = 18\ k_{\text{B}}T$ and stretching stiffness per nucleosome $c_s = 0.7$ pN/nm, in line with the results shown in Figure 4.2B. The dashed blue line reflects the extension of a DNA template with singly wrapped nucleosomes. The dashed black lines mark the forces and extensions examined during the subsequent rotation experiment. **B)** Rotation-extension curves of the same molecule as in panel A at forces of 0.5 pN (orange), 2 pN (dark red) and 5 pN (light red). Grey curves reflect the measurements with a reversed direction of magnet rotation. Solid black lines reflect the torsional spring model using the parameters described in panel A together with a torsional stiffness $c_t = 3 \pm 1$ pN·nm^2 and a twist-stretch coupling constant $c_{ts} = 0.1$ pN·nm. At 0.5 pN, the extension of the fiber initially remains nearly constant upon the application of positive turns. Beyond +25 turns or - 5 turns, the tether is observed to shorten. Similarly, at 2 pN little length reduction is initially observed, suggesting that the positive twist is absorbed by the chromatin fibers. The application of negative turns at a force of 2 pN did not affect the tether extension consistent with torque-induced melting of the DNA handles. At 5 pN, the response of the fiber to rotation exhibits an apex at +18 turns equal to the extension of the tether at 7 pN (panel A), consistent with twist-induced unstacking (see main text). Further application of positive turns again reduces the extension of the fiber, consistent with its restacking (see main text). **C)** Table summarizing the parameters used in the quantification of curves in panels A and B. **D)** Representative torque-twist measurement on a 167-NRL chromatin fiber at 2 pN (red). Data was offset to equate the torque plateau at negative twist with the DNA melting torque of -10 pN·nm. The dotted grey line represents the predicted torque build-up in the DNA handles alone. The solid black line shows the restoring torque of the DNA-fiber tether quantified with a torsional model yielding a torsional stiffness $k_t = 3$ pN·nm^2. The solid blue line is the prognozed torque that includes a correction for twist in tetrasomes. In the experiment, upon the application of positive twist, the torque in the fiber is initially constant and increases linearly after >15 turns. The slope of the torque upon the application of the negative turns closely follows that of the predicted torque curve for bare DNA. **E)** Schematic summarizing the aforementioned structural changes in the DNA-chromatin tether under torsion. Torsionally relaxed 167-NRL fiber (twist = 0) cannot absorb negative turns, and as such the entire linking number change is absorbed by the DNA handles. The consequences of imposed positive twist depend on the level of tension and may involve unstacking of chromatin fiber followed by changes in its chirality. This delays the formation of DNA plectonemes compared to negative twist.

4.2.4 The torsional modulus of chromatin fibers can be determined experimentally and computationally

To quantify the observed response of chromatin tethers to imposed turns, we analyzed the rotation-extension curves with a torsional spring model. To extract mechanical parameters that specifically describe the chromatin fiber, we separated out the contribution of the DNA handles from that of the fiber. To do so, we first quantified the measured rotation-extension curves of a bare DNA molecule (Fig. S6B) with approximately the same contour length as the DNA handles (1.9 kb). We employed the formulas based on Refs. [51, 52] (Supplementary Information) and captured the under-winding, over-winding and buckling transitions of DNA using fixed values of the contour length L (646 nm), the stretch persistence length P (50 nm), the intrinsic (force-independent) twist persistence length C (100 nm) and the twist persistence length of plectonemic DNA C_p (24 nm). The effective (force-dependent) twist persistence length of DNA, C_t, was expressed as: $C_t = \left(1 - \frac{C}{4P}\sqrt{\frac{k_\mathrm{B}T}{PF}}\right)$, where F is the applied force, k_B is the Boltzmann constant, and T is the temperature. We next independently measured the effective torsional stiffness of DNA using magnetic torque tweezers (Fig. S5). Fits of the linear regime yielded a torsional persistence length of 79 ± 5 nm at 1.7 ± 0.3 pN (Fig. S6D) (see Supplementary Information and Fig. S7 for torque data with corresponding force-extension curves of DNA), in agreement with previous observations [53]. This result was furthermore in agreement with the torsional stiffness employed to model the rotation-extension curves (Fig. S6B). We subsequently employed the parameters deduced from these two complementary approaches to deduce the torsional properties of chromatin fiber.

Our torsional spring model is based on a statistical mechanics framework that describes chromatin unfolding [39]. Here, we extend the previously described model by taking into account the supercoiling of rotationally constrained DNA handles, and the twisting of the chromatin fiber. In brief (see Supplementary Information and Fig. S8 for further details), the model distributes the applied twist (ΔLk) between the DNA handles (ΔLk_DNA) and the chromatin fiber (ΔLk_fiber). Under the assumption that an equal torque $\mathcal{T}$ acts both on the chromatin fiber and the DNA handles, the change in linking number ΔLk is distributed between these two components in a manner governed by their torsional properties:

$$\begin{aligned} \mathcal{T} &= \mathcal{T}_\mathrm{fiber} = \mathcal{T}_\mathrm{DNA} \\ \Delta Lk_\mathrm{fiber}(\Delta Lk, \mathcal{T}) &= \Delta Lk - \Delta Lk_\mathrm{DNA}(\Delta Lk, \mathcal{T}) \end{aligned} \tag{4.1}$$

The torsional spring model describes the chromatin fiber as a Hookean torsional spring characterized by several parameters: c_t - the twist modulus of the fiber per nucleosome ($\mathrm{pN} \cdot \mathrm{nm}^2$); N - the number of nucleosomes in a fiber;

nucleosomes	tetrasomes	unstacking energy (k_BT)	stiffness pN/nm	twist modulus pN·nm^2	ΔLk_{stack}
32	8	18	0.8	4	-0.35
32	4	24	1.3	4	-0.35
32	10	21	1.1	4	-0.35
29	2	25	1.2	4	-0.35
30	4	23	0.7	4	-0.3
29	7	25	1.2	3	-0.35
29	7	24	1.2	4	-0.35
29	10	24	1.2	3.5	-0.35
34	13	24	1.2	3.5	-0.35
28	10	20	0.6	4	-0.35

Table 4.1
Parameters from the quantitative analysis of ten individual 167-NRL fibers with the torsional spring model.

z_0 - the extension per single nucleosome, which is about 1.5 nm [52]. In addition, we included a twist-stretch coupling modulus for the chromatin fiber.

The DNA handles were described by a separate set of parameters, as described above. We used these parameters to quantify the change in the linking number of the DNA handles in the chromatin tether by employing the dependence (derived in the Supplementary Information):

$$\Delta Lk_{\mathrm{DNA}} = \frac{Lc_t}{Nz_0C_tk_{\mathrm{B}}T + Lc_t}\Delta Lk \tag{4.2}$$

Once the $\Delta Lk_{\mathrm{fiber}}$ and ΔLk_{DNA} were established, the torsional spring model allowed to analyze the rotation-extension curves of chromatin tethers of a known number of nucleosomes N. By varying the twist modulus c_t of the chromatin fiber, the applied turns were differently distributed between the fiber and DNA handles. We obtained the best match with the data in Fig. 4.3B using a twist-stretch coupling factor of 0.1 pN·nm and the following force-dependent values of the effective chromatin fiber twist modulus: $c_t = 2$ pN · nm^2 at 0.5 pN and 3 pN · nm^2 at 2 pN and 4 pN · nm^2 at 5 pN. As shown in Fig. S8, smaller (larger) values of the twist modulus c_t delayed (expedited) the buckling transition of the DNA handles. These results, divided by the value of k_BT at room temperature (4.1 pN · nm), yield a torsional persistence length of $\sim$ 1 nm, which is hundred times lower than that of DNA. The values of the twist modulus and persistence length, obtained by modelling experimental rotation-extension curves in the extension regime wherein nucleosome remain stacked, indicate that chromatin fibers feature high torsional flexibility.

Lastly, to describe the unstacking and restacking observed in the rotation-extension curve at 5 pN, we included the chromatin handedness (deduced from the asymmetry of the rotation curve) in the energy term of the torsional Hookean

spring (see Supplementary Section 4.5.4). By setting the unstacking energy to 18 k_BT (Fig. 4.2B), a value close to that measured for rotationally unconstrained fibers, we deduced the linking number change per the unstacked pair of nucleosomes. The modelled curve at 5 pN (Fig. 4.3B, light red) accurately captures the unstacking and restacking transition, including the characteristic peak in the curve, when the value of $\Delta Lk_{\text{unstack}}$ is set to -0.4. This is consistent with the value deduced from the heparin experiment (see Discussion and the overview of parameters of ten independent 167-NRL fibers in Table 4.1). Overall, from applying the torsional spring model to the data, we observed that all fibers display a similarly high torsional flexibility.

4.2.5 The response of chromatin fibers to torsion does not vary with NRL

We have also examined several aspects of the torsional response of 197-NRL fibers. As for 167-NRL fibers, we studied the force-induced unfolding of rotationally constrained fibers both in a relaxed state (Fig. S2) and in the presence of supercoiling (Fig. S4). We also measured the extensions and torques in these fibers at constant force and under excessive linking number change (Fig. 4.4B, D). As for 167-NRL fibers, we applied a torsional spring model to the data and deduced whether the distinct fiber geometry, resulting from the longer Nucleosome Repeat Length, resulted in altered torsional properties.

In the stretching experiments, we observed that the stiffness of rotationally constrained 197-NRL fibers (0.2 ± 0.1 pN/nm) was the same as in the rotationally unconstrained tethers (Fig. S2B). More importantly, these values were on average 3 times smaller than in 167-NRL chromatin fibers. In earlier work, we attributed this compliance to the stretching of a one-start, solenoidal helix which has a lower stiffness relative to a two-start zig-zag fiber [39, 42]. Although the stretching properties of these fibers appear to be different, the application of turns impacted the 197-NRL fibers in a similar manner as 167-NRL fibers. Fig. 4.4B shows that the 197-NRL fiber also absorbed positive twist and exhibited the properties of a left-handed superhelix with a twist modulus of $c_t = 1$ pN $\cdot$ nm^2 at 0.5 pN, $c_t = 2$ pN $\cdot$ nm^2 at 1.5 pN, and $c_t = 3$ pN $\cdot$ nm^2 at 3.5 pN, which makes them slightly more compliant than 167-NRL fibers. We observed, however, that the tether length slowly decreased when positive twist was applied at low tension. We could capture this behaviour by invoking a twist-stretch coupling factor of 0.8 pN $\cdot$ nm. Thus, quantitative analysis of 197-NRL fibers indicates that its torsional flexibility exceeds that of 167-NRL fibers. This reduced torsional stiffness was supported by direct torque measurements that exhibited a very shallow slope in the positive torque regime (Fig. 4.4D). Overall, despite differences in higher-order structures, the values of c_t differ only slightly between 167-NRL and 197-NRL fibers. As a result, the large compliancy of chromatin fiber to twist appears to be universal, irrespective of its higher-order structure.

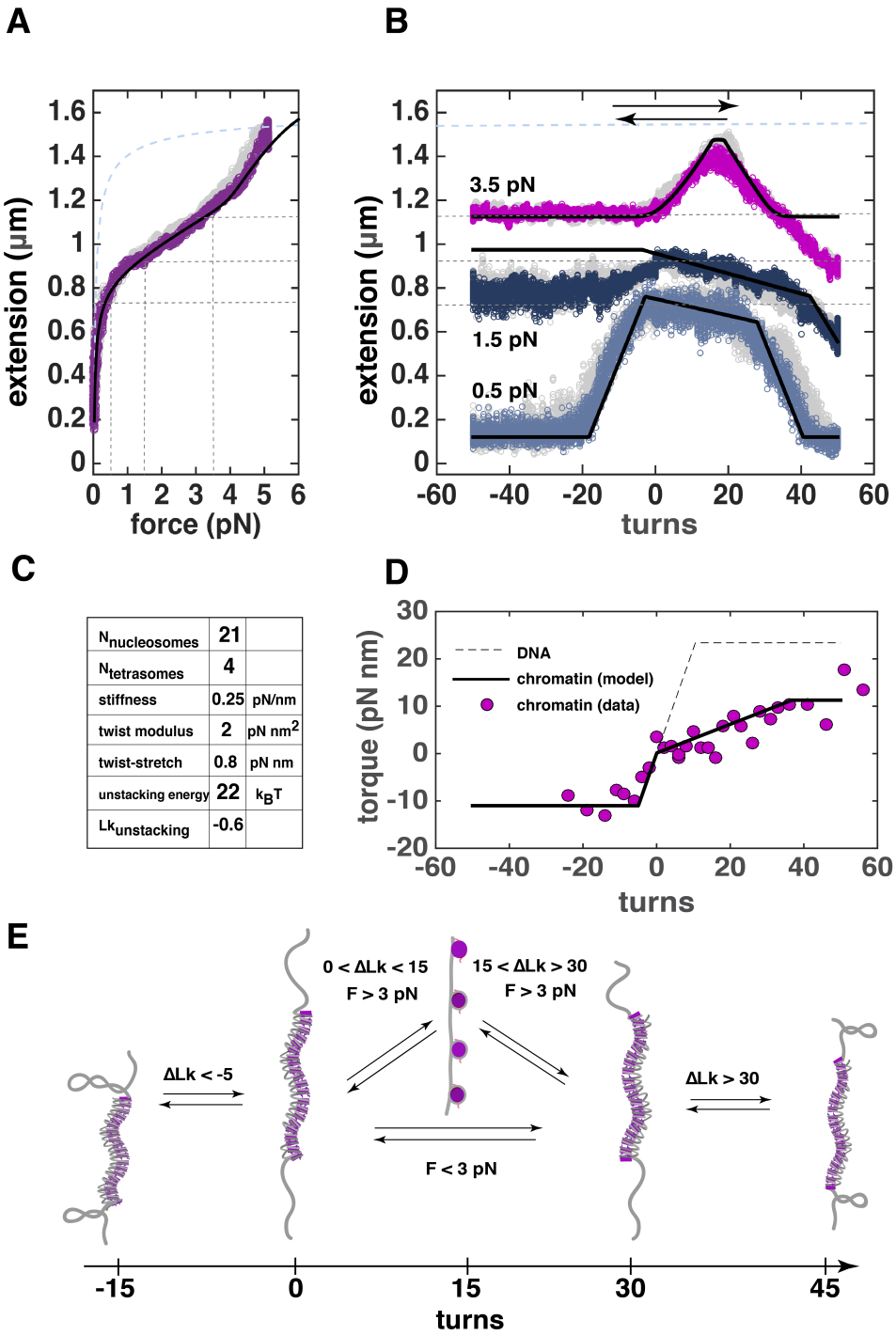

$N_{nucleosomes}$	21	
$N_{tetrasomes}$	4	
stiffness	0.25	pN/nm
twist modulus	2	pN nm^2
twist-stretch	0.8	pN nm
unstacking energy	22	k_BT
$Lk_{unstacking}$	-0.6	

Figure 4.4
197-NRL fibers fold into a left-handed, one-start fiber that responds similarly to torsion as the 167-NRL fibers See the figure caption on the next page.

Figure 4.4
197-NRL fibers fold into a left-handed, one-start fiber that responds similarly to torsion as the 167-NRL fibers. A) Force-extension curve of a rotationally constrained 25·197 chromatin fiber. The initially compacted fiber is stretched under force (violet) and observed to unstack at 4.5 pN. When the force is subsequently decreased, the fiber is observed to refold to its initial configuration (grey). The solid black line reflects the best fit to the statistical mechanics model with: $N_{\text{nucleosomes}} = 21, N_{\text{tetrasomes}} = 4$, unstacking energy $\Delta G_1 = 22\ k_{\text{B}}T$ and stretching stiffness per nuclesome $c_s = 0.25$ pN/nm. The dashed blue line reflects the extension of a DNA template with partially wrapped nucleosomes. The dashed black lines mark the forces and extensions examined during the subsequent rotation experiment. **B)** Rotation-extension curves of the same molecule as in panel A at forces of 0.5 pN (blue), 1.5 pN (dark grey) and 3.5 pN (pink). Grey curves reflect the measurements with a reversed direction of magnet rotation. Solid black lines reflects the torsional spring model using the parameters described in panel A together with a torsional stiffness $c_t = 2 \pm 1$ pN·nm^2 and twist-stretch coupling constant $c_{ts} = 0.8$ pN·nm. As in 167-NRL fibers, at 0.5 pN, the extension of the 197-NRL fiber initially remains nearly constant upon the application of positive turns. Beyond +25 turns or -5 turns, the tether is observed to shorten. The same occurs beyond 5 negative turns. At 2 pN a small reduction in extension is initially observed upon the application of positive twist, followed by the supercoiling of the DNA handles. The application of negative turns did not affect the extension of the tether. At 5 pN, the response of the fiber to rotation exhibits an apex at +19 positive turns whose extension equals the extension of the untwisted tether at 7 pN (panel A), consistent with twist-induced unstacking of the fiber (see main text). Further application of positive turns again reduces the extension of the fiber, consistent with its restacking (see main text). **C)** Table summarizing the parameters used in the quantification of curves in panels A and B. **D)** Representative torque-twist measurement on a 197-NRL chromatin fiber at 2 pN (violet). Data was offset to equate the torque plateau at negative twist with the DNA melting torque of -10 pN·nm. The dotted grey line represents the predicted torque build-up in the DNA handles alone. The solid black line shows the restoring torque of the DNA-fiber tether quantified with a torsional spring model yielding a torsional stiffness $k_t = 2$ pN·nm^2. In the experiment, upon the application of positive turns, the torque in the fiber increases slowly. The slope of the torque curve upon the application of negative turns closely follows that of the predicted torque curves for bare DNA. **E)** Schematic summarizing the aforementioned structural changes in a DNA-chromatin tether under torsion. Torsionally relaxed 197-NRL fiber (twist = 0) cannot absorb negative turns, and as such the entire linking number change is absorbed by the DNA handles. The consequences of imposed positive twist depend on the level of tension and may involve unstacking of nucleosomes in the chromatin fiber followed by changes in its chirality. This delays the formation of DNA plectonemes compared to negative twist.

4.3 Discussion and conclusions

The supercoiling of DNA is a fundamental factor in regulating gene expression and affecting chromatin structure [54], even in the presence of topoisomerases that neutralize some of the torsional stress *in vivo* [55–57]. Here, we have employed single-molecule studies to present a comprehensive characterization of compact chromatin fibers under tension and torsion. Our study of rotationally constrained chromatin fibers goes beyond previous single-molecule assays that focused on the dynamics of non-interacting nucleosomes [43, 45, 46]. Here, we have extensively probed the mechanical aspects of higher-order structures of

chromatin maintained by nucleosome-nucleosome interactions.
In contrast to these previous studies, our force-extension and rotation-extension measurements at forces below 4 pN exhibited no hysteresis between forward and backward stretching or twisting cycles. In particular, we observed the elastic, anisotropic response under rotational constraint of two types of fibers, 167- and 197-NRL, which were previously shown to fold into two-start and one-start conformations, respectively. We demonstrated that both fibers adopt a left-handed chirality and are capable of absorbing positive twist. In this way, the nucleosomes in chromatin fibers are protected from unstacking at forces below 5 pN and torques below 10 pN·nm. A remarkable observation is that continued application of positive twist resulted in twist-induced unstacking of chromatin, followed by refolding of the chromatin fiber. Overall, we find that the structure adopted by stacked nucleosomes allows for the effective absorption of twist. This implies that chromatin fiber constitutes a topological buffer that can absorb some tension and torsion without decompacting the nucleosome-wrapped DNA. We therefore propose that the secondary structure of chromatin can thus influence the *in vivo* dynamics of DNA processing by enzymatic motors that induce its supercoiling by keeping chromatin unfolding local, and thereby it plays an important role in controlling gene expression.

To ascertain that our samples folded into compact chromatin fibers, we carefully evaluated the effect of nucleosome-nucleosome interactions on the topology of the DNA in a chromatin fiber. To quantify the chirality, we defined the linking number per nucleosome in a folded fiber as: $Lk_{\mathrm{fiber}} = \Delta Lk_{\mathrm{nuc}} + \Delta Lk_{\mathrm{stack}}$. Although each nucleosome contains 1.7 turns of DNA, the linking number of a single nucleosome (ΔLk_{nuc}) in isolation has been measured to equal -1 in biochemical experiments [28]. Direct measurement of the linking number change upon assembly of individual nucleosomes [43] in freely-orbiting magnetic tweezers [58] revealed $\Delta Lk_{\mathrm{nuc}} = -1.2 \pm 0.3$ turns. Bancaud *et al.* measured the change in linking number upon histone disassembly from an array of non-interacting nucleosomes and reported $\Delta Lk_{\mathrm{nuc}} = -0.8 \pm 0.1$ turns [45]. In our single-molecule assay, in which we ensured via the use of appropriate salt concentrations that nucleosomes were properly stacked into a folded fiber, we directly measured for Lk_{fiber}, which we found to equal -1.35 ± 0.02 (Fig. S1) in 167-NRL fibers. We attribute this extra negative twist, relative to ΔLk_{nuc}, to the additional looping in the folded fiber that results in superhelix formation. In a 167-NRL fiber, which folds into a left-handed zig-zag superhelix, the linker DNA crosses back and forth between the two stacks of nucleosomes. This implies that a full turn of the linker DNA is constrained by a pair of nucleosomes, from which one would predict $\Delta Lk_{\mathrm{stack}} = \frac{-1}{2} = -0.5$. By subtracting the established $\Delta Lk_{\mathrm{nuc}} = -1$ from the obtained $Lk_{\mathrm{fiber}} = -1.35$ (inset Fig. 4.1C), we measured the linking number change of the linker DNA as $\Delta Lk_{\mathrm{stack}} = -0.35$, which is close to the predicted value, and the difference could be accommodated by undertwisting the linker DNA. Overall, this interpretation is compatible with

a superhelical folding of nucleosomal arrays into a zig-zag fiber mediated by the H4-tail internucleosomal contacts. Such bridging, confirmed in our previous single-molecule experiments with H4-tails cross-linked to the acidic patch of H2A [42], stabilizes the looping of the DNA that we showed here quantitatively.

In parallel, we analyzed the linking number Lk_{fiber} of 167-NRL fibers by modelled and experimentally obtained rotation-extension curves. By using a torsional spring model, we inferred a very similar value of $\Delta Lk_{\mathrm{stack}} \cong -0.4$ (Table 4.1). As explained in Fig. S8, this parameter was confirmed by analyzing the rotation-extension curves at forces above 3 pN. The largest extensions observed in these measurements (Fig. 4.3B) equalled those measured in force-extension curves at 7 pN (Fig. 4.3A), which is the regime of an unstacked array of singly wrapped octamers or tetramers. Knowing the composition of the fiber (Fig. 4.3C), it follows that 18 positive turns were necessary to induce the unstacking of the 167-NRL chromatin with 26 nucleosomes (Fig. 4.3B). This results in an estimation of $\Delta Lk_{\mathrm{stack}} = \frac{18}{-26} = -0.7$. This value is larger than those inferred from a torsional spring model or from the shift in the rotation curve, presumably because the twist absorbed by the DNA handles is not taken into account in this simple estimation. Other uncertainties, irrespective of the approach, arise from the unknown helical twist of the linker DNA between consecutive nucleosomes in the folded fiber and the aforementioned linking number paradox. Nevertheless, our three different estimations all yield a negative linking number of the looped linker DNA, which underscores the left-handed chirality of chromatin fibers.

Further analysis of the rotation-extension curves at tension above 3 pN reveals a remarkable phenomenon of a twist-induced refolding of the unstacked chromatin fiber. We observed in two separate assays that excessive positive twist refolds both the two-start fiber (Fig. 4.3B and Fig. S3) and the one-start fiber (Fig. 4.4B and Fig. S4). Thus, at sufficient force (> 3 pN), the unstacking transition appears to be reversed by torque in an unprecedented manner. The structure of such over-twisted fibers may involve the formation of the so-called reversomes (speculative right-handed nucleosomes [59]) or even the reconfiguration of the entire left-handed chromatin fiber to a superhelix with opposite handedness. Importantly, the tensions and torques involved in this phenomenon are appropriate to the *in vivo* context, as they are within the range accessible to, for example, RNA polymerases [60]. Possibly, such twist-induced refolding could be a functional event during transcription termination; however, further studies are necessary to unravel more details of this striking unstacking-restacking transition.

Although we observed that the extension and the stiffness of both 167- and 197-NRL fibers were unaffected by the presence of a rotational constraint, nonetheless an increased force was required to achieve the unstacking. This effect derives predominantly from the high torsional stiffness of the DNA handles, that need to accommodate the released twist, rather than from an inherently stronger interaction between the nucleosomes themselves. As a result, the large

linking number stored in the fiber (Lk_{fiber}) cannot freely dissipate (*e.g* by swiveling the ends of DNA handles) when a rotationally constrained tether is unfolded. By subtracting the fitted unstacking energy of unconstrained fibers (21 k_BT) from that of constrained fibers (27 k_BT), we estimated $\sim$ 6 k_BT of energy required for the over-twisting of DNA handles [39] (Fig. 4.2B and Fig. S2B). In our extended torsional spring model that includes the change in linking number, we uncoupled the contribution of the DNA handles from the entire tether, and obtained a good match between the data and the model with the unstacking energy of 18 $\pm$ 2 k_BT and 22 $\pm$ 2 k_BT for 167-NRL and 197-NRL fibers, respectively (Fig. 4.3C and Fig. 4.4C), which are consistent with values reported earlier for unconstrained fibers. Overall, our quantitative analysis of chromatin unfolding captures many previously undisclosed aspects of chromatin structure, including the rotational reconfiguration within the fiber.

We also quantitatively analyzed the elastic response of chromatin at low force regime, in which stacked nucleosomes maintain the higher-order structure. The measured torsional stiffness of folded chromatin fibers appears to be dramatically smaller than that of bare DNA. The torsional modulus per nucleosome, obtained by the model, translates to a torsional persistence length of $\sim$ 1 nm, which is about hundred times shorter than that of DNA. Such torsional plasticity means that chromatin can absorb large twists without building up much torque. This was supported by direct torque measurements in which positive twist applied to the chromatin tether resulted in a smaller build-up of torque than in bare DNA. A maximal torque of $\sim$ 10 pN $\cdot$ nm was reached at $\sim$ +25 turns, after which supercoiling of the DNA handles ensued, as evident from the reduction of the tether length. The torque threshold is lower than that generated by polymerases (15 pN $\cdot$ nm) [60], suggesting that torsional stress alone cannot induce chromatin unfolding. The slow build-up of torque in chromatin was, in some fibers, enhanced by the presence of a near zero-torque plateau in the first positive 10-15 turns. This could not be attributed to the disassembly of histones, since no simultaneous change in extension was observed (Fig. S9 and Fig. S10). We interpret this plateau regime as a transition of free tetrasomes (as shown by Vlijm *et al.* [43]) that reside on the DNA handles of our reconstituted fibers. We previously proposed that tetrasomes can by themselves constitute a torque reservoir [61], and it appears that this effect matters also in the presence of folded chromatin fibers. Upon correction of the torsional spring model with tetrasomes, the modelled curves (Fig. 4.3D) well align with the experimental data and reinforce the goodness of our torsional spring model.

Lastly, we point out how the aforementioned free tetrasomes were also able to affect the dynamics of plectoneme formation in the handles of chromatin tethers. To fit the bare DNA rotation curves (Fig. S6), we modelled the plectonemic DNA with a twist persistence length C_p of 24 nm [51, 52] (see Supplementary Information). To properly describe the slope in the rotation-extension curves of chromatin tethers at large twist (Fig. 4.3B and 4.4B), however, we had

to decrease the twist persistence length of plectonemic DNA to $C_p = 12$ nm, suggesting a reduction in the diameter of the supercoils. We attribute this decreased size to the presence of tetrasomes on the DNA handles: wrapping DNA around a tetrasome reduces the plectoneme loop size. It should also reduce the buckling torque, in agreement with the observed buckling transition in the rotation-extension curves of chromatin tethers. Indeed, the torque never reached the buckling torque for bare DNA, *i.e.* $\sim$ 20 pN·nm at 2 pN, as most of the twist was absorbed by the chromatin fiber. Thus, a full description of the behaviour of folded chromatin requires taking into account the effect of nearby tetrasomes.

In this work, we have presented a comprehensive study of chromatin fibers at physiologically relevant levels of tension, torsion, and buffer conditions. Chromatin plays an important role in regulating the dynamics of processes such as DNA transcription or replication, in which supercoiling is generated. The observations reported here highlight a multitude of relaxation mechanisms that chromatin fibers can employ under torsional stress. Our results support the anticipated role of chromatin in the "twin supercoiled domain" model and potentially the higher-order folding of chromatin may locally reinforce this effect. A possible scenario would involve an interplay of a folded chromatin fiber and a less compact array of non-interacting nucleosomes located near the actively transcribed *locus* (Fig. 4.1A). At a short distance from a transcription fork, chromatin is subjected to increasing tension and torque that is generated by the distant molecular motor (*e.g* RNAp). In this situation, the chromatin fiber could buffer the incoming positive supercoiling and facilitate the progression of transcription along the open chromatin in the closest proximity to RNAp. As the polymerase progresses, it may reach stacked nucleosomes and the effective force and torque may become high enough to locally distort the higher-order structure. Our data reveal that the absorption of positive supercoiling by the soft chromatin fiber prevents the global build-up of torque. Nevertheless, locally the force and twist may be sufficient to unstack nucleosomes. The remarkable refolding transition observed at excessive positive torsion may be a self-regulatory response that could function as a transcription repressor for nearby genes.

Based on these findings we propose that the response of chromatin to torsion demonstrated here can be highly relevant at the level of so-called topologically-associated domains (TADs) found *in vivo* [62], which could isolate such torsional buffers in the genome. These structures have been reported as long-distance transductors of torsional stress that was not released by topoisomerases.
Overall, our study indicates that nucleosome stacking significantly impacts the response of chromatin to twist and increases its flexibility. Collectively, the torsional elasticity of the fully folded fibers and the conformational changes of the tetrasomes indicate that large amount of twist can be absorbed *via* structural changes within folded chromatin fibers. All together ensures that torsionally rigid genomic DNA can be efficiently stored in the nucleus and

simultaneously processed during its replication or transcription.

4.4 Materials and methods

4.4.1 DNA constructs and chromatin assembly

Two pUC18 plasmids (Novagen) with multiple tandem repeats of the Widom-601 sequences were used as DNA templates for chromatin reconstitution. Plasmid 1 contained 30 repeats of the Widom-601 sequences spaced with 20 bp linkers (NRL = 167 bp), whereas plasmid 2 contained 25 repeats of the Widom 601-sequences with 50 bp linkers (NRL = 197 bp). Both plasmids were digested with Bsa*I* and Bse*YI*, and the resulting linearized fragments were separated by gel electrophoresis. The bands representing 7040 bp (plasmid 1) and 6955 bp (plasmid 2) DNA (both including ∼2000 bp of non-601 handles) were extracted and purified. In parallel, 600 bp DNA fragments were prepared with PCR on the pUC18 plasmid template using 10% biotin-16-dUTP or digoxigenin-11-dUTP. After amplification, these fragments were digested with Bsa*I* and Bse*YI*, respectively, and ligated to the previously linearized 601-DNA. The exact protocol is described in Ref. [63].
Wild-type human histone octamer (Epicypher) was mixed with labelled 601-DNA arrays and reconstituted into chromatin fibers using salt dialysis as in our previous work. More detailed protocols are available in Ref. [64].

4.4.2 Flow cell preparation

A clean cover slip was coated with 0.1% nitrocellulose (Ladd Research) in amylacetate solution and subsequently mounted onto a polydimethylsiloxane (Dow Corning) flow cell with a pre-cut channel. The flow cell was incubated with 10 ng/μl anti-digoxigenin (Sigma-Aldrich) for 2 h and then passivated with 4% bovine serum albumin (w/v) and 0.1% Tween-20 overnight at 4 °C. Polystyrene reference beads (1 μm, Ademtech) were flushed into the channel and incubated at room temperature for 30 min. Then 20 ng/ml of reconstituted fibers in measurement buffer (100 mM KCl, 2 mM $MgCl_2$, 10mM HEPES, pH 7.5, 10 mM NaN_3, 0.2% BSA, 0.1% Tween-20) was flushed into the flow cell and incubated at room temperature for 10 min. Magnetic beads from stock (either 1 μm diameter MyOne or 2.8 μm diameter M270 streptavidin-coated superparamagnetic beads, Invitrogen) were diluted 1000 times in the measurement buffer and injected into the flow chamber. Finally, untethered beads were flushed out with the measurement buffer. In the experiments with MyOne beads, the measurement buffer enriched with 250 ng/μl heparin was flushed into the flow cell after the force and twist measurements, in order to dissociate histone octamers from the tethered DNA.

4.4.3 Magnetic tweezers

The home-built magnetic tweezers setup used in this study was described previously in Ref. [65]. After mounting the flow cell [64] on the microscope, the sample was illuminated from the top by a LED light (Lumitronix). The transmitted light was collected by a 60× oil-immersion objective (Olympus) and focused onto a CMOS camera (Teledyne Dalsa) operating at an acquisition rate of 58 Hz. The bead position was tracked with nanometer accuracy using a custom-written tracker software [66].

Moving a pair of cubic magnets towards the tethered bead increased the force whereas rotating the magnets changed the degree of supercoiling of the tether (ΔLk) by ± 1 per turn. The applied rotation rate was 1 turn per second. The bead position was tracked in real-time without filtering or averaging. Tethers were initially stretched up to 6 pN and directly refolded to the initial state. Subsequently, selected tethers were supercoiled at 1.5 pN to assess their rotational constraint. Finally, force-extension curves were measured between 0 and 50 pN. The acquired data was analyzed using LabVIEW software by fitting the statistical mechanics model presented in Ref. [39]. Extension-twist curves were analyzed with the torsional spring model (Supplementary Information).

4.4.4 Magnetic torque tweezers

To perform magnetic torque measurements, the pair of cubic magnets was replaced by a cylindrical magnet with a small side magnet attached on it (Fig. S5) as in Ref. [67]. The chromatin fibers were stretched at ~ 2 pN while 10 negative turns were applied. Forces were calibrated for individual tethers as in Ref. [65]. Upon magnet rotation, the bead traced out a circular trajectory, whose center was determined in order to assess the exact attachment point of the DNA to the bead. Using this information, the bead's X,Y coordinates could be translated into radial coordinates to determine subsequently the angular position of the tether [56, 58, 67, 68]. Furthermore, the fluctuations of the relaxed tether were measured to quantify the angular trap stiffness. Finally, a series of measurements was performed in which various degrees of positive or negative twist was applied, while the corresponding shift in the angular position of the bead was measured. The restoring torque present in the tethered molecule could be calculated at each value of the applied turns by multiplying the angular shift by the trap stiffness. The resulting torque curves were offset such that the minimal values of the torques measured equaled the value of the DNA melting torque (-10 pN · nm) [56]. The criteria described in Ref. [67] were used to select torque curves for further analysis.

4.5 Supplementary Information

Here we describe the theoretical framework to describe the influence of torsion on our tether, which consists of a chromatin fiber surrounded by bare DNA handles. The analytical model partitions the linking number change ΔLk between the fiber (ΔLk_{fiber}) and the DNA handles (ΔLk_{DNA}) that was calculated by imposing equal torque in the entire tether:

$$\mathcal{T} = \mathcal{T}_{\text{DNA}} = \mathcal{T}_{\text{fiber}} \tag{4.3}$$

By modelling the rotation-extension curves and the torque-rotation curves such that they well describe the experimental data, we obtain torsional properties of chromatin fibers.

4.5.1 Model of elastic response of DNA to torsion

The behaviour of DNA under torsion can be described by the Worm-Like-Chain (WLC) model with three different, co-existing conformations: twisted, plectonemic and denatured (melted) [52]. We simplify this description by combining the WLC model with one of the dominant conformations of DNA at given linking number density (twisted worm-like-chain, worm-like-chain with plectonemes, or denatured state). Such approximation well captures the properties of DNA at low linking number change, since the coexistence of all three states occurs only in specific force and twist regimes [52] not employed in our experiments.

To describe the extension of DNA under tension and torsion, we derive the free energy of stretched and twisted DNA ($G_{\text{DNA}} = G_{\text{WLC}} + G_{\text{twist}}$) and find the critical linking number change that results in supercoiling or melting of the DNA duplex.

The free energy of twisted DNA is described by a parabolic function:

$$\begin{aligned} \frac{G_{\text{DNA}}(F, \Delta Lk)}{L} &= \frac{G_{\text{WLC}}(F) + G_{\text{twist}}(\Delta Lk)}{L} = \\ &= -\left(F - \sqrt{\frac{F k_{\text{B}} T}{P}}\right) + \frac{k_{\text{B}} T C_t}{2}\left(\frac{2\pi \Delta Lk_{\text{DNA}}}{L}\right)^2 \end{aligned} \tag{4.4}$$

where L is the contour length of the DNA (in nm), F is the force (in pN), $k_{\text{B}}T$ is the thermal energy (4.1 pN $\cdot$ nm at room temperature), P is the bending persistence length of DNA (set to 50 nm), ΔLk_{DNA} is the excess linking number of the DNA, C_t is the effective (force-dependent) twist persistence length: $C_t = C_{lim}(1 - \frac{C_{lim}}{4P}\sqrt{\frac{k_{\text{B}}T}{FP}})$, where C_{lim} is the intrinsic (force-independent) twist persistence length (set to 100 nm).

By taking the derivative of the free energy with respect to force, we can deduce the extension of twisted DNA :

$$\begin{aligned}\frac{z_{\mathrm{DNA}}(F,\Delta Lk)}{L} &= \frac{z_{\mathrm{WLC}}(F)+z_{\mathrm{twist}}(\Delta Lk)}{L} = \\ &= 1-\frac{1}{2}\sqrt{\frac{k_{\mathrm{B}}T}{PF}}-\frac{C^2}{16}\Big(\frac{2\pi\Delta Lk_{\mathrm{DNA}}}{L}\Big)^2\Big(\frac{k_{\mathrm{B}}T}{PF}\Big)^{\frac{3}{2}}\end{aligned} \tag{4.5}$$

Initially, the excess excess linking number will induce the DNA to over-wind or under-wind, leading to the build-up of twist energy. This will generate a torque in the molecule:

$$\mathcal{T}_{\mathrm{DNA}} = C_t\frac{2\pi\Delta Lk_{\mathrm{DNA}}}{L}k_{\mathrm{B}}T \tag{4.6}$$

When a torque reaches a critical value, known as the buckling torque, DNA buckles into a plectonemic conformation with a buckling torque:

$$\mathcal{T}_{\mathrm{buck}} = \sqrt{\frac{2k_{\mathrm{B}}TC_p(F-\sqrt{\frac{Fk_{\mathrm{B}}T}{P}})}{1-\frac{C_p}{C_t}}} \tag{4.7}$$

where C_p is the twist persistence length of plectonemic DNA (set to 24 nm) [51].

By rearranging terms in 4.7, it follows that the maximum excess linking number that can be absorbed by DNA prior to buckling equals:

$$\Delta Lk_{\max} = \frac{\mathcal{T}_{\mathrm{buck}}L}{2\pi k_{\mathrm{B}}TC_t} \tag{4.8}$$

Beyond the buckling torque, the DNA coexists in the twisted and plectonemic conformation. The total extension of the DNA decreases linearly with further applied turns according to:

$$\frac{\Delta z_{\mathrm{DNA}}}{\Delta Lk_{DNA}} = \frac{2\pi\left(1-\frac{1}{2}\sqrt{\frac{k_{\mathrm{B}}T}{PF}}-\frac{C^2}{16C_t^2}\left(\frac{k_{\mathrm{B}}T}{PF}\right)^{\frac{3}{2}}\left(\frac{\mathcal{T}_{\mathrm{buck}}}{k_{\mathrm{B}}T}\right)^2\right)}{\frac{\mathcal{T}_{\mathrm{buck}}}{k_{\mathrm{B}}T}\left(\frac{1}{C_p}-\frac{1}{C_t}\right)} \tag{4.9}$$

As a result, there is an increase of the free energy of plectonemic DNA which equals:

$$\Delta G_{\mathrm{DNA}} = 2\pi\mathcal{T}_{\mathrm{buck}}\Delta Lk_{DNA} \tag{4.10}$$

When negative turns are applied to DNA under low force, it will first underwind and then, at a critical value of torque, it will buckle and form plectonemes, as in the case of positive turns. However, there is an additional critical negative torque, that results in melting (or denaturation) of the DNA duplex. This denaturation torque $\mathcal{T}_{\mathrm{melt}}$, which equals -10 pN $\cdot$ nm [52, 56], limits the build-up of twist energy at negative turns. If the calculated buckling torque (Eq. 4.7) is smaller than the denaturation torque $\mathcal{T}_{\mathrm{melt}}$, the DNA will coexist in twisted and plectonemic conformations. If the buckling torque is higher than -10pN $\cdot$ nm, the DNA will coexist in two different conformations, twisted and melted. For a small linking number density, we consider the extensions of melted and twisted DNA to be identical [52]. By rearranging terms in Eq. 4.7, it follows that the maximum twist that DNA can absorb prior to melting equals:

$$\Delta Lk_{\mathrm{max}} = \frac{\mathcal{T}_{\mathrm{melt}} L}{2\pi k_{\mathrm{B}} T C_t} \tag{4.11}$$

The corresponding free energy gain of melted DNA per turns equals:

$$\Delta G_{\mathrm{DNA}} = 2\pi \mathcal{T}_{\mathrm{melt}} \Delta Lk_{\mathrm{DNA}} \tag{4.12}$$

In summary, when turns are applied, the extension of DNA follows the Eq. 4.5. Beyond the critical point (defined by Eq. 4.8 or Eq. 4.11), this extension reduces linearly with turns (by the factor calculated in Eq. 4.9) or remains constant, respectively. Rotation - extension curves modelled with the aforementioned dependencies and the parameters: $L = 1900$ nm; $P = 50$ nm; $C_{\mathrm{lim}} = 100$ nm and $C_p = 24$ nm well describe the experimental data presented in Fig. S6.

4.5.2 Model of elastic response of chromatin to torsion

Similarly to DNA, we calculate the energy of the chromatin fiber under torsion. A chromatin fiber can be considered as a Hookean spring with an elastic energy that is dependent quadratically on the change in extension and twist:

$$G_{\mathrm{fiber}} = \frac{1}{2}\frac{c_s}{N z_0}(\Delta z_{\mathrm{fiber}})^2 + \frac{1}{2}\frac{c_t}{N z_0}(2\pi \Delta Lk_{\mathrm{fiber}})^2 + \frac{c_c}{N z_0}(\Delta z_{\mathrm{fiber}})(2\pi \Delta Lk_{\mathrm{fiber}}) \tag{4.13}$$

where N is the number of nucleosomes in the fiber, z_0 is the size of a single nucleosome (set to 1.5 nm), c_s is the stretch modulus of the fiber per nucleosome (pN/nm), c_t is the twist modulus of the fiber per nucleosome (pN$\cdot$nm^2), c_c is the twist-stretch coupling of the fiber (pN $\cdot$ nm). The parameter $\Delta z_{\mathrm{fiber}}$ corresponds to the extension change of the chromatin fiber per nucleosome that is induced by force or torque. $\Delta Lk_{\mathrm{fiber}}$ is the excess linking number of the chromatin fiber per nucleosome.

The linking number change will lead to the build-up of twist energy. This will generate a torque in the molecule:

$$\mathcal{T}_{\text{fiber}} = c_t \frac{2\pi \Delta Lk_{\text{fiber}}}{N z_0} \tag{4.14}$$

This dependency allows to infer the torsional stiffness of the chromatin fiber, provided that the linking number change ΔLk_{fiber} and the torque $\mathcal{T}_{fiber}$ is known. In the subsequent section, we describe how to quantify these parameters from the experimental data that comprise the dynamics of chromatin handles and DNA handles.

4.5.3 Distribution of the linking number between the chromatin fiber and DNA handles

In our experiments, the tether consists of a chromatin fiber that is flanked by ~ 2 kbps DNA handles. The total excess linking number exerted by twisting the tether must be distributed between the DNA handles and the chromatin fiber (Fig. S8A). The linking number change in the chromatin fiber is therefore reduced with respect to the total excess linking number due to the presence of DNA handles (Fig. S8B):

$$\begin{aligned} \Delta Lk &= \Delta Lk_{\text{DNA}} + \Delta Lk_{\text{fiber}} \\ \Delta Lk_{\text{fiber}} &= \Delta Lk - \Delta Lk_{\text{DNA}} \end{aligned} \tag{4.15}$$

To calculate how the applied twist is distributed, we combine the Equations 4.3, 4.6 and 4.14. It follows that: :

$$C_t \frac{\Delta Lk_{\text{DNA}}}{L} k_{\text{B}}T = c_t \frac{\Delta Lk_{\text{fiber}}}{N z_0} \tag{4.16}$$

By rearranging terms in the Eq. 4.16 we calculate the twist absorbed by the DNA handles (ΔLk_{DNA}). The simplest dependency (excluding twist-stretch coupling) is then:

$$\Delta Lk_{\text{DNA}} = \frac{L c_t}{N z_0 C_t k_{\text{B}}T + L c_t} \Delta Lk \tag{4.17}$$

This equation for the excess linking number in DNA handles is then combined with Eq. 4.6 to calculate the critical twist that induces supercoiling or denaturation of DNA handles. Due to the presence of a soft chromatin fiber, these transitions will occur at a different excess linking number (ΔLk) than in the case of a tether with DNA only.

Knowing the distribution of the excess linking number (see Eq. 4.15 and Eq. 4.17), and the elastic response of DNA handles and chromatin fiber, we can calculate the extension of the DNA-fiber tether as a function of force and the applied turns:

$$z(F, \Delta Lk, N) = z_{\mathrm{DNA}}(F, \Delta Lk_{\mathrm{DNA}}) + z_{\mathrm{fiber}}(F, \Delta Lk_{\mathrm{fiber}}, N) \tag{4.18}$$

The formula above applies until ΔLk_{DNA} exceeds the critical value defining the buckling or melting transition. Beyond this point, the extension of the tether is determined by attributing the applied turns entirely to the dynamics of plectonemes (as in Eq. 4.9) or the denaturing DNA. Note that the plectoneme growth in the presence of histone proteins was described with a different persistence length C_p (see Discussion). In this regime, the excess linking number will lead to the build-up of energy of supercoiled or melted DNA handles, without generating torque build-up in the chromatin fiber. The resulting change in extension follows:

$$z(F, \Delta Lk, N) = z_{\mathrm{DNA}}(F, \Delta Lk) \tag{4.19}$$

This model is applicable at forces below 3 pN when chromatin fiber remains in its compact state. The application of turns at higher tension (> 3.5 pN) results in the chromatin unstacking and hence the extension of the DNA-chromatin tether. In the next section, we describe how the statistical mechanics model employed in our earlier work [39] is extended to capture the chirality and the twist-induced unstacking of the chromatin fiber.

4.5.4 Computational determination of twist-induced chromatin unstacking

As shown in our experiments, unstacking of chromatin (induced by either force or twist) yields with an increased tether length and a change in the distribution of the linking number between the fiber and DNA handles. Breaking a single nucleosome-nucleosome contact in a 167-NRL fiber leads to an increase in extension of ~ 76 bp (linker DNA and unwrapped first nucleosomal turn) and $\sim +0.4$ change in linking number (as inferred from the experiments with heparin, see Fig. S1) that must be accommodated by the DNA handles. Additionally, the unstacking comes with its own free energy cost, G_u. Here, rather than modelling a two-step unstacking transition as we reported previously in Ref. [39], for simplicity, we model the unstacking transition to consist of a single step. We next calculate the free energy of the stretching of the chromatin fiber and take into account the handedness of the nucleosome and the additional writhe of the linker DNA in the folded chromatin superhelix Lk_{fiber}.

This handedness of the fiber is defined by taking into account the linking number of a single nucleosome and the additional linking number of the linker DNA:

$$Lk_{\mathrm{fiber}} = \Delta Lk_{\mathrm{DNA}} + \Delta Lk_{\mathrm{stack}} \tag{4.20}$$

where ΔLk_{stack} is the linking number of the linker DNA in the chromatin fiber per nucleosome. The free energy of the fiber is then described by the function:

$$G_{\text{fiber total}} = \frac{1}{2}\frac{c_s}{Nz_0}(\Delta z_{\text{fiber}})^2 + \frac{1}{2}\frac{c_t}{Nz_0}(2\pi Lk_{\text{fiber}} + \Delta Lk_{\text{fiber}})^2 + \\ + \frac{c_c}{Nz_0}(\Delta z_{\text{fiber}})(2\pi Lk_{\text{fiber}} + \Delta Lk_{\text{fiber}}) \tag{4.21}$$

We then calculate all probable conformations with the Boltzmann distribution. For a finite number of nucleosomes we can numerically calculate the partition function that includes the energy of the DNA handles and the chromatin fiber:

$$Z = \sum_{i=0}^{N} \binom{N}{i} \exp\left(-\frac{G_{\text{DNA}} + G_{\text{fiber total}} + iG_u - Fz(F, \Delta Lk + iLk_{\text{fiber}}, i)}{k_{\text{B}}T}\right) \tag{4.22}$$

where i is the number of nucleosomes that unfolded, and $\binom{N}{i}$ is a binomial coefficient that takes the degeneracy of nucleosome unfolding into account [39]. The expected value of total extension at a given force and an excess linking number is then given by:

$$\left\langle z(F, \Delta Lk, N) \right\rangle = \\ Z^{-1} \sum_{i=0}^{N} z(F, \Delta Lk + iLk^0_{\text{fiber}}, i) \binom{N}{i} \exp\left(-\frac{G_{\text{DNA}} + G_{\text{fiber}} + iG_u - Fz)}{k_{\text{B}}T}\right) \tag{4.23}$$

Figure S8B and S8C show how the torsional modulus and the handedness of the chromatin fiber calculated by our model impact the resulting rotation-extension behaviour. We therefore used this model to interpret the measured rotation-extension datasets of chromatin fibers and obtained reproducible results shown in Table 4.1 of the main text.

4.6 Supplementary Figures

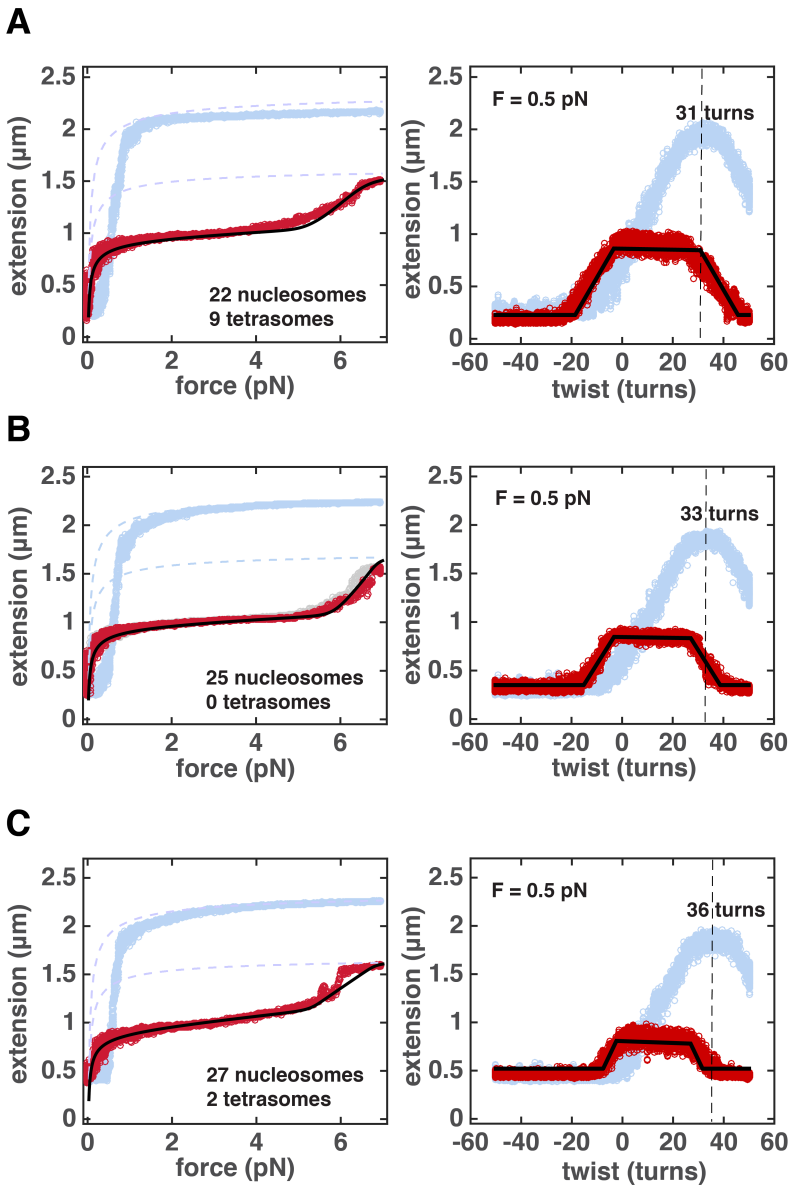

Figure S1
Chromatin fiber superhelix stores excessive linking number. See the detailed figure caption on the next page.

Figure S1

Chromatin fiber superhelix stores excessive linking number. Left panels: Force-extension curves of three 167-NRL chromatin fibers (red) with corresponding extensions of deproteinized tethers after treatment with heparin (blue). Black lines are the fit obtained by the statistical mechanics model [39] used to quantify the number of nucleosomes in the fiber ($N_{\text{nucleosomes}} = 22, 25, 27$ in left panels A,B,C, respectively). Blue dotted lines are the WLC extensions that indicate the length of unstacked fiber ($\sim 1.5\ \mu m$) and bare DNA template without nucleosomes ($\sim 2.2\ \mu m$). The remaining ~ 700 nm of folded DNA would unwrap at higher forces in discrete 25 nm steps revealing at least $700/25 = 28$ NCPs in studied fibers, as in Fig. 4.2. **Right panels:** Corresponding rotation-extension curves of chromatin fibers (red) shown in left panels supplemented with rotation-extension curves of deproteinized tethers (blue). Experiments were taken at 0.5 pN of force. Dotted lines mark the peak of the DNA rotation curve. The shift of the peak with respect to zero twist indicates the linking number that was stored in the chromatin fiber.

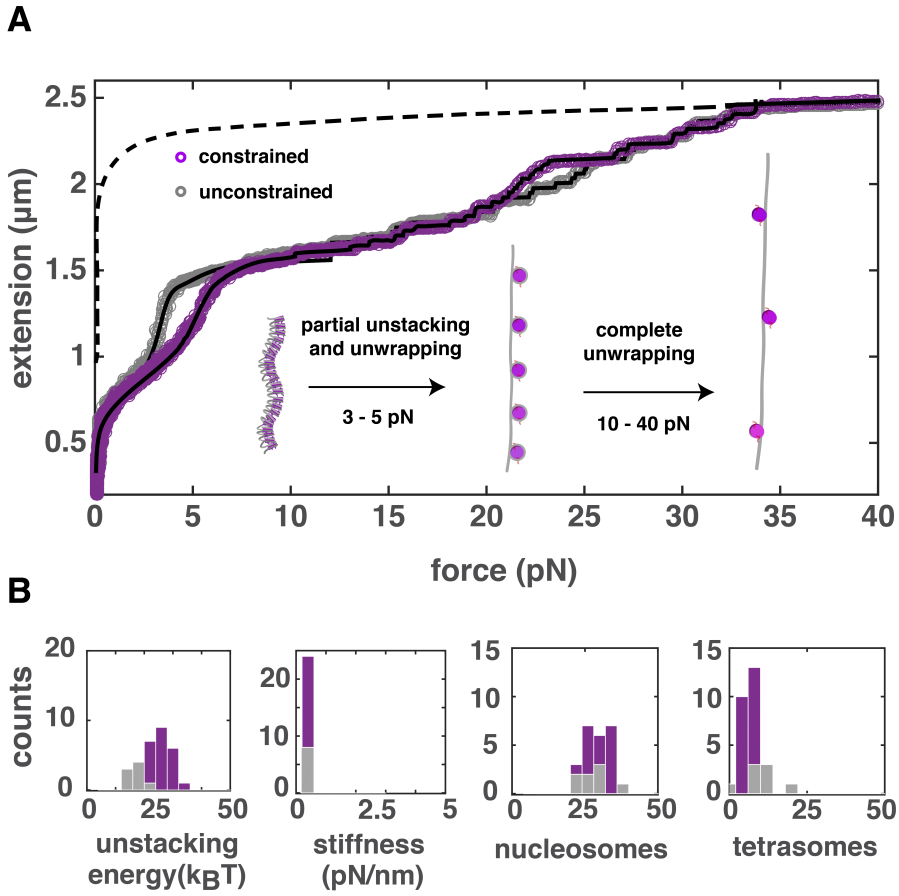

Figure S2

Stacking of the 197-NRL fiber is stabilized by torsional constraint. A) A force - extension curve of 197-NRL chromatin fibers assembled on a 601-DNA template that was rotationally constrained (violet) and unconstrained (grey). Both curves were analyzed with the statistical mechanics model [39] (black lines) that yielded with $N_{\text{nucleosomes}} = 31$ and $N_{\text{nucleosomes}} = 32$ for the constrained and the unconstrained fiber, respectively. The extension of bare 7 kb DNA template is plotted with the WLC model (dotted lines). *Inset*: a cartoon visualizing main conformational changes in chromatin fibers described in the text. **B)** Quantitative analysis of rotationally constrained 167-NRL fibers (n = 24, violet) and unconstrained ones (n = 8, grey) with the statistical mechanics model. Both populations have 30 ± 5 and 29 ± 6 (mean ± SD) assembled core particles, respectively, including nucleosomes and tetrasomes. The stretching stiffness of 0.3 and 0.2 ± 0.1 pN/nm for constrained and unconstrained fibers, respectively, is similar to values obtained in our previous work [39, 42]. The fitted mean unstacking energy of 26 ± 4 $k_{\text{B}}T$ in rotationally constrained fibers is larger than in unconstrained molecules (17 ± 2 $k_{\text{B}}T$).

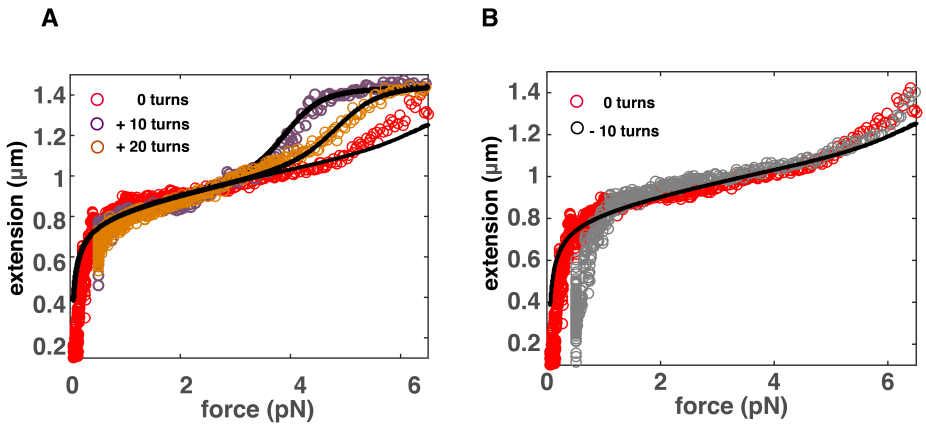

Figure S3

Torque regulates the unstacking of the 167-NRL chromatin fiber. Force-extension curves of the 167-NRL chromatin fiber with 20 nucleosomes obtained at positive (A) and negative (B) linking number. Solid lines are the fits obtained by the statistical mechanics model. The fiber was pre-twisted, subsequently stretched with low forces to induce its unstacking and then refolded to its initial configuration (not shown). The rupture force decreased upon external positive torque reaching the minimum at 3 pN (brown), after pre-twisting with 10 turns. Excessive positive torque changed this tendency and stabilized the fiber. The unstacking transition measured after applying 20 positive turns (orange) required more force than in the preceding stretching cycle. Negative twist did not affect the unstacking transition but induced supercoils in the DNA handles (panel B).

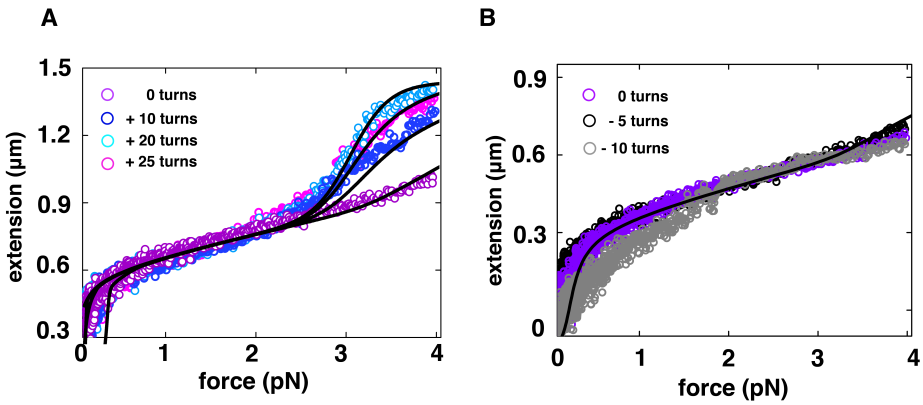

Figure S4

Torque regulates the unstacking of the 197-NRL chromatin fiber. Force-extension curves of the 197-NRL chromatin fiber with 25 nucleosomes obtained at positive (A) and negative (B) linking number. Solid lines are the fits obtained by the statistical mechanics model. The fiber was pre-twisted, subsequently stretched with low forces to induce its unstacking and then refolded to its initial configuration (not shown). The rupture force decreased upon external positive torque reaching the minimum at 2.5 pN (light blue), after pre-twisting with 20 turns. Excessive positive twist changed this tendency and stabilized the fiber. The unstacking transition measured after applying 25 positive turns (pink) required more force than in the preceding stretching cycle. Negative torque did not affect the unstacking transition but induced supercoils the DNA handles (panel B).

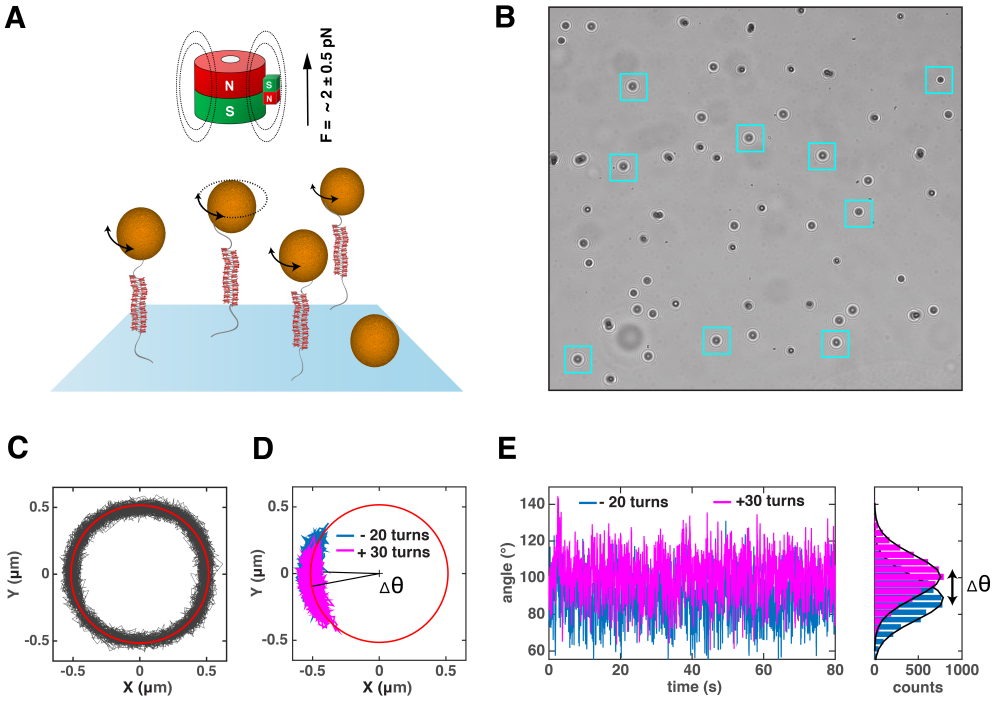

Figure S5

Multiplexed magnetic tweezers with a cylindrical magnet configuration enable direct torque measurement on many individual molecules. A) A schematic drawing showing molecules stretched with ∼ 2 pN by a cylindrical magnet with a small cubic magnet attached to its side (out of scale). Magnetic field lines generated by the cylindrical magnet (dotted lines) are oriented in parallel to tethers axis. In the absence of the side magnet, a bead that is tethered exactly below the center of the cylindrically-shaped magnet would fluctuate around the tether axis and draw a full circle (dotted circle). Addition of a small side magnet provides with a small transverse field (not shown) that constrains the free rotation of the bead. Additionally, it allows to apply torque to molecules by rotation of the magnet, as in classic magnetic tweezers with two cubic magnets. A non-magnetic bead that is attached to the glass surface serves as a reference bead. **B)** A fragment of the field of view with selected tethers for torque measurement. **C)** Tracking of the X,Y position of the tether under rotation. A circle was fitted through the data to obtain its radius. **D)** Fluctuations of the tether in X,Y plane under fixed cylindrical magnet configuration with a small side magnet. Upon application of twist, the tether experience a restoring torque that shifts the arc that represents tether's radial fluctuations. **E)** X,Y fluctuations transformed into polar coordinates to obtain the shift in the angle necessary to quantify the restoring torque.

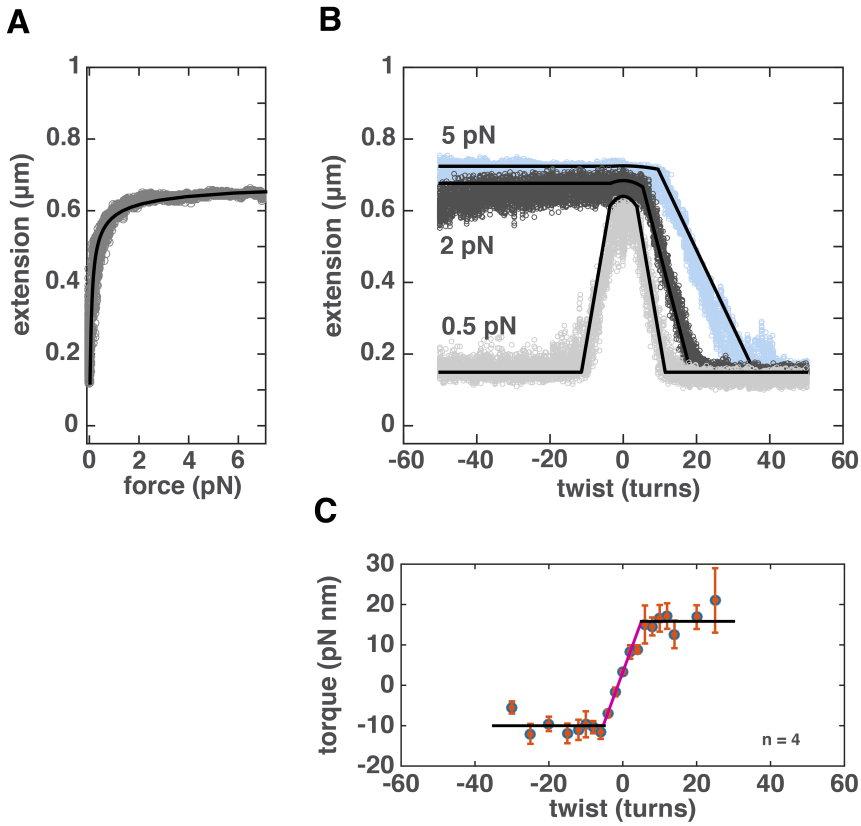

Figure S6

Modelling supercoiling of DNA. A) A force-extension curve of 1.9 kb DNA molecule fitted to a WLC model yielded a persistence length $P = 46$ nm. **B)** A rotation-extension curve of the molecule shown in panel A obtained at 0.5 pN (grey) and 2 pN (black) and 5 pN (blue). At low force, the curve is symmetric with respect to zero twist. The extension decreased linearly as the DNA forms plectonemes. At higher tension, negative twist favors DNA melting that does not contribute to a detectable change in the tether's extension. Black lines represent modelled rotation curves with the effective torsional stiffness of DNA $C_t = 70$ nm at 0.5 pN, $C_t = 80$ nm at 2 pN, $C_t = 83$ nm at 5 pN and torsional persistence length of plectonemic DNA $C_p = 24$ nm. **C)** The averaged torque curve from 4 DNA molecules measured simultaneously at $\sim$ 2 pN. Between -5 and +5 turns, the torque changes linearly. Beyond this regime, the curve remains flat, indicating no torque build-up which occurs upon structural changes such as DNA melting or supercoiling. An independent measure of the torsional stiffness is obtained by fitting the slope of the curve. The fitted $C_t = 79\ nm$ is consistent with the values obtained by quantifying rotation curves.

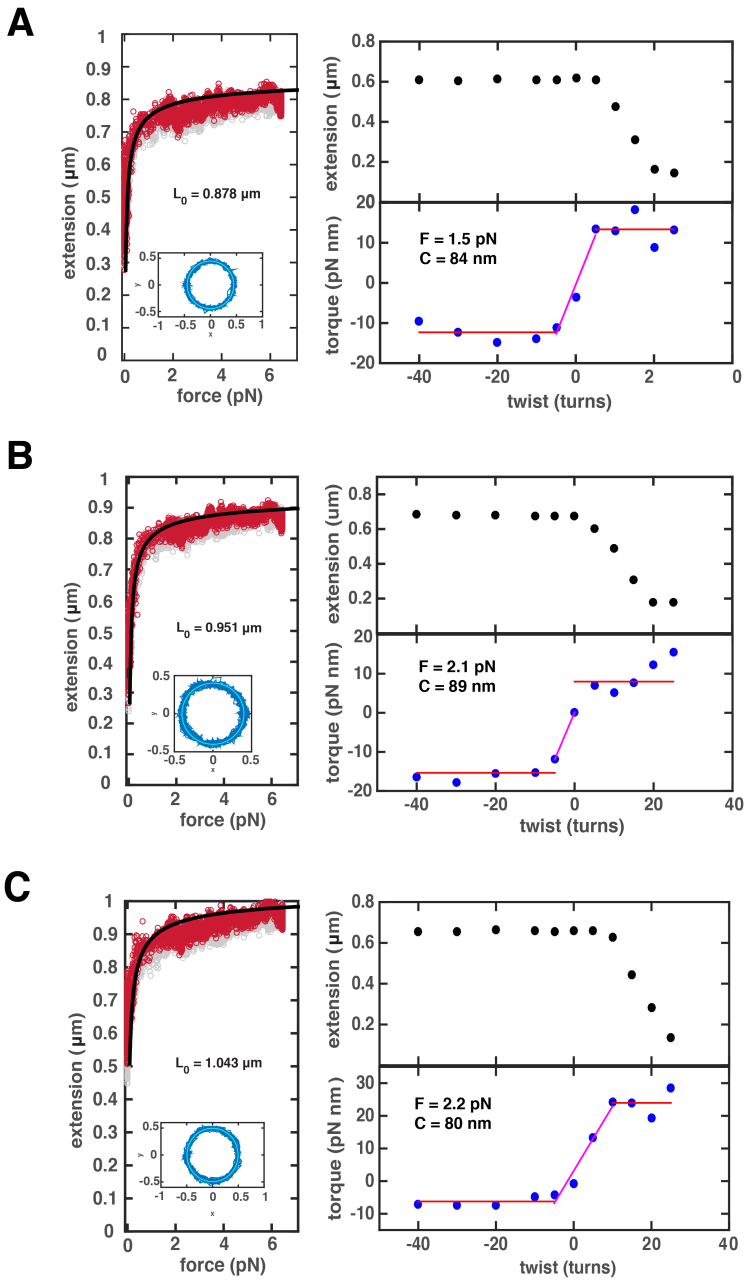

Figure S7
Multiplexed torque measurements of DNA molecules. See the detailed figure caption on page 116.

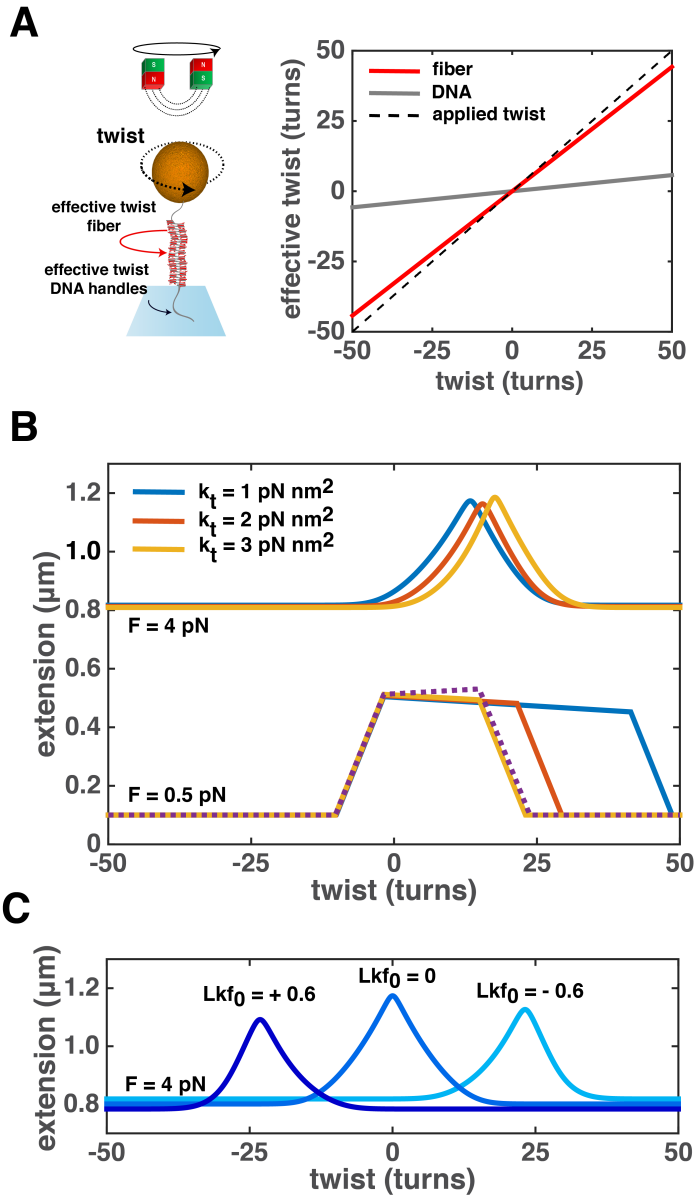

Figure S8
The effect of individual parameters in the statistical mechanics model on rotation-extension curves See the detailed figure caption on the next page.

Figure S8

Fig. S7. Multiplexed torque measurements of DNA molecules. A-C) Three representative curves obtained by tracking X,Y fluctuations of tethers under a cylindrical magnet configuration as in Fig. S5. Left panel: force-extension curve of the measured DNA molecule obtained with classic MT approach, fitted with a WLC model with the persistence length of 45 nm. Data was offset to account for the "hidden" length of tether due to the off-center attachment to the bead. *Inset*: X,Y fluctuations obtained upon magnet rotation were used to measure the hidden length. Right panel: Torque points (bottom trace) with the corresponding extension measured at this particular measurement point (top point). The pink line is the linear fit of the slope that is used to quantify torsional stiffness. Red lines indicate the melting and buckling point.

Fig. S8. The effect of individual parameters in the statistical mechanics model on rotation-extension curves. A) A cartoon of the tethered molecule indicating distribution of twist between the DNA and chromatin fiber with a plot of the twist build-up in those elements. **B)** A modelled rotation-extension curves of chromatin with 25 nucleosomes with different twist moduli. This parameter affects the buckling point (0.5 pN) and shifts the peak of the curve at 4 pN. The dotted line shows the curve modelled with the same parameters as in the yellow trace, but with negative twist-stretch coupling factor. **C)** A rotation-extension curve of the same type of fiber as in panel B, modelled with different linking number change upon unstacking.

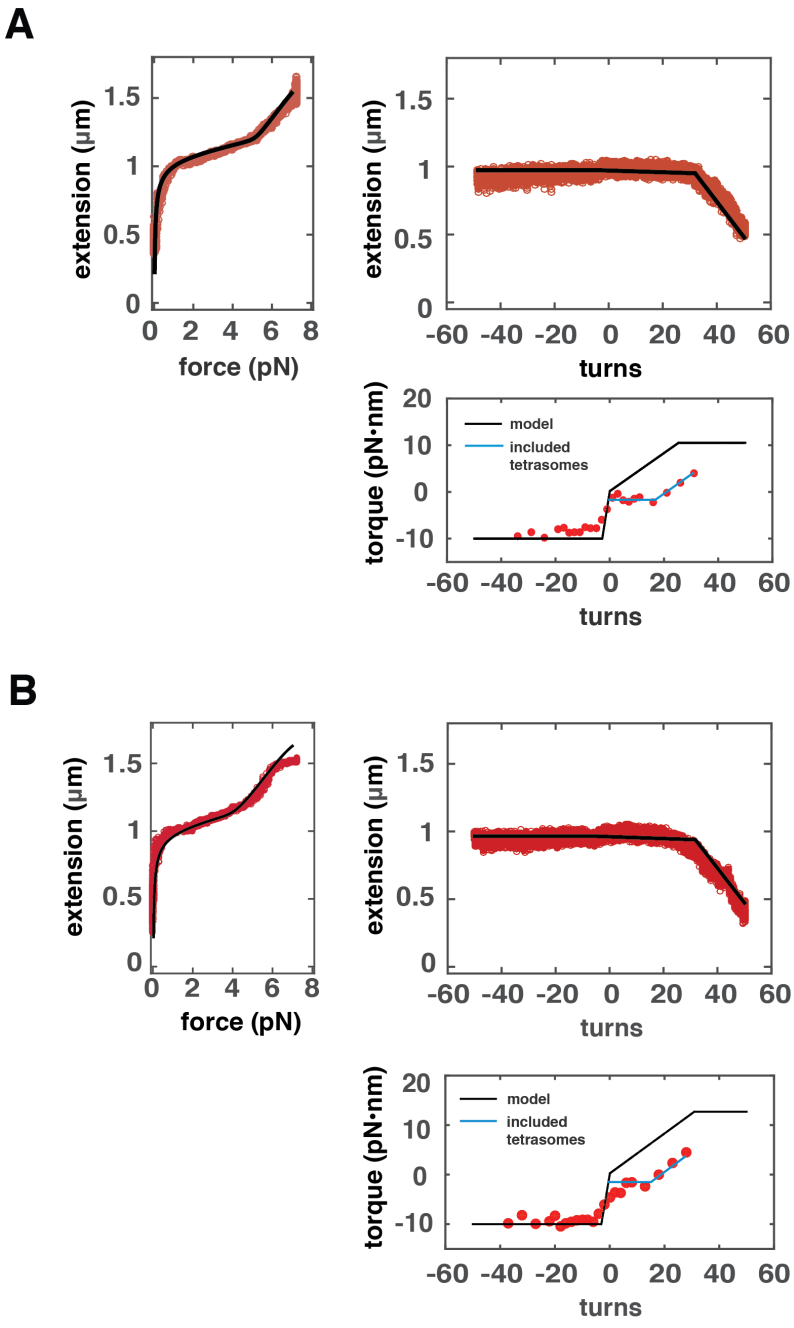

Figure S9
Torque measurements in 167-NRL with corresponding force-extension and rotation extension curves. See the detailed figure caption on the page 119.

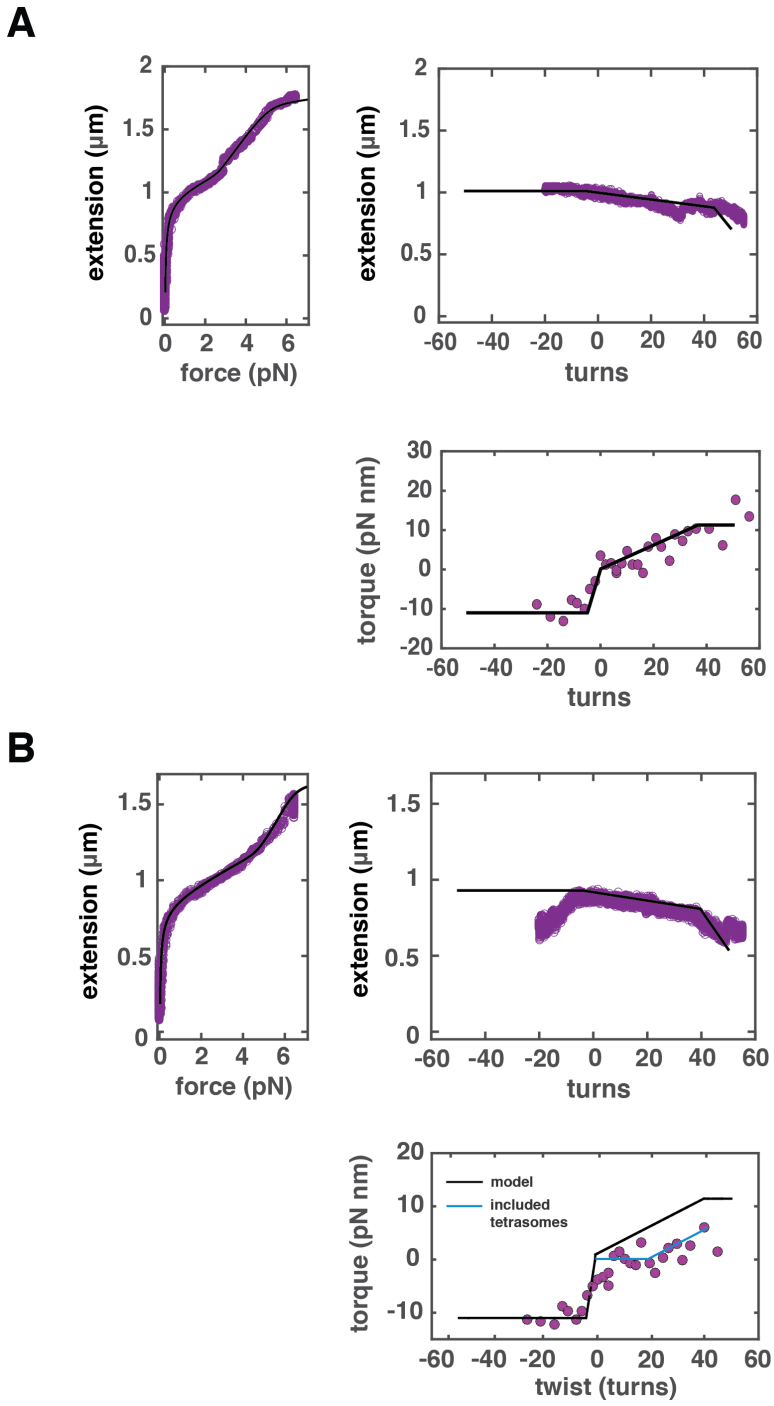

Figure S10
Torque measurements in 197-NRL with corresponding force-extension and rotation extension curves. See the detailed figure caption on the next page.

Figure S10

Fig. S9. Torque measurements in 167-NRL with corresponding force-extension and rotation extension curves. A) Selected molecules were analyzed as in Fig. 4.3. Top left panel shows the force-extension data (red) and the modelled curve (black) with parameters $N_{\text{nucleosomes}} = 24, N_{\text{tetrasomes}} = 2$, unstacking energy $dG_1 = 22\ k_{\text{B}}T$, stretching stiffness per nuclesome $C_s = 0.85$ pN/nm and twist modulus $C_t = 3$ pN $\cdot$ nm^2. Top right panel represents the rotation-extension curve recorded at 2 pN modelled with the same parameters. Bottom panel shows the measured restoring torque as a function of the applied twist. The black line is the prognozed torque from the model. The blue line is the prognozed torque that includes a correction for twist in tetrasomes. **B)** Similar analysis of another molecule yielding parameters: $N_{\text{nucleosomes}} = 24, N_{\text{tetrasomes}} = 0$, unstacking energy $dG_1 = 23\ k_{\text{B}}T$, stretching stiffness per nuclesome $C_s = 0.75$ pN/nm and twist modulus $C_t = 3$ pN $\cdot$ nm^2.

Fig. S10 . Torque measurements in 197-NRL with corresponding force-extension and rotation extension curves. A) Selected molecules were analyzed as in Fig. 4.4. Top left panel shows the force-extension data (violet) with the modelled curve (black) with parameters $N_{\text{nucleosomes}} = 21, N_{\text{tetrasomes}} = 1$, unstacking energy $dG_1 = 17\ k_{\text{B}}T$, stretching stiffness per nuclesome $C_s = 0.3$ pN/nm and twist modulus $C_t = 2$ pN $\cdot$ nm^2.Top right panel represent the rotation-extension curve recorded at 2 pN. Bottom panel shows the measured restoring torque as a function of the applied twist. The black line is the prognozed torque from the model. The blue line is the prognozed torque that includes a correction for twist in tetrasomes. **B)** Similar analysis of another molecule yielding parameters: $N_{\text{nucleosomes}} = 31, N_{\text{tetrasomes}} = 15$, unstacking energy $dG_1 = 18\ k_{\text{B}}T$, stretching stiffness per nuclesome $C_s = 0.4$ pN/nm and twist modulus $C_t = 3$ pN $\cdot$ nm^2.

Bibliography IV

[1] Roger D. Kornberg. "Structure of chromatin". In: *Annu Rev Biochem.* 46 (1977), pp. 931–54.

[2] Karolin Luger et al. "Crystal structure of the nucleosome core particle at 2.8Å resolution". In: *Nature* 389 (1997), pp. 251–260. ISSN: 0028-0836. DOI: 10.1038/38444.

[3] Sheila S. Teves, Christopher M. Weber, and Steven Henikoff. "Transcribing through the nucleosome". In: *Trends in Biochemical Sciences* 39.12 (2014), pp. 577–586. DOI: 10.1016/j.tibs.2014.10.004.

[4] Karolin Luger. "Dynamic nucleosomes". In: *Chromosome Research* 14.1 (2006), pp. 5–16. ISSN: 09673849. DOI: 10.1007/s10577-005-1026-1.

[5] Andrew Flaus and Tom Owen-Hughes. "Mechanisms for nucleosome mobilization". In: *Biopolymers* 68.4 (2003), pp. 563–578. ISSN: 00063525. DOI: 10.1002/bip.10323.

[6] Nick Gilbert and Bernard Ramsahoye. "The relationship between chromatin structure and transcriptional activity in mammalian genomes". In: *Briefings in Functional Genomics and Proteomics* 4.2 (2005), pp. 129–142. ISSN: 14739550. DOI: 10.1093/bfgp/4.2.129.

[7] Gregory D. Bowman and Michael G. Poirier. "Post-translational modifications of histones that influence nucleosome dynamics". In: *Chemical Reviews* 115 (2015), pp. 2274–2295. ISSN: 15206890. DOI: 10.1021/cr500350x.

[8] Thomas Jenuwein and C. David Allis. "Translating the histone code". In: *Science* 293.5532 (2001), pp. 1074–80. ISSN: 1530-8561. DOI: 10.1126/science.1063127.

[9] Yahli Lorch, Barbara Maier-Davis, and Roger D. Kornberg. "Mechanism of chromatin remodeling". In: *Proceedings of the National Academy of Sciences* 107.8 (2010), pp. 3458–3462. ISSN: 0027-8424. DOI: 10.1073/pnas.1000398107.

[10] Beat Fierz. "Dynamic Chromatin Regulation from a Single Molecule Perspective". In: *ACS Chemical Biology* 11.3 (2016), pp. 609–620. ISSN: 15548937. DOI: 10.1021/acschembio.5b00832.

[11] Nicole Happel and Detlef Doenecke. "Histone H1 and its isoforms: Contribution to chromatin structure and function". In: *Gene* 431 (2009), pp. 1–12. ISSN: 03781119. DOI: 10.1016/j.gene.2008.11.003.

[12] Melody A. Lever et al. "Rapid exchange of histone H1.1 on chromatin in living human cells". In: *Nature* 408.6814 (2000), pp. 873–876. ISSN: 00280836. DOI: 10.1038/35048603.

[13] Harold Weintraub. "The nucleosome repeat length increases during erythropoiesis in the chick". In: *Nucleic Acids Research* 5.4 (1978), pp. 1179–1188. ISSN: 03051048. DOI: 10.1093/nar/5.4.1179.

[14] Daria A. Beshnova et al. "Regulation of the Nucleosome Repeat Length In Vivo by the DNA Sequence, Protein Concentrations and Long-Range Interactions". In: *PLoS Computational Biology* 10.7 (July 2014). Ed. by Ioshikhes, e1003698. ISSN: 15537358. DOI: 10.1371/journal.pcbi.1003698.

[15] Jean Marc Victor et al. "Pulling chromatin apart: Unstacking or Unwrapping?" In: *BMC Biophysics* 5 (2012), p. 21. ISSN: 2046-1682. DOI: 10.1186/2046-1682-5-21.

[16] Kazuhiro Maeshima, Saera Hihara, and Mikhail Eltsov. "Chromatin structure: Does the 30-nm fibre exist in vivo?" In: *Current Opinion in Cell Biology* 22.3 (2010), pp. 291–297. ISSN: 09550674. DOI: 10.1016/j.ceb.2010.03.001.

[17] Thomas Schalch et al. "X-ray structure of a tetranucleosome and its implications for the chromatin fibre". In: *Nature* 436.7047 (2005), pp. 138–141. ISSN: 00280836. DOI: 10.1038/nature03686.

[18] Andrew Routh, Sara Sandin, and Daniela Rhodes. "Nucleosome repeat length and linker histone stoichiometry determine chromatin fiber structure." In: *Proceedings of the National Academy of Sciences of the United States of America* 105.26 (2008), pp. 8872–8877.

[19] Guohong Li and Danny Reinberg. "Chromatin higher-order structures and gene regulation". In: *Current Opinion in Genetics and Development* 21.2 (2011), pp. 175–186. ISSN: 0959437X. DOI: 10.1016/j.gde.2011.01.022.

[20] Feng Song et al. "Cryo-EM study of the chromatin fiber reveals a double helix twisted by tetranucleosomal units". In: *Science* 344.6182 (2014), pp. 376–380. ISSN: 10959203. DOI: 10.1126/science.1251413.

[21] J. C. Wang. "Helical repeat of DNA in solution." In: *Proceedings of the National Academy of Sciences* 76.1 (1979), pp. 200–203. ISSN: 0027-8424. DOI: 10.1073/pnas.76.1.200.

[22] Leroy F. Liu and James C. Wang. "Supercoiling of the DNA template during transcription". In: *Proceedings of the National Academy of Sciences* 84 (1987), pp. 7024–7027. ISSN: 0027-8424. DOI: 10.1073/pnas.84.20.7024.

[23] James C. Wang and A. Simon Lynch. "Transcription and DNA supercoiling". In: *Current Opinion in Genetics and Development* 3.5 (1993), pp. 764–768. ISSN: 0959437X. DOI: 10.1016/S0959-437X(05)80096-6.

[24] David J. Clark and Gary Felsenfeld. "A nucleosome core is transferred out of the path of a transcribing polymerase". In: *Cell* 71.1 (1992), pp. 11–22. ISSN: 00928674. DOI: 10.1016/0092-8674(92)90262-B.

[25] Sheila S Teves and Steven Henikoff. "Transcription-generated torsional stress destabilizes nucleosomes." In: *Nature Structural & Molecular biology* 21.1 (2014), pp. 88–94. ISSN: 1545-9985. DOI: 10.1038/nsmb.2723.

[26] Catherine Naughton et al. "Transcription forms and remodels supercoiling domains unfolding large-scale chromatin structures". In: *Nature Structural & Molecular Biology* 20.3 (2013), pp. 387–395. ISSN: 15459993. DOI: 10.1038/nsmb.2509.

[27] Lacramioara Bintu et al. "The elongation rate of RNA polymerase determines the fate of transcribed nucleosomes". In: *Nature Structural & Molecular Biology* 18.12 (2011), pp. 1394–1399. ISSN: 15459993. DOI: 10.1038/nsmb.2164.

[28] Ariel Prunell. "A topological approach to nucleosome structure and dynamics: The linking number paradox and other issues". In: *Biophysical Journal* 74.5 (1998), pp. 2531–2544. ISSN: 00063495. DOI: 10.1016/S0006-3495(98)77961-5.

[29] Benedetta Dorigo et al. "Nucleosome arrays reveal the two-start organization of the chromatin fiber". In: *Science* 306.5701 (Nov. 2004), pp. 1571–1573. ISSN: 00368075. DOI: 10.1126/science.1103124.

[30] Nikolay Korolev, Alexander P. Lyubartsev, and Lars Nordenskiöld. "A systematic analysis of nucleosome core particle and nucleosome-nucleosome stacking structure". In: *Scientific Reports* 8.1 (2018), p. 1543. ISSN: 2045-2322. DOI: 10.1038/s41598-018-19875-0.

[31] Karolin Luger, Mekonnen L. Dechassa, and David J. Tremethick. "New insights into nucleosome and chromatin structure: An ordered state or a disordered affair?" In: *Nature Reviews Molecular Cell Biology* 13.7 (2012), pp. 436–447. ISSN: 14710072. DOI: 10.1038/nrm3382.

[32] Kazuhiro Maeshima et al. "Liquid-like behavior of chromatin". In: *Current Opinion in Genetics and Development* 37 (2016), pp. 36–45. ISSN: 18790380. DOI: 10.1016/j.gde.2015.11.006.

[33] Horng D. Ou et al. "ChromEMT: Visualizing 3D chromatin structure and compaction in interphase and mitotic cells". In: *Science* 357.6349 (2017). ISSN: 10959203. DOI: 10.1126/science.aag0025.

[34] Jeffrey C. Hansen et al. "The 10-nm chromatin fiber and its relationship to interphase chromosome organization." In: *Biochemical Society transactions* 46.1 (2018), pp. 67–76. ISSN: 1470-8752. DOI: 10.1042/BST20170101.

[35] Viviana I. Risca et al. "Variable chromatin structure revealed by in situ spatially correlated DNA cleavage mapping". In: *Nature* 541.7636 (2017), pp. 237–241. ISSN: 0028-0836. DOI: 10.1038/nature20781.

[36] Shujun Cai et al. "The in situ structures of mono-, di-, and trinucleosomes in human heterochromatin". In: *Molecular Biology of the Cell* 29.20 (2018). Ed. by Kerry S. Bloom, pp. 2450–2457. ISSN: 1059-1524. DOI: 10.1091/mbc.E18-05-0331.

[37] Yujia Cui and Carlos Bustamante. "Pulling a single chromatin fiber reveals the forces that maintain its higher-order structure". In: *Proceedings of the National Academy of Sciences* 97.1 (2000), pp. 127–132. ISSN: 0027-8424. DOI: 10.1073/pnas.97.1.127.

[38] Nicolaas Hermans et al. "Toehold-enhanced LNA probes for selective pull down and single-molecule analysis of native chromatin". In: *Scientific Reports* 7.1 (2017), p. 16721. ISSN: 20452322. DOI: 10.1038/s41598-017-16864-7.

[39] He Meng, Kurt Andresen, and John van Noort. "Quantitative analysis of single-molecule force spectroscopy on folded chromatin fibers". In: *Nucleic Acids Research* 43.7 (2015), pp. 3578–3590. ISSN: 13624962. DOI: 10.1093/nar/gkv215.

[40] Philip J. J. Robinson et al. "EM measurements define the dimensions of the '30-nm' chromatin fiber: evidence for a compact, interdigitated structure." In: *Proceedings of the National Academy of Sciences of the United States of America* 103.17 (2006), pp. 6506–11. ISSN: 0027-8424. DOI: 10.1073/pnas.0601212103.

[41] Shirley Mihardja et al. "Effect of force on mononucleosomal dynamics". In: *Proceedings of the National Academy of Sciences* 103.43 (2006), pp. 15871–15876. ISSN: 0027-8424. DOI: 10.1073/pnas.0607526103.

[42] Artur Kaczmarczyk et al. "Single-molecule force spectroscopy on histone H4 tail-cross-linked chromatin reveals fiber folding". In: *Journal of Biological Chemistry* 292.42 (2017), pp. 17506–17513. ISSN: 1083351X. DOI: 10.1074/jbc.M117.791830.

[43] Rifka Vlijm et al. "Nucleosome assembly dynamics involve spontaneous fluctuations in the handedness of tetrasomes". In: *Cell Reports* 10.2 (2015), pp. 216–225. ISSN: 22111247. DOI: 10.1016/j.celrep.2014.12.022.

[44] Maxim Y. Sheinin et al. "Torque modulates nucleosome stability and facilitates H2A/H2B dimer loss". In: *Nature Communications* 4 (2013), p. 2579. ISSN: 20411723. DOI: 10.1038/ncomms3579.

[45] Aurélien Bancaud et al. "Structural plasticity of single chromatin fibers revealed by torsional manipulation". In: *Nature Structural and Molecular Biology* 13.5 (2006), pp. 444–450. ISSN: 15459993. DOI: 10.1038/nsmb1087.

[46] Aurélien Bancaud et al. "Nucleosome Chiral Transition under Positive Torsional Stress in Single Chromatin Fibers". In: *Molecular Cell* 27.1 (2007), pp. 135–147. ISSN: 10972765. DOI: 10.1016/j.molcel.2007.05.037.

[47] Qinming Chen et al. "Regulation of Nucleosome Stacking and Chromatin Compaction by the Histone H4 N-Terminal Tail-H2A Acidic Patch Interaction". In: *Journal of Molecular Biology* 429.13 (2017), pp. 2075–2092. ISSN: 10898638. DOI: 10.1016/j.jmb.2017.03.016.

[48] Jan Lipfert et al. "Magnetic torque tweezers: Measuring torsional stiffness in DNA and RecA-DNA filaments". In: *Nature Methods* 7.12 (2010), pp. 977–980. ISSN: 15487091. DOI: 10.1038/nmeth.1520.

[49] Terence R. Strick, Vincent Croquette, and David Bensimon. "Single-molecule analysis of DNA uncoiling by a type II topoisomerase". In: *Nature* 404.6780 (2000), pp. 901–904. ISSN: 0028-0836. DOI: 10.1038/35009144.

[50] M. Borens. "Action of Heparin on Nuclei: Solubilization of Chromatin enabling the Isolation of Nuclear Membranes". In: *Nature* 244.5410 (1973), pp. 28–30. ISSN: 0028-0836. DOI: 10.1038/244028a0.

[51] John F. Marko. "Torque and dynamics of linking number relaxation in stretched supercoiled DNA". In: *Physical Review E - Statistical, Nonlinear, and Soft Matter Physics* 76.2 (Aug. 2007), p. 021926. ISSN: 15393755. DOI: 10.1103/PhysRevE.76.021926.

[52] He Meng et al. "Coexistence of Twisted, Plectonemic, and Melted DNA in Small Topological Domains". In: *Biophysical Journal* 106.5 (2014), pp. 1174–1181. ISSN: 00063495. DOI: 10.1016/j.bpj.2014.01.017.

[53] Jan Lipfert et al. "Double-stranded RNA under force and torque: Similarities to and striking differences from double-stranded DNA". In: *Proceedings of the National Academy of Sciences* 111.43 (2014), pp. 15408–15413. ISSN: 0027-8424. DOI: 10.1073/pnas.1407197111.

[54] Samuel Corless and Nick Gilbert. "Investigating DNA supercoiling in eukaryotic genomes". In: *Briefings in Functional Genomics* 16.6 (2017), pp. 379–389. ISSN: 20412657. DOI: 10.1093/bfgp/elx007.

[55] Allyn J. Schoeffler and James M. Berger. "DNA topoisomerases: harnessing and constraining energy to govern chromosome topology". In: *Quarterly Reviews of Biophysics* 41.01 (2008), pp. 41–101. ISSN: 0033-5835. DOI: 10.1017/S003358350800468X.

[56] Amit Sharma and Alfonso Mondragón. "DNA topoisomerases". In: *Current Opinion in Structural Biology*. Methods in Molecular Biology 5.1 (1995). Ed. by Duncan J. Clarke, pp. 39–47. ISSN: 0959440X. DOI: 10.1016/0959-440X(95)80007-N.

[57] Fedor Kouzine et al. "The functional response of upstream DNA to dynamic supercoiling in vivo". In: *Nature Structural and Molecular Biology* 15.2 (2008), pp. 146–154. ISSN: 15459993. DOI: 10.1038/nsmb.1372.

[58] Jan Lipfert et al. "Freely orbiting magnetic tweezers to directly monitor changes in the twist of nucleic acids". In: *Nature Communications* 2.1 (2011). ISSN: 20411723. DOI: 10.1038/ncomms1450.

[59] Rifka Vlijm et al. "The supercoiling state of DNA determines the handedness of both H3 and CENP-A nucleosomes". In: *Nanoscale* 9.5 (2017), pp. 1862–1870. ISSN: 2040-3364. DOI: 10.1039/C6NR06245H.

[60] Jie Ma, Lu Bai, and Michelle D. Wang. "Transcription under torsion". In: *Science* 340.6140 (2013), pp. 1580–1583. ISSN: 10959203. DOI: 10.1126/science.1235441.

[61] Orkide Ordu et al. "Modification of the histone tetramer at the H3-H3 interface impacts tetrasome conformations and dynamics". In: *The Journal of Chemical Physics* 148.12 (2018), p. 123323. ISSN: 0021-9606. DOI: 10.1063/1.5009100.

[62] Job Dekker and Edith Heard. "Structural and functional diversity of Topologically Associating Domains". In: *FEBS Letters* 589 (2015), pp. 2877–2884. ISSN: 00145793. DOI: 10.1016/j.febslet.2015.08.044.

[63] Thomas B. Brouwer et al. "Unraveling DNA organization with single-molecule force spectroscopy using magnetic tweezers". In: *Methods in Molecular Biology*. Vol. 1837. Humana Press, New York, NY, 2018, pp. 317–349. ISBN: 9781493986750. DOI: 10.1007/978-1-4939-8675-0_17.

[64] Artur Kaczmarczyk et al. "Probing chromatin structure with magnetic tweezers". In: *Methods in Molecular Biology*. Vol. 1814. Humana Press, New York, NY, 2018, pp. 297–323. ISBN: 9781493985913. DOI: 10.1007/978-1-4939-8591-3_18.

[65] Zhongbo Yu et al. “A force calibration standard for magnetic tweezers”. In: *Review of Scientific Instruments* 85.12 (2014), p. 123114. ISSN: 10897623. DOI: 10.1063/1.4904148.

[66] J. P. Cnossen, D. Dulin, and N. H. Dekker. “An optimized software framework for real-time, high-throughput tracking of spherical beads”. In: *Review of Scientific Instruments* 85.10 (2014). ISSN: 10897623. DOI: 10.1063/1.4898178.

[67] Franziska Kriegel et al. “Probing the salt dependence of the torsional stiffness of DNA by multiplexed magnetic torque tweezers”. In: *Nucleic Acids Research* 45.10 (2017), pp. 5920–5929. DOI: 10.1093/nar/gkx280.

[68] Xander J. A. Janssen et al. “Electromagnetic torque tweezers: A versatile approach for measurement of single-molecule twist and torque”. In: *Nano Letters* 12.7 (2012), pp. 3634–3639. ISSN: 15306984. DOI: 10.1021/nl301330h.

Chapter 5

Linker histone H1 stabilizes nucleosome stacking in chromatin fibers

Linker histones function as regulators of chromatin structure and its dynamics. Although the interaction of the linker histone with the Nucleosome Core Particle has been extensively studied, its influence on the compaction of chromatin fibers remains less well understood. Here, we reconstituted nucleosomal arrays with linker histone H1 and applied piconewton forces that unfold the higher-order structure of chromatin fibers. We analyzed the resulting force-extension relation with a statistical physics model that captures non-equilibrium transitions and inferred that linker histones increase the nucleosome stacking energy by 3 k_BT. To quantify the size of the discrete chromatin unstacking ruptures, we employed a novel step-finding algorithm and concluded that chromatin fibers containing H1 yield asymmetrically unwrapped chromatosomes following unstacking. Our results indicate that linker histones do not influence the geometry of higher-order chromatin structures but rather help stabilize them. By resolving the mechanisms of this regulation, we can extend our understanding of the role of linker histones in the regulation of gene expression.

This chapter is based on: Kaczmarczyk A., Hermans N., Rodriguez de Mercado R., Vendel K., Nordenskiöld L., van Noort S.J.T., "Linker histone H1 stabilizes nucleosome stacking in chromatin fibers", *manuscript in preparation.*

5.1 Introduction

The basic unit of chromatin, the Nucleosome Core Particle, consists of 147 bp of DNA wrapped around a histone octamer composed of the H3-H4 tetramer and two H2A-H2B dimers [1]. A fifth histone, known as the linker histone (LH), can interact with the NCP and form a structure called the chromatosome [2]. The abundance of chromatosomes in eukaryotic chromatin varies, but in many cells it is comparable to that of nucleosomes, suggesting an important role of linker histones in chromatin folding [3].

Linker histones are proteins with a three-domain structure: a short N-terminal domain, a central globular domain that binds to the nucleosome dyad and a positively charged C-terminal domain that interacts with 10 - 20 bp of the linker DNA [4–6]. In the human genome, eleven different genes encode multiple isoforms of linker histones (*e.g* H1, H1.1, H5) that feature different binding modes to the NCPs [3, 7].

Structural studies of chromatosomes by EM and X-ray crystallography have shown that LHs play a major role in sealing the nucleosomal DNA around the histone octamer [6, 8], thus preventing its spontaneous breathing and sliding along the DNA [9, 10]. On the other hand, the interaction of LH with nucleosomes is highly dynamic, featuring transient binding and releasing of linker histones [11]. By this means, linker histones appear to regulate the stability of nucleosomes, which can constitute a roadblock for RNA polymerases *in vivo* [12]. Transcriptionally active regions of chromatin are less saturated with LH compared to silenced heterochromatin, suggesting that LH, indeed, acts as a general repressor of DNA metabolic processes [3]. *In vivo* studies indicate, however, that this regulation is not constitutive. Upon the knock-out of a gene coding for LH, minor phenotypic changes were observed and an alternative linker histone isoform was expressed [13]. This shows that the expression of linker histones is carefully maintained, and its role may be essential for establishing genome homeostasis.

The mechanism of gene regulation by linker histones may span beyond the level of single nucleosomes. MNase digestion assays on isolated cell nuclei have shown a correlation between the Nucleosome Repeat Length (NRL) and the number of LH molecules per nucleosome [14]. On average, 0.9 LH per nucleosome was found in regions with larger NRLs. LH binding to a nucleosome affects the electrostatic balance, since positively charged linker histones shield the negative charge of the linker DNA. Moreover, the presence of LH constrains the angle of the linker DNA entering and exiting the nucleosome. This leads to distinct geometries of chromatin fibers, as measured by cryo-EM [6]. It has been also suggested that the binding mode of LH can further impact the higher-order structure of chromatin. Recently, Zhou et al. reported that H1 binds asymmetrically to the one of linker DNA arms, whereas H5 interacts symmetrically with both linkers [15]. However, the differences in the topology of the resulting

chromatin fibers have not been resolved yet.

Due to the heterogeneity of natively purified chromatin and its sensitivity to the salt conditions, understanding of the higher order structure of chromatin has been challenging. Apart from the influence of LH and the NRL, chromatin structure is dynamically regulated by post-translational modifications (PTMs) and chromatin remodellers [16, 17]. All these sources of heterogeneity impeded structural characterization of chromatin folding *in vivo*.

Early *in vitro* reports indicated that linker histones are essential for chromatin compaction. Routh *et al.* showed that nucleosomal arrays with NRL = 197 bp were folded *in vitro* as beads-on-a-string and condensed into a 30 nm solenoid fiber only upon saturation with LH [18]. In contrast, zig-zag fibers with a short, straight linker DNA (NRL = 167 bp) were assembled into compact fibers in the absence of linker histones [19]. It was concluded that LH facilitates bending of the linker DNA which is required for nucleosome stacking into a one-start superhelix.

Our recent single-molecule force spectroscopy experiments on cross-linked chromatin fibers [20] and Monte Carlo simulations [21] indicated, however, that interactions between nucleosomes via histone tails can compensate the increased energy for bending the linker DNA in one-start fibers in the absence of LH. This suggests that linker histones may only be auxiliary mediators of chromatin compaction.

To gain mechanistic insight into the interaction of linker histones with chromatin, we used magnetic tweezers to unfold chromatin fibers with linker histone H1. In our previous work, we showed that linker histone did not influence the chromatin fiber geometry at forces below the unstacking transition [22]. Due to limited forces applied in these experiments and the increased unstacking force by LH, we were not able to resolve the unfolding pathway of such fibers. Here, we induced chromatin unstacking and DNA unwrapping from H1(+) chromatin fibers and compared their force-extension relation with H1(-) fibers. We confirmed that the compliance of the fibers was not affected by H1 and that H1 stabilized the stacking of nucleosomes. We developed a statistical mechanics model to quantify the non-equilibrium unstacking transitions and quantified the increased unstacking energy of H1(+) chromatin fibers. A novel step-finding algorithm allowed us to resolve discrete unstacking events and infer the most probable unwrapping mode of the H1(+) 197-NRL fibers. Overall, our findings provide insight into the role of linker histones in chromatin folding dynamics that may lead towards a better understanding of the regulatory mechanisms employed by LH in native chromatin.

5.2 Results

5.2.1 Chromatin higher-order structure is stabilized by the linker histone

We reconstituted nucleosomal arrays on a DNA template with multiple Widom-601 sequences separated by 50 bp of linker DNA (NRL = 197 bp). Under physiological conditions, these well-defined arrays condense into elastic solenoidal fibers stabilized by nucleosome stacking (schematically depicted in Fig. 5.1A) [20, 23]. To determine how the properties of 197-NRL fibers are affected by linker histones, we separately reconstituted H1(+) chromatin by dialyzing the 197-NRL DNA template against stoichiometric ratio of canonical histones and linker histone H1. To assess the differences in the level of compaction, we performed an electrophoretic band-shift assay. As shown in Fig. 5.1B, the mobility of nucleosomal arrays in the agarose gel decreased when the DNA was saturated with histone octamers. When chromatin fibers were supplemented with linker histone, the fibers migrated faster, resulting in a downward band-shift (Fig. 5.1C). The higher mobility of the H1(+) chromatin fibers reflected their increased condensation due to binding of the H1 to nucleosomes [24].

Subsequently, we used magnetic tweezers to probe the dynamics of single chromatin fibers with and without linker histones. First, as a reference, fibers without H1 were subjected to force to distort their higher-order structure and induce DNA unwrapping from nucleosomes. All the molecules presented in Fig. 5.2A featured similar unfolding patterns, which we interpreted quantitatively in our earlier work [23]. H1(-) 197-NRL chromatin fibers, flanked by $\sim$ 2 kb bare DNA handles, extend linearly until nucleosome-nucleosome interactions rupture, and simultaneously the outer turn of the nucleosomal DNA unwraps. This transition, that we denote here as nucleosome unstacking, corresponds with the plateau at 3 - 4 pN in the force-extension curves. It is followed by discrete unfolding steps at forces above 10 pN that arise from the DNA unwrapping from individual, now partially wrapped nucleosomes*. Importantly, the low force unstacking transition is in thermodynamic equilibrium, meaning that the unstacking is reversible. This is seen as an overlap in force-extension data between consecutive pulling and releasing cycles (Fig. S1).

We next added the linker histone H1 to the pre-assembled fibers that were tethered in the flow cell. More specifically, we first characterized the H1(-) 197-NRL fibers by measuring force-extension curves up to 7 pN. Subsequently, we refolded the initial fiber structure by reducing the force to $\sim$ 0.2 pN and then rinsed the flow chamber with the measurement buffer containing linker histone (See Methods). Upon subsequent stretching up to 40 pN, we obtained force-extension curves of H1(+) chromatin fibers that appeared more heterogeneous

*More detailed explanation of the force-extension curves and the model used for their interpretation can be found in Supplementary Information and in Chapter 2.

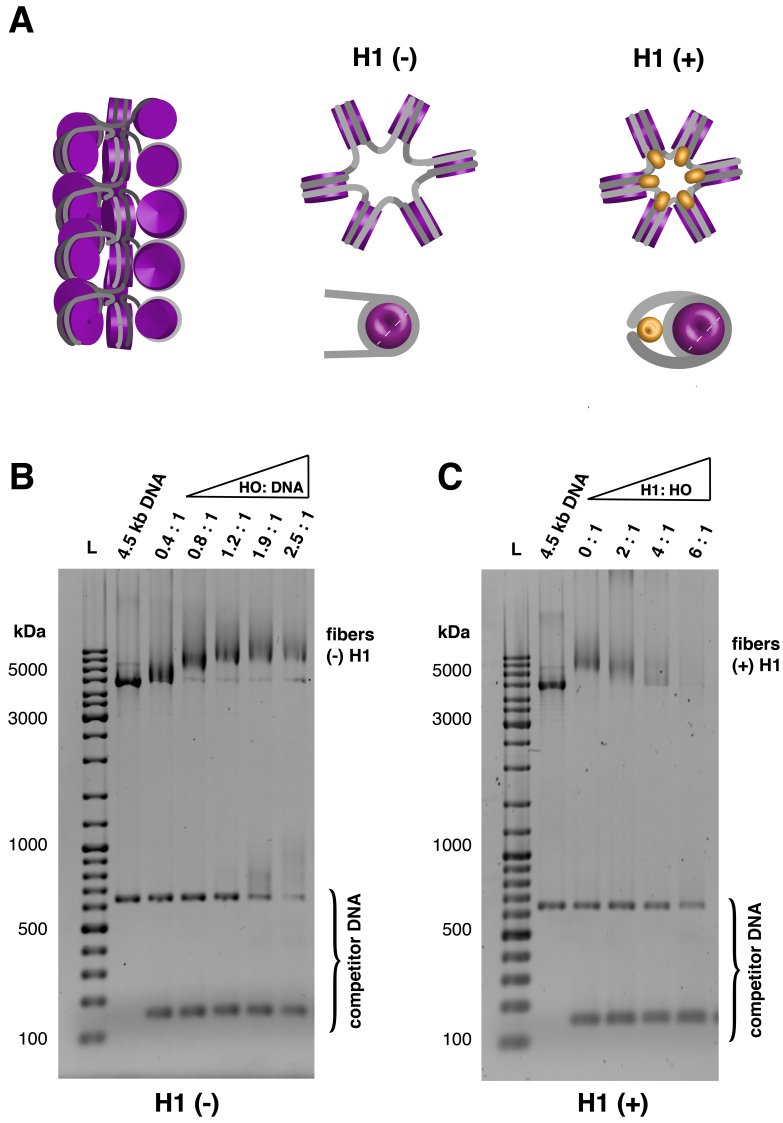

Figure 5.1
Linker histone H1 compacts solenoid fibers. **A)** A schematic drawing of a folded 197-NRL fiber (left) and top projections of an H1(-) and H1(+) fiber (upper middle and upper right, respectively). Binding of the linker histone H1 near the nucleosome dyad has been suggested to increase the stability of a nucleosome and constrains the angle between the nucleosome and the linker DNA. **B)** Electrophoretic mobility shift assay of reconstituted chromatin fibers without linker histone H1. As the histone:DNA ratio increases, reconstituted nucleosome arrays migrate slower through the agarose gel. The consecutive bands on the gel (lanes 3-7) are gradually shifted with respect to the bare DNA (lane 2). Upon full saturation of the 601-DNA template, excessive histones start to assemble on the competitor DNA (lane 6-7). **C)** The same band-shift assay of fibers with an optimal histone octamer:DNA ratio (titration 1.2:1 in panel B) titrated with increasing linker histone (H1) concentration. A downward band shift with increasing linker histone concentration results from the compaction of fibers by H1.

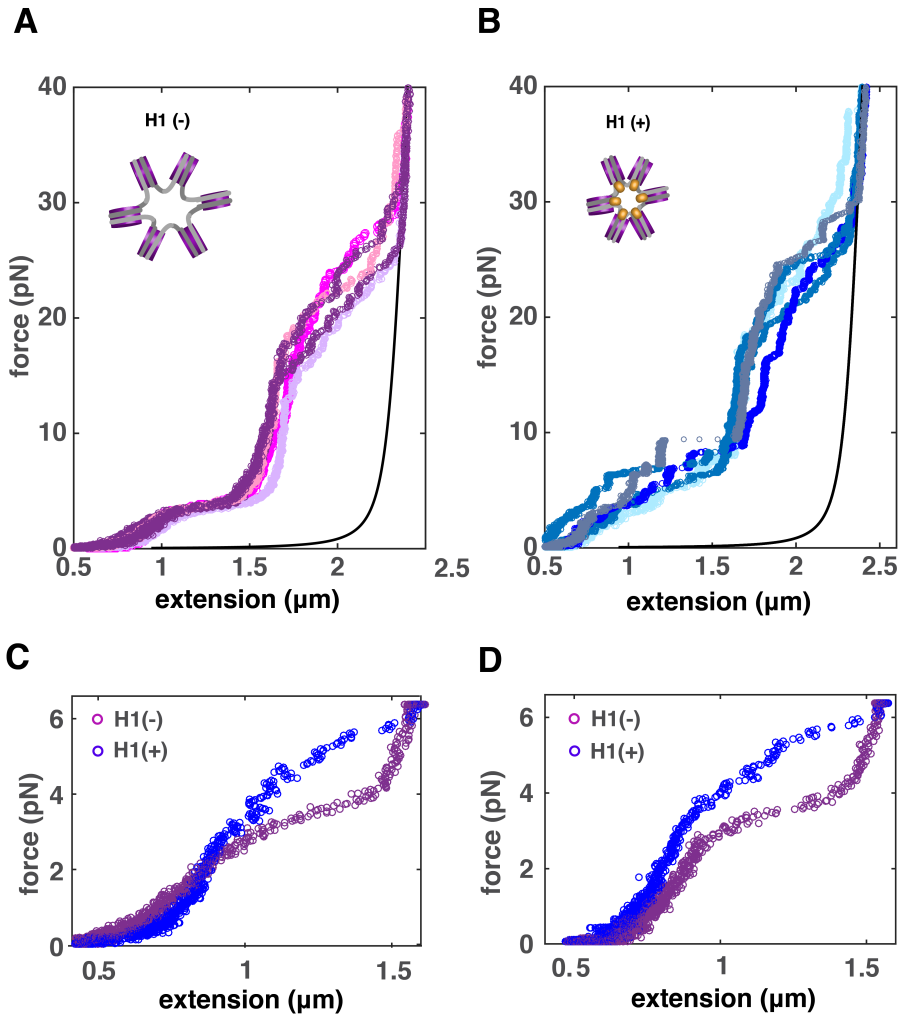

Figure 5.2
Linker histone H1 stabilizes nucleosome stacking. A) Force-extension curves of 5 representative 25·197-NRL fibers. Fibers undergo the unstacking transition at 3.5 pN followed by step-wise unwrapping of singly wrapped nucleosomes. **B)** Force-extension curves of 197-NRL fibers with linker histone H1 added to the flow cell post reconstitution. The curves are more heterogeneous at the low force regime. The unstacking transition is no longer gradual as in H1(-) fibers and occurs at higher forces. **C, D)** Comparison of the same tether stretched up to 7 pN in the absence of the linker histone (violet) and subsequently upon addition of the H1 to the flow cell (blue). The H1(+) fiber remains folded at 4 pN and unstacks in discrete steps at forces between 4 - 6 pN.

at the low force regime (Fig. 5.2B) compared to H1(-) fibers. Further stretching resulted in the step-wise unwrapping of individual nucleosomes, similarly to H1(-) fibers. This indicates that the linker histone influenced the unstacking of chromatin fiber but not the final DNA unwrapping at high forces. A closer look at the low force regime of the same molecule stretched in these two conditions revealed that H1(+) chromatin fibers unstacked in discrete rupture steps occurring between 4 - 7 pN (Fig. 5.2 C,D), which is a higher force compared to H1(-) fibers featuring gradual unstacking at 3.5 pN. In contrast, the linear stretching below 3 pN was only moderately affected by H1. We observed similar effects in 167-NRL fibers that were reported to form zig-zag fibers (Fig. S2). Overall, the most important effect of H1 is that it stabilizes chromatin fibers against unstacking.

5.2.2 Chromatin unstacking enhances H1 dissociation

The experiments described above involved stretching the chromatin fibers that were supplemented with H1 after tethering in the flow cell. We also tested chromatin fibers consisting of pre-reconstituted chromatosomes. We assembled H1(+) chromatin by salt dialysis and stretched the fibers in the measurement buffer in the absence of H1. Consistent with Figs. 5.2C, D, we observed discrete ruptures at forces exceeding 4 pN, instead of a force plateau at 3.5 pN (Fig. 5.3A). Interestingly, in contrast to H1(-) fibers (Fig. S1), the refolding curve of H1(+)

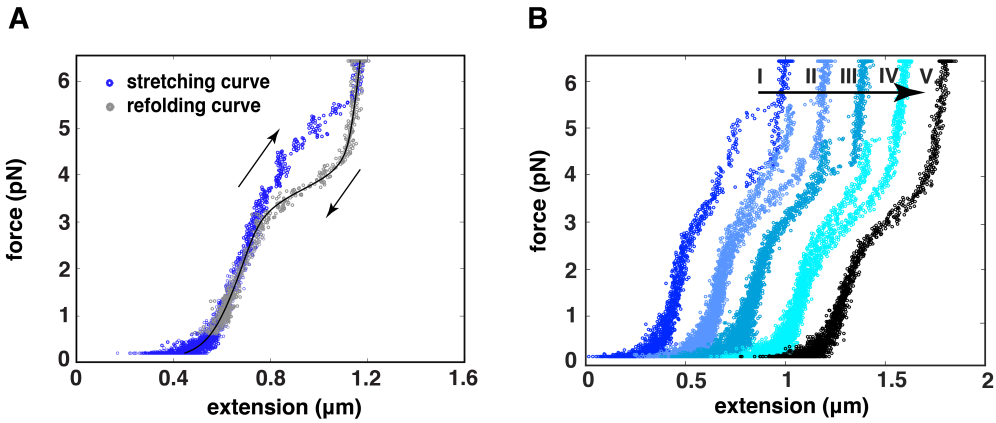

Figure 5.3
Linker histones disassemble when chromatin fibers are overstretched. A) A force-extension curve of the H1(+) reconstituted fiber stretched in the absence of linker histone in the measurement buffer. The hysteresis above 3 pN indicates a non-equilibrium transition. Below 3 pN, the F-E curve overlaps in the pull and release curve. **B)** A H1(+) tether pulled 5 times reveals the gradual dissociation of H1. Traces were offset in x-axis by 250 nm for clarity.

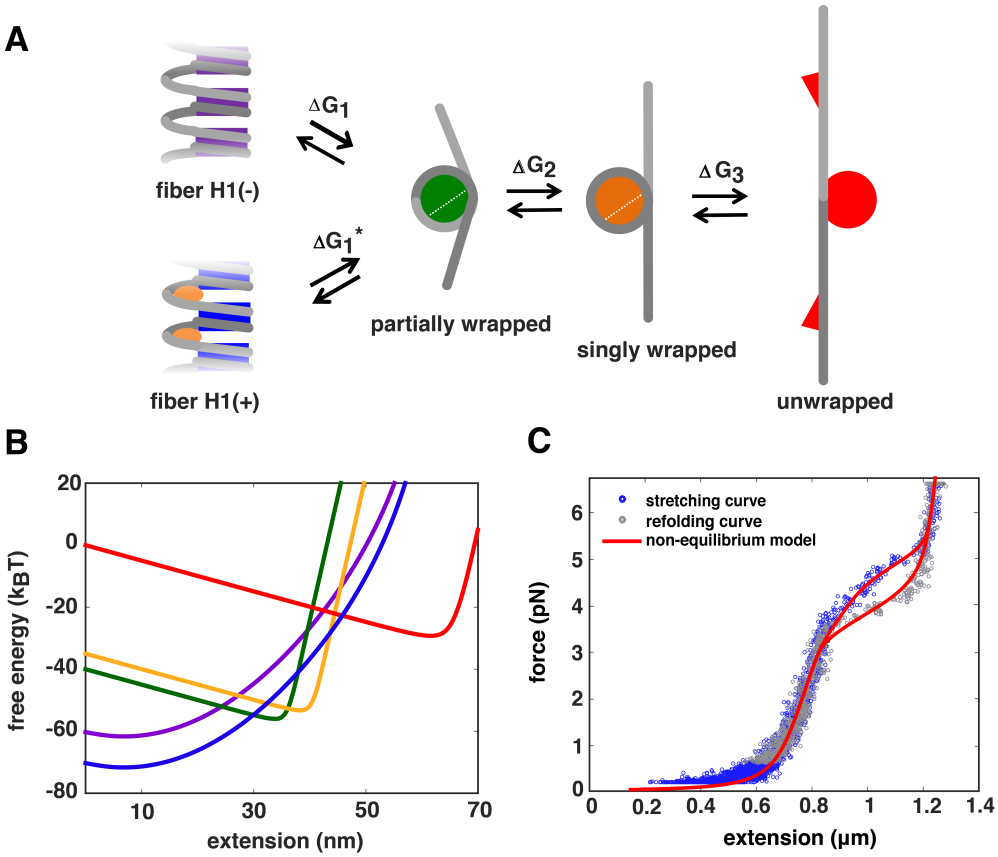

Figure 5.4

A non-equilibrium model allows to quantify the stacking energy of chromatosomes. A) A graphical representation of chromatin states under force. When interactions between adjacent nucleosomes or chromatosomes break, the fiber unstacks and simultaneously DNA partially unwraps from nucleosomes. Partially wrapped nucleosomes further extend and ultimately the remaining inner nucleosomal DNA turn unwraps. The breaking of histone-histone and histone-DNA interactions in each transition requires free energy. **B)** Free energy landscape (F = 2 pN) of the five conformations presented in panel A. See Fig. S4 for the force dependence of this energy landcape. **C)** F-E curve of H1(+) chromatin assembled on 15·601 DNA plotted together with the non-equilibrium model (red) using parameters: $N_{chromatosomes} = 14$, $k_{folded} = 0.26\ pN/nm$, $\Delta G_1^* = 22\ k_BT$, $\Delta G_2 = 5\ k_BT$.

fibers did not overlap entirely with the stretching curve, implying H1 dissociation during the measurement. The hysteresis vanished after five consecutive pull and release cycles (Fig. 5.3B), after which the F-E curve resembled that of H1(-) fiber. The slopes of all the F-E curves remained unaffected, meaning that the compliance of the chromatin fiber was the same in the presence and absence of H1. Thus, within single fibers that were reconstituted with stoichiometric amounts of LH, we confirmed that binding of the linker histone stabilized the nucleosomes stacking in 197-NRL chromatin fibers but did not affect its solenoidal one-start structure.

The non-equilibrium unfolding observed here indicates that the pulling rate exceeded the transition rate from the fully compacted fiber to partially wrapped nucleosomes (Fig. 5.4A). We investigated the unstacking mechanism of the H1(+) fibers further by quantification of this non-equilibrium transition. Therefore, we extended the equilibrium model presented in Ref. [23] to account for the energy barrier and transition rates from one conformation to another (Fig. 5.4B) (see Supplementary Information for further details). We used the fitting parameters from the equilibrium model and introduced three new parameters that characterize linker histones in the chromatin fiber: the unstacking energy per chromatosome ΔG_1^*, the number of chromatosomes and the transition rate k. The latter depends on the free energy barrier between the fiber and singly wrapped conformations: $k = k_0\, e^{-\Delta G_{\mathrm{barrier}}}$ (Eq. 5.12), where k_0 is the attempt rate. The free energy $\Delta G_{\mathrm{barrier}}$ is fully defined by the force-dependent energy-extension curves of the two states, as plotted in Fig. 5.2B and Fig. S4B. We fitted the curve of the extension of the H1(+) 197-NRL fiber (Fig. 5.4C) and obtained the unstacking energy of ΔG_1^* of 22 $k_{\mathrm{B}}T$. This is 3 $k_{\mathrm{B}}T$ larger than the unstacking energy of the H1(-) fiber (ΔG_1 = 19 $k_{\mathrm{B}}T$). Our single-molecule stretching experiments and subsequent analysis thus revealed that the linker histones' dissociation from the NCP is enhanced after unstacking and that the presence of chromatosomes increases the stacking energy by 3 $k_{\mathrm{B}}T$.

5.2.3 Quantification of discrete unstacking steps reveals asymmetric unwrapping of chromatosomes

Lastly, we investigated the discrete steps at the low force regime (Fig. 5.2 C,D, and Fig. 5.3A) that define chromatin unstacking. The ruptures represent the same transition from a fully folded fiber to partially wrapped nucleosomes, as in H1(-) fibers. However, in the presence of stable chromatosomes, unfolding intermediates at low force regime could be directly resolved. We measured the number of base pairs released in each unfolding event in 15 individual chromatin fibers using a novel step-finding algorithm that more accurately detects transitions at low force regime (see Supplementary Information).

The method was validated by quantifying the unwrapping steps at the force range of 15 - 35 pN. Figure 5.5C shows the histogram of unwrapping step sizes

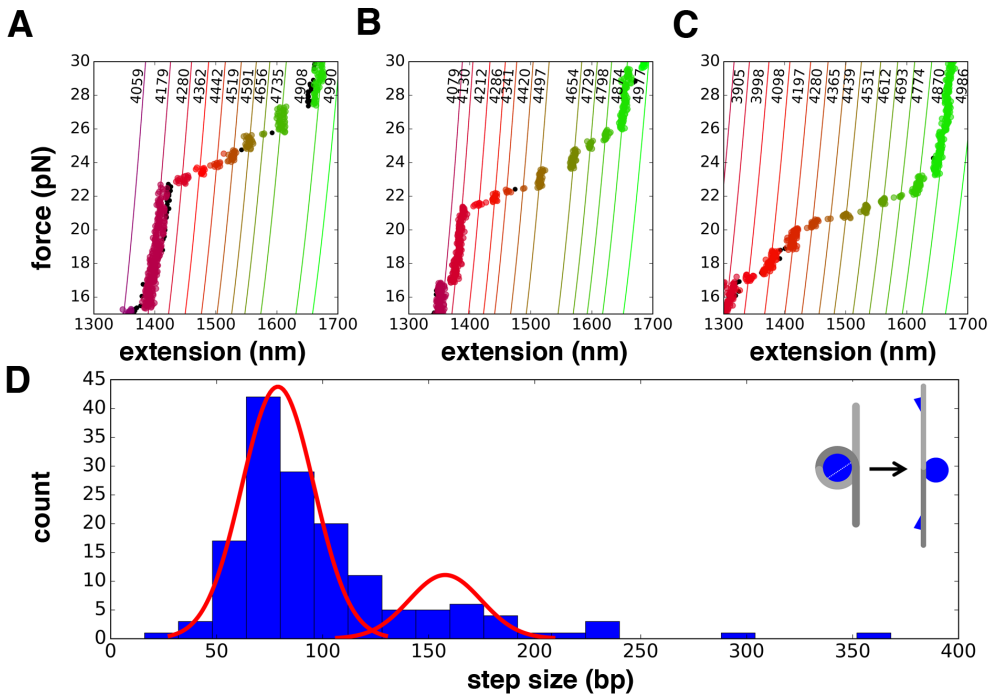

Figure 5.5
Quantification of discrete unwrapping steps yields a uniform distribution of step size. A-C) Unwrapping events at high force regime for 3 different molecules. Each state is labeled with the contour length in base pairs. **D)** Histogram of step sizes indicating the length of DNA released upon unwrapping of inner nucleosomal turn from multiple nucleosomes in 15 independent chromatin fibers. The step size is defined by the difference in contour length between two states. A double Gaussian describing a mean step size of m = 78.9 ± 0.3 bp is shown in red.

with a clear peak at ∼ 80 bp, that corresponds with the number of base pairs wrapped around a singly wrapped nucleosome [23]. Since some of the nucleosomes could unwrap simultaneously, the histogram has a smaller second peak at twice the step size (∼ 160 bp). To refrain from discretization effects, we fitted a double error function to the cummulative distribution to retrieve the number of base pairs. The fit yielded a mean step size of = 78.9 ± 0.3 bp (mean ± SE) that agreed well with previous results obtained from a t-test step finding algorithm [23].

We next employed this novel method to quantify the unstacking steps observed in the presence of H1. This proved to be less trivial than the quantification of steps at high force. Due to the simultaneous Hookean extension of the fiber and the low stiffness of the tether at low force, the resulting large thermal fluctuations obscured small rupture events. Nevertheless, we detected clear transitions that extended well beyond the length of the linker DNA between

a pair of chromatosomes (Fig. 5.6A), consistent with the simultaneous unstacking and partial DNA unwrapping that we corroborated earlier from pulling on the H1(-) fibers [23]. The histogram in Fig. 5.6D reveals a multitude of step sizes between 50 to 300 bp. These non-uniform transitions represent the unstacking of individual or multiple chromatosomes, that is slower than the same transition in nucleosome arrays without H1, which made it possible to resolve individual unstacking events.

Depending on the DNA unwrapping mechanism and the binding mode of the linker histones, the release of the outer turn of DNA from chromatosomes can yield different extensions. In the case of an equal number of base pairs being unwrapped from both sides of a nucleosome (symmetric unwrapping), we expect a ∼106 bp step size that corresponds to the unwrapping of the two halves of nucleosomal outer turn (56 bp, [23]) and the release of the total 50 bp of linker DNA. In the histogram (Fig. 5.6), however, counts are generally the lowest near the step sizes of 100, 200 and 300 bp, suggesting different pathway of unstacking.

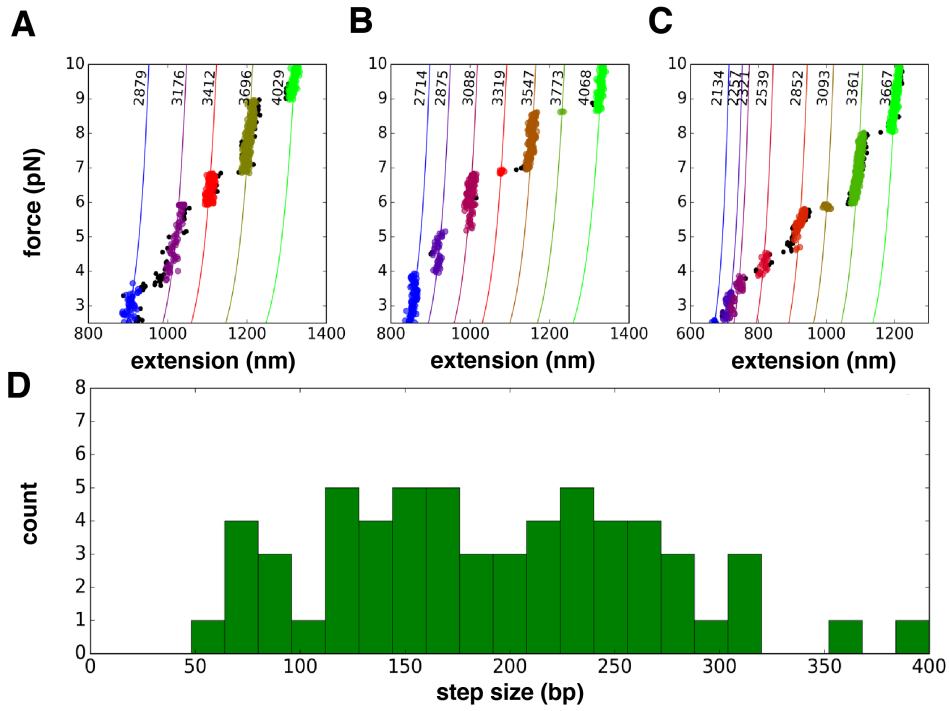

Figure 5.6
Step size distribution for unstacking of chromatosomes in 197-NRL H1(+) fibers yields a wide distribution of unstacking steps. A-C) Low force transitions in 3 different molecules. Each state is labeled with the contour in base pairs. **D)** Histogram of the unstacking steps in 15 different chromatin fibers. The step size is defined by the difference in contour length between two successive states.

A more probable interpretation assumes asymmetric unwrapping of the nucleosomes. Such asymmetric unwrapping was observed in the absence of linker histone in a study that combined spFRET with optical tweezers [9]. In this mechanism (Fig. 5.7B), in addition to half of the linker DNA that is released upon unstacking, the outer turn of the nucleosomal DNA unwraps from one side. This effect might be reinforced in the case of an asymmetric binding of H1, as suggested in Refs. [15, 25]. The crystal structure of nucleosomes shows 14 DNA-histone contacts, and leaves 7-8 bp on both sides of the nucleosome unconstrained. This lengthens the "effective" linker DNA length to 65 bp and shortens the unwrapping length to 52 bp (Fig. 5.7A). An unstacked nucleosome pair contains then the effective linker length plus 0, 1 or 2 unwrapping lengths, for a total of 65, 117 or 169 bp, respectively. These lengths match better with the observed peaks in the distribution. Larger steps can only be attributed to multiple simultaneous unstacking events, yielding: 65 + 117 = 182 bp, 65 + 169 = 234 bp or 117 + 169 = 286 bp. Tentatively, we therefore interpret the 234 bp peak as the simultaneous asymmetric unwrapping and unstacking of 3 nucleosomal particles. Note that this interpretation sufficiently explains the force-extension of H1(-) fibers, though the presence of linker histones may slow down the stacking and/or unstacking reaction. Only by stabilizing the nucleosomes with H1, we could resolve the mechanism of unstacking, as chromatin fibers without linker histone feature faster and reversible dynamics. Importantly, the observation of asymmetric unwrapping for the case of H1 histones is consistent with the work of Zhou *et al.* and White *et al.* [15, 25] who reported the off-dyad binding in H1 histones in contrast to on-dyad H5 chromatosomes.

Overall, without the detailed knowledge of the exact geometry of the linker histone binding, we could explain the distribution of step sizes since unstacking is directly followed by unwrapping into partially wrapped nucleosomes. When a nucleosome is unwrapped on one side, its neighbor is forced to unwrap to the other side. In the presence of multiple nucleosomes on the DNA, a wide distribution of step sizes is generated due to a combination of many unstacking and unwrapping transitions. In summary, by studying the role of H1 in chromatin with single-molecule force spectroscopy, we have inferred that LH stabilized chromatin fibers and we resolved the mechanistic details of chromatin fiber (un-)folding.

5.3 Discussion and conclusions

In this work, we compared chromatin fibers containing wild-type histone octamers with similar chromatin fibers reconstituted with the linker histone H1. Linker histones are important components influencing the compaction of nucleosomal arrays into chromatin fibers. Here, we showed that both the extension

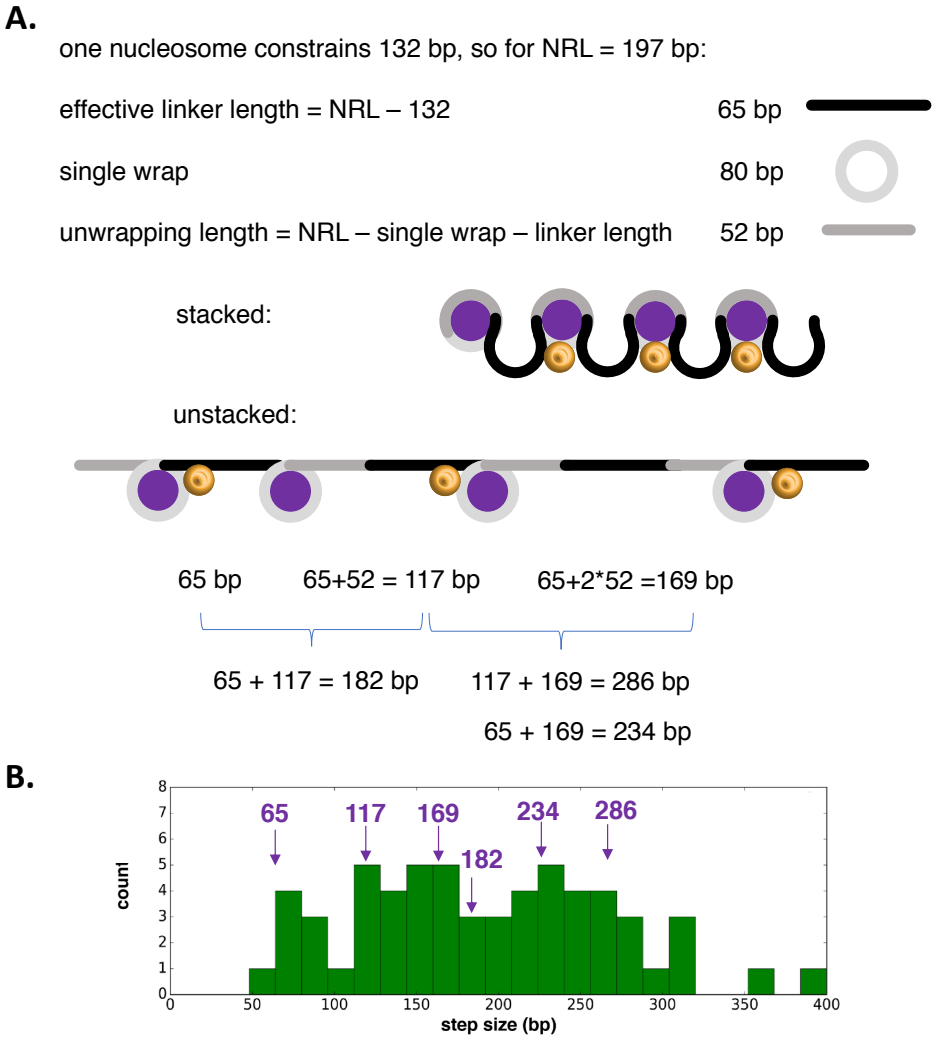

Figure 5.7
Proposed unstacking mechanism in H1(+) 197-NRL fibers. A) Schematic of the unstacking with the explanation of the corresponding extensions. Linker histones (shown in gold) bind to the dyad and at least one linker DNA. Upon unstacking and asymmetric unwrapping, the LH-dyad interaction and one LH-linker DNA interaction may persist. Note that the same unwrapping mechanism could exist in absence of LH, but rapid refolding obscure these intermediates. **B)** Histogram of unstacking steps in 15 independent molecules as in Fig. 5.6D.

and the compliance of the fibers are unaffected by the presence of H1. However, we demonstrated that nucleosome stacking in chromatin fibers does become more stable upon the addition of the linker histone. This could explain the more condensed chromatin structures that have been reported before [26]. We described the force-extension curves of H1(+) 197-NRL chromatin fibers with a non-equilibrium model that yielded an increased unstacking energy by 3 k_BT relative to H1(-) fibers. By analyzing the discrete unstacking steps occurring at low forces, we resolved transitions that indicate asymmetric DNA unwrapping from chromatosomes. These results shed new light on the chromatin fiber dynamics and the role of the linker histone in its folding.

At first, we performed gel electrophoresis on both types of chromatin fibers and showed that fibers become more compacted in the presence of H1. However, our single-molecule force spectroscopy data did not reveal changes in the compliance of chromatin fibers upon the enrichment with the H1. The low force regime that describes the tether stiffness yielded the same linear extension in H1(+) and H1(-) fibers. Quantitative analysis with the equilibrium model [23] yielded a slightly higher average stiffness of chromatin fibers with H1 ($k_{\text{folded}} = 0.28 \pm 0.07$ pN/nm vs. $k_{\text{folded}} = 0.18 \pm 0.05$ pN/nm, Supplementary Fig. S3). In individual fibers, however, the slope of the F-E curve did not change upon disassembly of H1, that ensued following repeated stretching and refolding cycles (Fig. 5.3). It is possible that the stiffness of the tether might be affected by the aspecific binding of H1 to the DNA handles. To minimize these effects, we used the lowest possible concentrations of linker histone (~ 1 μM) and applied a small force (~ 0.2 pN) while adding the H1 to the flow cell. It has been suggested that H1 preferentially binds to DNA junctions [27], therefore keeping the DNA handles stretched allowed us to minimize the unspecific binding. The successive H1 dissociation from individual tethers confirms that non-specific binding of H1 plays a minor role in our experiments.

We prepared the 197-NRL chromatosome fibers with two methods: co-reconstitution with H1 during the salt dialysis and the assembly of chromatosomes on tethered chromatin fiber in the magnetic tweezers. Both approaches resulted in quantitatively similar force-extension curves, though in the first case, H1 dissociation was irreversible, due to the absence of H1 in the measurement buffer. This suggests that the supplementation of the H1 at low concentration favoured in the specific binding of linker histone to the nucleosomal dyad.

Quantification of the unstacking step sizes observed in H1(+) fibers with our previous t-test method [23] was challenging at low force regime due to the linear extension of the folded fiber. Here, we measured discrete rupture events using a novel step-finding algorithm with 1 bp resolution. We obtained the average step size of the inner nucleosomal turn unwrapping of 79 bp for both H1(+) and H1(-) fibers. The new step-finding algorithm that we developed enables now to quantify nucleosome unstacking transition without knowing the NRL or symmetry of unwrapping *a priori*. This is an important step to quantify

natively assembled chromatin, where nucleosomes are distributed with various distances, which can influence stacking interactions.

Here, the unstacking events of H1(+) chromatin fibers featured a broad distribution of step sizes. We interpreted these results by taking account of the asymmetric unwrapping of chromatosomes upon unstacking that was observed in nucleosomes *in vitro* by Ngo *et al.* [9]. We speculate that such a mechanism occurs independent of the geometry of the linker histone binding. Knowing that H1 binds to the dyad and one or two linker DNAs, only the second interaction needs to break to allow unwrapping. Indeed, it appears that not all the contacts are broken, because our force-extension curves are to some extent reversible (Fig. 5.3B). In the case of symmetric binding (interaction with the dyad and two DNA linkers), it may be stochastic which side breaks first. Still, one linker DNA-H1 interaction can be stronger than the other. Asymmetric binding (two interactions) would automatically lead to asymmetric unwrapping because one side of the chromatosome is stabilized by the linker DNA-H1-dyad interaction. In the case of asymmetric binding, the orientation may be arbitrary, leading to the same distribution of step sizes. All together, we cannot discriminate between asymmetric and symmetric binding of the linker histone. However, the data clearly support the hypothesis of the asymmetric DNA unwrapping. Such a phenomenon can have implications *in vivo*, for example in maintaining the directionality of transcription. Linker histones can also affect the kinetics of this process, for instance by slowing down and, thus regulating, the gene expression.

5.4 Materials and methods

5.4.1 DNA and chromatin preparation

pUC-18 plasmid (Novagen) containing 15 or 25 repeats of Widom-601 sequence spaced by 50 bp of linker DNA (NRL = 197 bp) was digested using Bsa*I* and Bse*YI* enzymes (NE BioLabs). The linearized fragments with 601 repeats and 2030 bp of flanking DNA were subsequently labelled as in Ref. [28]. In brief: a Klenow reaction was performed to fill in the overhangs with digoxigenin-11-dUTP at the Bsa*I* site and biotin-16-dUTP at the Bse*YI* site. The labelled DNA was purified by Promega Wizard SV Gel PCR cleanup kit and subsequently mixed with stoichiometric ratios with *Drosophila* histone octamer (co-reconstituted with H1) or wild-type human histone octamer (Epicypher) at 2 M NaCl. Chromatin fibers were reconstituted overnight by a salt dialysis in Slide-A-Lyzer 10000× MWCO MINI dialysis tubes (Thermo Scientific). A titration series of 601-DNA:HO ratios between 0.8 and 1.5 was prepared and dialyzed against 100 mM, 1× TE pH 7.5 buffer overnight. The origin of histones qualitatively did not affect the results of the single-molecule force spectroscopy experiments.

5.4.2 Chromatin with linker histone

Lyophilizated *Drosphila* H1 histone stock (provided by Prof. L. Nordenskiöld, NTU, Singapore) was dissolved in 1 M NaCl, 50 mM Tris-HCl at pH 8.8 (final concentration 14 μg/μl). Reconstitution of chromatosome arrays with recombinant *Drosphila* histone octamers was performed similarly to that of nucleosomal arrays. An optimal ratio of 601-DNA and HO established in the previous reconstitution was used and titrated with increasing concentration of the linker histone, following Ref. [26]. A titration series of DNA HO:H1 ratios between 1:1.2:0.5 to 1:1.2:5 was dialyzed against 100 mM NaCl, 1× TE, pH 7.5 buffer overnight. Afterwards, the dialysis tubes were transferred to a folding buffer containing 100 mM NaCl, 2 mM $MgCl_2$ and 1× TE.

10 μl of each titration was fixed in formaldehyde (0.05 %) and loaded on a 0.7 % agarose gel in 0.2x TB and the band-shift assay was performed to select the titration with the most optimal LH concentration. Gels were stained with 1× ethidium bromide and the bands were visualized on the ChemiDoc UV imager.

Alternatively, chromatin fibers with linker histones were formed by adding the H1 stock (0.5 mM) to the flow cell (500× dilution) with tethered H1(-) chromatin fibers.

5.4.3 Flow cells

Flow cells were assembled from 2 coverslips, 24 × 40 mm and 24 × 60 mm (Menzel Gläser), sandwiched between a Polydimethylsiloxane (PDMS, Sylgard) mold. The bottom slide was coated with 0.1 % nitrocellulose in amyl-acetate (Ladd Research Industries). Subsequently, the assembled flow cell was incubated with 300 μl of 10 ng/μl sheep anti-digoxigenin (Sigma-Aldrich). Next, 300 μl of the passivation buffer consisting of 4 % *(w/v)* Bovine Serum Albumin (BSA, Sigma-Aldrich) and 0.2 % *(w/v)* Tween-20 (Sigma-Aldrich) was added and incubated at 4 degrees C overnight. Experiments were performed in measurement buffer (MB) that consisted of: 100 mM KCl, 2 mM $MgCl_2$, 10 mM NaN_3, 10 mM HEPES pH 7.5 and 0.4 % *(w/v)* BSA. Flow cells were washed with the buffer prior to measurements. 500 μl of 40 pg/μl chromatin in MB was incubated for 10 min at room temperature. Next, 20 μl of M270 magnetic beads (Invitrogen) were washed three times in 1× TE buffer and diluted 500 times in MB before they were flushed into the flow cell. After 10 min the flow cell was washed again with MB and the tethered chromatin fibers were ready for force spectroscopy.

In the experiments with H1(-) chromatin fibers, linker histone was introduced into the flow cell. 1 μl of the 14 μg/μl stock solution was dilluted in 500 μl of the MB buffer and injected into the flow cell (final H1 concentration of the H1: 28 ng/μl, $\sim$ 1 μM). Prior to the H1 assembly, the tethered molecules were

stretched with 0.2 pN force to prevent non-specific interactions of chromatosomes with the surface and the non-specific binding of H1 to bare DNA.

5.4.4 Magnetic tweezers

A home-built magnetic tweezer set-up was used, consisting of: a 25 Mpix camera (CMOS Vision GmbH), a frame grabber (National Instruments), a 40× oil objective (NA = 1.3, Nikon Corporation), an infinity-corrected tube lens (ITL200, Thorlabs), a 100 μW 645 nm LED (IMM Photonics GmbH), a multi-axis piezo scanner P-517.3CL (Physik Instrumente), two 5 mm cube magnets N50 (Supermagnete, Webcraft), a hollow shaft Stepper Motor (Casun) and two M-126.2S1 translation stages (Physik Instrumente).

By changing the magnet position between 0.1 - 10 mm above the flow cell, the force was increased and decreased exponentially in the range of 0.05 and 70 pN. Multiple beads were tracked in real-time using a custom tracking algorithm based on Fast Fourier Transform cross-correlation of a 100 pixels region of interest around a bead with a computer-generated image featuring cylindrically symmetric pattern of interference signals. Computer-controlled magnet movements and synchronous real-time bead tracking were implemented in LabVIEW (National Instruments).

5.5 Supplementary Information

5.5.1 Non-equilibrium statistical mechanics model

Here, we introduce a non-equilibrium model based on the statistical mechanics model (equilibrium model) presented in [23]. This extended quantitative framework combines the elastic response of DNA and chromatin fiber under tension and accounts for the energy barriers between different conformations of unfolding chromatin. Such model allows to capture and quantify the force-extension curves in H1(+) chromatin fibers that feature hysteresis.

Elasticity of DNA and a chromatin fiber

The elasticity of a DNA molecule is described by the extensible Worm-Like Chain (WLC) model [29], where the free energy $G(f, L)$ is given by:

$$G_{\mathrm{DNA}}(f, L) = -L\left[f - \sqrt{\frac{f k_{\mathrm{B}} T}{A}} + \frac{f^2}{2S}\right] + f z_{\mathrm{DNA}} \tag{5.1}$$

with f the force, L the contour length of the DNA, A the persistence length, k_{B} the Boltzmann constant, T the temperature and S the DNA stretching modulus.

Taking the derivative with respect to force and equating this to zero leads to the extension of DNA as a function of force:

$$z_{\mathrm{DNA}}(f, L) = L\left[1 - \frac{1}{2}\sqrt{\frac{k_{\mathrm{B}}T}{fA}} + \frac{f}{S}\right]. \tag{5.2}$$

When force is applied to a chromatin fiber, different stages of extension can be identified (Fig. 5.4A). For a chromatin fiber that consists of N nucleosomes, every nucleosome can be in any of four conformations (stacked, partially wrapped, singly wrapped or fully unwrapped). When all nucleosomes are in the stacked state, the free energy of the fiber is described by:

$$G_{\mathrm{fiber}}(f) = \frac{f^2}{2k} \tag{5.3}$$

with k the stiffness of the fiber (pN/nm) and f the applied force [23]. The Hookean extension of the fiber is then:

$$z_{\mathrm{fiber}}(f) = \frac{f}{k} + z_0. \tag{5.4}$$

with z_0 - the nucleosome line density of a folded fiber (set to 1.7 nm).

Equilibrium model

In the equilibrium model, we quantify the distribution of all the conformations as a function of force. Per nucleosome, we express the free energy of conformations:

$$G_{\mathrm{stacked}}(f) = \frac{f^2}{2k} \tag{5.5a}$$

$$G_{\mathrm{partially\ wrapped}}(f) = G_{\mathrm{DNA}}(f, L_{\mathrm{partially\ wrapped}}) + \Delta G_1 \tag{5.5b}$$

$$G_{\mathrm{singly\ wrapped}}(f) = G_{\mathrm{DNA}}(f, L_{\mathrm{singly\ wrapped}}) + \Delta G_1 + \Delta G_2 \tag{5.5c}$$

$$G_{\mathrm{fully\ unwrapped}}(f) = G_{\mathrm{DNA}}(f, L_{\mathrm{fully\ unwrapped}}) + \Delta G_1 + \Delta G_2 + \Delta G_3 \tag{5.5d}$$

where G_{DNA} is the energy of the unwrapped DNA and the linker DNA as in Eq. 5.1, ΔG_j is the free energy associated with the corresponding transition and L_i is the contour length of all free DNA in a particular conformation. For a fully unwrapped nucleosome, $L_{\mathrm{fully\ unwrapped}}$ equals to the Nucleosome Repeat Length (NRL), while for intermediate states: $L_{\mathrm{partially\ unwrapped}}$ corresponds to NRL $- 147 + L_{\mathrm{unwrapped\ length}} = 197 - 147 + 40 = 90$ bp; $L_{\mathrm{singly\ unwrapped}}$ corresponds to NRL $- L_{\mathrm{wrapped\ length}} = 197 - 80 = 107$ bp.

These free energies can be combined with the extension z for each nucleosome as a function of the applied force f:

$$z_{\text{stacked}}(f) = \frac{f}{k} + z_0 \tag{5.6a}$$

$$z_{\text{partially wrap}}(f) = z_{\text{DNA}}(f, L_{\text{partially wrap}}) \tag{5.6b}$$

$$z_{\text{singly wrapped}}(f) = z_{\text{DNA}}(f, L_{\text{singly wrapped}}) \tag{5.6c}$$

$$z_{\text{fully unwrapped}}(f) = z_{\text{DNA}}(f, L_{\text{fully unwrapped}}) \tag{5.6d}$$

where z_{DNA} follows Eq. 5.2.

The force-extension relation for the whole chromatin fiber is the sum of the contributions of all N nucleosomes and of the DNA handles:

$$z_{\text{tot}}(f) = \sum_{i=1}^{N} z_i(f) + z_{\text{DNA}}(f, L_{\text{handles}}) \tag{5.7a}$$

$$G_{\text{tot}}(f) = \sum_{i=1}^{N} G_i(f) + G_{\text{DNA}}(f, L_{\text{handles}}) \tag{5.7b}$$

with z_i the extension of the i^{th} nucleosome and G_i the free energy of that nucleosome, calculated with Eq. 5.6 and Eq. 5.5, respectively.

If the nucleosomes are indistinguishable, one has to correct for degeneracy of the energy of each conformation by introducing a degeneracy factor D:

$$D(\text{state}) = \prod_{i<j} \binom{n_i + n_j}{n_i} \tag{5.8}$$

with n_i the number of nucleosomes in state i. For fibers with the NRL of 197 bp, which were showed to have a one-start structure [20], nucleosomes unstack independently and the degeneracy factor is required. With this degeneracy factor, the Boltzmann-averaged extension of the fiber as a function of force becomes:

$$\langle z_{\text{tot}}(f) \rangle = \frac{\sum_{\text{states}} z_{\text{tot}}(f)\, D(\text{state}) \exp^{-(G_{\text{tot}}(f) - f z_{\text{tot}})/k_{\text{B}}T}}{\sum_{\text{states}} D(\text{state}) \exp^{-(G_{\text{tot}}(f) - f z_{\text{tot}})/k_{\text{B}}T}} \tag{5.9}$$

This equation was fitted to the force-extension curves with the following parameters: total length of the DNA construct $L_{\text{DNA}} = 4985$ bp or 6955 bp (for 15·601 and 25·601 DNA template, respectively), persistence length of DNA $A = 50$ nm, stretching modulus $S = 1000$ pN, NRL = 197 bp, number of nucleosomes N_{nuc}, extension of a nucleosome in fully folded state $z_0 = 1.5$ nm, stiffness of the fiber k, number of tetrasomes N_{unfolded}, number of bp unwrapped in the partially wrapped state $L_{\text{unwraped length}}$, the free energies ΔG_1, ΔG_2, ΔG_3

and the degeneracy factor (from Eq. 5.8). In addition to these parameters, we include an offset in extension z_{offset}, to correct for the fact that the chromatin fiber is usually not bound exactly to the bottom of the bead.

Non-equilibrium model

With the expressions for G and z in Eq. 5.5 and 5.6 we can numerically find an expression of free energy (G) as a function of extension (z) for each of the five conformations at any force. We simplified the equilibrium model described above by distinguishing three different states of nucleosome under force: stacked, singly wrapped and unwrapped.

Subtracting the work (fz) from the calculated free energy G results in the energy landscape shown in Fig. 5.4B and Fig. S4B. From this energy landscape, one can calculate the probability for each nucleosome to be in a certain state j at a force f with the Boltzmann equation:

$$P_j(f) = \sum_z \frac{\exp^{-(G_j(z)-fz)}}{\sum_{z,j} \exp^{-(G_j(z)-fz)}} \tag{5.10}$$

which is normalized by requiring that the total probability to be in any of the three conformations equals one. This is similar to the equilibrium model, but now we include deformations within each of these states, rather than taking only the most probable extension of each state.
The average extension of a nucleosome $\langle z_j \rangle$ in a certain state j at any force is thus calculated by integration of the probability over all extensions:

$$\langle z_j \rangle(f) = \frac{\int z(f) \exp^{-G_j(z)-fz} dz}{\int \exp^{-G_j(z)-fz} dz} \tag{5.11}$$

which was done numerically.

Figure S4B shows that there is an energy barrier in between states at different forces. The height of these barriers determines the rate of the transitions. These rates ($k_{i,j}^{\text{forward}}$ and $k_{i,j}^{\text{backward}}$) can be calculated with:

$$k_{i,j}^{\text{forward}}(f) = k_0 \exp\left(-\frac{\Delta G_{i,j}^{\text{barrier}}(f)}{k_{\text{B}}T}\right) \tag{5.12a}$$

$$k_{i,j}^{\text{backward}}(f) = k_0 \exp\left(-\frac{\Delta G_{i,j}^{\text{barrier}}(f) + \Delta G_{i,j}}{k_{\text{B}}T}\right) \tag{5.12b}$$

with k_0 the attempt rate to pass the barrier, $\Delta G_{i,j}$ the difference between the free energy of two states and $\Delta G_{i,j}^{\text{barrier}}$ the height of the energy barrier.

A Markow chain describes the changes in the chromatin fiber as a function time (t) and force (f). The transition rates are used to calculate a state transition matrix, whose product with a vector of the probabilities $P_j(t)(f)$

(from Eq. 5.10) results in the new vector $P_j(t + \Delta t)(f)$.
This new $P_j(t + \Delta t)(f)$ is used to calculate the extension of the chromatin fiber, by summing the extensions of all chromatosomes, nucleosomes, and tetrasomes, taking the probability of conformation j into account:

$$z(t, f) = N \sum_j P_j(t, f) \langle z_j(f) \rangle \tag{5.13}$$

where N is the total number of chromatosomes/nucleosomes/tetrasomes. This is repeated for each step in a force trajectory changing linearly. The extension of the DNA handles as a function of force, which does not show hysteresis, is added to obtain the total extension of the tether, which can then be plotted as a function of force.

5.5.2 Quantification of discrete unfolding steps

To model the discrete steps in force-extension curves, we identified the number of free base pairs L_{DNA} released in each unstacking or unwrapping transition. Here, we also simplified the statistical mechanics model described in the previous paragraph by distinguishing three different states of nucleosome under force: stacked, singly-wrapped and unwrapped. The folded fiber was modelled for this purpose with a Freely-Jointed-Chain (FJC) model, which yields a linear extension as a function of force, up to $f = 10$ pN. The extension of the DNA was described with a WLC model as in Eq. 5.2.

Freely-Jointed-Chained

We used here a FJC to model the extension of a folded chromatin fiber, although the fiber itself cannot be considered as a polymer of randomly oriented rigid segments. The advantage of a FJC model over the previously used Hookean spring model is that a freely jointed chain initially extends linearly at low force but the stiffness increases rapidly at forces exceeding half of the full extension. So while there is no numerical difference in the extension and the energy for small forces up to the unstacking transition, using a FJC prevents unrealistic extensions of the chromatin fiber at large forces.

At small forces ($fb \ll k_B T$), the stiffness of the fiber can be related to the Kuhn length b [29]:

$$k_{\mathrm{FJC}} = 3 \frac{k_{\mathrm{B}} T}{b L_{\mathrm{nuc}}} \tag{5.14}$$

where k_{FJC} is the stiffness per nucleosome, k_{B} is the Boltzmann constant, T is the absolute temperature and for L_{nuc} we take twice the height of a nucleosome (nm). The extension z_{FJC} depends on force f and length L and is given

by the Langevin function:

$$z_{\mathrm{FJC}}(f, L) = L\left[\coth\left(\frac{fb}{k_{\mathrm{B}}T}\right) - \frac{k_{\mathrm{B}}T}{fb}\right] \tag{5.15}$$

where $\coth(x)$ is the hyperbolic cotangent.

At low force, $z_{\mathrm{FJC}} \propto k_{\mathrm{FJC}}$ and a FJC behaves like a Hookean spring. At high force, the extension is limited to an imaginary contour length of the nucleosome stack L, which we set to ~ 50 nm:

$$\lim_{f\to\infty} z_{\mathrm{FJC}} = L = Nb \tag{5.16}$$

Identification of discrete states

The total extension $z_{\mathrm{tot}}(f)$ of the tether is sum of the extension of the stacked fiber plus the extension of the free DNA:

$$z_{\mathrm{tot}}(f) = N_{\mathrm{stacked}} z_{\mathrm{nuc}}(f) + z_{\mathrm{DNA}}(f, L) \tag{5.17}$$

with the number of nucleosomes N_{stacked} that is stacked in the chromatin fiber. The contour length of the free DNA L, is the sum of the DNA handles and the unwrapped length:

$$L_{\mathrm{DNA}} = L_{\mathrm{handles}} + \sum_{N_{\mathrm{unstacked}}} \mathrm{NRL} - L_{\mathrm{wrapped}} \tag{5.18}$$

where $N_{\mathrm{unstacked}}$ is the number of nucleosomes that unstacked from the folded fiber.

To recover the discrete states in the force-extension curve, we plotted the expected states according to Eq. 5.17 for increasing the amount of free DNA (Fig. S5) in 50 bp increments, though we analyzed the data with 1 bp increments. Subsequently, we calculated the probability that a given data point belongs to a particular state characterized by contour length S_L using the Z-score. The Z-score is a measure for the distance between a point and its expected value in terms of standard deviations and can be written as:

$$Z = \frac{|X - \mu|}{\sigma} \tag{5.19}$$

where X is the measured value, μ is the expected value and σ is the standard deviation. In the case of force-extension measurements, X is the measured extension at a certain force and μ is the extension calculated by the combination of a WLC and a FJC (Eq. 5.17). The expected standard deviation σ_{exp} of the extension can be expressed in terms of a measurement error and thermal fluctuations:

$$\sigma^2_{\mathrm{exp}} = \sigma^2_{M_{\mathrm{err}}} + \sigma^2_{\mathrm{TF}} \tag{5.20}$$

where $\sigma_{Merr} \approx 5$ nm and the thermal fluctuations σ_{TF} can be calculated using equipartition for the deviation of the extension from equilibrium:

$$\frac{1}{2}k_{\mathrm{B}}T = \frac{1}{2}\frac{dF}{dz}\sigma_{\mathrm{TF}}^2 \tag{5.21}$$

where the stiffness ($\frac{dF}{dz}$) can be calculated from the force-extension data.

The probability that a data point i belongs to a certain state S_L can now be written as:

$$P_i(S_L) = 1 - \mathrm{erf}\,(Z) \tag{5.22}$$

This yields a probability between 0 and 1; the bigger the probability, the the more likely a point is in the given state.

By summing the probabilities for all points for each state defined by L and normalizing it, a probability density distribution is obtained that indicates which states are most likely occupied during the force ramp (Fig. S5):

$$P(S_L) = \frac{\sum\limits_i P_i(S_L)}{\sum\limits_S \sum\limits_i P_i(S_L)} \tag{5.23}$$

The peaks in the probability density distribution indicate the states that are most likely to exist. States were assigned only when they were composed of two or more data points. In addition, the probability density must be at least $2 \times (\sum_S \sum_i P_i(S_L))^{-1}$, *i.e* consisting of at least 2 data points. In the example in Fig. S5, 19 states were found.

Merging states

Sometimes clusters of points appeared to be wrongly divided into multiple states. In Fig. S5, two separate states were found for the group of points indicated by the arrow. In order to correct this, the states were merged if the data of the clusters fulfilled specific criteria. Since the data is expected to be normally distributed, the Z-score could again be used to attribute a group of data points to each separate state. The threshold was set at 2σ, which should capture 95% of the points. Again, σ was based on the expected standard deviation (Eq. 5.20). Alternatively, a merged state with a contour length that is calculated by the weighted average of the points belonging to both initial states was evaluated. The following criteria were set to determine whether two states were merged into this new state:

1. Each of the two initial states must have at least 50% of the data within 2σ of the other state;
2. The merged state must have at least 80% of the points within 2σ.

An example is shown in Fig. S6. Initially, two states were found for a group of data points, as indicated by the peaks in the probability density distribution

(Fig. S5B). These two states have 75% of the points within 2σ of the other state. The merged state with a contour length of free DNA that is the weighted average of the two old states, has 96% of the points within 2σ. Both criteria hold so the new state was enforced. Of the 19 states in Fig. S5C, 15 remained in Fig. S6C. Removing falsely identified states from the data resulted in more accurate transitions.

Unwrapping step sizes

A double error function was fitted to the cumulative step size distribution to retrieve the number of base pairs in the inner turn wrap:

$$\mathcal{N}(x) = a_1 \left[1 + \mathrm{erf}\left(\frac{x-\mu}{\sigma\sqrt{2}}\right)\right] + a_2 \left[1 + \mathrm{erf}\left(\frac{x-2\mu}{\sigma\sqrt{2}}\right)\right] \tag{5.24}$$

where a_1, a_2 are the amplitudes of the first and second Gaussian, μ is the mean step size and σ is the standard deviation.

5.6 Supplementary Figures

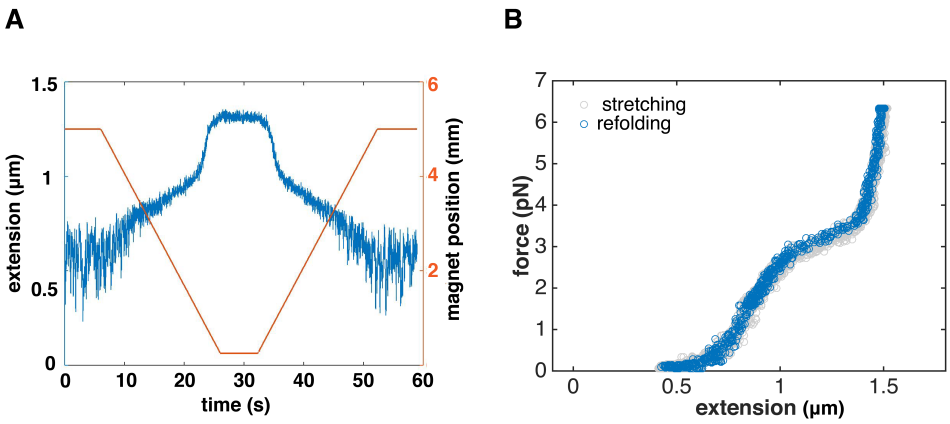

Figure S1
H1(-) 197-NRL fibers unfold in thermal equilibrium. A) A time trace representing the unstacking and restacking of a 197-NRL fiber induced by force (regulated by changing the magnet position). **B)** Representation of the same data as a force-extension curve. The refolding curve (grey) overlaps with the stretching curve (blue) indicating no histone loss and rapid restacking of the solenoid fiber to its initial configuration. The unstacking/restacking transition is in equilibrium, provided that the applied forces do not exceed 8-10 pN.

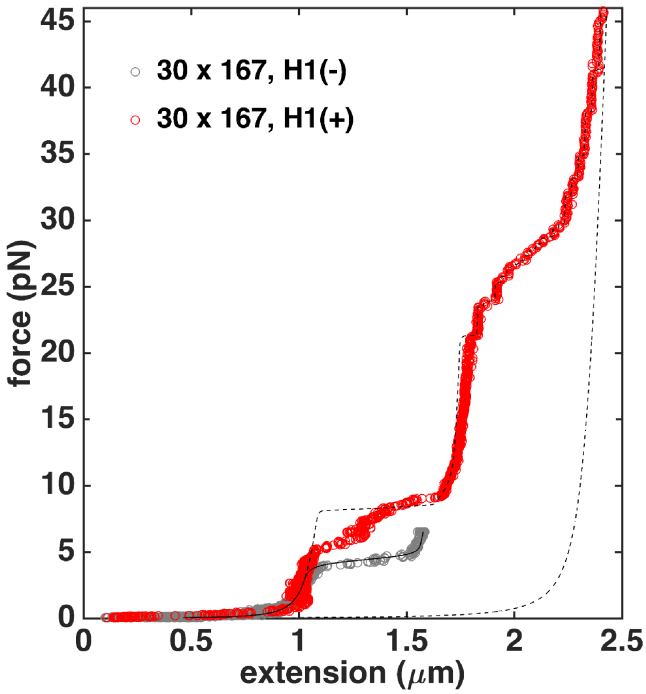

Figure S2

167-NRL fibers are stabilized by the linker histone H1. Force-extension curve of a 30·601 167-NRL chromatin fiber in the absence of the linker histone (grey) and the same molecule stretched with high forces after supplementing the measurement buffer with H1 (red). As in 197-NRL fibers, upon adding the H1, the linear stretching regime below 3 pN remained intact and the unstacking transition occurred at larger forces (ruptures between 6 - 9 pN instead of a 4.5 pN plateau).

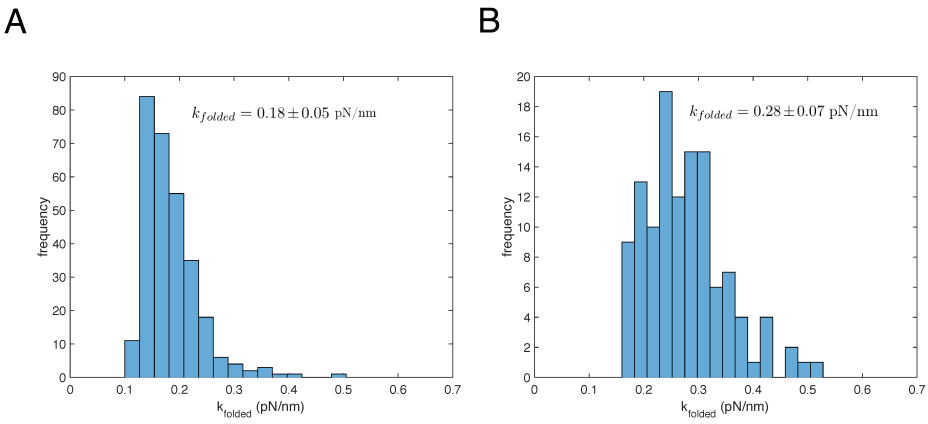

Figure S3

Stiffness of the H1(+) 197-NRL is on average higher than that of H1(-) 197-NRL fibers. A) Histogram showing the distribution of the stiffness obtained from the fitting the F-E curves of chromatin fibers reconstituted in the absence of H1. The average value is calculated to be $k_{\text{folded}} = 0.18 \pm 0.05$ pN/nm (mean ± SD). **B)** Histogram showing the distribution of the stiffness obtained from the fitting the release trace of F-E curves of chromatin fibers reconstituted with WT histone octamers and H1. The average value is $k_{\text{folded}} = 0.28 \pm 0.07$ pN/nm (mean ± SD).

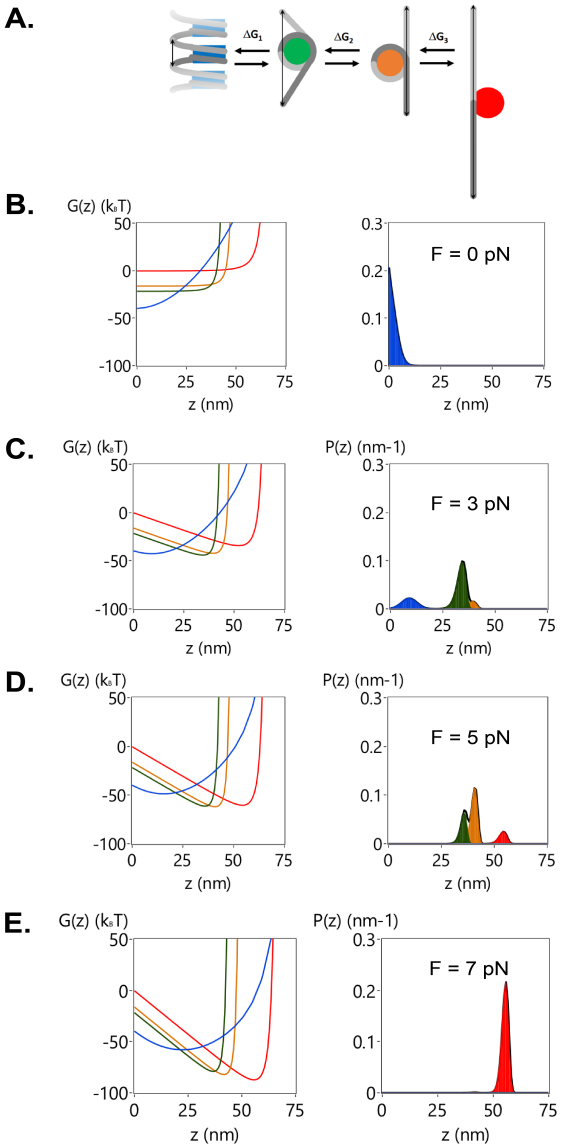

Figure S4

The energy landscape describes the distribution of conformations at different forces. A) A graphical representation of chromatin states under force. **B-E)** Energy landscape calculated at forces of 0, 3, 5 and 7 pN (left panels) and the corresponding probability distribution of each state (right panels). Colors correspond to distinct conformations of the fiber: stacked, partially wrapped, singly wrapped, unwrapped states, as depicted in panel A.

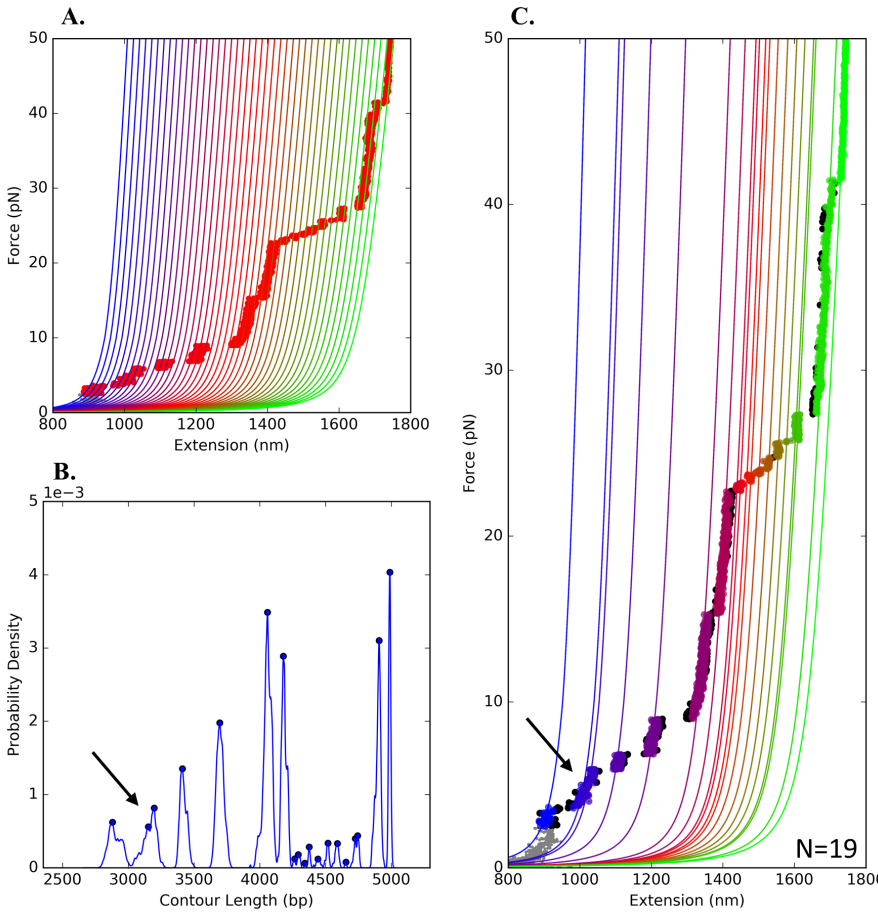

Figure S5

Extraction of discrete states in force-extension curves. A) Possible states of chromatin unfolding according to Eq. 5.17. For clarity, only states separated by 50 bp are shown, although 1 bp intervals states were tested. **B)** Probability distribution for all states in 1 bp steps. **C)** Colored lines show the states corresponding to the peaks in the probability distribution. Each state is plotted in a different color and data points within 2σ of a state are shown in the same color. Data points that could not be attributed to a distinct state are shown in black. The grey data points (f $<$ 10 pN) were not used during this analysis.

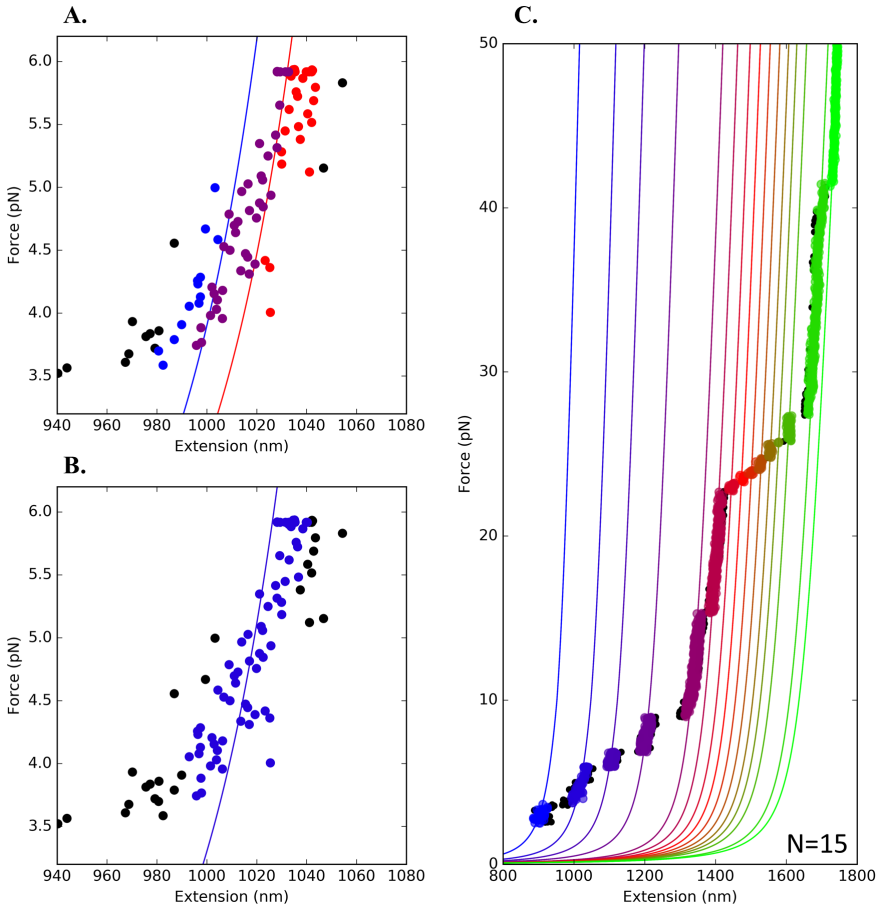

Figure S6

Merging states based on overlapping probability density distributions. A) Close-up of the second cluster of data points in Fig. S5C. The red and blue state represent two closely spaced peaks indicated by the arrow in Fig. S5B. Data points within 2σ of a state are shown in the same color as the line representing the state. Overlapping points (i.e. within 2σ of both states) are shown in purple. **B)** Result after merging states of (A). The cluster is now described by one state. The merged state is the weighted average of the two initial states. Note though that more points were not assigned (black). **C)** Full force-extension curve after merging. Each cluster is described by a single state.

Bibliography V

[1] Roger D. Kornberg. "Structure of chromatin". In: *Annu Rev Biochem.* 46 (1977), pp. 931–54.

[2] Robert T. Simpson. "Structure of the chromatosome, a chromatin particle containing 160 base pairs of DNA and all the histones". In: *Biochemistry* 17.25 (1978), pp. 5524–5531. ISSN: 0006-2960. DOI: 10.1021/bi00618a030.

[3] Nicole Happel and Detlef Doenecke. "Histone H1 and its isoforms: Contribution to chromatin structure and function". In: *Gene* 431 (2009), pp. 1–12. ISSN: 03781119. DOI: 10.1016/j.gene.2008.11.003.

[4] Peter G. Hartman et al. "Studies on the Role and Mode of Operation of the Very-Lysine-Rich Histone H1 in Eukaryote Chromatin: The Three Structural Regions of the Histone H1 Molecule". In: *European Journal of Biochemistry* 77.1 (1977), pp. 45–51. ISSN: 14321033. DOI: 10.1111/j.1432-1033.1977.tb11639.x.

[5] Alan P. Wolffe. "Histone H1". In: *International Journal of Biochemistry and Cell Biology* 29.12 (1997), pp. 1463–1466. ISSN: 13572725. DOI: 10.1016/S1357-2725(97)00026-5.

[6] Feng Song et al. "Cryo-EM study of the chromatin fiber reveals a double helix twisted by tetranucleosomal units". In: *Science* 344.6182 (2014), pp. 376–380. ISSN: 10959203. DOI: 10.1126/science.1251413.

[7] F Thoma, T Koller, and A Klug. "Involvement of histone H1 in the organization of the nucleosome and of the salt-dependent superstructures of chromatin." In: *The Journal of cell biology* 83.2 Pt 1 (Nov. 1979), pp. 403–27. ISSN: 0021-9525.

[8] Philip J. J. Robinson and Daniela Rhodes. "Structure of the '30 nm' chromatin fibre: A key role for the linker histone". In: *Current Opinion in Structural Biology* 16.3 (2006), pp. 336–343. ISSN: 0959440X. DOI: 10.1016/j.sbi.2006.05.007.

[9] Thuy T.M. Ngo et al. "Asymmetric unwrapping of nucleosomes under tension directed by DNA local flexibility". In: *Cell* 160.6 (2015), pp. 1135–1144. ISSN: 10974172. DOI: 10.1016/j.cell.2015.02.001.

[10] David A Hill and Anthony N Imbalzano. "Human SWI/SNF nucleosome remodeling activity is partially inhibited by linker histone H1". In: *Biochemistry* 39.38 (2000), pp. 11649–11656. ISSN: 00062960. DOI: 10.1021/bi001330z.

[11] Melody A. Lever et al. "Rapid exchange of histone H1.1 on chromatin in living human cells". In: *Nature* 408.6814 (2000), pp. 873–876. ISSN: 00280836. DOI: 10.1038/35048603.

[12] Sheila S. Teves, Christopher M. Weber, and Steven Henikoff. "Transcribing through the nucleosome". In: *Trends in Biochemical Sciences* 39.12 (2014), pp. 577–586. DOI: 10.1016/j.tibs.2014.10.004.

[13] Christopher L. Woodcock, Arthur I. Skoultchi, and Yuhong Fan. "Role of linker histone in chromatin structure and function: H1 stoichiometry and nucleosome repeat length". In: *Chromosome Research* 14.1 (2006), pp. 17–25. ISSN: 09673849. DOI: 10.1007/s10577-005-1024-3.

[14] Yuhong Fan et al. "H1 Linker Histones Are Essential for Mouse Development and Affect Nucleosome Spacing In Vivo". In: *Molecular and Cellular Biology* 23.13 (2003), pp. 4559–4572. ISSN: 0270-7306. DOI: 10.1128/MCB.23.13.4559-4572.2003.

[15] Bing Rui Zhou et al. "Structural Mechanisms of Nucleosome Recognition by Linker Histones". In: *Molecular Cell* 59.4 (2015), pp. 628–638. ISSN: 10974164. DOI: 10.1016/j.molcel.2015.06.025.

[16] Gregory D. Bowman and Michael G. Poirier. "Post-translational modifications of histones that influence nucleosome dynamics". In: *Chemical Reviews* 115 (2015), pp. 2274–2295. ISSN: 15206890. DOI: 10.1021/cr500350x.

[17] Beat Fierz. "Dynamic Chromatin Regulation from a Single Molecule Perspective". In: *ACS Chemical Biology* 11.3 (2016), pp. 609–620. ISSN: 15548937. DOI: 10.1021/acschembio.5b00832.

[18] Andrew Routh, Sara Sandin, and Daniela Rhodes. "Nucleosome repeat length and linker histone stoichiometry determine chromatin fiber structure." In: *Proceedings of the National Academy of Sciences of the United States of America* 105.26 (2008), pp. 8872–8877.

[19] Thomas Schalch et al. "X-ray structure of a tetranucleosome and its implications for the chromatin fibre". In: *Nature* 436.7047 (2005), pp. 138–141. ISSN: 00280836. DOI: 10.1038/nature03686.

[20] Artur Kaczmarczyk et al. "Single-molecule force spectroscopy on histone H4 tail-cross-linked chromatin reveals fiber folding". In: *Journal of Biological Chemistry* 292.42 (2017), pp. 17506–17513. ISSN: 1083351X. DOI: 10.1074/jbc.M117.791830.

[21] Babette E de Jong et al. "Rigid Basepair Monte Carlo Simulations of One-Start and Two-Start Chromatin Fiber Unfolding by Force." In: *Biophysical journal* 115.10 (2018), pp. 1848–1859. ISSN: 1542-0086. DOI: 10.1016/j.bpj.2018.10.007.

[22] Marteen Kruithof et al. "Subpiconewton dynamic force spectroscopy using magnetic tweezers." In: *Biophysical journal* 94.6 (2008), pp. 2343–2348. ISSN: 00063495. DOI: 10.1529/biophysj.107.121673.

[23] He Meng, Kurt Andresen, and John van Noort. "Quantitative analysis of single-molecule force spectroscopy on folded chromatin fibers". In: *Nucleic Acids Research* 43.7 (2015), pp. 3578–3590. ISSN: 13624962. DOI: 10.1093/nar/gkv215.

[24] Van A. T. Huynh, Philip J. J. Robinson, and Daniela Rhodes. "A method for the in vitro reconstitution of a defined '30 nm' chromatin fibre containing stoichiometric amounts of the linker histone". In: *Journal of Molecular Biology* 345.5 (2005), pp. 957–968. ISSN: 00222836. DOI: 10.1016/j.jmb.2004.10.075.

[25] Alison E. White, Aaron R. Hieb, and Karolin Luger. "A quantitative investigation of linker histone interactions with nucleosomes and chromatin". In: *Scientific Reports* 6 (2016). ISSN: 20452322. DOI: 10.1038/srep19122.

[26] Philip J. J. Robinson et al. "EM measurements define the dimensions of the '30-nm' chromatin fiber: evidence for a compact, interdigitated structure." In: *Proceedings of the National Academy of Sciences of the United States of America* 103.17 (2006), pp. 6506–11. ISSN: 0027-8424. DOI: 10.1073/pnas.0601212103.

[27] Patrick Varga-Weisz, Kensal Van Holdei, and Jordanka Zlatanoval. "Preferential Binding of Histone H1 to Four-way Helical Junction DNA". In: *The Journal of Biological Bhemistry* 268.28 (1993), pp. 20699–20700.

[28] Artur Kaczmarczyk et al. "Probing chromatin structure with magnetic tweezers". In: *Methods in Molecular Biology*. Vol. 1814. Humana Press, New York, NY, 2018, pp. 297–323. ISBN: 9781493985913. DOI: 10.1007/978-1-4939-8591-3_18.

[29] Carlos Bustamante et al. "Single-molecule studies of DNA mechanics". In: *Current Opinion in Structural Biology* 10.3 (2000), pp. 279–285. ISSN: 0959440X. DOI: 10.1016/S0959-440X(00)00085-3.

Chapter 6

Summary

Every eukaryotic cell within a complex organism must accommodate a genetic code that is stored as very long DNA molecules. In humans, the DNA is composed of almost 3 billion base pairs, which would measure more than 1 meter in a stretched configuration. In order to fit the entire genome in a micrometer-sized cell nucleus, eukaryotic DNA is organized into chromatin. Chromatin is a DNA-protein complex that features many levels of condensation. The basic structural unit of chromatin is called the nucleosome, which consists of almost 50 nanometers of DNA wrapped around an octamer of histone proteins. Interactions between nucleosomes in chromatin facilitate the compaction of DNA by several orders of magnitude.

While being densely compacted, DNA is subject to multiple processes, particularly its replication and transcription. In order to regulate these processes, the structure and composition of chromatin must be very dynamic. Mechanistically, the regulation involves reorganization of DNA packing by the repositioning, assembly or disassembly of nucleosomes. These transitions are aided by enzymes that can unwind, stretch and separate the two strands of bare DNA and, by doing so, generate forces and torques necessary to unfold chromatin.

The effects of tension and torsion on bare DNA and single nucleosomes have been extensively studied *in vitro* with single-molecule techniques. This has generated a detailed understanding of the physical properties of DNA and revealed the dynamic nature of nucleosomes. However, in the crowded environment of cells, nucleosomes are rarely present in isolation, and the nucleosomal arrays may form higher-order structures with distinct mechanical properties. By now, it has not been resolved how multiple nucleosomes compact into chromatin fibers in cells, and how this affects DNA accessibility. Due to the complex nature and the typical diameter of 10 - 100 nanometers, the structure of chromatin fibers *in vivo* could not be captured by traditional imaging techniques. Knowing these details would provide many new insights into the mechanisms of gene expression (epigenetic regulation) which, upon malfunction, may cause severe diseases. Therefore, the aim of this thesis is to increase the understanding of chromatin folding and its dynamics. To resolve topological changes in the un-

folding chromatin fibers, single-molecule magnetic tweezers were employed and statistical mechanics was used to quantify the experimental results.

Magnetic tweezers are a unique tool to study the topology and mechanical properties of chromatin fibers. This single-molecule force- and torque-spectroscopy technique allows to directly measure both the extension of individual reconstituted chromatin fragments with nanometer accuracy as well as the forces involved in their (un-)folding. The higher-order structure of different chromatin fibers was previously inferred from fitting a statistical mechanics model to the force-extension data. The results presented in this dissertation focus on the interactions between nucleosomes that contribute to the stacking of nucleosomes into a fiber structure.

In order to study the dynamics of chromatin fibers, the existence and stability of different topologies of such fibers were first established. The nucleosomal arrays were prepared via salt dialysis (**Chapter 2**) on a DNA template with multiple repeats of 601-sequences, separated with a fixed length of linker DNA, 20 bp or 50 bp (Nucleosome Repeat Length, NRL = 167 and 197, respectively). Such well-defined substrates have been instrumental in structural studies of chromatin *in vitro*, specifically in investigating how the spacing between adjacent nucleosomes impacts the geometry of compacted fibers. The most detailed electron microscopy and crystallography structures showed two stacks of nucleosomes connected by straight linker DNA (two-start, zig-zag fiber). However, alternative structures (such as a one-start, solenoid fiber) have also been proposed. In the stretching experiments performed here by magnetic tweezers, a two-start folding of 167-NRL fibers and a one-start folding of 197-NRL was inferred (**Chapter 3**).

The interpretation that 197-NRL fibers fold into a one-start solenoid was previously questioned, however, with the counterargument that the obtained force-extension curves could be interpreted as gradually unwrapping arrays of non-interacting nucleosomes. To address this issue, it was essential to directly show that nucleosome-nucleosome contacts are broken in 197-NRL fibers upon stretching. Thus, the existence of such interactions would be an indicator of nucleosome stacking. For this purpose, chemical bonds were introduced between neighboring nucleosomes of chromatin fibers containing mutant histones H4-V21C and H2A-E64C (**Chapter 3**). These histones had a cysteine residue at the acidic patch (H2A) and at the end of the histone tail (H4) that allowed for site-specific cross-linking, confirmed by the increased rupture forces of the individual fibers. This result indicated that the flexible histone tails that protrude out of the nucleosomes are responsible for interactions between neighboring nucleosomes. These experiments established also that the rupture of chromatin fibers that was observed at 4 pN, both in fibers with the NRL of 167 bp and 197 bp, should be attributed to the unstacking of nucleosomes. By this means, the existence of two alternative chromatin higher-order structures was inferred. These interpretations influenced the conclusions drawn further in this thesis.

Importantly, the folding of one-start and two-start chromatin fibers was shown in the absence of linker histones (**Chapter 5**). The linker histone (LH) is an additional histone protein that can interact with the nucleosome and form a structure called the chromatosome. Early studies indicated that linker histones are essential for chromatin compaction. However, the stretching experiments performed here on chromatin fibers without linker histones indicated that interactions between nucleosomes (discussed in **Chapter 3**) are sufficient to compensate the increased energy for bending the linker DNA that is required to form one-start solenoid chromatin fibers. In **Chapter 5**, it was shown that both the extension and the compliance of chromatin fibers were not affected by the presence of linker histones. Instead, chromatin fibers became more stable upon the addition of the linker histone H1, such that the unstacking transition occurred at higher force. Since the unstacking transition of fibers with linker histone was slower, compared to the fibers without H1, the unstacking of single chromatosome pairs could be resolved. By using a novel step-finding algorithm, an asymmetric mechanism of unwrapping was inferred from analyzing the discrete transitions in force-extension curves. Overall, linker histones affected the dynamics of chromatin fiber unstacking, but not its higher-order structure.

Once the folding of chromatin fibers was carefully analyzed, the response of 167-NRL and 197-NRL fibers to torsion was studied by magnetic tweezers and magnetic torque tweezers (**Chapter 4**). The application of twist to reconstituted chromatin fibers, by rotating magnetic field, mimicked the effect of torsional stress *in vivo*. Such mechanical stress has been proposed to be generated in cells by polymerases progressing along the DNA during its replication and transcription and is thought to induce the unwrapping of nucleosomes. Here, the impact of force and torque on compact chromatin fibers was investigated. In contrast to individual nucleosomes and sparsely decorated nucleosomal arrays, the twist-induced structural changes in the studied chromatin fibers were reversible, indicating a large degree of torsional elasticity of chromatin. This was tested by direct torque measurements that confirmed the hypothesis that chromatin fibers effectively act as a twist buffer. Moreover, a left-handed chirality of one-start and two-start chromatin fibers was inferred. Surprisingly, the response of chromatin to positive twist featured different signatures depending on the force applied during twisting. The most striking observation was the twist-induced unstacking and subsequent restacking of the chromatin fiber. These findings provide a new mechanism of chromatin supercoiling that is directly relevant for all processes that generate torsional stress in the eukaryotic genome.

In conclusion, using single-molecule force spectroscopy, structural changes of DNA and chromatin fibers were resolved and quantified. Due to nucleosome-nucleosome interactions, the mechanical properties of folded nucleosomal arrays clearly differ from those of isolated nucleosomes. Such folding of nucleosomes into secondary chromatin structures opens up a plethora of regulatory pathways

for controlling the level of DNA organization in cells. Single-molecule force- and torque-spectroscopy experiments and statistical mechanics models presented in this thesis can now be used for studying more complex substrates. For example, probing the dynamics of chromatin fibers with post-translational histone modifications would indicate how epigenetic modifications regulate the stability of nucleosome stacking. The experimental assays presented in this thesis are also applicable to studying natively purified chromatin samples, which can reveal more direct insights into chromatin folding *in vivo*.

Samenvatting

Elke eukaryotische cel in een complex organisme bevat een genetische code die wordt opgeslagen in de vorm van hele lange DNA-moleculen. In mensen bestaat het DNA uit bijna 3 miljard basenparen, wat uitkomt op een streng van meer dan 1 meter lang wanneer deze helemaal zou worden uitgerold. Om dit hele genoom in een micrometer grote celkern te laten passen, wordt het eukaryote DNA georganiseerd in chromatine. Chromatine is een DNA-eiwit complex dat wordt gekenmerkt door zijn vele niveaus van condensatie. Het fundamentele bouwblok van chromatine wordt het nucleosoom genoemd, wat bestaat uit bijna 50 nanometer aan DNA dat rondom een octameer van histoon-eiwitten gewonden is. Interacties tussen nucleosomen in chromatine condenseren het DNA enkele ordes van grootte, zodat het in de celkern past.

Ondanks dat DNA stevig ingepakt zit, kan het onderhevig zijn aan verschillende processen, zoals replicatie, het kopiëren van DNA, en transcriptie, het uitlezen van DNA. Om deze processen te reguleren is de structuur en compositie van chromatine zeer dynamisch. Transcriptie-regulatie houdt mechanisch gezien in dat nucleosomen herpositioneren, gevormd en afgebroken worden. Enzymen helpen bij deze transities door het DNA te ontwinden, uit te rekken of de twee strengen DNA uit elkaar te trekken; hierbij wordt kracht en torsie gecreëerd die nodig zijn om chromatine te laten ontvouwen.

De effecten van kracht en torsie op kaal DNA en individuele nucleosomen zijn uitgebreid bestudeerd *in vitro* met technieken die de resolutie halen om DNA per individueel molecuul te meten. Door deze experimenten is er een gedetailleerd begrip ontstaan over de fysische eigenschappen van DNA en is de dynamica van individuele nucleosomen in kaart gebracht. Echter, in het drukke milieu van een cel zijn nucleosomen nooit geïsoleerd aanwezig, en vormen zij verschillende hogere orde structuren van chromatine, met elk hun eigen mechanische eigenschappen. Het is moeilijk gebleken om systemen van meerdere nucleosomen, opgevouwen tot chromatinevezels, af te beelden. Hierdoor is tot nu toe weinig bekend over welke invloed dit opvouwen heeft op de toegankelijkheid van het DNA. Door de complexe aard en de geringe diameter van 10 - 100 nanometer, hebben traditionele beeldvormende meettechnieken de structuur van chromatine *in vivo* nog niet kunnen vastleggen. Wanneer deze structuren bekend zouden zijn, zou dit vele nieuwe inzichten over de

mechanismen van genexpressie (epigenetische regulatie) opleveren die, wanneer defect, ernstige ziektes kunnen veroorzaken. Het doel van dit proefschrift is het vouwen en de dynamiek van chromatine beter te begrijpen. Om de topologische veranderingen in ontvouwende chromatine fibers te meten, wordt hier gebruik gemaakt van een magnetisch pincet. De gemeten data konden vervolgens geïnterpreteerd worden door middel van statistische fysica.

Het magnetische pincet is een uniek gereedschap om de topologie en mechanische eigenschappen van chromatine vezels te bestuderen. Deze 'single-molecule' kracht- en torsie-spectroscopie techniek, maakt het mogelijk om de extensie van individuele chromatinevezelfragmenten te meten met nanometer nauwkeurigheid, en daarbij ook de krachten die gepaard gaan bij het ontvouwen te kwantificeren. De hogere orde structuren van verschillende chromatinevezels kunnen worden afgeleid door het fitten van een op de statistische fysica gebaseerd model aan de kracht-uitstrekking data. De resultaten in dit proefschrift focusseren zich op de interactie tussen nucleosomen die door stapeling van nucleosomen bijdragen aan de chromatine vezel structuur.

Om de dynamiek van chromatine fibers te bestuderen, zijn eerst de stabiliteit van verschillende topologieën van zulke fibers getest. Zogenaamde 'kralen kettingen' van nucleosomen werden bereid via zout dialyse (**Hoofdstuk 2**) met behulp van een DNA substraat bestaande uit herhalingen van zogenaamde 601-sequenties. Door deze speciale DNA sequentie was het mogelijk om nucleosomen van elkaar te scheiden met een vaste lengte aan linker DNA, 20 bp of 50 bp (corresponderend met een nucleosoom herhalingslengte, NHL = 167 en 197, respectievelijk). Zulke goed gedefinieerde substraten zijn essentieel voor studies naar de structuur van chromatine *in vitro*. Specifiek hebben we deze substraten gebruikt om erachter te komen hoe de afstand tussen nucleosomen de geometrie van de opgevouwen fibers beïnvloedt. De meest gedetailleerde elektronenmicroscopie en kristallografie metingen hebben laten zien dat twee stapels van nucleosomen aan elkaar verbonden waren door recht linker DNA (de twee-start of zig-zag fiber). Alternatieve structuren, zoals een één-start, (solenoïde) fiber, zijn echter ook voorgesteld als mogelijkheid. De strek-experimenten, hier gedaan met de magnetische pincetten, laten zowel een twee-start vouwing van 167-NHL fibers als een één-start vouwing van 197-NHL fibers zien (**Hoofdstuk 3**).

De interpretatie dat 197-NHL fibers opvouwen tot een één-start solenoíde werd voorheen betwijfeld, met als argument dat de verkregen kracht-extensie curves verklaard konden worden door aan te nemen dat nucleosomen geleidelijk ontvouwen en geen interactie met elkaar hebben. Om deze kwestie te adresseren, was het essentieel om te laten zien bij welke kracht nucleosoom-nucleosoom interacties worden verbroken als de fibers worden uitgerekt. Hiervoor werden chemische verbindingen gelegd tussen naast elkaar liggende nucleosomen van chromatine fibers die de mutant histonen H4-V21C en H2A-E64C bevatten (**Hoofdstuk 3**). Deze histonen hadden een cysteïne residu bij zowel het zure gedeelte van histoon H2A als aan het einde van de histoon H4 staart, zodat

het mogelijk was om deze via specifieke cross-linking covalent aan elkaar te verbinden. De cross-linking werd bevestigd door de verhoging van de kracht die nodig is om de individuele fibers kapot te trekken. Dit resultaat toont aan dat de flexibele histoon staarten die uit het nucleosoom steken verantwoordelijk zijn voor de interacties tussen de naast elkaar liggende nucleosomen. Deze experimenten lieten ook zien dat het openbreken van chromatine fibers, wat zowel bij de 167-NHL als de 197-NHL fibers rond een kracht van 4 pN gebeurt, moet worden toegekend aan zowel het verbreken van de stapeling van nucleosomen als de gedeeltelijke ontvouwing van nucleosomen. Hieruit werd geconcludeerd dat er twee alternatieve hogere orde nucleosoom structuren bestaan. Deze interpretaties vormen de basis voor het onderzoek in de volgende hoofdstukken van dit proefschrift.

Een belangrijk resultaat is dat zowel één-start als twee-start chromatine fibers kunnen vouwen in hogere orde structuren in afwezigheid van linker histoon (**Hoofdstuk 5**). Het linker histoon (LH) is een additioneel histoon eiwit dat interacties kan aangaan met het nucleosoom. Samen wordt dit complex een chromatosoom genoemd. Eerdere studies gaven aan dat linker histonen essentieel zijn voor het compact maken van chromatine. De strek-experimenten die hier gedaan zijn op chromatine fibers zonder linker histonen, laten echter zien dat interacties tussen nucleosomen (zie **Hoofdstuk 3**) sterk genoeg zijn om de energie benodigd voor het buigen van het linker DNA in een één-start solenoïde fiber te compenseren. In **Hoofdstuk 5**, laten we zien dat zowel de extensie als de elasticiteit van chromatine fibers niet beïnvloed wordt door de aanwezigheid van linker histonen. In plaats daarvan werden de chromatine fibers stabieler met de toevoeging van een linker histoon H1, zodat het verbreken van de nucleosoomstapels plaats vond bij hogere krachten. Omdat het verbreken van nuclesoom stapels in fibers met linker histonen langzamer was, vergeleken met fibers zonder H1, kon het verbreken van de interacties tussen individuele nucleosomen bekeken worden. Gebruikmakend van een nieuw analyse algoritme dat discrete transities in de kracht-extensie curves herkent, konden we concluderen dat nucleosomen asymmetrisch ontvouwen. Linker histonen beïnvloeden dus met name de dynamiek van het stapelen van nucleosomen in chromatine fibers, maar de hogere orde structuren zelf veranderen niet.

Vervolgens, werd de reactie van 167-NHL en 197-NHL fibers op torsie bestudeerd met behulp van magnetische pincetten en magnetische torsie pincetten (**Hoofdstuk 4**). Het draaien van gereconstrueerde chromatine fibers door het magnetisch veld te draaien, bootst het effect van torsie als gevolg van transcriptie na. Er is voorgesteld dat zulke mechanische spanningen gegenereerd worden in cellen door polymerasen wanneer deze over het DNA bewegen gedurende replicatie en transcriptie, en dat deze spanningen de nucleosomen ontvouwen. In contrast met individuele nucleosomen en ketens van nucleosomen die geen interactie met elkaar hebben, waren de structurele veranderingen resulterend uit het draaien van de chromatine vezels omkeerbaar, wat aangeeft dat chro-

matinevezels een grote rotatie-elasticiteit hebben. Dit werd getest door directe moment-metingen, die bevestigden dat chromatine fibers werken als buffers voor torsie. Bovendien werd een linkshandige chiraliteit van zowel de één-start als twee-start chromatine structuren afgeleid. Verassend genoeg werd het respons van chromatine op positieve draaiingen (tegen de klok in) gekenmerkt door verschillende configuraties, afhankelijk van de kracht die werd toegepast tijdens het draaien. De meest opvallende observatie was dat de interacties tussen nucleosomen in eerste instantie worden verbroken door positieve draaiingen om vervolgens weer op te stapelen in gevouwen chromatine fibers bij overmatige draaiing. Deze bevindingen tonen een nieuw mechanisme voor het open ontvouwen van chromatine dat relevant is voor alle processen die torsie genereren op het eukaryotische genoom.

Het vouwen van nucleosomen in een secundaire chromatine structuur kan belangrijk zijn voor de regulatie van genen in cellen en het is daarom van belang om meer inzicht te krijgen in achterliggende mechanismen. Door krachtspectroscopie toe te passen op individuele moleculen, konden structurele veranderingen van DNA en chromatine vezels bekeken en gekwantificeerd worden. De mechanische eigenschappen van gevouwen chromatine structuren zijn door de nucleosoom-nucleosoom interacties duidelijk anders dan die van geïsoleerde nucleosomen. De kracht- en torsie-spectroscopie en de statistisch-mechanische modellen die gebruikt zijn in dit proefschrift, kunnen nu ook gebruikt worden voor het bestuderen van complexere substraten. Het onderzoeken van de dynamiek van chromatine fibers met zogenaamde post-translatie modificaties van histonen zou bijvoorbeeld inzicht kunnen opleveren hoe epigenetische modificaties de stabiliteit van chromatine vouwing reguleren. De experimenten die in dit proefschrift worden gepresenteerd kunnen ook toegepast worden op gepurificeerde chromatine monsters, die meer inzicht kunnen leveren in het vouwen van chromatine *in vivo*.

List of publications

1. "Chromatin fibers stabilize nucleosomes under torsional stress"
   Kaczmarczyk A., Meng H., Ordu O., van Noort S.J.T., Dekker N. H.,
   submitted.
2. "Linker histone H1 stabilizes nucleosome stacking in chromatin fibers"
   Kaczmarczyk A., Hermans N., Rodriguez de Mercado R., Vendel K., Nordenskiöld L., van Noort S.J.T.,
   manuscript in preparation.
3. "Rigid Basepair Monte Carlo Simulations of One-Start and Two-Start Chromatin Fiber Unfolding by Force"
   de Jong B., Brouwer T.B., **Kaczmarczyk A.**, Visscher B., van Noort S.J.T.,
   Biophysical Journal 115, 1-12, (2018).
4. "Unraveling DNA Organization with Single-Molecule Force Spectroscopy Using Magnetic Tweezers."
   Brouwer T.B., **Kaczmarczyk A.**, Pham C., van Noort S.J.T.,
   in: Bacterial Chromatin. Methods in Molecular Biology, 1837:317-351 (2018).
5. "Probing chromatin structure with magnetic tweezers"
   Kaczmarczyk A., Brouwer T.B., Pham C., Dekker N.H, van Noort S.J.T.,
   in: Nanoscale Imaging. Methods in Molecular Biology, 1814:297-323 (2018).
6. "Single-molecule force spectroscopy on histone H4 tail cross-linked chromatin reveals fiber folding"
   Kaczmarczyk A., Allahverdi A., Brouwer T.B., Nordenskiöld L., Dekker N.H., van Noort S.J.T.,
   Journal of Biological Chemistry, 292 (42), 17506-17513 (2017).

Curriculum vitae

I was born on 2nd of February, 1988, in Ruda Śląska, Poland. From early adolescence, my interests were directed towards natural sciences. In 2007, I finished the high school education at Liceum Ogólnokształcące in Bytom, Poland, where I followed extensive biology and chemistry courses. After that, I was admitted to the Silesian University of Technology in Gliwice, Poland, where I started the Engineer study programme in Biotechnology. I graduated with distinction in 2011 and continued with the Master study programme at the same university. Under the supervision of Dr. Magdalena Skonieczna and Prof. Wiesław Szeja, I investigated the oxidative damage of DNA in cancer cells, which was the subject of my master thesis.

After completing my undergraduate studies in 2012, I moved abroad to start an internship in the lab of Prof. Jens Michaelis at Ulm University, Germany. Under the guidance of Katarzyna Krzemień, I developed an interest in chromatin biology and single-molecule biophysics, which motivated me to pursue an academic career. Shortly after, I applied for the joint PhD position at Leiden University and Delft University of Technology, The Netherlands. The project, supervised equally by Prof. John van Noort and Prof. Nynke H. Dekker, brought together the expertise of the two research labs in single-molecule force- and torque-spectroscopy techniques with the goal to study the dynamics of chromatin fibers.

As a PhD candidate, I supervised two bachelor students: Raùl Wijfies, Wendy Blonk, and one master student, Kim Vendel. I also assisted in teaching the bachelor course 'The Physics of Life Processes', that was taught by Prof. Doris Heinrich. Several times I presented my research projects at conferences in Europe and in the U.S., which helped me to establish new collaborations (*e.g.* with Hannah Wheeldon from Edinburgh University).

Apart from these scientific activities, I joined the board of Leidse Promovendus Overleg (LEO), that is an organization of PhD students involved in organizing events and supporting PhD candidates at Leiden University.

In October 2018, I moved to the United Kingdom, where I started my post-doctoral position in the lab of Prof. David Rueda at Imperial College London.